# THERMAL ASPECTS OF CORROSION OF STEEL IN CONCRETE

Effect of low temperature on the resistivity and the cathodic reaction rate.

*By:*

*Jan-Magnus Østvik Jr.*

The Norwegian University of Science and Technology

Department of structural engineering

N – 7034 Trondheim

Norway

November 2004

***To my wife Guri,***

***your encouragement and endless patience***

***was vital for this project.***

# ACKNOWLEDGEMENTS

I wish to express my gratitude to the Norwegian Public Roads Administration and Norwegian Research Council for financing this work.

Many people have contributed and helped me through the four years of study, thank you:

- *Øystein Vennesland*, for being my main supervisor, guiding and encouraging me through all phases of my study.

- *Claus K. Larsen*, for being my co-supervisor, your patience and guidance has been vital for my progress.

- *M$^{a}$Carmen Andrade Perdrix*, for receiving me at Instituto Eduardo Torroja in Madrid, your hospitality and being my mentor in electrochemistry.

- *Erik J. Sellevold*, for constructive criticism and for our very useful discussions.

- *Dirch Bager,* for performing the Calorimetric test and useful discussions.

- *Finn Fluge and Kjersti K. Dunham*, for keeping my project economy healthy.

- *Helge Rødsjø, Kjell Kristiansen, Svein Lorentsen and Ove Loraas* for assisting me in my laboratory work.

- *Colleagues at Instituto Eduardo Torroja*, for making my stay in Madrid an unforgettable journey both professionally and personally.

- *Colleagues at the Norwegian Public Roads Administration and the Norwegian University of Science and Technology*, for all the encouragements and for making the work more joyful.

- *My Dad, Jan M. Østvik*, for creating and nurturing my interest for corrosion of steel in concrete.

Last but not least I want to express my warmest gratitude to my wife, *Guri*, and to my lovely daughters, *Emma* and *Marie*, for your great encouragement, sacrifice and patience. I apologise to you and to all my friends for any neglect while I selfishly perused my goal.

Trondheim, November 2004

Jan-Magnus Østvik

# SUMMARY

The underlying causes and processes of reinforcement corrosion are quite well investigated and understood, however, there are some aspects not extensively investigated. One such aspect is the effect of temperature on the corrosion process in concrete, and especially the corrosion behaviour in the low temperature range.

Concrete due to its porous nature has pore solution present in a liquid state, even at very low temperatures in its smallest pores. Given the presence of liquid, and provided oxygen is present, it is likely that corrosion is possible at even very low temperatures.

In Norway where a considerable number of concrete structures are directly exposed to climatic conditions below 0°C, the effect of low temperatures on corrosion is an important topic.

During the course of this study, corrosion of steel in concrete was indirectly investigated by monitoring thermal effects on two of the main parameters for steel corrosion in concrete, cathodic reaction rate and the electrical resistivity of concrete. The experiments were performed on two concrete mixes (water/binder – ratio (w/b) of 0.4 and 0.6) for various curing conditions. The experimental programme can be summarised as follows:

- The cathodic reaction rate
  - Stationary polarisation
    - Polarisation: -0.6 V/MMO
    - Temperature range: -40°C ≤ T ≤ 40°C
    - Intervals: 5°C change every 24 hours
    - Moisture content: 55% ≤ DCS ≤ 99%
  - Cathodic polarisation curves
    - Scanning interval: 0 V/MMO – -1.2 V/MMO
    - Scan rates: 0.1 V/15 minutes,
      0.1 V/ 24 hours
    - Temperature: 20°C, 0°C and -20°C

- The electrical resistivity of concrete
  - Measurement techniques:
    - Electrochemical Impedance Spectroscopy
    - Positive Feedback
    - Potential Square Pulse
  - Temperature (constant): 20°C, 2°C, -14°C and -28°C
  - Moisture content: 30% ≤ DS ≤ 100%

The thermal response of these two corrosion parameters provides valuable indications on actual embedded corroding systems.

The results from the cathodic reaction rate experiments show that the cathodic reaction rate at stationary polarisation of -0.6 V/MMO (approximately -0.5 V/SCE) decreases with decreasing temperature. The cathodic reaction rate at -40°C is about 5 to 8% of the corresponding

reaction rate at 0°C, and at +40°C the reaction rate is increased to between 150 to 650% the rate at 0°C. In general, the changes are largest for the concrete with w/b ratio of 0.6, which has a much higher initial reaction rate (at 0°C) than w/b 0.4.

In the temperature range -40°C ≤ T ≤ 0°C the thermal changes in the cathodic reaction rate followed the Arrhenius law quite well. The calculated activation energy constants were in the range 2500 – 5000 K confirming values already reported. No clear and uniform correlation between the activation energy constants and the properties of the concretes was found. However, considerable hysteresis effects for the variants with the initial highest moisture contents were found. These effects were attributed to ice formation in the largest capillaries. The amount of ice in the concretes was determined by low temperature calorimetry. This verified the presence of quite substantial amounts of ice at the lowest temperatures (-40°C).

In the temperature range 0°C ≤ T ≤ 40°C the thermal changes in the cathodic reaction rate did in some cases follow the Arrhenius law and in some cases not. The reaction rate appeared to approach an upper limit. This may be due to decreasing solubility of oxygen for increasing temperature, and that the reaction is decelerated by the supply of reactants. The effect appeared to be strongest for the concrete with w/b ratio of 0.4. This observation strengthens the indication of transport and accessibility related deceleration. Inhibition of the reaction increasingly occurred for temperatures higher than 20°C.

The cathodic polarisation experiments (0 to -1.2 V/MMO) indicated that the equilibrium potentials of the electrodes were quite unaffected by temperature. Furthermore, the cathodic reaction rate showed a Tafel region with slopes in the range (-0.1 to -0.2 V/decade) which is similar to reported values for oxygen reduction on platinum (-0.12 V/decade). The variation from the ideal slope was attributed to changes in the oxide layers and interfering red-ox reaction due to the presence of a passive oxide layer and impurities on the electrode surface. In the low overpotential range (0 to -0.3 V) the polarisation behaviour appeared relatively unaffected by temperature. Only small changes in the equilibrium potential were observed for decreasing temperatures. These changes may have been introduced by forgoing polarisation.

The fast scan rate (-0.1 V every 15 minutes) generally induced higher values for the reaction rate than the slow scan rate (-0.1 V every 24 hours). The results are more or less parallel showing the same trend. However, one should be aware that the fast scan rate is in the first peak of the potentiostatic transient while the slow scan rate is assumed to be in a more or less quasi steady state. Of practical reasons (time) the fast scan rate was chosen for further polarisation experiments.

At decreasing temperatures the reaction rate approaches a situation similar to concentration polarisation at increasing overpotentials. This situation occurred on cathodic overpotentials more negative than -0.3 V and the effect appeared to be magnified for decreasing temperatures. This indicates that even though the solubility of oxygen in water increases for decreasing

temperatures the effect of increased concentration of dissolved oxygen did not increase its availability at low temperatures.

The lowest temperature for these polarisation experiments was -20°C and only small amounts of ice should be present at this temperature. The small amounts of ice were presumably not enough to affect the reaction rate profoundly.

It must be emphasised that the cathodic polarisation curves are presented without automatic compensation for the ohmic drop.

The results from the electrical resistivity of concrete experiments show that the electrical resistivity of concrete is greatly affected by both temperature and the moisture condition of the concrete.

In general, the electrical resistivity of concrete increases with decreasing temperature and follows the Hinrichson-Rasch law (diversion of the Arrhenius law) quite well. The calculated activation energy constants from the results were in the range 2000 – 5000 K and appear to be relatively unaffected by the initial moisture content and the concrete quality.

The totally saturated specimens had non-linear behaviour in the Arrhenius plots. The non-linear behaviour was attributed to ice formation in the largest capillaries.

The electrical resistivity increases strongly with decreasing moisture content. Below certain moisture content levels the resistivity increases

very much stronger with decreasing moisture content. At higher moisture contents than these critical levels, the increase appears to be dependent on the mix characteristics (i.e. w/b ratio, silica content, cement content). At moisture contents lower than these critical levels the increase appears to be independent of the mix characteristics. The results, using some assumptions, indicate that a critical thickness of the conductive adsorbed water layers were reached at the breaking levels, forcing the conductive pathways into very small pores where the conduction is hindered by restricted mass transport.

By combining the effects of temperature and moisture condition on electrical resistivity, it was found that the moisture content had a similar effect for all the four constant temperatures investigated. The temperature resulted in a shift towards a higher level for decreasing temperatures, indicating that the moisture sensitivity is independent of temperature.

Measurements by Electrochemical Impedance Spectroscopy (EIS) gave information on the concrete's dielectric properties. In general, a typical impedance spectrum for concrete could be described by a suppressed semicircle that indicated that the concrete had distributed relaxation times.

The distributed relaxation times indicate several parallel conductive phases, i.e. the impedance describes the different phases of conduction in concrete (e.g. cement particles, liquids, and adsorbate). The magnitude of the suppression was not much affected by temperature.

In addition, the results showed that the frequency at maximum capacitance was decreasing for decreasing temperatures. This indicates that the frequency corresponding to zero capacitive contribution also had a similar temperature dependency. The results indicate that the appropriate measurement frequency for obtaining the actual resistance of the concrete decreases for decreasing temperature.

Furthermore the dielectric constant appears to increase for increasing moisture content. Due to limited data it is not possible to be conclusive; however, this trend is coherent with the theory. The calculated dielectric constants were in the range 10 – 15.

Resistivity was measured using three techniques, where two of the techniques were compared: EIS and Positive Feedback. EIS measurements were regarded as "true", and the comparison revealed a rather limited range of resistivities (up to 17 kΩm) which could be reliably measured with positive feedback.

Using the results from the experimental work and making some assumptions, it can be concluded that corrosion rate decreases strongly with decreasing temperature, although this reduction cannot be quantified.

The main conclusions of this study are:

1) The cathodic reaction rate of passive steel embedded in concrete decreases with decreasing temperature.

2) Ice formation in the capillaries generates a considerable hysteresis effects on the cathodic reaction rate of steel in concrete.

3) The cathodic polarisation behaviour of steel is temperature dependent.

4) The electrical resistivity of concrete increases with decreasing temperature.

5) The electrical resistivity of concrete is governed by the moisture condition of concrete, increasing with decreasing moisture content.

# TABLE OF CONTENTS

# NOTATIONS, UNITS AND ABBREVIATIONS

| Symbol | Unit | Description and/or definition |
|---|---|---|
| $a$ | [K] | activation energy constant |
| $A$ | [K] | activation energy constant |
| $A$ | [$m^2$] | area |
| $A$ | [$sec^{-1}$] | constant |
| $A$ | [-] | scaling factor (Arrhenius law) |
| $A_e$ | [$m^2$] | area of the electrode |
| $C_{cem}$ | [kg $m^{-3}$] | cement in the dosage |
| $c$ | [kg $m^{-3}$] | concentration |
| $C$ | [kg $m^{-3}$] | oxygen concentration in the pore solution |
| $c_i$ | [mole $m^{-3}$] | concentration of ions |
| *const* | [-] | constant (scaling factor/mathematics) |
| *CSH* | [-] | Calcium – Silicate – Hydrates |
| *DCS* | [-] | Degree of Capillary Saturation |
| *DS* | [-] | Degree of Saturation |
| $D_i$ | [$m^2$ $sec^{-1}$] | diffusion coefficient of species |
| $D_{ox}$ | [$m^2$ $sec^{-1}$] | oxygen diffusion coefficient |
| $e$ | $1.6 \cdot 10^{-19}$ C | electron charge |
| $E$ | [V] | potential |
| $E$ | [V $m^{-1}$] | strength of the electrical field |
| $E_a$ | [kJ $mole^{-1}$] | activation energy |
| $E_a$ | [V] | anodic potential |
| $E_c$ | [V] | cathodic potential |
| $E_{eq}$ | [V] | equilibrium potential |

| Symbol | Unit | Description and/or definition |
|---|---|---|
| $F$ | [-] | constant |
| $F$ | 96485 C/mol | Faradays constant ($1F = e \cdot N_A$) |
| $F$ | [-] | Formation factor |
| $I$ | [A] | current |
| $i$ | [A/m$^2$] | current density |
| $I_0$ | [A] | cell current at temperature $T_0$ |
| $i_0$ | [A/m$^2$] | exchange current density |
| $i_a$ | [A/m$^2$] | anodic (dissolution)current density |
| $i_c$ | μA/cm$^2$ | cathodic (reduction) current density |
| $i_c$ | [A/m$^2$] | cathodic current density |
| $i_L$ | [A/m$^2$] | limiting current density |
| $k$ | [-] | shape factor for the aggregate particles |
| $k$ | [sec$^{-1}$] | thermal velocity factor |
| $k_p$ | kg/m | moisture permeability coefficient |
| $L$ | [m] | length |
| $L_e$ | [m] | effective path |
| $m$ | [-] | shape factor |
| $N_A$ | $6.02 \cdot 10^{23}$ mol$^{-1}$ | Avogadro number |
| $R$ | [Ω] | electrical resistance of the section |
| $R$ | 8.315 J/K mol | gas constant |
| $R_1$ | [Ωm] | electrical resistivity at temperature $T_1$ |
| $R_2$ | [Ωm] | electrical resistivity at temperature $T_2$ |
| $RH$ | [%] | Relative Humidity (abbreviation for text) |
| $r_m$ | [m] | meniscus radius of water |
| $R_o$ | [Ωm] | electrical resistivity of the porous rock when saturated with water |

| Symbol | Unit | Description and/or definition |
|---|---|---|
| $R_w$ | [Ωm] | electrical resistivity of the water contained in the porous rock |
| $R_\Omega$ | [Ω] | electrical resistance |
| $T$ | [°C or K] | temperature |
| $t$ | [s] | time |
| $T$ | [-] | tortuosity |
| $S$ | [kg/m$^3$] | total amount of solids in the dosage: (cement + additions + aggregates) |
| $u_i$ | [m$^2$ V$^{-1}$ s$^{-1}$] | ionic mobility |
| $V_a$ | [-] | volume fraction of particles |
| $v_i$ | [m s$^{-1}$] | Ionic migration rate |
| $V_m$ | [-] | volume fraction of the matrix |
| $w_{es}$ | [%] | evaporable water |
| $W_{nf}$ | [%] | non-frozen water |
| $W_g$ | [-] | cement content factor $(1- C_{cem} /S)$ |
| $x$ | [m] | distance |
| $z$ | [-] | valence of ions |
| $\alpha$ | [-] | coefficient of temperature for the material |
| $\alpha_{cement\ paste}$ | [-] | coefficient of temperature, without aggregates in the mix |
| $\alpha_{dosage}$ | [-] | coefficient of temperature for the tested dosage |
| $\beta$ | [-] | kinetic parameter (transfer coefficient) |
| $\beta_e$ | [-] | symmetry factor |
| $\delta$ | [m] | thickness of the diffusion layer |
| $\varphi$ | [%] | Relative Humidity (for equations) |

| Symbol | Unit | Description and/or definition |
|---|---|---|
| $\sigma$ | [N/m$^2$] | tension (also surface tension) |
| $\Delta E$ | [V] | potential difference |
| $\Delta T$ | [K] | temperature difference ($T_0$ - T) |
| $\eta_c$ | [V] | cathodic overpotential |
| $\eta_L$ | [V] | overpotential for concentration polarisation |
| $\kappa$ | [$\Omega^{-1}$m$^{-1}$] | electrical conductivity |
| $\rho$ | [Ωm] | electrical resistivity ( $\rho_\Omega = R_\Omega \cdot A / l$ ) |
| $\rho_0$ | [Ωm] | electrical resistivity at a temperature of reference $T_0$ (normally 25°C) |
| $\rho_a$ | [Ωm] | electrical resistivity of the particles |
| $\rho_m$ | [Ωm] | electrical resistivity of the matrix |
| $\varphi$ | [-] | fractional volume of the water contained in the rock |

# 1

# INTRODUCTION

*This chapter gives the background and the objectives for the thesis and the experimental work. An overview of the thesis is given at the end of the chapter.*

## 1.1 Background

Concrete normally provides reinforcing steel with excellent corrosion protection. The highly alkaline environment in concrete results in the formation of a very stable passive film on the reinforcement. In addition, concrete can be proportioned to have a low permeability, reducing the risk of penetration of aggressives and increasing the electrical resistivity. High electrical resistivity impedes the flow of electrochemical corrosion currents.

The major cause of severe corrosion of steel reinforcement is penetration of chloride ions through the concrete and on to the steel. In marine environments the threshold (critical for corrosion) chloride content at the depth of the reinforcement is often reached only a few years after installation/construction.

Widespread use of de-icing salts can also reduce the service life of concrete structures on or along the roads. Chloride induced corrosion in concrete causes localised attack or so-called pitting. Corrosion of reinforcing steel in concrete may also be initiated by carbonation. $CO_2$ in the atmosphere reacts with $Ca(OH)_2$ and the *CSH* phase in concrete, thereby reducing the pH in concrete to near neutral. The intensity of the corrosion is normally much lower for corrosion due to carbonation compared to chloride induced corrosion.

The economical consequences due to corrosion of steel in concrete are substantial. The corrosion problem must be considered as one of the largest single infrastructure problems facing industrialised countries.

For steel embedded in atmospherically exposed concrete the only likely cathode reaction is reduction of dissolved oxygen given in Equation 1.1. The corresponding anodic dissolution of steel is normally written as in Equation 1.2.

$$\tfrac{1}{2} O_2 + H_2O + 2e^- \rightarrow 2OH^- \qquad \textit{(Equation 1.1)}$$

$$Fe \rightarrow Fe^{2+} + 2e^- \qquad \textit{(Equation 1.2)}$$

When iron is dissolved it reacts with oxygen and forms ferrous hydroxide, ferric hydroxide and later hydrated ferric oxide as shown in Equations 1.3, 1.4 and 1.5 respectively. This means that for both anodic and cathodic reactions, the water and oxygen content are controlling factors.

$$Fe^{2+} + 2OH^- \rightarrow Fe(OH)_2 \qquad \text{(Equation 1.3)}$$

$$4Fe(OH)_2 + O_2 + 2H_2O \rightarrow 4Fe(OH)_3 \qquad \text{(Equation 1.4)}$$

$$2Fe(OH)_3 \rightarrow Fe_2O_3 \cdot H_2O + H_2O \qquad \text{(Equation 1.5)}$$

Another significant parameter is temperature. The effect of temperature on corrosion has previously been investigated [1, 2]. These investigations, however, have focused on temperatures higher than water freezing point, and very few results on lower temperatures have been reported.

In the Nordic countries a substantial percentage of the most important infrastructure is located in areas with several months with mean temperatures lower than 0°C. Previously, it has been generally accepted that rebar corrosion will not propagate during these cold periods due to temperature control of the corrosion processes. Observations of significant current flows in cathodic protection systems, even in very low temperatures (-15°C or lower), questions the assumption of no propagation at low temperatures.

This project was initiated by The Norwegian Public Roads Administration (NPRA) as a part of a national programme "The lifecycle of concrete structures"

## 1.2 Objectives

The main objectives for the project have been to:

1. Investigate the effect of temperature on the cathodic reaction rate.
   Establish the correlation between temperature and the cathodic reaction rate and evaluate if this reaction governs the corrosion rate.

2. Investigate the effect of temperature on electrical resistivity and other electrical properties of concrete.
   Find a correlation between electrical resistivity and other electrical properties of concrete and temperature. Define effect of porosity and moisture content.

3. Estimate the effect of temperature on the corrosion rate.

## 1.3 Scope of work

Corrosion of steel is in general dependent on four elements:

1. An anode where the metal is oxidised
2. A cathode where a reduction process occurs
3. An electrical contact between the anode and the cathode
4. An ionic conduction pathway provided by an electrolyte

This thesis is built based around the four above mentioned elements. By concentrating on elements 2 and 4 it is expected to find a relation between temperature and the expected corrosion behaviour of embedded steels in concrete.

In the following paragraphs the layout of the thesis is given.

Chapter 2 defines the basic theories concerning corrosion of steel in concrete. A certain level of general understanding of corrosion is expected of the reader; hence, the detailing level of basic theories is kept to a minimum. At the end of the chapter a starting point for the experimental work is given.

Chapter 3 is a summary of the experimental work performed within the scope of this study. The different materials, experiments and equipment used are described in detail.

Chapter 4 presents the results and the associated discussion of these from the effect of temperature on the cathodic reaction rate.

Chapter 5 presents the results and associated discussion on the influence of temperature, moisture and concrete quality on the electrical resistivity of concrete. Some evaluations of the temperature influence on other electrical properties are also given.

Chapter 6 ties the observations from both chapter 4 and 5 together and estimates the effect of temperature on corrosion of steel in concrete. The obtained results are compared with results available in the literature.

Chapter 7 is the overall conclusions within the framework of the study.

# 2

# THEORETICAL BACKGROUND

*This chapter gives the theoretical background for this project. The cathodic processes and the kinetics of the cathodic reactions are reviewed along with properties affecting the electrical resistivity of concrete.*

## 2.1 Introduction and starting point for the literature review

The surface of a corroding metal contains both anodic and cathodic sites, and acts as a mixed electrode. In general, the mixed metal theory [3] states that on the anodic sites the metal atoms pass into the solution as positively charged, hydrated ions (anodic oxidation) and the excess of electrons flows through the metal to cathodic sites. To form a cathodic area, an electron acceptor, like dissolved oxygen or hydrogen ions, must be present to consume the excess electrons released by the oxidation reaction at the anodic locations (cathodic reduction).

These two reactions form an electrochemical couple and describe the metal corrosion process as a combination of an anodic oxidation, such as dissolution of iron, and a cathodic reduction, such as oxygen reduction.

The electrons released at the anodic site must be consumed elsewhere on the metal surface establishing the corrosion reaction. The process is completed by the transport of ions through the aqueous phase, leading to the formation of corrosion products at the anodic sites. These corrosion products can either be soluble (e.g. ferrous chloride) or insoluble (e.g. rust, hydrated ferric oxide) [4].

To summarise; corrosion of steel requires a complete cell established by four main elements: an anode, a cathode, an electrical connection and an electrolytic contact between the reaction sites.

To monitor the anodic reaction directly can be problematic. To measure the anodic reaction rate the electrode needs to be polarised around its corrosion potential either by an incremental polarisation change (linear polarisation) or by a short term electrical pulse (galvanostatic pulse). Such change in polarisation introduces more uncertainties and obstructs repeated measurements until the system has returned to its new equilibrium state. In addition repeated measurements of the instantaneous anodic reaction rate indicate that the anodic reaction rate may vary greatly according to Tuutti [5].

The focus of this literature review is mainly the processes occurring at the cathodic electrode and the electrical resistivity of concrete.

For further details on theoretical background for this review it is referred to the reference list [1-10].

## 2.2 Cathodic reactions in concrete

In alkaline and oxygen rich electrolytes, such as atmospherically exposed concrete, the overall corrosion reaction can be a single reduction process or a combination of reduction processes along with dissolution of iron. The most frequent cathodic reaction in atmospherically exposed concrete is reduction of oxygen [1 – 9] expressed by Equation 2.1.

*4 – electron pathway:* $O_2 + 2H_2O + 4e^- \rightarrow 4OH^-$ *(Equation 2.1)*

According to Yeager [11] this reaction may go directly (direct 4 – electron pathway) as given by Equation 2.1 or by a secondary state producing an instable super oxide (peroxide pathway), as expressed in Equation 2.2.

*Peroxide pathway:* $O_2 + H_2O + 2e^- \rightarrow HO_2^- + OH^-$ *(Equation 2.2)*

The peroxide pathway is either completed by a further reduction reaction (Equation 2.3) or a decomposition reaction (Equation 2.4):

*Reduction reaction:* $HO_2^- + H_2O + 2e^- \rightarrow 3OH^-$ *(Equation 2.3)*

*Decomposition reaction:* $2HO_2^- \rightarrow 2OH^- + O_2$ *(Equation 2.4)*

The sum of reactions for the peroxide pathway is in both cases equivalent to the sum of reactions for the direct 4 – electron pathway. The distinction of these two parallel pathways may be quite marginal. Superoxide [$(O_2^-)_{ads}$, $(HO_2)_{ads}$] and peroxide [$(O_2H^-)_{ads}$, $(H_2O_2)_{ads}$] adsorbed states may be involved in both reaction pathways but the peroxide pathway favours the adsorbed state especially when impurities are present at the electrode surface. It is therefore likely that the oxygen reduction in concrete involves superoxide and/or peroxide formation.

In more localised corrosion a combination of oxygen reduction and reduction of protons ($H^+$ - ions) and/or water may occur. In severely localised corrosion, termed "pitting" corrosion, reduction of protons will be the main contributor for the cathodic reaction due to lack of oxygen. Decreasing oxygen concentrations leads to large cathodic overpotentials and therefore favours these reactions. Proton reduction (Hydrogen gas formation) is given in Equation 2.5 and water reduction in Equation 2.6.

*Proton reduction:* $2H^+ + 2e^- \rightarrow H_2$ *(Equation 2.5)*

*Water reduction:* $2H_2O + 2e^- \rightarrow H_2 + 2OH^-$ *(Equation 2.6)*

These electrode reactions occur mainly in the low potential range (lower than -0.9 V/SCE).

Another aspect of interest is the effect of the passivating oxide and hydroxide layer generated on the electrode surface of embedded steels in concrete, commonly termed passive film.

These oxihydroxides generate due to the alkalinity of the pore water. The pore water has a pH in the range 12 – 14 dependent on the properties of the concrete mix and exposure.

Sato [12] stated that the formation of a passive film is an ongoing and self-maintaining process mainly dependent on the potential difference, ΔE, at the oxide/solution interface.

$$i_a = const \cdot \exp\left(\frac{\beta z F}{RT} \cdot \Delta E\right) \qquad \textit{(Equation 2.7)}$$

Where:

| | | |
|---|---|---|
| $i_a$ | anodic current density | [A/m$^2$] |
| *const* | constant (scaling factor) | |
| $\beta$ | kinetic parameter (transfer coefficient) | |
| $z$ | valence (number of electrons) | |
| $\Delta E$ | Potential difference on the oxide/solution interface | [V] |
| $T$ | Temperature | [K] |
| $R$ | Gas constant | 8.315 J/K mole |
| $F$ | Faraday constant | 96 485 C/mole |

Equation 2.7 is derived from the Butler Volmer Equation. The constant, *const* represents the exchange current density, but has been regarded as a constant for later mathematical manipulation. The kinetic parameter, β, represents the anodic transfer coefficient.

The anodic (dissolution) current density has been observed to be independent of the electrode potential in acidic solutions [12].

The potential difference in the oxide/solution interface is determined by the following electrochemical reaction [12]:

$$H_2O = O_{ox}^{2-} + 2H_{aq}^{+} \qquad \textit{(Equation 2.8)}$$

Hence, it is directly influenced by the pH in the solution [12]:

$$\Delta E = const + \frac{RT}{F}\ln[H^+] \qquad \textit{(Equation 2.9)}$$

Where:

| | | |
|---|---|---|
| $\Delta E$ | Potential difference on the oxide/solution interface | [V] |
| *const* | constant | |
| $[H^+]$ | concentration of hydrogen ions | |
| $T$ | Temperature | [K] |
| $R$ | Gas constant | 8.315 J/K mole |
| $F$ | Faraday constant | 96 485 C/mole |

By combining Equations 2.7 and 2.9 a linear-logarithmic correlation between the anodic dissolution current density and the pH of the solution is given [12]:

$$\log(i_a) = const - \beta z \cdot pH \qquad \textit{(Equation 2.10)}$$

Where:

| | | |
|---|---|---|
| $i_a$ | anodic current density | [A/m$^2$] |
| *const* | constant | |
| $\beta$ | kinetic parameter (transfer coefficient) | |
| $z$ | valence (number of electrons) | |

Potentiostatic experiments performed by Pruckner [13] showed that this dependency is near linear-logarithmic also in alkaline aqueous solutions (Figure 2. 1).

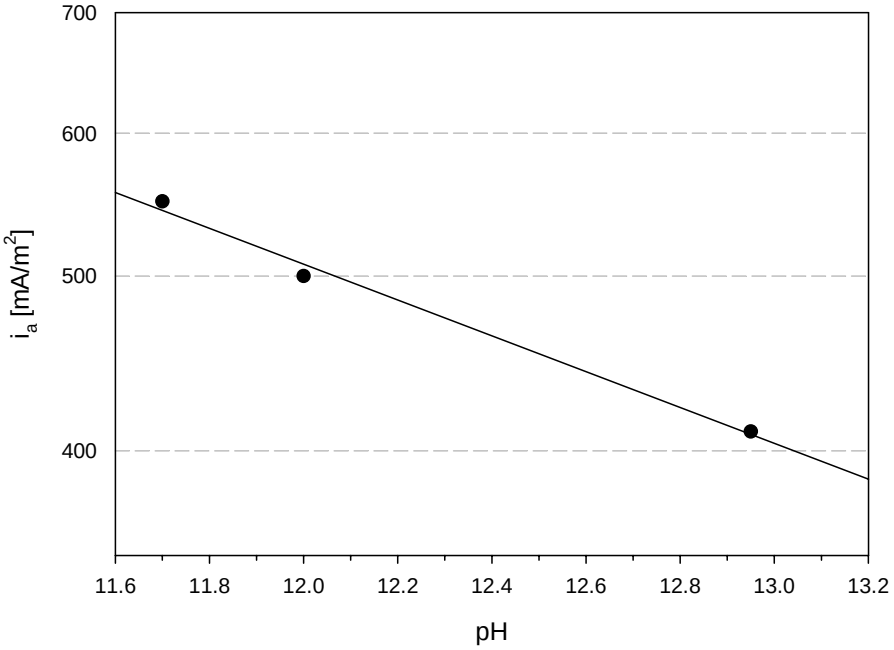


*Figure 2. 1 Dependency on the anodic dissolution current in the passive regime on pH. (Current density in logarithmic presentation). After Pruckner [13].*

The formation of a passive film is dependent upon the presence of dissolved oxygen in the pore water solution. The stability of the passive film is limited in presence of aggressive ions. Breakdown of the passive state generally occurs due to presence of chloride ions in sufficient amounts or due to decreasing pH.

Andrade, Merino, Nóvoa, Pérez and Soler [14] characterised the passive layer on iron in alkaline solutions as generally formed with a dense inner layer at the electrode surface mainly consistent of magnetite ($Fe_3O_4$), and more amorphous outer layer consisting of $\gamma$-$Fe_2O_3$ and bound water. The

two phases have nearly the same oxygen sub lattice with $Fe^{2+}$ and $Fe^{3+}$ occupying only slightly different octahedral and tetrahedral interstices.

Stratmann, Bohnenkamp and Engell [15] stated that the oxidation of $Fe_3O_4$ to $\gamma$-$Fe_2O_3$ is a reversible process.

$$3Fe_3O_4 \rightleftharpoons 4\gamma \cdot Fe_2O_3 + Fe^{2+} + 2e^- \qquad \textit{(Equation 2.11)}$$

The bound water molecules in combination with the polymer like frame of $\gamma$-$Fe_2O_3$ form a physical barrier for diffusion of iron ions. Due high conductivity the reduction processes at the oxide/solution interface is maintained by a very low anodic dissolution current density.

How these oxides and hydroxides interact in the total cathodic reaction when polarised is not clear in the reviewed literature. However, it is probable since the oxidation of $Fe_3O_4$ to $\gamma$-$Fe_2O_3$ is a reversible process, that some conversion of oxides will take place under polarised conditions and act in the total reaction.

Recent research performed by Vennesland [16] shows that heavy polarised steel (chloride extraction) in concrete gained thickness of the oxide layer as a result of the polarisation. These observations support the theory of interaction in the total cathodic reaction.

## 2.3 Factors controlling the cathodic reaction rate

### 2.3.1 Cathodic polarisation and reaction kinetics

How much the electrode is polarised is related to its overpotential, η (the driving force). Increased cathodic overpotential, $\eta_c$, results in an increase in cathodic reaction rate. This is measured as an increase in current density on the electrode. If there is plentiful supply of reactants (e.g. dissolved oxygen) then the relationship between current density and the overpotential can be described by the Butler-Volmer Equation [3]:

$$i_c = i_0 \left[ e^{\frac{-\beta F}{RT}\eta_c} \right] \qquad \textit{(Equation 2.12)}$$

Where:

| | | |
|---|---|---|
| $i_c$ | cathodic current density | [A/m$^2$] |
| $i_0$ | exchange current density | [A/m$^2$] |
| $\beta$ | transfer coefficient | |
| $\eta_c$ | cathodic overpotential | [V] |
| $T$ | Temperature | [K] |
| $R$ | Gas constant | 8.315 J/K mole |
| $F$ | Faraday constant | 96 485 C/mole |

For equation 2.12 to be valid the overpotential must be sufficiently negative (numerically greater than ($RT/\beta_e F$)). If it is assumed that the energy barrier at the electrode surface is symmetrical ($\beta_e = 0.5$) then the

overpotential has to be numerical greater than -50 mV at room temperature (293 K).

Funahishi and Young [17] listed the major steps involved in cathodic polarisation of steel in concrete (seen in context of cathodic protection):

1. The supply of oxygen is ensured by oxygen dissolving into the concrete pore solution from the surrounding atmosphere.

2. Oxygen is transferred by diffusion through the concrete pore solution from the concrete surface towards the reaction sites of the concrete
3. Oxygen reaches the adjacent areas of the cathodic electrode

4. The reaction on the cathodic electrode is one or both of the following:

    a. Oxygen is reduced at the cathodes existing on the steel, and hydroxide ions are produced given that the steel potential is more positive than the hydrogen equilibrium potential

    b. The anodic sites on the cathodic polarised steel (mixed metal electrode) decrease due to the supply of electrons

5. The hydroxide ions that are generated by oxygen reduction are transported away from the steel interface by diffusion and the electrostatic field generated by the cathodic protection system.

When the rate of the cathodic reaction is controlled by steps 4a and 4b, the cathodic polarisation is controlled by activation polarisation. However, if the rate of the reaction is limited by mass transport (steps 1-3 and step 5) the cathodic reaction rate is controlled by concentration polarisation.

When the current density approaches a limiting value ($i_L$) this can be caused by either one or a combination of inhibited transport of dissolved oxygen to the electrode surface and limited transport of hydroxide from the electrode surface. This is a situation referred to as concentration polarisation. The magnitude of $i_L$ will then depend on environmental factors such as temperature.
An Evans diagram illustrating concentration polarisation is given in Figure 2. 2.

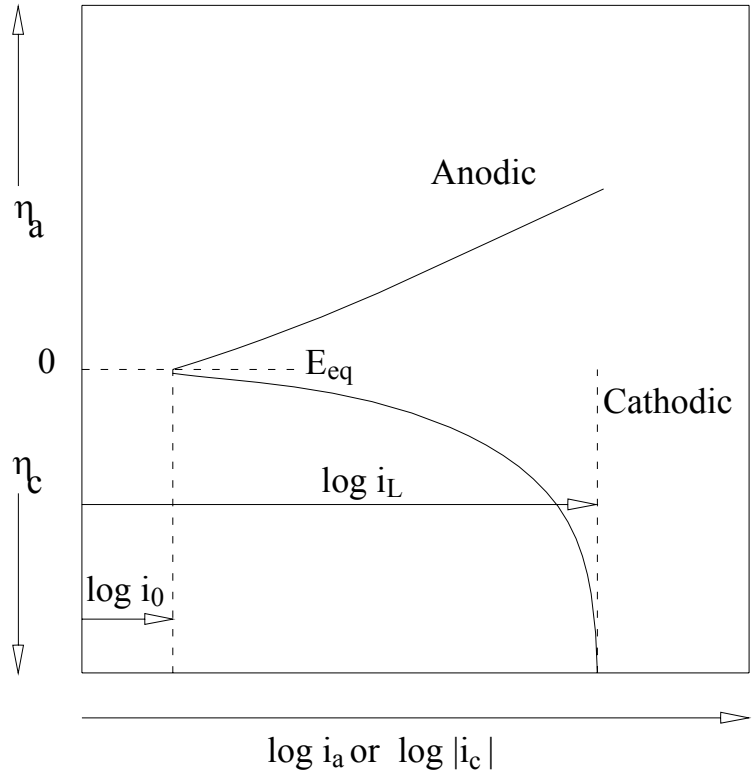


*Figure 2. 2 Polarisation curve for an electrode process such as oxygen reduction under concentration polarisation. Based on Page [4].*

The $O_2$ – concentration in the pore liquid affects both the driving force (the overpotential) and the activity. By decreasing the $O_2$ concentration the absolute value of the potential will increase, but the activity (current density) will decrease.

An example showing the effect of oxygen concentration on value of $E_{corr}$ for passive steel in concrete is given in Figure 2. 3.

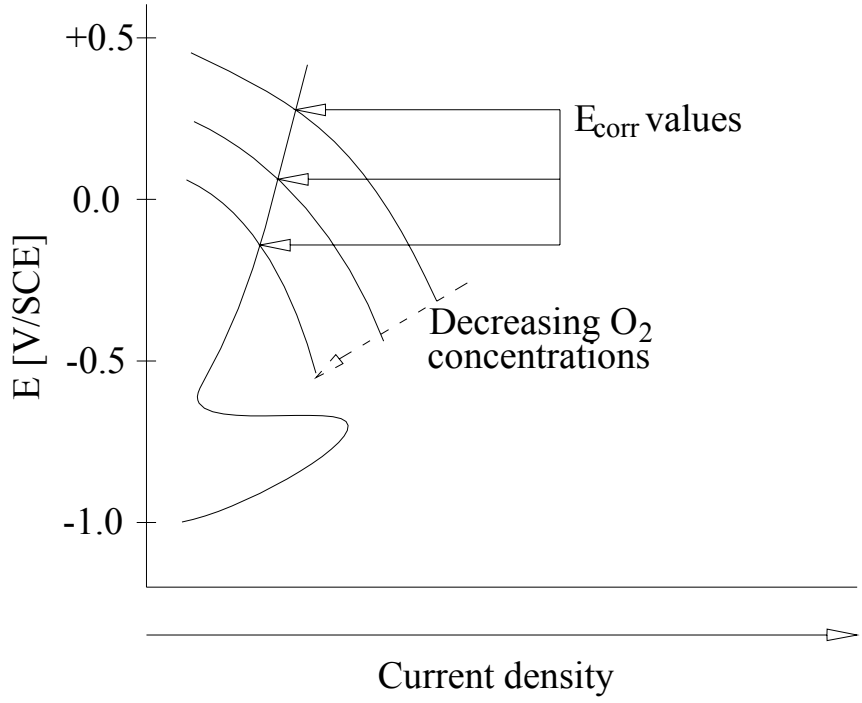


*Figure 2. 3 Evans Diagram showing the effect of oxygen concentration on the value of $E_{corr}$ of passive steel rebar. Based on Page [4].*

From Figure 2. 3 it is indicated that the cathodic polarisation curves will change by decreasing oxygen concentrations and that the equilibrium potentials of the electrode also will decrease by decreasing $O_2$ – concentrations.

The theory behind concentration polarisation in the Nernst diffusion layer gives a relationship between overpotential and current density involving concentration polarisation for a cathodic reaction at 25°C [3]:

$$\eta_L = \frac{0.059}{z \cdot \log\left(i_L - \frac{i}{i_L}\right)} \qquad \textit{(Equation 2.13)}$$

Where:

| | | |
|---|---|---|
| $\eta_L$ | overpotential for concentration polarisation | [V] |
| $z$ | valence (number of electrons) | |
| $i$ | Current density | [A/m$^2$] |
| $i_L$ | limiting current density | [A/m$^2$] |

Equation 2.13 has its origin in Nernst Equation where the concentration is replaced by the current density generated by the concentration gradient [3].

The limiting current density can be calculated as follows (for oxygen reduction) according to Bockris et al. [3]:

$$i_L = -4F \cdot D_{ox} \cdot \left( \frac{C}{\delta} \right) \qquad \textit{(Equation 2.14)}$$

Where:

| | | |
|---|---|---|
| $i_L$ | limiting current density | [A/m$^2$] |
| $F$ | Faraday constant | 96 485 C/mole |
| $D_{ox}$ | oxygen diffusion coefficient | [m$^2$/sec] |
| $C$ | oxygen concentration in the pore solution | [kg/m$^3$] |
| $\delta$ | thickness of the diffusion layer | [m] |

Equation 2.14 is derived from Fick's first law of diffusion.

By Equations 2.13 and 2.14 it is possible to calculate the limiting current density and the corresponding overpotential; however, the practical value of such calculations is minimal. In practice, the rate of the cathodic reaction could partially be controlled by mass transfer (bulk diffusion of oxygen) and partially by kinetics of the anodic reaction (mixed metal electrode). In addition oxides on the surface of the electrode may inhibit the oxygen diffusion (through the oxide layer) to the electrode surface.

Funahishi and Young [17] stated that the limiting current density and the corresponding overpotential would be difficult to estimate due to several influencing parameters.

Jäggi, Elsener and Böhni [18] stated that from the open circuit potential until the diffusion limiting current occurs the kinetics of the cathodic oxygen reduction is mainly controlled by charge transfer. This region is often termed: Tafel region. In this region the current potential correlation is linear – logarithmic. The ideal Tafel gradient for oxygen reduction (on platinum without diffusion) is -0.12 V/decade [3].

However, polarisation curves recorded in an electrochemical flow cell by Jäggi, Elsener and Böhni [18] indicated that the Tafel gradient may change presumably not affected by diffusion phenomena. They reported Tafel gradients in the range from -0.222 to -0.239 V/decade dependent on the temperature ranging from 5 to 47°C. The Tafel gradients showed no uniform change by temperature, found from their published results.

The same authors found that the age of the passive film (and presumably the thickness of it) inhibits oxygen reduction compared to oxygen reduction on platinum. This inhibition increased with prolonged age of the passive film.

### 2.3.2 Temperature effect on the cathodic reaction rate

The effect of temperature on systems dependent upon the presence of oxygen is complicated since there are two conflicting factors:

Factor 1: Most aqueous solutions are in contact with the atmosphere and contain oxygen. The saturated solubility of oxygen in pure water at 25°C is only about $10^{-3}$ mol/dm$^3$ and the solubility decreases significantly by increasing temperature according to Funahishi and Young [17]. The relationship between temperature and the solubility of oxygen in pure water in the temperature range 0°C – 80°C is shown in Figure 2.4.

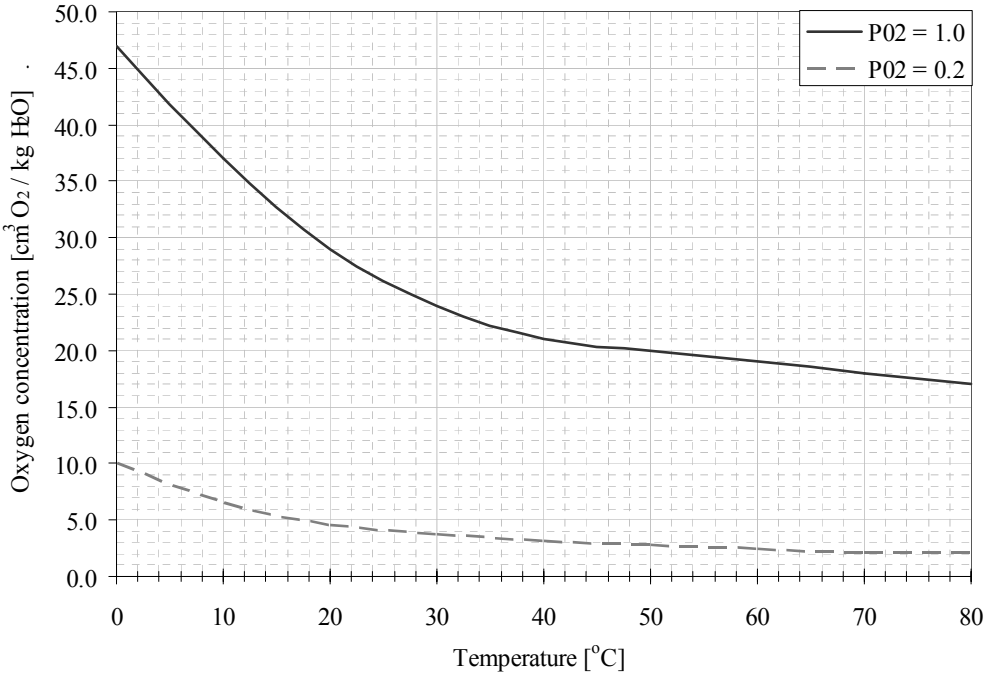


*Figure 2. 4 The solubility of oxygen in water for 1 atm and 0.2 atm pressures of oxygen. After Funahishi and Young [17].*

Factor 2: Oxygen diffusion in concrete increases by increasing temperature according to Vennesland [20]. The temperature related increase of the transport of oxygen may compensate for the reduced solubility of oxygen in water.

In addition to the oxygen availability the chemical reduction reaction itself has a temperature dependency. In 1889 S.A Arrhenius found that a change in temperature changes the rate of a chemical reaction exponentially [3]:

$$k = A \cdot e^{\left(-\frac{E_a}{RT}\right)} \qquad \textit{(Equation 2.15)}$$

Where:

| | | |
|---|---|---|
| $k$ | thermal velocity factor | [$sec^{-1}$] |
| $A$ | constant | [$sec^{-1}$] |
| $E_a$ | activation energy | [kJ/mole] |
| $R$ | Gas constant | 8.315 J/K mole |
| $T$ | Temperature | [K] |

At higher temperatures, the probability that two molecules will collide is higher. This higher collision rate results in a higher kinetic energy, which has an effect on the activation energy of the reaction. The activation energy is the amount of energy required to ensure that a reaction happens.

The quantity of the activation energy for a given reaction expresses temperature dependency (or sensitivity) for the reaction.
The temperature sensitivity of many chemical reactions can be explained by the Arrhenius equation; however, it cannot be regarded as a universal law.

For an electrochemical process such as oxygen reduction the temperature influence on the resulting current would then be [19]:

$$I = I_0 \cdot e^{-\left(a\left[\frac{1}{T}-\frac{1}{T_0}\right]\right)} \qquad \textit{(Equation 2.16)}$$

Where:

| | | |
|---|---|---|
| $I$ | cell current at temperature T | [A] |
| $I_0$ | cell current at temperature $T_0$ | [A] |
| $a$ | activation energy constant | [K] |
| $T / T_0$ | Temperature | [K] |

The activation energy constant, $a$, is equal to ($E_a$/R) in the Arrhenius equation (Equation 2.15).

The cathodic oxygen reduction and especially its temperature dependency have not been studied extensively. However, Jäggi, Böhni and Elsener [19] showed that the activation energy constant, $a$ (according to Equation 2.16), for oxygen reduction is in the range of 4310 K in simulated pore

solution (pH 13.5) and slightly lower in mortar (4250 K). The anodic and cathodic partial reactions temperature dependency was shown to be similar to that of the overall macrocell current.
By numerical modelling of the macrocell current with the polarisation curve of the anodic and cathodic partial reactions along with the mortar resistivity, Jäggi, Böhni and Elsener [19] achieved to calculate the temperature influence on the macrocell current. These numerical calculations were in good agreement with their experimental research. The experiments were performed in the temperature range of 0°C to +50°C.

Vennesland [20] investigated the effect of temperature on the oxygen transport through submerged concrete by stationary polarisation. He found an increase in current density from 0.5 $mA/m^2$ to 1.2 $mA/m^2$ for an increase of temperature from 1°C to 30°C. If it is assumed that this increase follows Arrhenius, then the increase would correspond to an activation energy constant of about 2500K calculated from Equation 2.16.

Vennesland [20] further found that the activation energy for the diffusion constants for oxygen in concrete in the same temperature interval was 15kJ/mole. This corresponds to an activation energy constant of approximately 1800K. He concludes that temperature has a substantial effect on the oxygen reduction at steel embedded in concrete.

The activation energy constant for diffusion of oxygen for oxygen was found to be lower than that of the oxygen reduction process. This observation may be an indicator of that the diffusion of oxygen is less temperature dependent than the reduction process. It is then probable that

the availability of reactants (dissolved oxygen) would not impair the reaction at lower temperature. Since oxygen diffusion has not been studied at temperatures below 0°C no direct conclusion can be taken from the available literature.

Elsener, Flükiger, Woytas and Böhni [21] reported on-site measurements in a temperature range from -10°C to 18°C. In this range they observed an increase in macrocell current density from 5.5 $mA/m^2$ to 22 $mA/m^2$ corresponding to an activation energy constant of 3789K.

Raupach [22] states that the influence of temperature on the corrosion rate can not be generally described by an activation energy constant due to its dependency of several other parameters. Especially, it is very dependent on the degree of water saturation.

The found activation energy constants found in the literature give little basis to conclude on an appropriate level of activation energy constants. It is, however, clear that the cathodic reaction rate and related phenomena show a temperature dependency and that the activation energy constant is in the range 2500K – 5000K. This quite extensive range of activation energy constants indicates that the reaction is not only the influencing parameter, substantiating the statement of Raupach [22].

### 2.3.3 Influence of the moisture condition of concrete on the cathodic reaction rate

The moisture content of concrete defines the amount of pores that contains water, either totally water filled or as adsorbed layers on the pore walls. The amount of pores which contains water strongly influence the concretes overall ability to transport charged particles. In order for oxygen reduction to occur, water has to be present both on the cathodic electrode surface and also interconnected with the corresponding anode. The continuity of these wet pores will influence the rate of the reaction.

Andrade, Alonso and Garcia [23] stated that the moisture level appeared to have the dominant effect on the rebar corrosion process. They state that with ideal conditions for oxygen availability at the electrode surface the reaction could be inhibited by the amount of active surface. It appears as the moisture contents could be correlated to the part of the pores giving the contact to the electrodes (reaction sites). At a critical low moisture content the electrode connection is dried out, and no reaction is possible.

Due to these dry spaces the amount of active electrode surface will decrease, a process that is found as a decrease in the overall reaction current, although the premises for oxygen availability improves. Normally, the reaction rates are related to the full surface of the exposed steel, while in some cases the actual active surface may be very much smaller.

Andrade, Alonso and Garcia [23] illustrated this by four cases of humidity and the corresponding active surface for reaction. Since their investigations mainly were performed with eyes to the correlation between oxygen availability and the corrosion rate of steel in concrete their conclusions are not directly transferable to cathodic reaction rate. However, the amount of surface available for the cathodic reaction to proceed is clearly a rate determining step for the cathodic reaction.

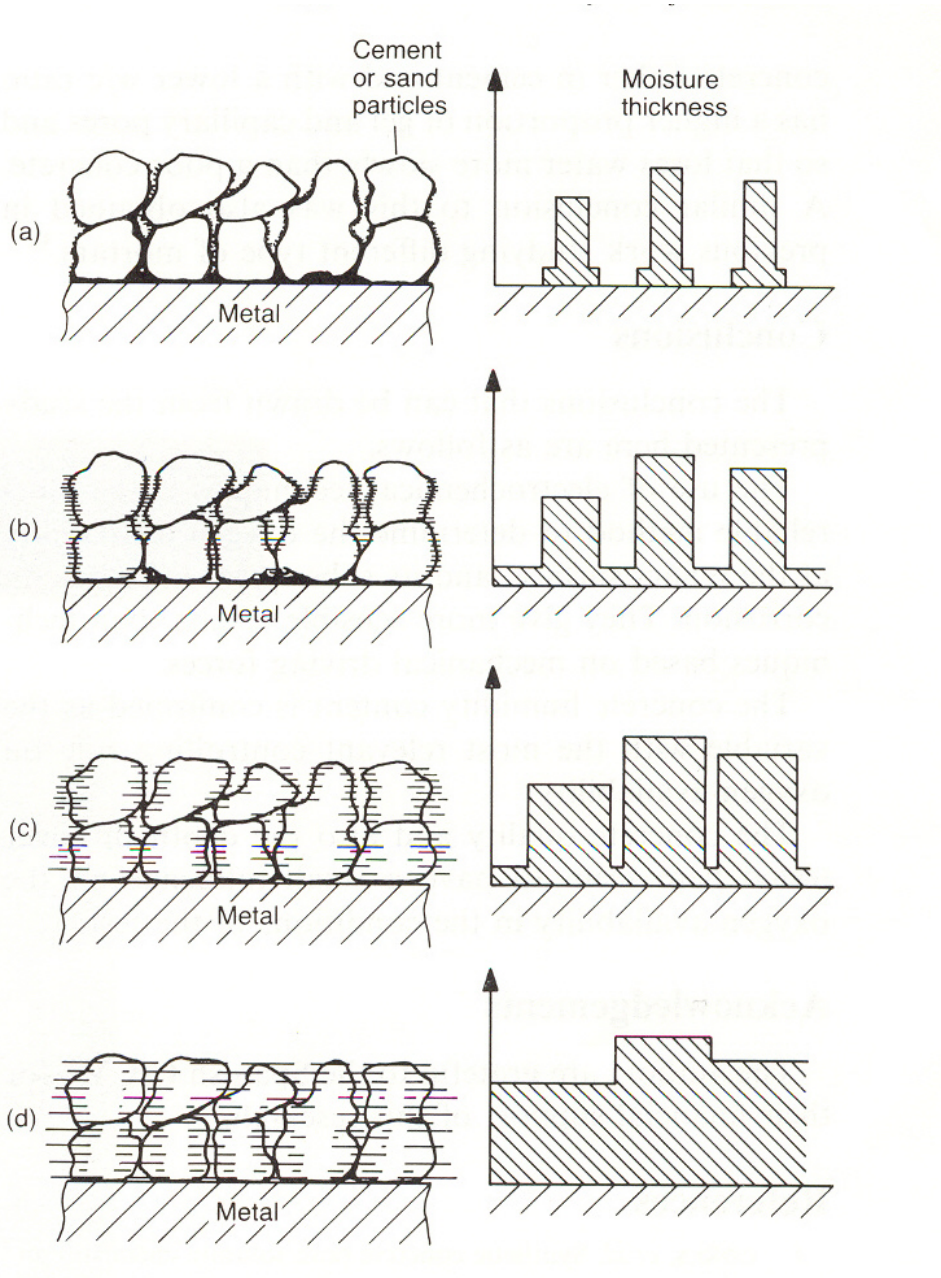


*Figure 2. 5 Scheme of the moisture content evolution in concrete pores, a) low humidity, b) medium humidity, c) high humidity and d) saturated conditions. After Andrade, Alonso and Garcia [23].*

Funahishi and Young [17] found that in highly dried concrete (dried for 72 hours at 50°C) the cathodic reaction process appeared to be controlled by

the diffusion of hydroxide ions produced on the steel surface because of the thin electrolyte existing on the steel surface. Furthermore, they found that the polarisation behaviour in wet concrete is completely different from that of steel in simulated pore solution.

Raupach [24], however, stated different results than Funahishi and Young [17] in his investigations. Here it is stated that the effect of wetting could be separated in four different cases.

1. *"Permanently dry conditions (RH less than 100% and no further wetting) lead to that the $O_2$ – diffusion was not significant. The cathodic and anodic polarisation resistances control the reaction rate."*

2. *"Short-term water application (wetting by spray, fog, splashed water or in natural form of a rain shower) did not lead to oxygen deprivation at the steel surface".* In this case he found that the change in the conductivity of the concrete cover lead to changes in the reaction rate.

3. *"Long-term water application (wetting in such a manner that the reinforcement is in totally saturated concrete) lead to oxygen deprivation at the steel surface and lead to a considerable decrease in cathodic reaction rate."*

4. *"Permanently water saturated (total water saturation of the entire probe/structural part etc.) lead to control of the cathodic reaction rate by diffusion of oxygen to the electrode surface."*

Since these investigations are not directly comparable it is difficult to draw any conclusion on the effect of moisture state on the cathodic reaction rate other than for totally saturated conditions where oxygen diffusion seems to dominate the reaction rate; and that the active reaction surface of the electrode must be dependent upon the amount of water present in the pores.

The extremes (saturated and extremely dry) appear to be relatively well defined, however, on intermediate and more relevant moisture contents the information in the reviewed literature is scarce.

### 2.3.4 Influence of the concrete properties on the cathodic reaction rate

The concrete properties are important for the cathodic reaction rate by means of availability of oxygen at the electrodes and removal of hydroxide from the electrode. Both these processes are assumed to be dominated by diffusion.

Previously, diffusion has been discussed in terms of electrochemistry, i.e. how the species move in the diffusion layer surrounding the electrodes. The bulk concrete itself has different properties for transport of species and these are most likely related to the moisture conditions in concrete as much as the layout of the pore system.

The transport of gases, water or ionised aqueous solutions in concrete takes place through pore spaces in the cement paste matrix or in micro cracks. A variety of different physical and/or chemical mechanisms may occur simultaneously. Considering the variations in pore sizes, pore filling and temperature, it is likely that the transport of media through concrete is not dominated by a single mechanism according to [26].

An experimental investigation of the transport characteristics of a given concrete is therefore limited to measured effective values. It is impossible to elude secondary mechanisms occurring. The flow of media must be considered as one single dominating mechanism in a model in order to interpret the obtained values. Despite the fact that possibly a large part of the transport is due to coterminous transport processes.

It is probable that the concrete properties are determining the transport conditions in concrete. However, it has not been found any direct information on how the physical properties of concrete affect the cathodic reaction rate directly. It is supposed that since the layout of the concrete pore system is very important for the transport mechanisms it is also very important for the availability of oxygen at the cathodic electrode as well as it is important for the removal of hydroxide ions from the cathodic electrode.

The electrolytic contact between the anodic- and the cathodic electrode is vital for the overall reaction rate of the corrosion reaction as stated in Chapter 1.

Since the information available on the effect of concrete properties on the cathodic reaction especially it is referred to section 2.6 where these properties are discussed in terms of effect on electrical resistivity. The same parameters that affect the electrical resistivity are assumed to have a reversed effect on the cathodic reaction rate.

## 2.4 Electrical resistivity of concrete

The electrical resistivity is defined by Esbach and Souders [27] as the electrical resistance of a conductor of unit volume and constant cross section in which the current is continuously and uniformly distributed.

It can be viewed more simply as the electrical resistance between two opposing faces of unit cube of material. This is the volume resistivity, and if some current leaks along the surface of conductor, then a surface resistivity factor must be taken into account according to Harper [28]. The electrical resistivity, ρ, can be found by:

$$\rho = \frac{R \cdot A}{L} \qquad \textit{(Equation 2.17)}$$

Where:

| | | |
|---|---|---|
| $\rho$ | electrical resistivity | [Ωm] |
| $R$ | electrical resistance of the section | [Ω] |
| $A$ | area defined by the opposing electrodes | [$m^2$] |
| $L$ | distance between the electrodes | [m] |

The electrodes have to be identically sized. The distance between the electrodes, $L$, should ideally be as small as possible to ensure linear current distribution.

In Figure 2. 6 an illustration of a unit cube for measuring the electrical resistivity is given. In a cube where all sides are equal (and 1), the measured $R$ is equal to $\rho$.

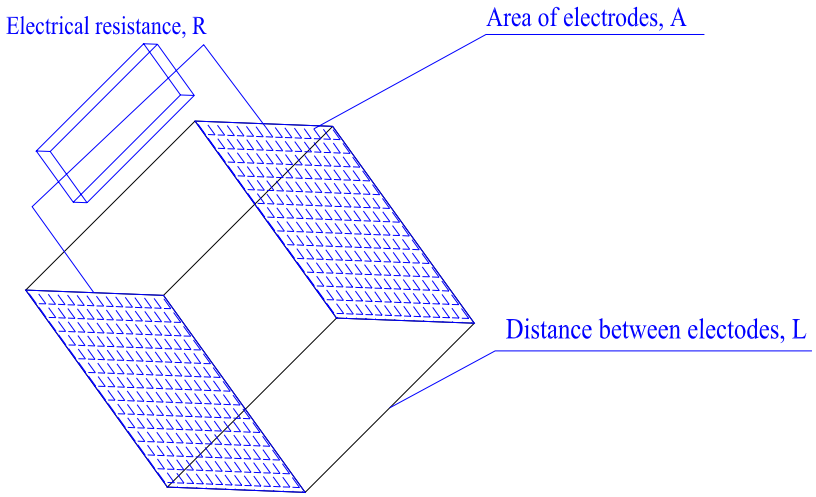


*Figure 2. 6 A principal illustration of a unit cube for resistivity measurements*

The range of the electrical resistivity of a porous material such as concrete depends very much on its moisture state. A very wet concrete may act as a semi – conductor ($\rho \approx 10^1$ Ωm) while an oven dried concrete may act more or less as an insulator ($\rho > 10^6$ Ωm) according to Whiting and Nagi [29]. The effect of moisture on the electrical resistivity will be discussed in section 2.6.

Concrete is a composite material, containing several components which electrical properties varies and the ideal theory of uniformly and continuously distributed current can not be used directly.

### 2.4.1 Ionic mobility, ionic strength and the electrical resistivity of solutions

Measurements of the electrical resistance of an electrolyte are performed by applying a voltage between two electrodes. This voltage results in an electrical field, *E*; in the solution that causes forces to the ions in the solution. The positive ions (cations) will migrate towards the negative electrode and the negative ions (anions) migrate towards the positive electrode. The rate of the movement of ions (ionic migration rate) is proportional to the electrical field by [21]:

$$v_i = u_i \cdot |z_i| \cdot E \qquad \textit{(Equation 2.18)}$$

Where:

| | | |
|---|---|---|
| $v_i$ | Ionic migration rate | [m $s^{-1}$] |
| $\|z_i\|$ | valence of ions | [-] |
| $u_i$ | ionic mobility | [$m^2$ $V^{-1}$ $s^{-1}$] |
| $E$ | strength of the electrical field | [V $m^{-1}$] |

The total current generated by the mass transport (the migration) is proportional to the strength of the field and the charge of the ion transport.

$$I = F \cdot A \cdot E \cdot \sum c_i \cdot u_i \cdot |z_i| \qquad \textit{(Equation 2.19)}$$

Where:

| | | |
|---|---|---|
| $I$ | total current through the cross section | [A] |
| $F$ | Faradays constant (96 487) | [A s mole$^{-1}$] |
| $A$ | cross sectional area | [m$^2$] |
| $E$ | strength of the electrical field | [V m$^{-1}$] |
| $c_i$ | concentration of ions | [mole m$^{-3}$] |
| $\|z_i\|$ | valence of ions | [-] |
| $u_i$ | ionic mobility | [m$^2$ V$^{-1}$ s$^{-1}$] |

The conductivity (i.e. the reciprocal of the electrical resistivity) of the solution will be:

$$\kappa\left(=\frac{1}{\rho}\right) = F \cdot \sum c_i \cdot u_i \cdot |z_i| \qquad \textit{(Equation 2.20)}$$

Where:

| | | |
|---|---|---|
| $\kappa$ | electrical conductivity | [$\Omega^{-1}$m$^{-1}$] |
| $\rho$ | electrical resistivity | [$\Omega$m] |
| $F$ | Faradays constant (96 487) | [A s mole$^{-1}$] |
| $c_i$ | concentration of ions | [mole m$^{-3}$] |
| $\|z_i\|$ | valence of ions | [-] |
| $u_i$ | ionic mobility | [m$^2$ V$^{-1}$ s$^{-1}$] |

A relation between the diffusion coefficient and the ionic mobility can be found as:

$$D_i = \frac{RT \cdot u_i}{|z_i| \cdot F} \qquad \textit{(Equation 2.21)}$$

Where:

| | | |
|---|---|---|
| $D_i$ | diffusion coefficient | [$m^2$ $sec^{-1}$] |
| $R$ | Gas constant | 8.315 J/K mole |
| $T$ | Temperature | [K] |
| $F$ | Faradays constant (96 487) | [A s $mole^{-1}$] |
| $\|z_i\|$ | valence of ions | [-] |
| $u_i$ | ionic mobility | [$m^2$ $V^{-1}$ $s^{-1}$] |

To estimate the individual contributions of the various species and their concentrations to the overall electrical conductivity of the solutions appears to be of little practical value. The electrical resistivity of pore solution normally is about 0.1 Ωm, while concrete resistivity seldom is less than 20 Ωm. Considering the big difference between the resistivity of the conductive solution and the composite as a whole, a small change in the electrolytic resistivity of the pore liquids is assumed to be of minor importance.

### 2.4.2 Concrete electrical resistivity theories

A variety of theories and models have been developed to explain the electrical resistivity of concrete. These models can be divided in two categories.

1. Composite materials theories. These theories attempt to predict resistivity as a function of the resistivity of each component of the composite and their volume and/or size factors.

2. Empirical models. By fitting experimental results to simple equations, coefficients for particular materials can be established.

Composite Materials Theories

Maxwell [30] was one of the first to attempt to explain electrical properties of composite materials in the 19$^{th}$ century. Originally, his attempts were derived in terms of conductivity. The Maxwell relationship can be shown in terms of electrical resistivity as shown in Equation 2.27.

$$\frac{\frac{\rho_m}{\rho}-1}{\frac{\rho_m}{\rho}+2}=V_a\frac{\frac{\rho_m}{\rho_a}-1}{\frac{\rho_m}{\rho_a}+2} \qquad \textit{(Equation 2.22)}$$

Where:

| | | |
|---|---|---|
| $\rho_m$ | electrical resistivity of the matrix | [Ωm] |
| $\rho$ | electrical resistivity of the composite | [Ωm] |
| $\rho_a$ | electrical resistivity of the particles | [Ωm] |
| $V_a$ | volume fraction of particles | [-] |

Aggregate resistivities may vary greatly [31] due to water adsorption, however, most concrete specifications limit sources to generally hard, low-adsorption aggregates.

Most of these aggregates have resistivities larger than $10^3$ Ωm, while the resistivity of the matrix is several orders of magnitude lower [32, 34, 35]. For practical applications the aggregate resistivity can be considered as infinite.

If $V_a$ is expressed as $1\text{-}V_m$, then the Maxwell relationship reduces to:

$$\rho = \rho_m \frac{3 - V_m}{2V_m} \qquad \textit{(Equation 2.23)}$$

Where:

| | | |
|---|---|---|
| $\rho_m$ | electrical resistivity of the matrix | [Ωm] |
| $\rho$ | electrical resistivity of the composite | [Ωm] |
| $V_m$ | volume fraction of the matrix | [-] |

Maxwell assumed that the particles were spherical and that the fractional volume of aggregate is so small that there are no interactions among the flowlines of current around the particles.

Fricke [33] deduced a similar equation for uniform ellipsoidal particles (the particles are still assumed non-conductive):

$$\rho = \rho_m \frac{(1+k) - V_m}{k \cdot V_m} \qquad \textit{(Equation 2.24)}$$

Where:

| | | |
|---|---|---|
| $\rho_m$ | electrical resistivity of the matrix | [Ωm] |
| $\rho$ | electrical resistivity of the composite | [Ωm] |
| $k$ | shape factor for the aggregate particles | [-] |
| $V_m$ | volume fraction of the matrix | [-] |

In Equation 2.18, Fricke introduced a shape factor, $k$, to describe the shape of the ellipsoids. For spherical particles, $k = 2$, and for a particular sand investigated by Fricke, $k = 1.4$ was found.

The resistivity of a composite consisting of non-conductive particles embedded in a conductive matrix may also be expresses in terms of an effective path, $L_e$. Since the current must travel a tortuous path because of obstructing particles, the effective path is longer than the dimension of the composite in the direction of the current [32].

Noting that the cross-sectional area of the matrix in a unit-cube is numerically equal to $V_m$, the resistivity of the composite may be written according to Monfore [32]:

$$\rho = \frac{\rho_m L_e}{V_m} \qquad \textit{(Equation 2.25)}$$

Where:

| | | |
|---|---|---|
| $\rho_m$ | electrical resistivity of the matrix | [Ωm] |
| $\rho$ | electrical resistivity of the composite | [Ωm] |
| $L_e$ | effective path | [m] |
| $V_m$ | volume fraction of the matrix | [-] |

Tortuosity, $T$, a term frequently used to describe the structure of rocks is related to the effective path, by Equation 2.31 [32]:

$$T = \left( \frac{L_e}{L} \right)^2 \qquad \textit{(Equation 2.26)}$$

Where:

| | | |
|---|---|---|
| $T$ | tortuosity | [-] |
| $L_e$ | effective path | [m] |
| $L$ | apparent path length | [m] |

*L* is the apparent path length, i.e. the actual dimension of the composite in the direction of the current flow.

Since the volume fraction of aggregates in concrete often exceeds 70% Maxwell's assumption of no interaction in current field from aggregates clearly is not a valid assumption.

Whittington et al [34] states that these theories would probably represent quite well the results for mortars since a mortar may be regarded as a single-size particle system in a conductive cement paste matrix. Monfore [32] did such experiments on mortars and found a fairly good agreement between his experimental results and the predictions from the models. For concrete, however, these models probably would fail due to the presence of various particle sizes present in the conductive cement paste matrix.

Empirical models – Formation factor approach

In studies of porous rock in oil-bearing reservoirs, Archie [36] found a relationship between the resistivity of the saturated rock and the resistivity of the fluid with which it was saturated. This ratio is termed the formation factor, *F*, in the relation known as Archie's law:

$$F = \frac{R_o}{R_w} = \varphi^{-m} \qquad \textit{(Equation 2.27)}$$

Where:

| | | |
|---|---|---|
| $F$ | Formation factor | [-] |
| $R_o$ | electrical resistivity of the porous rock when saturated with water | [Ωm] |
| $R_w$ | electrical resistivity of the water contained in the porous rock | [Ωm] |
| $\varphi$ | fractional volume of the water contained in the rock | [-] |
| $m$ | shape factor | [-] |

This equation is purely empirical, and is not substantiated in any physical models.

Archie's law were later generalised [37, 38]:

$$F = A \cdot \varphi^{-m} \qquad \textit{(Equation 2.28)}$$

where $F$ and $\varphi$ are as defined in Equation 2.32 and $A$ is an additional dimensionless constant.

Whittington et al. [34] applied Archie's law for concrete, defining $F$ as the ratio of the measured resistivity of the concrete to the resistivity of the cement paste and $\varphi$ as the volume fraction of cement paste in the concrete. By performing experiments on moist cured samples of relatively high w/b ratios concretes (w/b 0.6 and 0.8) Whittington et al. [34] found the values of the constants to be $A = 1.04$ and $m = 1.2$ for concrete.

In investigations by Jackson [38] and Morrely and Ford [39] the constant $A$ was in most cases fairly constant and close to 1 while $m$ varies with the particular mixture characteristics.

## 2.5 Relationship between corrosion rate of embedded reinforcements and electrical resistivity of concrete

The level of resistivity needed to prevent corrosion has been examined in various studies, with varying results. Most studies confirm that a resistance of 50 Ωm or lower will very likely result in corrosion occurring according to Elkey and Sellevold [40]. The level of resistivity for adequate protection against corrosion is more clouded. Several studies states that adequate protection is achieved at resistivity levels higher than 100 Ωm. While others suggest values up to 600 Ωm.

Berke et al. [41, 42] discovered two specimens with severe corrosion at resistivity levels of 430 Ωm and 730 Ωm, respectively. To define a level of adequate protection against corrosion is not easy, and a wider range must be considered. A suggestion for protection limit could be 1000 Ωm, but this has to be confirmed by a large statistical study according to Elkey and Sellevold [40].

The relationship between corrosion current and electrical resistance is given in Figure 2.8 after Cabrera et al. [43]

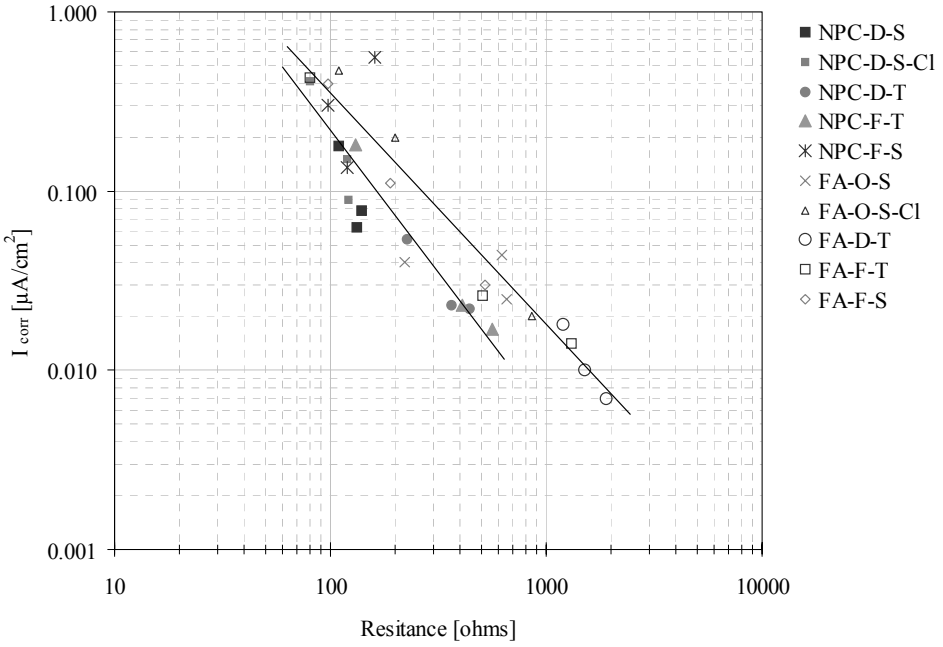


*Figure 2. 7 Relation between corrosion current and resistance. After Cabrera et al. [43]*

Andrade and Alonso [1] presented the relationship between the corrosion rate and the electrical resistivity for both laboratory measurements on mortar specimens (Figure 2.9) and measurements performed on real concrete structures (Figure 2.10). For both cases the results show a scatter, however, indicating a critical resistivity of about 1000 Ωm for corrosion confirming the above suggested protection limit.

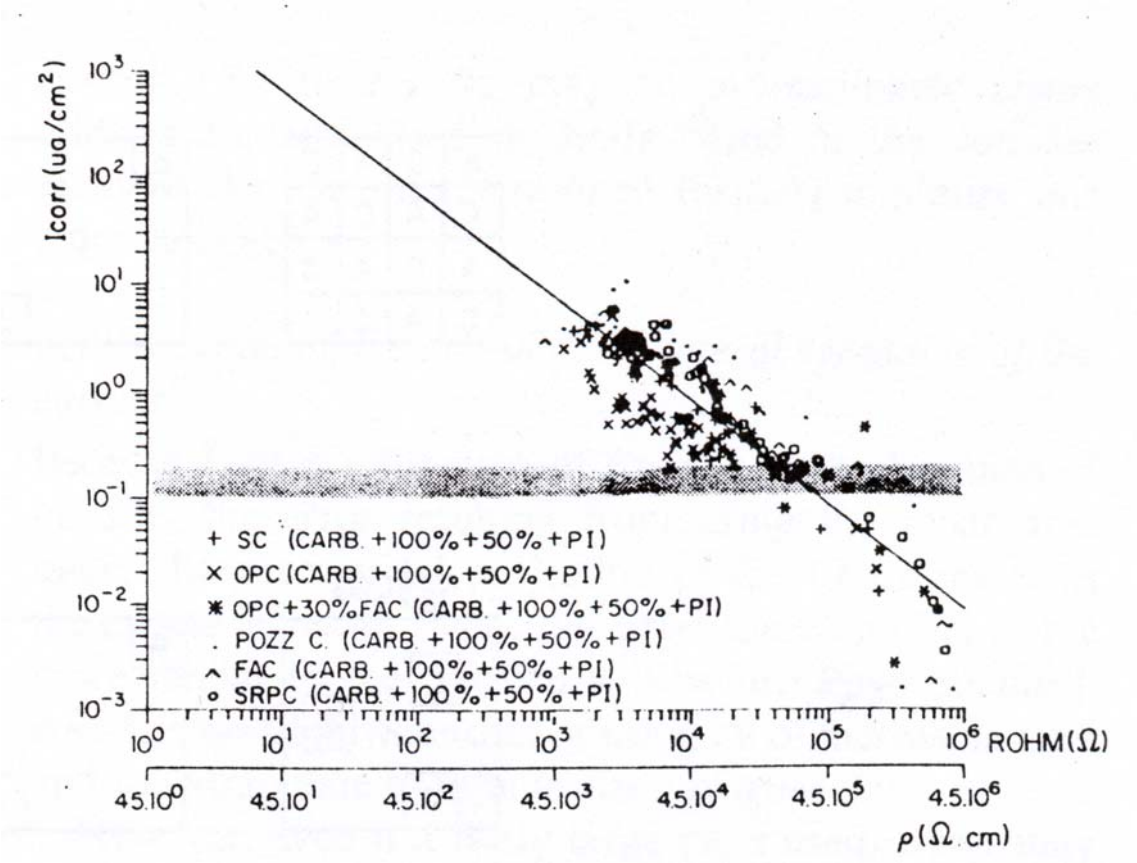


*Figure 2. 8 Dependence of $I_{corr}$ on electrical resistivity of carbonated mortars fabricated with several cement types. The scatter does not enable an accurate relationship. After Andrade and Alonso [1].*

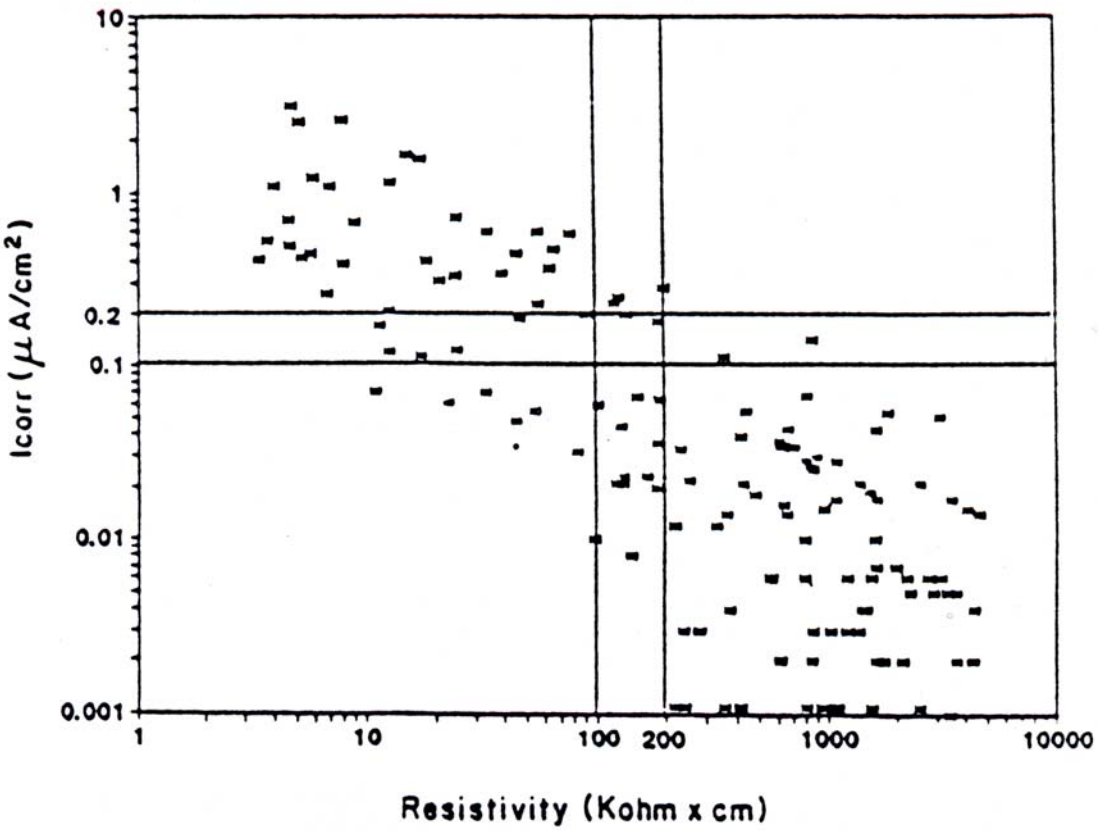


*Figure 2. 9 Relationships found in real structures (confined sensors) between Icorr and the resistivity. After Andrade and Alonso [1].*

Based on the results, Andrade and Alonso [1] characterised the risk of corrosion in respect to electrical resistivity.

*Table 2. 1 Characterisation of the corrosion risk level at various ranges of electrical resistivity according to Andrade and Alonso [1]. Resistivity is conversed from [kΩcm] to[Ωm].*

| **Resistivity [Ωm]** | **Risk levels** |
|---|---|
| *> (1000 – 2000)* | The corrosion rate values will be very low even if the concrete is carbonated or chloride contaminated |
| *100 – 1000* | Low to high corrosion rate |
| *< 100* | Resistivity is not the controlling parameter for the corrosion rate |

## 2.6 Factors influencing the electrical resistivity of concrete

### 2.6.1 Influence of the concrete mix proportions on the electrical resistivity of concrete

The electrical resistivity of concrete is related to the microstructure of the cement matrix, its pore structure, porosity and pore size distribution. It is also a function of the concentration of ions and their mobility in the pore solution [44, 45].

The cement chemistry, cement content, w/b-ratio and use of admixtures are factors which influence the microstructure of the cement matrix of concrete as well as the ionic strength of the pore water. Any influence on these properties affects the electrical resistivity of the concrete.

Although the resistivity of the concrete is mainly governed by the cement paste, changes in the aggregate type and amount influence the electrical resistivity [32].

Cement type

It has been shown by several authors [32, 46, 47] that cement containing high amounts of tricalcium aluminate ($C_3A$) generates higher resistivities than comparable cements with lower $C_3A$ content.

Monfore [32] attributed this to the absence of calcium hydroxide in the hydration products of $C_3A$. The difference is most profound at early ages due to the immediate formation of ettringite during hydration of $C_3A$. When comparing high-alkali and low-alkali cements Monfore [32] further found that the alkali content did not appear to have any practical significance on the electrical resistivity of concrete.

Cement content

Any changes in the in the volume fraction of cement matrix will lead to a change in the electrical resistivity of concrete. The resistivity is mainly influenced by the properties of the cement matrix, or the cement paste, as mentioned in the introduction of this section. The cement content and the w/b ratio used in the concrete mix determine the volume fraction of the cement paste. An increase in the cement content will lead to a decrease in electrical resistivity.

Huges et al. [48] found by measuring the electrical resistivity on 12 concrete mixes with various cement contents (300kgs/$m^3$ – 400kgs/$m^3$) that an increase in cement content decrease the electrical resistivity. This decrease was almost 20% as cement content increased from 300kgs/$m^3$ to 400kgs/$m^3$ for a concrete having a w/c of 0.5, and almost 25% for a concrete having a w/c of 0.55 by the same change in cement content.

Water – cement (binder) ratio

Water – cement ratio (or water – binder ratio) is one of the most important parameters controlling the performance of concrete. It has a significant effect on the strength and durability characteristics of concrete.

This parameter plays an important role for the microstructure of the cement paste and the ionic strength of the pore water solution. Evidently, this parameter is decisive for the development of the electrical resistivity of concrete.

Monfore [32] found that the resistivity increases as w/c – ratio decreases. The electrical resistivity of a cement paste having a w/c of 0.4 was about double that of a paste having a w/c of 0.6. The same trend has been verified by several authors [48, 49].

The electrical resistivity of cement paste is very much lower than that of concrete made of the same paste. It can be close to 1/5 of the companion concrete resistivity in some cases according to Whiting and Nagi [29].

Aggregates

It was stated in section 2.4.2 that the electrical resistivity of aggregate is very much higher than that of the cement paste. The electrical resistivity of aggregates depends on their water absorption abilities. Monfore [32] measured the electrical resistivities of several aggregates typically used for concrete. He found a correlation between water absorption and electrical resistivity. Sandstone and limestone that may absorb close to 10% by weight have quite low resistivities while marble and especially granite absorb little water and therefore sustain very high resistivities.

There is no specific study on the effect of type of aggregate on the electrical resistivity of concrete. One would expect that the resistivity of a concrete made with limestone aggregate would be less than that of a concrete made with granite aggregate, all other things being equal.

The amount of aggregate in a concrete mix is assumed to affect the electrical resistivity. Hughes et al. [48] measured the electrical resistivity of concretes containing a range of aggregate contents. They expressed the aggregate content as a multiple of the cement content. When the aggregate content was increased from 2.92 to 4.36 the resistivity increased from 48.6 to 57.3 Ωm, an increase of about 18%.

Silica fume additive

Silica fume is a by-product of the reduction of high-purity quarts with coal in electric furnaces in the production of silicon and ferrosilicon alloys. Silica fume consists of very fine vitreous particles with very high surface area compared to portland cement (approximately 100 times smaller).

Because of its very fine particles and pozzolanic characteristics, silica fume creates a very fine pore structure and a low ionic concentration in the pore solution [41]. This leads to a significant increase in electrical resistivity.

The influence of silica fume on the electrical resistivity increases by decreasing w/c ratios. Berke et al. [42] found an increase in resistivity of more than an order of magnitude by adding 15% silica fume (by mass of cement) compared to a similar mixture without silica fume additive (1400 Ωm compared to 130 Ωm). The mixture had a w/c ratio of 0.38.

### 2.6.2 Influence of the curing and construction practices on the electrical resistivity of concrete

The effects of curing regime and construction practices are not directly found in the literature. The changes in electrical resistivity relates to other properties more dominant. The pure effects from the casting and curing are not so easily extracted since the effect of the concrete's microstructure, moisture content and ambient temperature are more dominant with respect to the electrical resistivity. The effects of environmental aspects will be thoroughly discussed in the following.

### 2.6.3 Influence of moisture on the electrical resistivity of concrete

Moisture content is the most dominant factor for the electrical resistivity of concrete. Since almost all of the electrical current is distributed in the aqueous phase in concrete, the amount of water available for this distribution is highly dominant. When some of this pore water evaporates (dries out) there is less water for distributing the current flow, hence, the electrical resistivity increases.

It has been stated in the introduction of Chapter 2.4 that oven dried concrete acts as an insulator ($\rho > 10^6$ Ωm) while saturated concrete acts as a semi – conductor ($\rho \approx 10^1$ Ωm). This large difference in electrical resistivity has been verified by several authors [29, 40-44].

Hunkeler [45] indicates that the conductivity of concrete drops to practically zero at a relative humidity of approximately 40%. The binder phase in concrete still contains significant amounts of water at this RH. However, the water in the pores is essentially non-conductive. This effect is most likely due to surface forces that demobilises the ions dissolved in the pore water.

Hammond and Robson [47] measured the electrical resistivity of an oven-dried concrete to 400 MΩm. This large electrical resistivity is well in the range of insulators. This confirms the theory of that the conduction of current passes in the aqueous phase. Still this is an extreme case in which no conclusions can be made up on.

Gjørv, Vennesland and El-Busiady [49] studied the effect of moisture content on concrete specimens and related the moisture content to degree of water saturation. They studied water saturation from 40% to 100% and found the resistivities to change from 30 – 60 Ωm at 100% saturation to 1 – 60 kΩm at 40% saturation. The difference between low and high w/c ratios in electrical resistivity by drying was most pronounced for the lower levels of saturation.

An extraction of their results is given in Figure 2. 10.

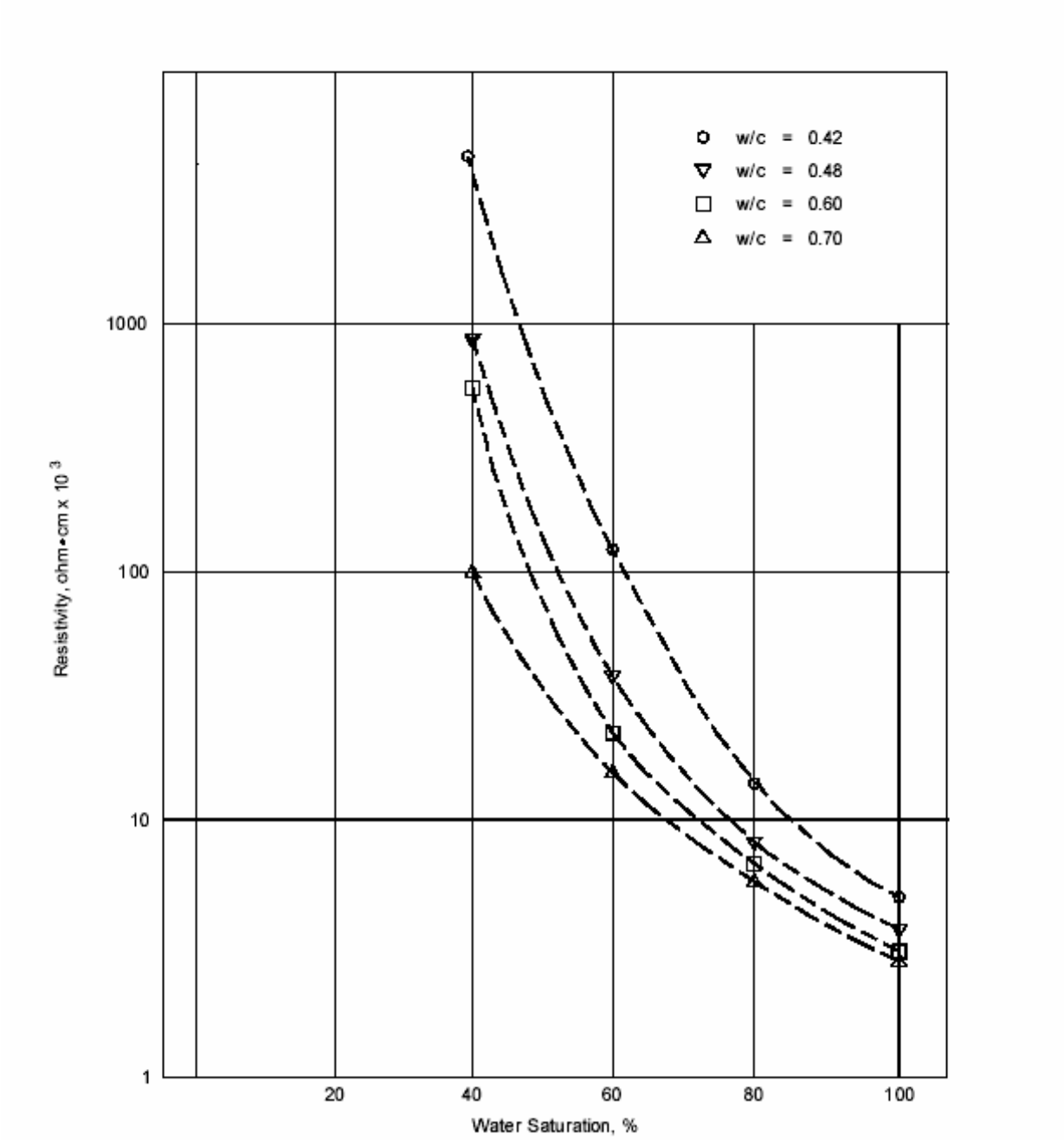


*Figure 2. 10 Effect of water-saturation on electrical resistivity of concrete. Extracted from Gjørv et al. [49].*

Elkey and Sellevold [40] investigated the effect of moisture on the electrical resistivity. They reported a dramatic increase in resistivity in the range of 40 – 60% saturation. They suggested that at this point the pore

system begins to lose continuity. This results in a more substantial change in available electrical flowpaths.

Sellevold, Larsen and Blankvoll [58] studied the electrical resistivity of samples taken from a post tensioned concrete bridge (Gimsøystraumen Bridge, balanced cantilevered box construction) after 14 years of service in severe marine climate. The samples were initially water saturated, then dried to the desired degrees of saturation. The electrical resistivity was determined as a function of degree of capillary saturation (70%<DCS<100%). The resistivities ranged from 100 Ωm at 100% saturation to 500 Ωm at 70% saturation. The in-situ degree of saturation was in the range of 80 – 90% which would correspond to concrete resistivities of 250 – 150 Ωm.

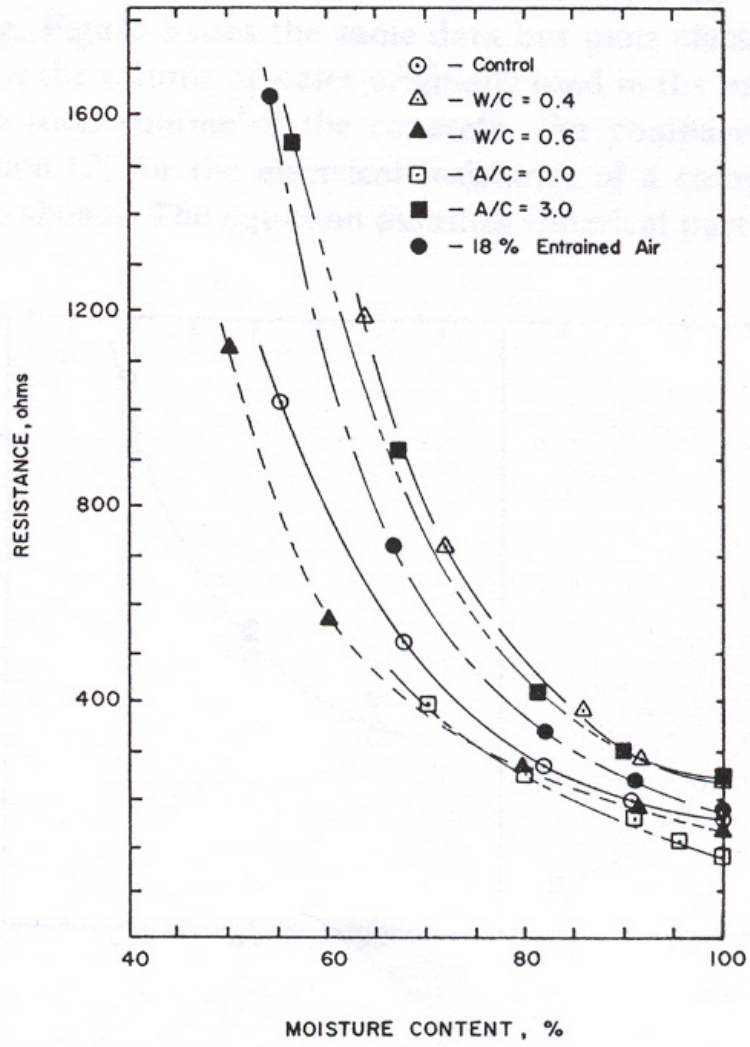


*Figure 2. 11 Influence of moisture content on electrical resistance of Portland Cement Concretes, after Woelfl and Lauer [59]*

Woelfl and Lauer [59] investigated the influence of moisture content on the electrical resistance for concretes of various w/c ratios, additives and entrained air contents. Their results are shown in Figure 2. 11.

### 2.6.4 Influence of temperature on the electrical resistivity of concrete

Like all materials the electrical resistivity of concrete is affected by temperature. This phenomenon is complicated by the change in the pore water chemistry that occurs along with change in temperature. According to McNeill [60] the temperature dependency is almost entirely dependent upon the behaviour of the electrolyte (pore water in concrete). At higher temperatures, more ions will dissolve into the pore water, and then precipitate as the solution cools.

As temperature increases, the viscosity of the fluid decreases, increasing the mobility of the conducting ions. This leads to a decrease in electrical resistivity of the porous material.

The fundamental variation of phenomena such as resistivity by temperature can be expressed by the Hinrichson-Rasch Law [61]:

$$R_2 = R_1 \cdot e^{A\left(\frac{1}{T_2} - \frac{1}{T_1}\right)} \qquad \textit{(Equation 2.29)}$$

Where:

| | | |
|---|---|---|
| $R_1$ | electrical resistivity at temperature $T_1$ | [Ωm] |
| $R_2$ | electrical resistivity at temperature $T_2$ | [Ωm] |
| $T_1$ | temperature | [K] |
| $T_2$ | temperature | [K] |
| $A$ | activation energy constant | [K] |

Figure 2. 12 shows a composite plot of data collected by Woelfl and Lauer [59] and data from Monfore [32] superimposed on a curve developed by Spencer [62]. This shows the multiplying factor needed to change a resistance taken at other temperatures to that measured at 70°F (21.1°C). The conformity of these independent studies suggests that the temperature phenomenon is independent of other concrete aspects such as porosity, cement content, w/b ratio etc.

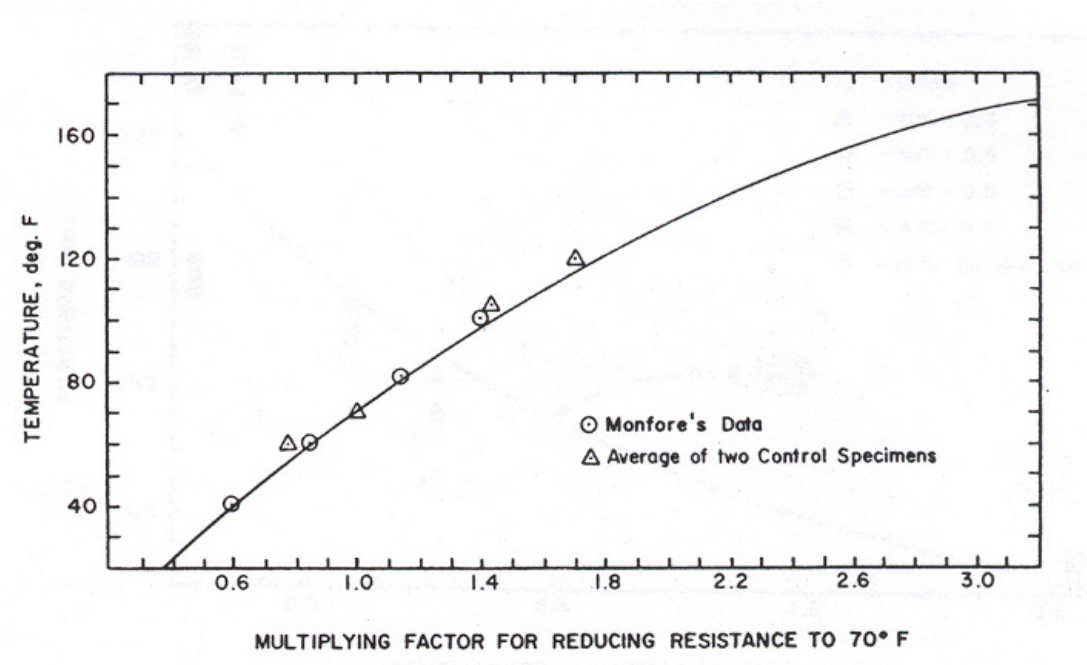


*Figure 2. 12 Spencer's temperature reduction curve, after Woelfl and Lauer [57]*

Hope and Ip [63] investigated the influence of temperature on resistivities of concretes across a range of w/c ratios. The concretes were cured at 70°F (21.1°C) for 54 days at 100% RH, and then placed over a salt solution at 75% RH for additional 14 days. The concretes were exposed to a series of different temperatures and the resistivities were measured.

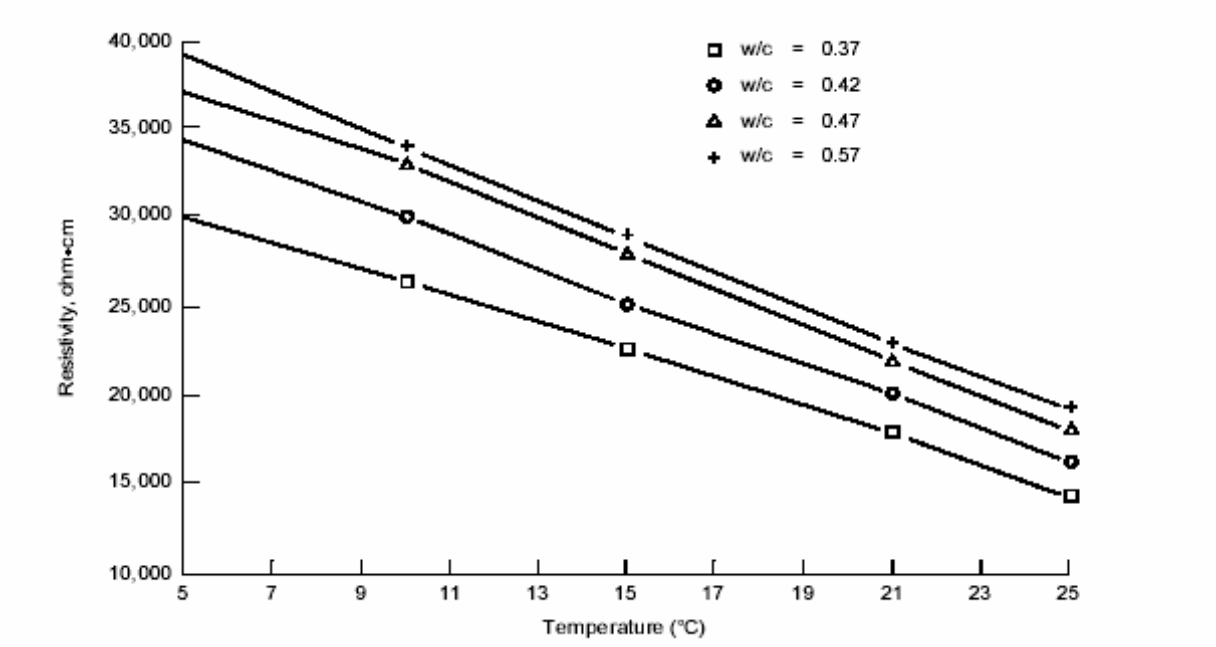


*Figure 2. 13 Influence of temperature on electrical resistivity of concrete across a range of w/c ratios, after Hope and Ip [63].*

Figure 2. 13 shows the results Hope et al. found. These results confirm the findings of Woelfl and Lauer [59] since the lines representing the mixes are more or less parallel. The data correspond to the Hinrichson-Rasch Law with an activation energy constant of approximately 2900 K for all mixes.

Monfore [32] found this constant for cement pastes to 2200 K while Elkey and Sellevold [40] note that the activation energy constant can vary from 2000 – 5000 K in some cases. This represents a temperature sensitivity of 3 – 5% per °C at 21°C which varies by moisture content. Decreased degree of saturation leads to an increased temperature sensitivity. This creates a second order problem if both moisture content and temperature is varying.

Castellote, Andrade and Alonso [64] standardised the electrical resistivity of mortar and concrete specimens at various temperatures to an equivalent resistivity at 25°C by the equation:

$$\rho = \rho_0 + \alpha \cdot \Delta T \cdot \rho_0 \qquad \textit{(Equation 2.30)}$$

Where:

| | | |
|---|---|---|
| $\rho$ | electrical resistivity at temperature T | [Ωm] |
| $\rho_0$ | electrical resistivity at a temperature of reference $T_0$ (normally 25°C) | [Ωm] |
| $\alpha$ | coefficient of temperature for the material | [-] |
| $\Delta T$ | temperature difference ($T_0$ - T) | [K] |

The coefficient of temperature for the material was characterised by the equation:

$$\alpha_{cement\ paste} = \alpha_{dosage} + Wg \cdot F \qquad \textit{(Equation 2.31)}$$

Where:

| | | |
|---|---|---|
| $\alpha_{cement\ paste}$ | coefficient of temperature, without aggregates in the mix | [-] |
| $\alpha_{dosage}$ | coefficient of temperature for the tested dosage | [-] |
| $Wg$ | (1-$C_{cem}$/S) | [-] |
| $C_{cem}$ | cement in the dosage | [kg/m$^3$] |
| $S$ | total amount of solids in the dosage: (cement+additions+aggeregates) | [kg/m$^3$] |
| $F$ | constant | [-] |

The values of the constant, F were determined numerically, and the resulting two expressions for standardisation were:

In the case, T<25°C:

$$2E^{-6} \cdot \Delta T \cdot \rho_0^2 + (1 + 0.664 \cdot \Delta T - 0.825 \cdot Wg \cdot \Delta T) \cdot (\rho_0 - \rho) = 0 \quad \textit{(Equation 2.32)}$$

In the case, T>25°C:

$$5E^{-0} \cdot \Delta T \cdot \rho_0^2 + (1 + 0.0564 \cdot \Delta T - 0.064 \cdot Wg \cdot \Delta T) \cdot (\rho_0 - \rho) = 0 \quad \textit{(Equation 2.33)}$$

### 2.6.5 Measurement techniques and Testing methods

There are many aspects around measurements of electrical resistivity that need to be concerned when evaluating results. The electrical apparatus and the circuitry are very important factors. For materials such as concrete interaction of the current loading ions occurs at the interface between electrode and electrolyte. When DC measurements are used a polarisation of the electrochemical double layer occurs due to these interactions. This leads to a false reading of the current response from the potential deviation. In addition a net transport of ions (migration) occurs due to the one-directional electrical field.

The arrangement and contact media used for the electrodes are important factors to consider. If the contact between the concrete and the electrodes is improperly done, a transition resistance is introduced in the system. This is often very hard to separate out, and may lead to erroneous results.

A wide variety of specimen types, electrode arrangements and testing methods have been used in the various studies of the electrical resistivity of concrete. Elkey and Sellevold [40] summarised a number of these investigations and sorted the parameters (Table 2.2). In the following a brief discussion of the main parameters is given.

*Table 2. 2 Summary of laboratory test methods for electrical resistivity of concrete, based on Elkey and Sellevold [40] with additions.*

| **Study** | **Voltage type** | **Frequency** | **Specimen description** | **Electrode type** | **Method of contact** |
|---|---|---|---|---|---|
| Andrade and Alonso 1995 [1] | Galvanostatic Pulse | Not available | On site, Cylinders in Lab. | Ring disc (stainless steel) | Wet sponge |
| Monfore, 1968 [32] | DC 4-10 V AC 2-8 V | 0.1-10 kHz | Cubes (1" and 4") | Brass plates (external) | Stiff graphite gel |
| Hammond & Robson, 1955 [47] | DC 55-3kV AC | 0.002-25 kHz | Cubes (4") Prisms (4x4x1") | Brass plates (external) | Stiff graphite gel |
| Hughes, 1985 [48] | DC 4-8 V AC 10V | 1 kHz | Cubes (150 mm) | Brass plates (external) | Fluid cement-paste (w/c = 0.5) |
| Woelfl and Lauer, 1979 [59] | AC 6 V | 60 Hz | Prisms (1x2x6") | slim rods (material N/A) | Cast in |
| Hauck, 1993 [62] | AC | Not available | Cylinders (Ø100 mm x 51 mm) | iron mesh (external) | Electrolytic solution |
| Hope, 1985 [65] | AC | 1 kHz | Prisms (25x25x100 mm) | Brass or steel rods | Cast in |
| Bracs, 1970 [66] | Not available | Not available | Cubes (6") | Steel wire | Cast In |
| Cabrera, 1994 [43] | AC 10V | 1 kHz | Cubes (100 mm) | Brass plates (external) | Fluid cement paste |
| Schissl, 1993 [67] | AC | 120 Hz | Not available | Multi-ring electrode | Cast in |
| Hansson, 1983 [68] | DC 3-9 V | | Prisms (90x70x50 mm) | Perforated steel plates (30x30mm) | Cast in |
| Bhargava and Rhenstrom, 1978 [69] | AC 0.5-1.5 V | 0.1-50 kHz | Prisms (40x40x160 mm) | Hardened Cement paste w/Pt black | Cast in |

Voltage and frequency

Measurements of the electrical resistivity of concrete have been performed using both direct current (DC) and alternating current (AC) at various frequencies. As initially mentioned application of a DC current causes a back electromotive force (back EMF), which alters the resistance readings. Migration will also occur due to this continuous electrical field, thereby altering the chemical composition of the electrolyte locally.

Most authors use AC current based techniques to eliminate the difficulties obtained by the DC current based ones. A variety of frequencies is found in the literature, ranging from 2Hz [47] to 50 kHz [69]. Bhargava and Rhenstrom [69] found by applying different voltages and frequencies that below 1 kHz some difference occurred between the various amplitudes (0.5, 1 and 1.5 V). On higher frequencies no such difference was found.

It is generally accepted that a measurement frequency of 1 kHz is appropriate for measuring the electrical resistance through a concrete volume.

Specimen size and shape

In terms of electrical resistivity a term “the bigger is better” would be appropriate. In a large sample inhomogeneities would play a lesser role for the measurements representing a large concrete mass. However, it is practically difficult and time consuming to condition such large specimens.

In Table 2.1 there are large variations on the specimen sizes and shapes. No conclusion on geometry can be given; it depends on the aims and objectives for the individual projects.

Electrode type and arrangement

The type and arrangement of electrodes determines the measurement quality and the reliability of the resistivity calculations. Face to face plate (or mesh) electrodes of intimate contact (or embedded) with the concrete would ideally give an excellent result due to a well defined concrete volume measured upon. While a rod or a point electrode would yield difficulties in calculating the electrical resistivity since the concrete volume is more uncertain.

Normally, metal electrodes are used for resistivity measurements. Either brass or steel plate electrodes applied on the surface of the specimen, or mesh electrodes embedded in the concrete while casting. Internal electrodes have the advantage of a consistent contact zone, while external electrodes may be affected by the amount of force applied to ensure appropriate contact. Elkey and Sellevold [40] noticed a decrease in resistivity when a greater force was applied to ensure contact. Their observation indicates that the contact zones for external electrodes less consistent than for internal electrodes.

## 2.7 Concluding remarks and starting point for the experimental work

The literature review given in the previous sections has shown that the cathodic reaction rate and the electrical resistivity depend on many parameters, especially on moisture content of the concrete and the temperature. For both subjects the knowledge is high, but very little information on low temperatures was found in the literature.

The effect of freezing temperatures on the concrete system is yet uncertain. Furthermore the concrete is a porous system which may allow water unfrozen at very low temperatures. This may allow corrosion to occur in the low temperature range.

Motivated in the above and the information obtained by the literature review, an experimental programme was developed. Details on the experimental programme are outlined in the following chapter.

# 3

# EXPERIMENTAL PROGRAMME

*This chapter gives an overview of the experimental programme and details on specimen design, sample preparation, mix proportion and test methods.*

## 3.1 Introduction

The experimental programme consists of two separate parts:

- Cathodic reaction rate – temperature dependence (CRR)
- Electrical resistivity – temperature dependence (ER)

In the first part the aim was to simulate a corrosion process by polarising an embedded black steel electrode system in concrete, and monitor the effect of temperature on the resulting current. This part is referred to as "CRR" in the following. Concrete samples with a 3-electrode system have been exposed to temperatures in the range from -40 °C up to +40 °C under constant polarisation of -0.6V/MMO.

In the second part measurements of the electrical resistance were performed on concrete slices with varying moisture contents and curing conditions. This part is named "ER" in the following. The measurements

have been performed by electrochemical impedance spectroscopy, positive feedback measurements and potential square pulse measurements. All measurements were performed at four constant temperatures between +20 °C and -28 °C. The effect of concrete composition, moisture state and curing conditions were investigated.

### 3.1.1 Choice of concrete qualities, curing and handling

Since many of the Norwegian concrete structures suffering from reinforcement corrosion were built in the nineteen seventies and early nineteen eighties it was decided to test one concrete quality based on know-how from that time, and to compare this to a modern high quality concrete.

The concrete qualities were both cast using the same cement type HSOPC (CEM I 52.5 LA). This cement type was not available in the seventies, however, to minimise the amount of variables this cement was chosen for both concrete qualities as a compromise.

The aggregate was of similar origin for both concretes. The main variables between the concretes were: water – binder ratio, cement content, silica fume addition. The low concrete quality was balanced for the low cement content by adding a finer sand fraction.

Curing of the specimens were chosen to water curing (immersed in water) and sealed curing (self-desiccation). It is common knowledge that bridge concretes due to often large dimensions of the structures will have curing

conditions somewhere between water-curing and self-desiccation. The outer layer of concrete will have sufficient supply of water to almost be considered as water cured while the concrete within this scale will self-desiccate.

Handling of the specimens was chosen as a combination of reasons.

- The sealing was applied to keep controlled moisture contents during testing and storage in both parts of the experimental programme.

- The airtight sealing was applied to minimise oxygen supply from the atmosphere (inside the chamber) in the CRR – experiments.

- Drying of the specimens at 40°C was chosen to have "extremely" dry specimens to widen the moisture range in the ER – experiments.

- Re-immersion of the specimens in the ER – experiments was chosen to optimise conditions for ice formation (e.g. high pore filling.)

### 3.1.2 Choice of temperature range

The aim was to simulate realistic temperatures for the artic climate in the range of -40°C and +40°C. In the planning phase of the temperature chamber it was evaluated to go beyond -40°C, but this idea was rejected due to cost issues. The temperature range was chosen to: $-40°C \leq T \leq 40°C$. This temperature range was used for the CRR – experiments.

In the ER – experiments the temperature range was determined by the capacity of the refrigerator and freezer available at IETcc in Madrid where large parts of the ER – experiments were performed. The range was chosen to four specific temperatures: 20°C, 2°C, -14°C and -28°C.

### 3.1.3 Choice of methodology in the CRR – experiments.

A direct investigation of the corrosion rate at different temperatures is practically complicated, especially at lower temperatures.

The introduction of a corrosive environment for the embedded steel by appointing chlorides to the mix and/or carbonate the samples introduces possible difficulties for interpretation, in addition to the practical difficulties and the time consumption. Therefore it was chosen to investigate the temperature effect on the cathodic reaction rate by polarisation.

## 3.2 Materials

Two concrete mixes have been tested in both parts of the experimental programme. Both compositions are based on concrete mixes used in the Norwegian building industry today. The mixes took into account the specimen dimensions; hence, the maximum aggregate size was set to 11mm. This small aggregate size resulted in a higher content of small particles needed. The behaviour was something between concrete and mortar.

The concrete compositions are based on the NPRA standard guidelines for concrete composition.

### 3.2.1 High quality concrete mix – SV 30.

The water-binder ratio for this concrete was 0.40. A low alkali HSOPC (CEM I 52.5 LA) was used. The cement content was 444.1 kgs/$m^3$. 8 % silica fume (of cement weight) was added in the mix.

The mix proportions are given in Table 3.1

*Table 3. 1 Specification of the mix proportions of the w/b 0.4 concrete*

| ***Materials*** | ***[kg/m$^3$]*** |
|---|---|
| *Cement: HSOPC, CEM I 52.5 LA (Norcem Anlegg)* | *444,1* |
| *Micro silica (Elkem)* | *35,5* |
| *Free water* | *182,3* |
| *Adsorbed water* | *11,3* |
| *Aggregate fraction 0-8 mm (Årdal natural)* | *993,2* |
| *Aggregate fraction 8-11mm (Årdal)* | *662,1* |
| *Super plasticizer (Sikament 92)* | *4,44* |
| *Air entrainment (Sika AER)* | *0,13* |
| *Proportioned Concrete density (kgs/m$^3$)* | *2328* |

### 3.2.2 Low quality concrete mix – SV 50.

The water-binder ratio for this concrete was 0.60. The same cement type as for the high quality concrete mix was used. The cement content was 340.8 kg/m$^3$. No silica fume was added in this mix.

The mix proportions are given in Table 3.2

*Table 3. 2 Specification of the mix proportions of the w/b 0.6 mixes*

| ***Materials*** | ***[kg/m$^3$]*** |
|---|---|
| *Cement: HSOPC, CEM I 52.5 LA (Norcem Anlegg)* | *340,8* |
| *Free water* | *190,9* |
| *Adsorbed water* | *12,0* |
| *Aggregate fraction 0-8 mm (Årdal natural)* | *704,8* |
| *Aggregate fraction 0-2 mm (Årdal natural washed)* | *352,4* |
| *Aggregate fraction 8-11mm (Årdal)* | *704,8* |
| *Super plasticizer (Sikament 92)* | *0,68* |
| *Air entrainment (Sika AER)* | *0,02* |
| *Proportioned Concrete density (kgs/m$^3$)* | *2306* |

### 3.2.3 Electrodes

The steel electrodes used in the "CRR" research are normal quality ribbed carbon steel reinforcement (Tempcore, B500C by Fundia). The diameter of the reinforcing steel was 8 mm. The area of the exposed part of the electrodes was calculated without including the area of the ribs.

The electrodes used in the "ER" research were stainless steel and acid resistant woven mesh electrodes. The steel quality was AISI 316 (Stainless steel fabric No. 8 by Burmeister). The diameter of the tread was 0.89 mm and with symmetrical mask width at 2.29 mm. The surface area of the electrode was considered to be equal to the area covered by the mesh. A principal drawing of the mat geometry is given in Figure 3.1.

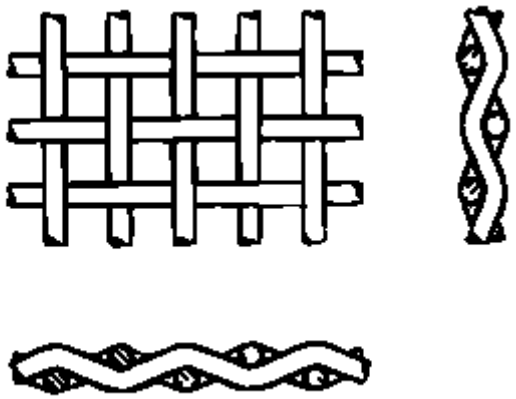

*Figure 3. 1 Drawing of the mesh electrode used in the Electrical resistivity - Temperature experiments. (Illustration from the Burmeister catalogue)*

As reference electrode an Activated Titanium Mesh (ATM) electrode was used. The reference electrodes were manufactured at NTNU.

The activated titanium mesh (LIDA®, 20mm wide and 0.6mm thick) was supplied in desired lengths.

The titanium mesh was cut in lengths of 40 mm and clamped around a copper wire. The cable used was a double isolated Ø2.5 mm copper wire with XLPE insulation. The copper part was stripped in lengths of 5 mm and the inner insulation for additional 5 mm. The titanium copper connection was subsequently sealed with glued heat-shrinkable tubing. The exposed area of the reference electrodes was approximately 2 $cm^2$.

A schematic picture showing the steps in production of the electrode is given in Figure 3.2.

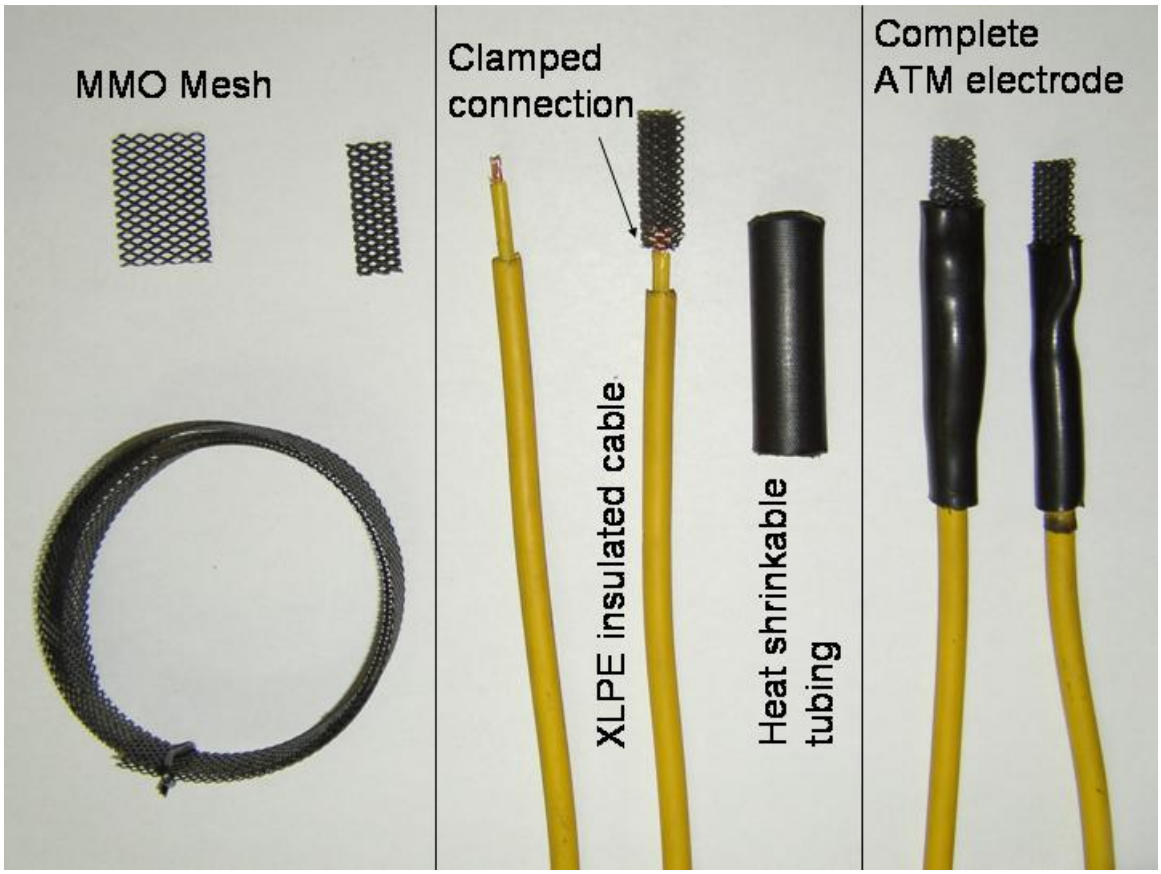


*Figure 3. 2 A schematic picture showing the processes in making the Activated Titanium Mesh – reference electrode*

## 3.3 Specimens

### 3.3.1 CRR specimens

The CRR – specimen with dimensions: 60x60x150 mm is shown in Figure 3.3. The electrodes were arranged in a 3-electrode system. The working electrode (WE) and counter electrode (CE) were black steel rebar electrodes, sealed with glued heat-shrinkable tubing in both ends. The average exposed steel area for both rebar electrodes was 17.6 $cm^2$. To be able to use banana plugs on the wires a 4 mm hole was drilled in both black steel electrodes. The third electrode (RE) is the ATM reference electrode described in section 3.2.3.

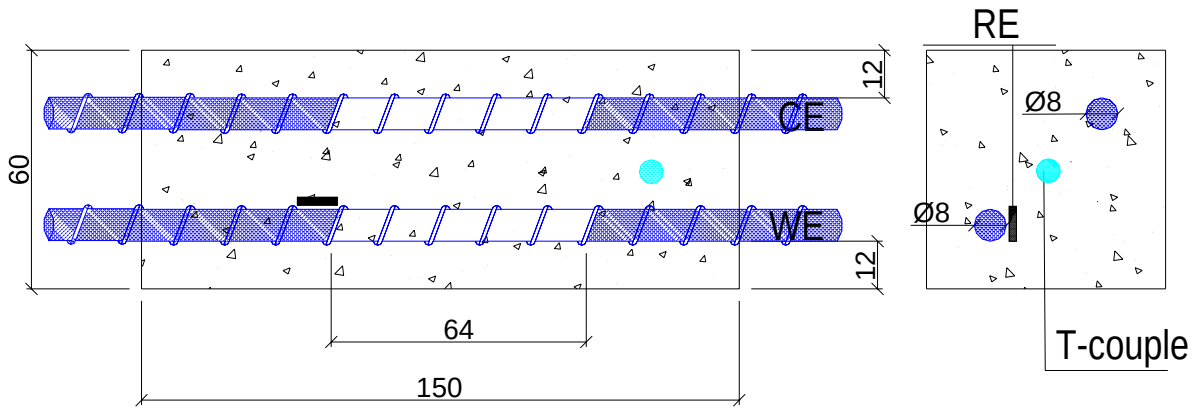


*Figure 3. 3 Drawing of the CRR – specimen (dimensions in mm)*

Figure 3.4 shows the electrode set – up. The reinforcement electrodes and the reference electrode are shown before they were cast. The reference electrode is placed close to the right of the working electrode (WE), and the counter electrode (CE) diagonally to the right on the picture. The reference electrode (RE) was placed as close to the working electrode as practically possible and still minimise the risk of failure due to short cutting of the circuit.

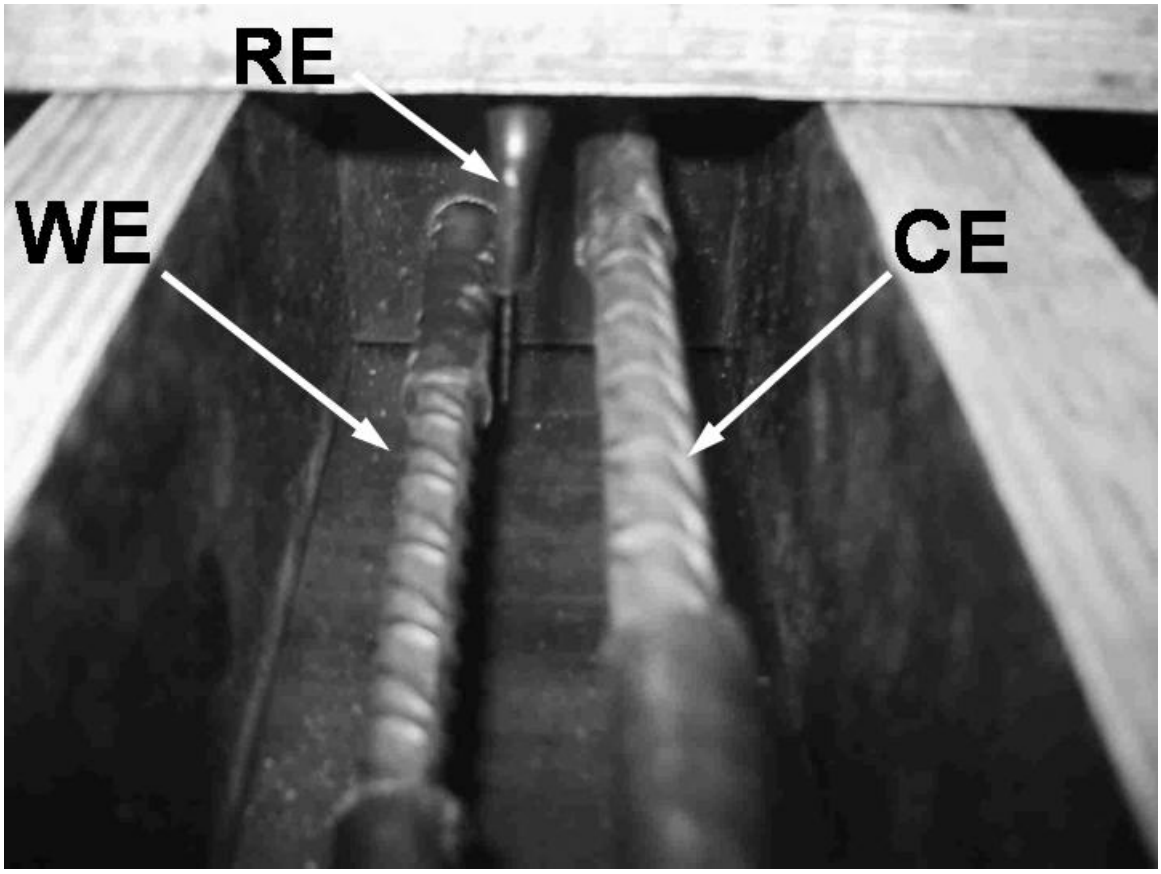


*Figure 3. 4 Picture of the electrode set-up in the mould before casting. The WE is the closest to the reference electrode, CE at the right.*

### 3.3.2 ER specimens

The ER – specimens were of dimensions: 100x100x28 mm. A principal drawing of the specimen is given in Figure 3.5. The samples held 2 parallel stainless steel mesh electrodes. To ensure a homogeneous aggregate content in the specimens, 100x100x1500 mm long concrete beams were cast, and then the specimens were sawed to the defined thickness of 28 mm from these. The electrodes have a concrete cover of 10 mm.

To ensure external electrical contact one stainless steel pin was soldered to each electrode for each specimen. The connection pins were subsequently sealed with heat-shrinkable tubing only stripped 2 – 4 mm in one end for connection by alligator clips.

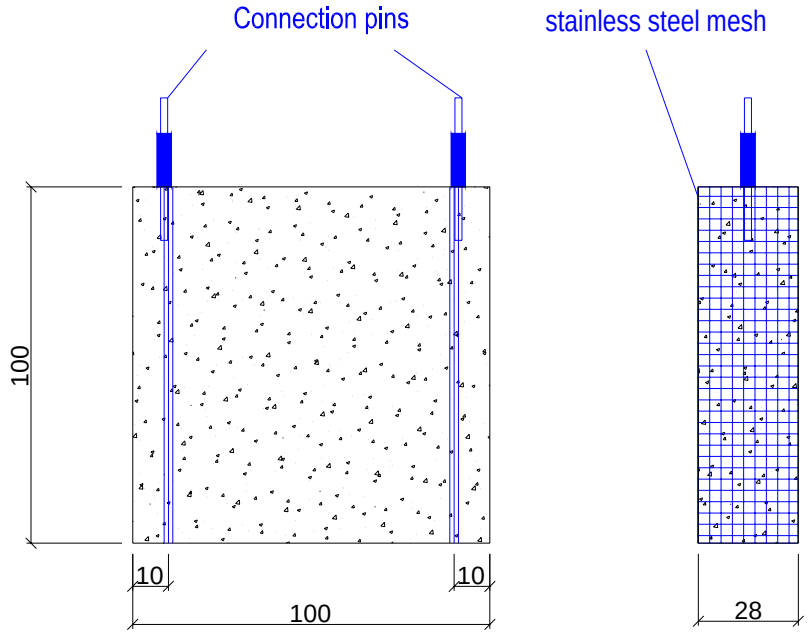


*Figure 3. 5 Drawing of the ER – specimen (dimensions in mm)*

## 3.4 Layout of the experimental programme

The test programme was performed in two parts. Each part includes two concrete mixes and a number of variants of curing regimes and moisture conditioning. The layout of the experiments and a detailed description of the different tests performed are described in this section.

### 3.4.1 Identification of the specimens

A descriptive identification system for all the specimens in both parts of the experimental programme was developed. Each specimen was given an identification which reflected the test part, run number, concrete quality (represented by w/b – ratio), curing condition and further handling along with a number describing its number in the series.

CRR specimens

In Table 3.3 an overview of the specimens tested in the CRR – experiments is given followed by one example of the identification for one of the specimens.

*Table 3. 3 Table showing the identification system for the CRR – experiments.*

| Experiment | C | | | | | | | | | | | | | | | |
|---|---|---|---|---|---|---|---|---|---|---|---|---|---|---|---|---|
| Run | 1 | | | | | | | | 2 | | | | | | | |
| Concrete | 0.4 | | | | 0.6 | | | | 0.4 | | | | 0.6 | | | |
| Curing | W | | S | | W | | S | | W | | S | | W | | S | |
| Sealing | U | | S | | U | | S | | U | S | U | S | U | S | U | S |
| Specimen no | 1-3 | | 1-3 | | 1-3 | | 1-3 | | 1-5 | 1-5 | 1-5 | 1-5 | 1-5 | 1-5 | 1-5 | 1-5 |

Specimen id:
**C1-0.4-S-S-1**

The curing conditions are termed W and S; W is water cured and S is self – desiccated. The sealing is termed U and S and reflects to whether the sample was sealed during testing or not; U is unsealed and S is sealed.

In order to illustrate the identification system an example is given:

The identification: C1-0.4-S-S-1 denotes that this specimen is tested in the CRR section, Run 1. The specimen was cast from the high quality concrete with water binder ratio 0.4 and cured in sealed conditions (self – desiccated) and sealed during testing. The number in the end reflects that it was number 1 of (in this case) 3 specimens.

ER specimens

The ER – experiments involved many runs and a quite extensive number of specimens. For each of these runs t multiple specimens were tested, and for practical reasons it is not possible to show all tested specimens in the same table.

As an example, Table 3.4 gives an overview of the specimens tested in Run 1 of the ER – experiments.

*Table 3. 4 Table showing the identification system for the ER – experiments, Run 1.*

| Experiment | R | | | | | | | |
|---|---|---|---|---|---|---|---|---|
| Run | 1 | | | | | | | |
| Concrete | 0.4 | | | | 0.6 | | | |
| Curing | W | | S | | W | | S | |
| Test condition | S | D | S | D | S | D | S | D |
| Specimen no | 1-3 | 1-3 | 1-3 | 1-3 | 1-3 | 1-3 | 1-3 | 1-3 |

Specimen id:
**R1-0.4-W-S-1**

In order to illustrate the identification system an example is given:

The identification: R1-0.4-W-S-1 gives that this specimen was tested in Run 1 of the ER – experiments. As for the CRR – experiments the number 0.4 is given in respect to w/b – ratio, hence the concrete quality. The

sample was water cured (W) and sealed without further conditioning (S). And that it was number 1 in a series of 3 parallel samples.

The ER – experiments involves several conditionings; S is sealed without further conditioning, D is dried for 1 week at 40 °C, Sr and Dr are the S and D specimens after being resaturated by water suction (immersed in water). All specimens were sealed during testing. A further description of each run will be given in a later paragraph in this chapter.

In order to summarise a principal schematic of the structure of the denomination of the specimens is presented in Figure 3.6.

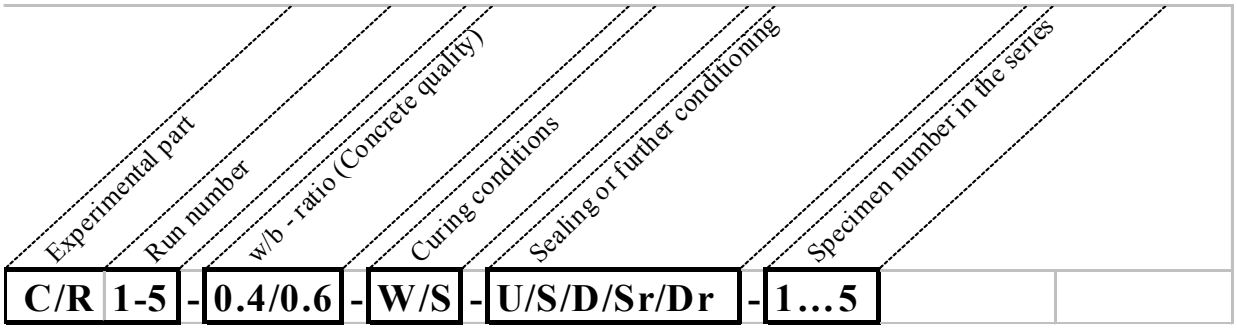


*Figure 3. 6 Schematic summary of the identification for the specimens*

### 3.4.2 Flowchart for the CRR – experiments

The CRR – experiments can be summarised in a flowchart. This is presented in Table 3.5.

*Table 3. 5 Flowchart table for the CRR – experiments*

| Experiment | C | | | | | | | | | | | | | | | |
|---|---|---|---|---|---|---|---|---|---|---|---|---|---|---|---|---|
| Run | 1 | | | | | | | | 2 | | | | | | | |
| Concrete | 0.4 | | | | 0.6 | | | | 0.4 | | | | 0.6 | | | |
| Curing | W | | S | | W | | S | | W | | S | | W | | S | |
| Sealing | U | | S | | U | | S | | U | S | U | S | U | S | U | S |
| Number of speciemens | 3 | | 3 | | 3 | | 3 | | 5 | 5 | 5 | 5 | 5 | 5 | 5 | 5 |
| Freezing [$^{o}$C] | $0^{o}$C - ($-40^{o}$C) | | | | | | | | $0^{o}$C - ($-40^{o}$C) | | | | | | | |
| Thawing [$^{o}$C] | $-40^{o}$C - $0^{o}$C | | | | | | | | $-40^{o}$C - $0^{o}$C | | | | | | | |
| Heating [$^{o}$C] | $0^{o}$C - $+40^{o}$C | | | | | | | | not tested | | | | | | | |
| Cooling [$^{o}$C] | $40^{o}$C - $0^{o}$C | | | | | | | | not tested | | | | | | | |
| Polarisation test | Scanning intervals 15min and 24h | | | | | | | | not tested | | | | | | | |
| Polarisation test | $20^{o}$C, $0^{o}$C, $-20^{o}$C | | | | | | | | not tested | | | | | | | |
| Moisture control | not tested | | | | | | | | Total water content | | | | | | | |

### 3.4.3 Flowchart for the ER – experiments

The ER – experiments were performed in 4 runs. The experimental part is summarised in Table 3.6.

*Table 3. 6 Flowchart table for the ER – experiments*

| Experiment | R | | | | | | | | | | | | | | | |
|---|---|---|---|---|---|---|---|---|---|---|---|---|---|---|---|---|
| Run | 1 | | | | | | | | 2 | | | | | | | |
| Concrete | 0.4 | | | | 0.6 | | | | 0.4 | | | | 0.6 | | | |
| Curing | W | | S | | W | | S | | W | | S | | W | | S | |
| Test condition | S | D | S | D | S | D | S | D | S | D | S | D | S | D | S | D |
| No of specimens | 3 | 3 | 3 | 3 | 3 | 3 | 3 | 3 | 2 | 1 | 1 | 1 | 2 | 1 | 1 | 1 |
| Freezing [°C] | 20°C, 2°C, -14°C, -28°C | | | | | | | | 20°C, 2°C, -14°C, -28°C | | | | | | | |
| Thawing [°C] | -28°C, -14°C, 2°C, 20°C | | | | | | | | -28°C, -14°C, 2°C, 20°C | | | | | | | |
| Weight control | Before and after | | | | | | | | Before and after | | | | | | | |
| Moisture control | Total water content | | | | | | | | not tested | | | | | | | |

| Experiment | R | | | | | | | | | | | | | | | |
|---|---|---|---|---|---|---|---|---|---|---|---|---|---|---|---|---|
| Run | 3 | | | | | | | | 4 | | | | | | | |
| Concrete | 0.4 | | | | 0.6 | | | | 0.4 | | | | 0.6 | | | |
| Curing | W | | S | | W | | S | | W | | S | | W | | S | |
| Test condition | S | D | S | D | S | D | S | D | Sr | Dr | Sr | Dr | Sr | Dr | Sr | Dr |
| No of specimens | 3 | 3 | 3 | 3 | 3 | 3 | 3 | 3 | 3 | 3 | 3 | 3 | 3 | 3 | 3 | 3 |
| Freezing [°C] | 20°C, 2°C, -14°C, -28°C | | | | | | | | 20°C, 2°C, -14°C, -28°C | | | | | | | |
| Thawing [°C] | -28°C, -14°C, 2°C, 20°C | | | | | | | | -28°C, -14°C, 2°C, 20°C | | | | | | | |
| Weight control | At all temperatures | | | | | | | | At all temperatures | | | | | | | |
| Moisture control | Total water content | | | | | | | | Total water content | | | | | | | |

## 3.5 Curing and preparation of specimens

Well cured samples (more than 80 days of curing) were used for all investigations.

The sealing used for some of the samples was an airtight plastic coated aluminium foil. The supplier of this type of foil was the food manufacturer IDUN.

### 3.5.1 Preparation and curing of CRR – specimens

The samples for the CRR – investigations were cast in tailored moulds. The specimens for Run 1 and Run 2 were cast from individual batches at different times. The samples were cured over night in the moulds covered with plastic after casting at a temperature of 20°C ± 1°C. After demoulding each specimen was either sealed to self-desiccate or put in a water container for water curing.

In the following it is given a description of the curing and conditioning which were performed for the concrete samples in this experimental section.

Water cured – Unsealed specimens (W-U specimens)

The specimens were water cured (at 20°C ± 1°C) after demoulding until the tests were initiated. The specimens were only surface dried with a cloth prior to the experiment. This curing and preparation was performed for both concrete compositions and used in both Run 1 and Run 2.

Water cured – Sealed specimens (W-S specimens)

The specimens were water cured as the W-U specimens. Then the specimens were sealed before they were placed in the temperature chamber. This conditioning was performed for both concrete compositions but was only tested in Run 2.

Self-desiccated – Unsealed specimens (S-U specimens)

The specimens were cured in isolated conditions after demoulding (self desiccated) in a temperate room (at 20°C ± 0.5°C, 80% RH) until start up of the experiments. The sealing was removed before they were placed in the temperature chamber. This conditioning was performed for both concrete compositions but was only tested in Run 2.

Self-desiccated – Sealed specimens (S-S specimens)

The specimens were cured as the S-U specimens. The specimens were kept sealed during the experiments also. This curing and preparation was performed for both concrete compositions and used in both Run 1 and Run 2.

### 3.5.2 Preparation and curing of ER – specimens

The specimens were cast as 1500 mm long beams. Two beams were cast for each concrete at the same point in time.

The beams were cured for 2 days in the moulds, covered with plastic to minimise the moist loss at a temperature of 20°C ± 1°C. Then the sawing of the specimens to the specified thickness of 28mm took place. After sawing each specimen was either sealed to self-desiccate or put in a water container for water curing after demoulding. The curing conditions were equal to that of the specimens for the CRR – specimens.

All specimens were after about 50 days of curing sealed with the same type of plastic coated aluminium foil used in the CRR – experiments and sent to Madrid for further conditioning and testing.

It is important to note that the samples tested in Run 4 were a resaturated version of the samples tested in Run 3. These specimens were saturated for 8 weeks to obtain as stable conditions as possible within the frame of this work. The samples tested in Run 4 were given a unique identification.

In the following a description of the curing and conditioning for the concrete samples in this experimental section is given.

Water cured – Sealed specimens (W-S specimens)

The specimens were cured in water (at 20°C ± 1°C) for 50 days after sawing, sealed and sent to Madrid. In Madrid the sealing was removed and the samples were stored in water for 1 week in water (at 20°C ± 2°C). Then the samples were taped along the electrodes and sealed using a fragile thin plastic foil in 5 layers. Some specimens were sent back to Norway for further testing in Run 3 and Run 4.

Water cured – Dried specimens (W-D specimens)

The specimens were initially handled as the W-S specimens. In Madrid the sealing was removed and the samples were oven dried at 40 °C for 1 week. The samples were then taped along the electrodes and sealed using a fragile thin plastic foil in 5 layers. Some specimens were sent back to Norway for further testing in Run 3 and Run 4.

Self-desiccated – Sealed specimens (S-S specimens)

The specimens were self-desiccated after sawing for 50 days (at 20°C ± 0.5°C, 80% RH), sealed and sent to Madrid. In Madrid the sealing was removed and replaced with tape along the electrodes and sealing by 5 layers of thin plastic foil. Some specimens were sent back to Norway for further testing in Run 3 and Run 4.

Self-desiccated – Dried specimens (S-D specimens)

The specimens were initially handled as the S-S specimens. In Madrid the sealing was removed and the samples were oven dried at 40 °C for 1 week. The samples were then taped along the electrodes and sealed using a fragile

thin plastic foil in 5 layers. Some specimens were sent back to Norway for further testing in Run 3 and Run 4.

Water cured – Sealed – Resaturated specimens (W-Sr specimens)

These specimens are based on the water cured – sealed specimens tested in Run 3. After finishing Run 3 the sealing and tape were removed and the specimens were resaturated in water (at 20°C ± 1°C). In this period the stability of the pore water chemistry was controlled by measuring the electrical resistivity. The specimens were considered as stable when the variation in electrical resistivity was less than ± 5%. This took approximately 8 weeks. The samples were then sealed by the plastic coated aluminium foil used on CRR – specimens and taped in all crossings and electrode holes.

Water cured – Dried – Resaturated specimens (W-Dr specimens)

These specimens are based on the water cured – dried specimens tested in Run 3. Further handling was equal to that of the W-Sr specimens.

Self-desiccated – Sealed – Resaturated specimens (S-Sr specimens)

These specimens are based on the self desiccated – sealed specimens tested in Run 3. Further handling was equal to that of the W-Sr specimens.

Self-desiccated – Dried – Resaturated specimens (S-Dr specimens)

These specimens are based on the self desiccated – dried specimens tested in Run 3. Further handling was equal to that of the W-Sr specimens.

## 3.6 Test programme CRR – experiments

### 3.6.1 Temperature effect on cathodic polarisation curves

A series of polarisation experiments were conducted, primarily to verify that the chosen potential level of -0.6 V/MMO was within the level where oxygen reduction is assumed to take place, secondly to observe any thermal effects on the appearance of the polarisation curves.

The potential range was from -0.1V/MMO down to -1.2V/MMO regardless of the systems equilibrium potential. The polarisation experiments were performed in steps. Two step-durations were initially tested. The short deviation was 0.1V every 15 minutes and the long was 0.1V every 24hours. These are termed fast scanning and slow scanning, respectively, in the following.

Polarisation experiments for all C1 specimens were done for both fast and slow scanning. The fast scanning was performed at three different temperatures of 20°C, 0°C and -20°C. All these polarisation experiments were done without IR – compensation.

### 3.6.2 Verification of the ATM reference electrode

In order to investigate the integrity, reproducibility and stability of the MMO reference electrode special reference cell specimens were manufactured. These specimens were made of w/b = 0.5 mortar. The specimens contain one embedded ATM electrode and one embedded Manganese ($MnO_2$) electrode. As an absolute reference an external standard calomel electrode ($SCE_{sat}$) was used. These measurements were compared with an external silver/silver chloride (0.1 M Ag/AgCl) reference electrode. Measurements at lower temperatures were also made, but without the third reference electrode. These samples were cured for less than 30 days when the experiments started.

### 3.6.3 Moisture content

Moisture control of the specimens in Run 2 was conducted by weighing before and after the experiments. In the end a full drying at 105 °C was done after resaturation and pressurisation (50 bar for 2 days) of the specimens.

In addition the ignition loss at 1000 °C of small samples of the concretes was measured to get an indication of the amount of chemically bound water.

### 3.6.4 Run 1

Run 1 contained less variants and parallel samples than Run 2. Run 1 started at 0 °C through -40 °C and back to 0 °C. The temperature changes were programmed to 5 °C steps every 24 hours. At the end of the temperature cycle the specimens were kept at 0 °C for more than 200 hours to control stability of the systems. After the period at 0 °C a heating cycle was performed. The temperature was changed from 0 °C up to +40 °C and then down to 0 °C again. The temperature was changed in 5 °C steps every 24 hours. An ideal temperature history for Run 1 is given in Figure 3.7.

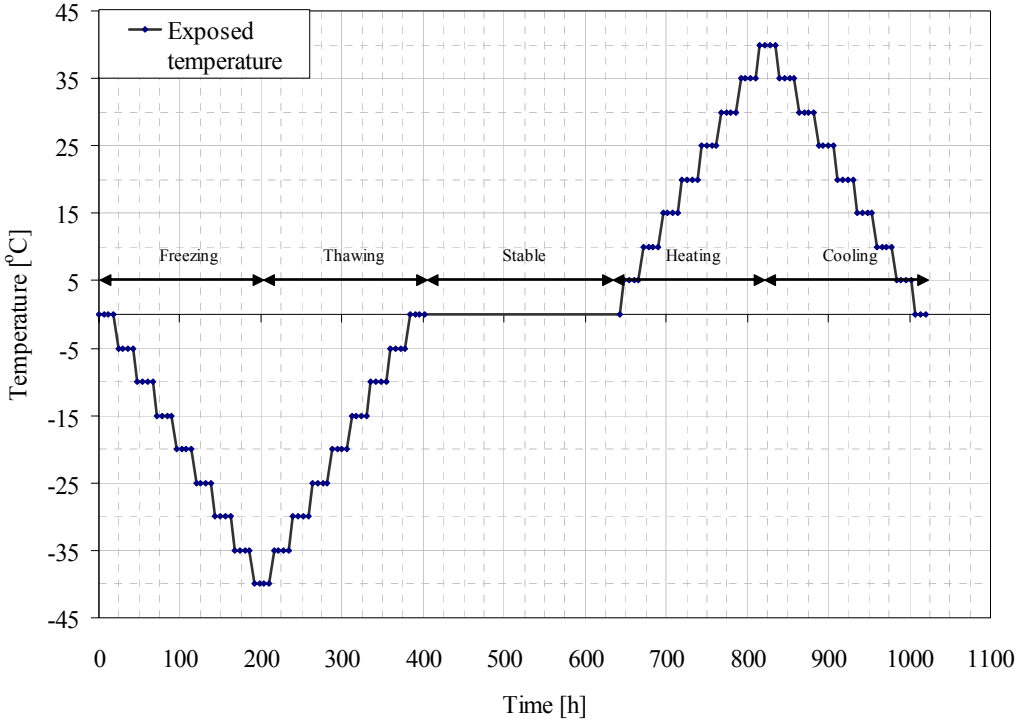


*Figure 3. 7 Ideal temperature history for Run 1*

In Table 3.7 the temperature intervals are shown corresponding to the arrow marked time intervals in Figure 3.7.

*Table 3. 7 Temperature intervals, range and duration*

| Name of interval | Temperature range | Duration [h] |
|---|---|---|
| Freezing | $0^{o}C$ - $(-40^{o}C)$ | 200 |
| Thawing | $(-40^{o}C)$ - $0^{o}C$ | 200 |
| Stable | $0^{o}C$ | 250 |
| Heating | $0^{o}C$ - $40^{o}C$ | 200 |
| Cooling | $40^{o}C$ - $0^{o}C$ | 200 |

For Run 1 no moisture control of the specimens was performed. Based on Run 2 some estimations of the moisture content in the samples were performed. The tested specimens for Run 1 and estimated moisture content are shown in Table 3.8. A discussion of the moisture content will be given in Chapter 4.

*Table 3. 8 Tested specimens in Run 1*

| Specimen Id | Temperature interval | | | | | | Tests | | | Age | DS* |
|---|---|---|---|---|---|---|---|---|---|---|---|
| | Freezing | Thawing | Stable | Heating | Cooling | Stability | Resistance | $\eta$ = - 0.6 | -0.1< $\eta$ < -1.2 | Start test | Start test |
| | | | | | | | | [V/MMO] | | [days] | [%] |
| C1-0.4-W-U-1 | X | X | X | X | X | | | X | X | 84 | |
| C1-0.4-W-U-2 | X | X | X | X | X | | | X | X | 84 | 99.0 |
| C1-0.4-W-U-3 | | | | | | X | | X | | 84 | |
| C1-0.4-S-S-1 | X | X | X | X | X | | | X | X | 84 | |
| C1-0.4-S-S-2 | X | X | X | X | X | | | X | X | 84 | 97.5 |
| C1-0.4-S-S-3 | | | | | | X | | X | | 84 | |
| C1-0.6-W-U-1 | X | X | X | X | X | | | X | X | 91 | |
| C1-0.6-W-U-2 | X | X | X | X | X | | | X | X | 91 | 98.0 |
| C1-0.6-W-U-3 | | | | | | X | | X | | 91 | |
| C1-0.6-S-S-1 | X | X | X | X | X | | | X | X | 91 | |
| C1-0.6-S-S-2 | X | X | X | X | X | | | X | X | 91 | 97.0 |
| C1-0.6-S-S-3 | | | | | | X | | X | | 91 | |
| *) estimated from Run 2 moisture data | | | | | | | | | | | |

### 3.6.5 Run 2

This run was an extended version of Run 1. An extended number of series and a higher number of parallel samples for each type were investigated. The temperature intervals freezing and thawing were executed in the same way as for Run 1. The stable temperature, heating and cooling intervals were not investigated.

In addition, measurements of the electrical resistance between the working electrode and the counter electrode were carried out. These measurements were performed by chronoamperometry at 1 kHz. The device (ResMES, by Protector) is automated and measurements were performed every 15 minutes.

Moisture control was performed on small pieces of the samples after finishing the temperature intervals according to paragraph 3.6.3. The tested specimens for Run 2 and calculated moisture content are shown in Table 3.9.

The temperature measurements were calibrated against melting ice during the experiments.

The temperature test cycle is shown in Figure 3.8.

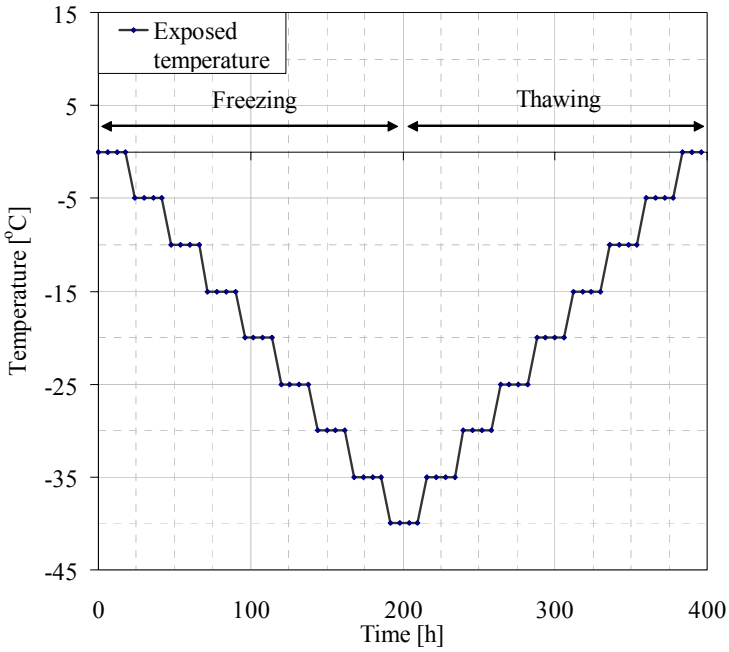


*Figure 3. 8 Ideal temperature history for Run 2*

*Table 3. 9 Tested specimens in Run 2*

| Specimen Id* | Temperature interval | | | | | | Tests | | | Age | DS |
|---|---|---|---|---|---|---|---|---|---|---|---|
| | Freezing | Thawing | Stable | Heating | Cooling | Stability | Resistance | $\eta$ = - 0.6 [V/MMO] | -0.1< $\eta$ < -1.2 | Start test [days] | Start test [%] |
| C2-0.4-W-U-1-3 | X | X | | | | | | X | | 82 | 99.2 |
| C2-0.4-W-U-4 | | | | | | X | | X | | 82 | |
| C2-0.4-W-U-5 | X | X | | | | | X | | | 82 | |
| C2-0.4-W-S-1-3 | X | X | | | | | | X | | 82 | 99.8 |
| C2-0.4-W-S-4 | | | | | | X | | X | | 82 | |
| C2-0.4-W-S-5 | X | X | | | | | X | | | 82 | |
| C2-0.4-S-U-1-3 | X | X | | | | | | X | | 82 | 97.4 |
| C2-0.4-S-U-4 | | | | | | X | | X | | 82 | |
| C2-0.4-S-U-5 | X | X | | | | | X | | | 82 | |
| C2-0.4-S-S-1-3 | X | X | | | | | | X | | 82 | 97.8 |
| C2-0.4-S-S-4 | | | | | | X | | X | | 82 | |
| C2-0.4-S-S-5 | X | X | | | | | X | | | 82 | |
| C2-0.6-W-U-1-3 | X | X | | | | | | X | | 90 | 98.6 |
| C2-0.6-W-U-4 | | | | | | X | | X | | 90 | |
| C2-0.6-W-U-5 | X | X | | | | | X | | | 90 | |
| C2-0.6-W-S-1-3 | X | X | | | | | | X | | 90 | 99.6 |
| C2-0.6-W-S-4 | | | | | | X | | X | | 90 | |
| C2-0.6-W-S-5 | X | X | | | | | X | | | 90 | |
| C2-0.6-S-U-1-3 | X | X | | | | | | X | | 90 | 96.9 |
| C2-0.6-S-U-4 | | | | | | X | | X | | 90 | |
| C2-0.6-S-U-5 | X | X | | | | | X | | | 90 | |
| C2-0.6-S-S-1-3 | X | X | | | | | | X | | 90 | 97.6 |
| C2-0.6-S-S-4 | | | | | | X | | X | | 90 | |
| C2-0.6-S-S-5 | X | X | | | | | X | | | 90 | |

*) Specimens 1-3 for each type has been placed in one row since the handling of these are equal.

## 3.7 Test programme ER – experiments

### 3.7.1 Measurement techniques

These measurements were performed based upon three different principles. The methods are briefly described below, and a description of the equipment used for measurements is given in section 3.8.2.

Electrochemical Impedance Spectroscopy (EIS)

The basis of EIS is to impose an external sinusoidal voltage signal with low amplitude and varying frequency to the electrode/electrolyte system (i.e. the concrete). The current response of the system is measured. The relation between the imposed AC voltage signal and the current response describes the impedance for the system in the form of a real and imaginary component. For more information on Electrochemical Impedance Spectroscopy see Feliu and Feliu [70] and Macdonald [71].

Positive feedback

In order to perform this type of measurements the potentiostat needs to have an extra circuit (positive feedback loop). This circuit is normally used to compensate for the ohmic drop between RE and WE in polarisation experiments. The positive feedback loop allows control of the resistance of the concrete by changing the circuit potential feeding a constant alternating current (AC) force (the magnitude of the current and the frequency is dependent upon the range of electrical resistance). For the concretes used

in these experiments the current was in the range of 1 μA – 100μA. When the resistivity of the medium exceeds that of the positive feedback loop the AC current feed is picked up by an oscilloscope, and the resistance of the circuit can be calculated by Ohms law.

Square pulse measurements

The basis of potential square pulse measurements (or chronoamperometry) is to impose a controlled potential difference in steps (at a given frequency) to the working electrode. The potential difference may be in either positive or negative direction or both. The current response will then be minimally affected by capacitive effects in the medium, and the electrical resistance may easily be measured.

### 3.7.2 Description of the different runs in the ER experiments

In the ER – experimental part a total of four different runs have been carried out, each one trying to improve from the previous run. In the following a description of the different runs and their objectives is given.

It is important to note that during storage and sending the samples lost a significant amount of moisture, and most of the samples tested in Runs 1, 2 and 3 had a very low degree of capillary saturation (DCS < 50%).

Run 1

Run 1 was performed on three parallel samples for each of the four different conditionings and for both concrete mixes. A total of 24 specimens were tested. A list of the tested specimens is given in Table 3.10.

The temperatures investigated were 20 °C (room temperature), 2°C, -14 °C and -28 °C. The samples were stored for minimum 36 hours at each temperature before the measurements took place.

The EIS measurements were performed at frequencies in the range from 100 Hz up to 40 MHz. The amplitude was selected to 10 mV for the sinusoidal voltage signal after some initial testing. The resolution was selected to 401 different frequencies, which was the maximum resolution of the equipment.

In the thawing part, from -28 °C and back to 20 °C, the measurements of electrical resistance were performed using the positive feedback loop on a potentiostat as described in paragraph 3.7.1. No parallel measurements of EIS and Positive feedback were performed in this run.

*Table 3. 10 List of the tested specimens in Run 1*

| Specimen Id. | Measurement techniques* | | | | | | Moisture control | | | | | Age | DS |
|---|---|---|---|---|---|---|---|---|---|---|---|---|---|
| | EIS | | P.Feed | | P.Sq.P | | Weighing | | | Further | | | |
| | Freezing | Thawing | Freezing | Thawing | Freezing | Thawing | Start | End | During | Resaturation | Drying (105°C) | Start test [days] | Start test [%] |
| R1-0.4-W-S-1 | X | | | X | | | X | X | | X | X | 90 | 93.8 |
| R1-0.4-W-S-2 | X | | | X | | | X | X | | X | X | 90 | 95.6 |
| R1-0.4-W-S-3 | X | | | X | | | X | X | | X | X | 90 | 95.1 |
| R1-0.4-W-D-1 | X | | | X | | | X | X | | X | X | 90 | 63.7 |
| R1-0.4-W-D-2 | X | | | X | | | X | X | | X | X | 90 | 67.6 |
| R1-0.4-W-D-3 | X | | | X | | | X | X | | X | X | 90 | 66.2 |
| R1-0.4-S-S-1 | X | | | X | | | X | X | | X | X | 90 | 73.3 |
| R1-0.4-S-S-2 | X | | | X | | | X | X | | X | X | 90 | 73.4 |
| R1-0.4-S-S-3 | X | | | X | | | X | X | | X | X | 90 | 74.0 |
| R1-0.4-S-D-1 | X | | | X | | | X | X | | X | X | 90 | 55.5 |
| R1-0.4-S-D-2 | X | | | X | | | X | X | | X | X | 90 | 57.2 |
| R1-0.4-S-D-3 | X | | | X | | | X | X | | X | X | 90 | 53.6 |
| R1-0.6-W-S-1 | X | | | X | | | X | X | | X | X | 90 | 96.0 |
| R1-0.6-W-S-2 | X | | | X | | | X | X | | X | X | 90 | 98.0 |
| R1-0.6-W-S-3 | X | | | X | | | X | X | | X | X | 90 | 98.2 |
| R1-0.6-W-D-1 | X | | | X | | | X | X | | X | X | 90 | 48.9 |
| R1-0.6-W-D-2 | X | | | X | | | X | X | | X | X | 90 | 44.1 |
| R1-0.6-W-D-3 | X | | | X | | | X | X | | X | X | 90 | 45.3 |
| R1-0.6-S-S-1 | X | | | X | | | X | X | | X | X | 90 | 61.2 |
| R1-0.6-S-S-2 | X | | | X | | | X | X | | X | X | 90 | 68.8 |
| R1-0.6-S-S-3 | X | | | X | | | X | X | | X | X | 90 | 71.7 |
| R1-0.6-S-D-1 | X | | | X | | | X | X | | X | X | 90 | 31.0 |
| R1-0.6-S-D-2 | X | | | X | | | X | X | | X | X | 90 | 32.1 |
| R1-0.6-S-D-3 | X | | | X | | | X | X | | X | X | 90 | 31.9 |

*) EIS: Electrochemical Impedance Spectroscopy, P.Feed: Positive Feedback
P.Sq.P: Potential Square Pulse (Chronoamperometry)

Run 2

In order to investigate the reliability of the measurement techniques a small series of samples was run through the temperature cycle. Eight specimens in total representing all conditionings for both concretes were tested. Parallel measurements with both EIS and Positive feedback measurements were carried out on both freezing and thawing. Additionally, two samples (R2-0.4-W-S-2 and R2-0.6-W-S-2) were resaturated using vacuum from their initial "dry state" and tested through the temperature cycle. These samples were added in order to observe prospective ice-nucleation.

The measurements were performed in the same way as Run 1. The only difference from Run 1 was that a lower resolution, 99 different frequencies, was chosen for the EIS measurements. Run 1 showed that disturbance from external sources was not an excessive problem. A list of the 10 tested specimens is given in Table 3.11.

*Table 3. 11 List of the tested specimens in Run 2*

| Specimen Id. | Measurement techniques* | | | | | | Moisture control | | | | | Age | DS** |
|---|---|---|---|---|---|---|---|---|---|---|---|---|---|
| | EIS | | P.Feed | | P.Sq.P | | Weighing | | | Further | | | |
| | Freezing | Thawing | Freezing | Thawing | Freezing | Thawing | Start | End | During | Resaturation | Drying (105°C) | Start test [days] | Start test [%] |
| R2-0.4-W-S-1 | X | X | X | X | | | X | X | | | | 120 | 76.0 |
| R2-0.4-W-S-2 | X | X | X | X | | | X | X | | | | 110 | 99.0 |
| R2-0.4-W-D-1 | X | X | X | X | | | X | X | | | | 120 | 72.0 |
| R2-0.4-S-S-1 | X | X | X | X | | | X | X | | | | 120 | 76.0 |
| R2-0.4-S-D-1 | X | X | X | X | | | X | X | | | | 120 | 71.0 |
| R2-0.6-W-S-1 | X | X | X | X | | | X | X | | | | 120 | 58.0 |
| R2-0.6-W-S-2 | X | X | X | X | | | X | X | | | | 110 | 99.0 |
| R2-0.6-W-D-1 | X | X | X | X | | | X | X | | | | 120 | 54.0 |
| R2-0.6-S-S-1 | X | X | X | X | | | X | X | | | | 120 | 63.0 |
| R2-0.6-S-D-1 | X | X | X | X | | | X | X | | | | 120 | 60.0 |
| *) EIS: Electrochemical Impedance Spectroscopy, P.Feed: Positive Feedback P.Sq.P: Potential Square Pulse (Chronoamperometry) | | | | | | | | | | | | | |
| **) Estimated moisture content based on data from Run 1 | | | | | | | | | | | | | |

Run 3

After finishing Run 2 in Madrid, the samples were sent back to Norway for further investigations. During the sending and storage after arrival most of the samples have had significant moist losses. It was then decided to perform a run with samples having the lower moisture contents. From a scientific point of view these low moisture states are of special interest.

The chamber used in the CRR experiments was programmed to the same temperature cycle as the previously performed ER – runs. A series of three parallel samples of each type, a total of 24 samples, were run through the

temperature cycle. In this run the measurement technique was potential square pulse measurements using handheld equipment. A list of the 24 tested specimens is given in Table 3.12.

*Table 3. 12 List of the specimens tested in Run 3*

| Specimen Id. | Measurement techniques* | | | | | | Moisture control | | | | | Age | DS |
|---|---|---|---|---|---|---|---|---|---|---|---|---|---|
| | EIS | | P.Feed | | P.Sq.P | | Weighing | | | Further | | | |
| | Freezing | Thawing | Freezing | Thawing | Freezing | Thawing | Start | End | During | Resaturation | Drying (105°C) | Start test [days] | Start test [%] |
| R3-0.4-W-S-1 | | | | | X | X | X | X | X | X | X | 350 | 70.9 |
| R3-0.4-W-S-2 | | | | | X | X | X | X | X | X | X | 350 | 73.4 |
| R3-0.4-W-S-3 | | | | | X | X | X | X | X | X | X | 350 | 76.2 |
| R3-0.4-W-D-1 | | | | | X | X | X | X | X | X | X | 350 | 64.8 |
| R3-0.4-W-D-2 | | | | | X | X | X | X | X | X | X | 350 | 66.1 |
| R3-0.4-W-D-3 | | | | | X | X | X | X | X | X | X | 350 | 66.1 |
| R3-0.4-S-S-1 | | | | | X | X | X | X | X | X | X | 350 | 62.1 |
| R3-0.4-S-S-2 | | | | | X | X | X | X | X | X | X | 350 | 65.2 |
| R3-0.4-S-S-3 | | | | | X | X | X | X | X | X | X | 350 | 66.1 |
| R3-0.4-S-D-1 | | | | | X | X | X | X | X | X | X | 350 | 56.6 |
| R3-0.4-S-D-2 | | | | | X | X | X | X | X | X | X | 350 | 55.3 |
| R3-0.4-S-D-3 | | | | | X | X | X | X | X | X | X | 350 | 57.6 |
| R3-0.6-W-S-1 | | | | | X | X | X | X | X | X | X | 350 | 47.6 |
| R3-0.6-W-S-2 | | | | | X | X | X | X | X | X | X | 350 | 50.9 |
| R3-0.6-W-S-3 | | | | | X | X | X | X | X | X | X | 350 | 51.9 |
| R3-0.6-W-D-1 | | | | | X | X | X | X | X | X | X | 350 | 42.0 |
| R3-0.6-W-D-2 | | | | | X | X | X | X | X | X | X | 350 | 41.8 |
| R3-0.6-W-D-3 | | | | | X | X | X | X | X | X | X | 350 | 41.9 |
| R3-0.6-S-S-1 | | | | | X | X | X | X | X | X | X | 350 | 45.6 |
| R3-0.6-S-S-2 | | | | | X | X | X | X | X | X | X | 350 | 46.2 |
| R3-0.6-S-S-3 | | | | | X | X | X | X | X | X | X | 350 | 46.6 |
| R3-0.6-S-D-1 | | | | | X | X | X | X | X | X | X | 350 | 37.4 |
| R3-0.6-S-D-2 | | | | | X | X | X | X | X | X | X | 350 | 37.4 |
| R3-0.6-S-D-3 | | | | | X | X | X | X | X | X | X | 350 | 37.8 |

*) EIS: Electrochemical Impedance Spectroscopy, P.Feed: Positive Feedback
P.Sq.P: Potential Square Pulse (Chronoamperometry)

Run 4

The same samples tested in Run 3 were resaturated by water suction for more than 50 days. The motivation of running the same samples as in Run 3 at much higher moisture contents was to observe directly the effect of moisture content in combinations with thermal effects. The specimens were given unique identification still being physically the same samples as tested in Run 3.

The specimens immersed in water for 8 weeks to ensure more or less stable conditions in the pore solution chemistry. The control was performed by measurements of the electrical resistivity. A variation less than ± 5% was set as the limit for acceptable stability. This took 8 weeks to achieve.

After achieving an acceptable level of stability the samples were sealed and run through the same temperatures as the previous runs. The measurements were performed by potential square pulse measurements.

A list of the tested specimens for Run 4 is given in Table 3.13.

*Table 3. 13 List of the tested specimens in Run 4*

| Specimen Id. | Measurement techniques* | | | | | | Moisture control | | | | | Age | DS |
|---|---|---|---|---|---|---|---|---|---|---|---|---|---|
| | EIS | | P.Feed | | P.Sq.P | | Weighing | | | Further | | | |
| | Freezing | Thawing | Freezing | Thawing | Freezing | Thawing | Start | End | During | Resaturation | Drying (105°C) | Start test [days] | Start test [%] |
| R4-0.4-W-Sr-1 | | | | | X | X | X | X | X | X | X | 350 | 99.6 |
| R4-0.4-W-Sr-2 | | | | | X | X | X | X | X | X | X | 350 | 99.6 |
| R4-0.4-W-Sr-3 | | | | | X | X | X | X | X | X | X | 350 | 99.7 |
| R4-0.4-W-Dr-1 | | | | | X | X | X | X | X | X | X | 350 | 99.7 |
| R4-0.4-W-Dr-2 | | | | | X | X | X | X | X | X | X | 350 | 100.0 |
| R4-0.4-W-Dr-3 | | | | | X | X | X | X | X | X | X | 350 | 99.8 |
| R4-0.4-S-Sr-1 | | | | | X | X | X | X | X | X | X | 350 | 99.4 |
| R4-0.4-S-Sr-2 | | | | | X | X | X | X | X | X | X | 350 | 99.6 |
| R4-0.4-S-Sr-3 | | | | | X | X | X | X | X | X | X | 350 | 99.7 |
| R4-0.4-S-Dr-1 | | | | | X | X | X | X | X | X | X | 350 | 99.9 |
| R4-0.4-S-Dr-2 | | | | | X | X | X | X | X | X | X | 350 | 99.7 |
| R4-0.4-S-Dr-3 | | | | | X | X | X | X | X | X | X | 350 | 99.7 |
| R4-0.6-W-Sr-1 | | | | | X | X | X | X | X | X | X | 350 | 99.0 |
| R4-0.6-W-Sr-2 | | | | | X | X | X | X | X | X | X | 350 | 98.7 |
| R4-0.6-W-Sr-3 | | | | | X | X | X | X | X | X | X | 350 | 98.9 |
| R4-0.6-W-Dr-1 | | | | | X | X | X | X | X | X | X | 350 | 98.7 |
| R4-0.6-W-Dr-2 | | | | | X | X | X | X | X | X | X | 350 | 99.3 |
| R4-0.6-W-Dr-3 | | | | | X | X | X | X | X | X | X | 350 | 98.6 |
| R4-0.6-S-Sr-1 | | | | | X | X | X | X | X | X | X | 350 | 99.0 |
| R4-0.6-S-Sr-2 | | | | | X | X | X | X | X | X | X | 350 | 99.0 |
| R4-0.6-S-Sr-3 | | | | | X | X | X | X | X | X | X | 350 | 98.6 |
| R4-0.6-S-Dr-1 | | | | | X | X | X | X | X | X | X | 350 | 98.8 |
| R4-0.6-S-Dr-2 | | | | | X | X | X | X | X | X | X | 350 | 99.0 |
| R4-0.6-S-Dr-3 | | | | | X | X | X | X | X | X | X | 350 | 98.8 |

*) EIS: Electrochemical Impedance Spectroscopy, P.Feed: Positive Feedback
P.Sq.P: Potential Square Pulse (Chronoamperometry)

Run 5

Run 5 was performed on two parallel samples for each of the four different conditionings and for both concrete mixes. A total of 16 specimens were tested. The specimens had not been put through any temperature cycle. The change of the electric resistance during resaturation and stabilisation were followed using potential square pulse measurements. All measurements have been performed at room temperature (at 20°C ± 1°C).

### 3.7.3 Moisture content

In Tables 3.10 – 3.13 the moisture control steps are shown for each run. The moisture control of the specimens was conducted by weighing before and after the experiments in all the runs. In runs 3 and 4 the samples were additionally weighed during testing to control whether or not the samples had larger moist loss at certain temperatures.

Resaturation of the specimens by immersion in tap water was performed in runs 1, 3 and 4. In addition to the supplementary Run 5 where moisture control was the main objective. In runs 3 and 4 the specimens were pressurised (at 50bar for approximately 3 days). After pressurisation the specimens in runs 3 and 4 were weighed in water in order to obtain the volume and, hence, enable porosity calculations. It is important to note that an absolute concrete volume, however, can not be found since the volumes of the electrodes are unknown. It is assumed that that this introduces an error less than 1%.

For runs 1, 3 and 4 the specimens were dried at 105°C for at least 96 hours to ensure that the dry weights of the specimens were as correct as possible.

## 3.8 Experimental setup

### 3.8.1 Experimental setup for CRR – experiments

The experimental system involves a chamber that generates temperatures in the range -40°C <T<+40°C, potentiostats that polarise cathodically in the range 0<E<-1.2V and equipment recording the current generated in the cell. Each parts of this will be separately described in the following. A picture of the experimental setup is shown in Figure 3.9.

Temperature chamber

The chamber with external dimensions 1250x2500x500 mm (width by length by height) is made of coated steel elements with polyurethane insulation. The chamber was manufactured especially for this project by PREPAN. The chamber can be opened from the top in all its length and width to ensure easy placing and handling of the specimens.

To provide cooling and heating an external compressor in combination with an internal heat exchanger was used. The heat exchanger was equipped with two powerful fans which ensured a good airflow inside the chamber. A heating element was also used to be able to provide higher temperatures than of the external surroundings. The system was designed to freeze down 200kgs of concrete to -40°C within 24 hours. The capacity

of thawing was ensured by a heating element of 1.5 kW mounted in the heat exchanger.

The system was controlled by a control system (DX9000 by Johnson Controls). This unit gives the opportunity to programme any temperature cycle within the cooling systems capacity.

The generator and heat-exchanger was supplied by TEAS. The planning was performed in cooperation with NTNU.

*Figure 3. 9 Picture of the Temperature chamber with cabling system*

Potentiostats

The potentiostats were especially made for this project (Protector POT50). A set of 50 equal potentiostats was manufactured with a common power supply. The potentiostats could be adjusted individually to a desired potential in the range $1.2 < E_{app} < -1.2$ V. All adjustments of the potential were performed manually. To control the adjustments the potentials were measured with a handheld Digital multi meter (Fluke 87 II) on the signal out contacts for each potentiostat.

Logging units

The logging equipment consisted of a SOLARTRON 3530 ORION data logger and a personal computer. The logging intervals were set to 30 minutes. A low scan rate was chosen (1/40 second per channel) in order to get optimal resolution based on interpolation of 5 individual measurements per channel.

### 3.8.2 Experimental setup for the ER – experiments

The experimental setup for this section contains several different measurement techniques. Descriptions of the techniques were given in section 3.7.1.

Temperature chamber

An ordinary refrigerator was used. (Miele KD 6452 S) The freezer part had the capacity to freeze down all the samples to -38°C within 24 hours. Due to the load on the compressor a minimum temperature of -28°C was chosen. The highest temperature available for the freezer part was -14°C. On maximum the refrigerator had capacity to keep a temperature of 2°C. Based on these facts four temperatures were chosen: 20°C, 2°C, -14°C and -28°C.

Electrochemical Impedance Spectroscopy equipment.

The experimental setup for this type of measurements consists of a measurement unit (HP 4194A Measurement unit), a impedance/gain-phase analyzer (HP 4194A Impedance/Gain-Phase Analyser) and a personal computer. This equipment has a frequency range from 100 Hz – 40 MHz. The measurements were performed in the whole range. In the initial run the highest possible resolution was chosen, 401 different frequencies, which gave an overall picture of the impedance of the concrete samples. Due to technical problems with handling such amounts of data, a lower resolution of 99 different frequencies were chosen for the later measurements.

A picture of the setup is given in Figure 3.10.


*Figure 3. 10 Picture of the equipment for the EIS measurements*

Positive feedback/Ohmic drop equipment

The measuring equipment for these types of measurements consisted of a potentiostat (AMEL – 551 – POTENTIOSTAT) and an oscilloscope (Kenwood CO-1303-D). All data recording was performed manually.

A picture of the setup is given in Figure 3.11.

*Figure 3. 11 Picture of the setup used for ohmic drop measurements*

Potential square pulse equipment

For these measurements a handheld LCR-meter (ESCORT ELC – 131D) was used. The measurements were all performed on a constant frequency at 1 kHz. All data recording was performed manually.

## 3.9 Determination of freezeable water, $w_f$, in concrete

To quantify the amount of water able to freeze in the pores of the respective concretes, testing with low temperature calorimetry was performed at Aalborg Portland in Denmark.

Small concrete specimens were sawn from well cured concrete cubes of both the w/b 0.4 and the w/b 0.6 concrete. The concretes were of approximately 600 days of age when the preparation of the specimens took place and had been water cured since casting.

After sawing the specimens were ground to dimensions:
d ≈15mm, l ≈ 70mm to fit in an air-tight cylindrical formed stainless steel test cell slightly larger than the specimens. The specimens were immersed in water for a few hours then sealed in airtight plastic bags, packed and sent to Denmark for testing.

The heat flow was measured using a low temperature CALVET Micro-calorimeter. The measurements were carried out in a scanning mode in the temperature range down to about -55°C where no further freezing is expected below this temperature. The cooling rate was approximately 3.3°C/h and the heating rate approximately 4.1°C/h.

# 4

# TEMPERATURE EFFECTS ON CATHODIC REACTION RATE

*This chapter gives a detailed description of the experimental results obtained in the investigation of the influence of temperature on the Cathodic Reaction Rate (CRR – experiments).*

## 4.1 Introduction

The CRR – experiments were carried out to investigate the effect of temperature and moisture on corrosion of steel in concrete. The experiments were performed on concrete specimens with a three electrode system (WE, CE and RE) in the temperature range $-40°C \leq T \leq 40°C$. The WE was continuously polarised at -0.6 V/MMO.

Information about the cathodic behaviour of steel in concrete gives basic knowledge in order to give a better forecast of the corrosion behaviour of steel in concrete.

## 4.2 Low temperature calorimetry – determination of frozen capillary water

When concrete is exposed to temperatures as low as -40°C some of the capillary water will freeze. Therefore it was performed low temperature calorimetry to determine the amount of water able to freeze in the tested concretes.

The recorded heat flow in concrete specimens that was measured during cooling and heating for the w/b 0.4 and the w/b 0.6 concretes are shown in Figure 4. 1 and Figure 4. 2.

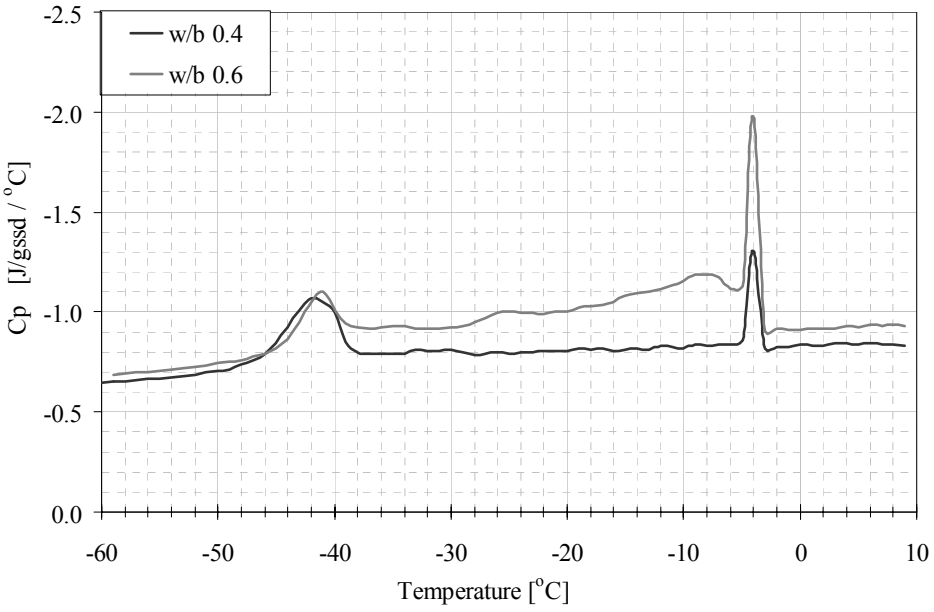


*Figure 4. 1 Heat flow during cooling for mature water cured concrete specimens of the w/b 0.4 and w/b 0.6 concrete. Cool 3.3°C/h.*

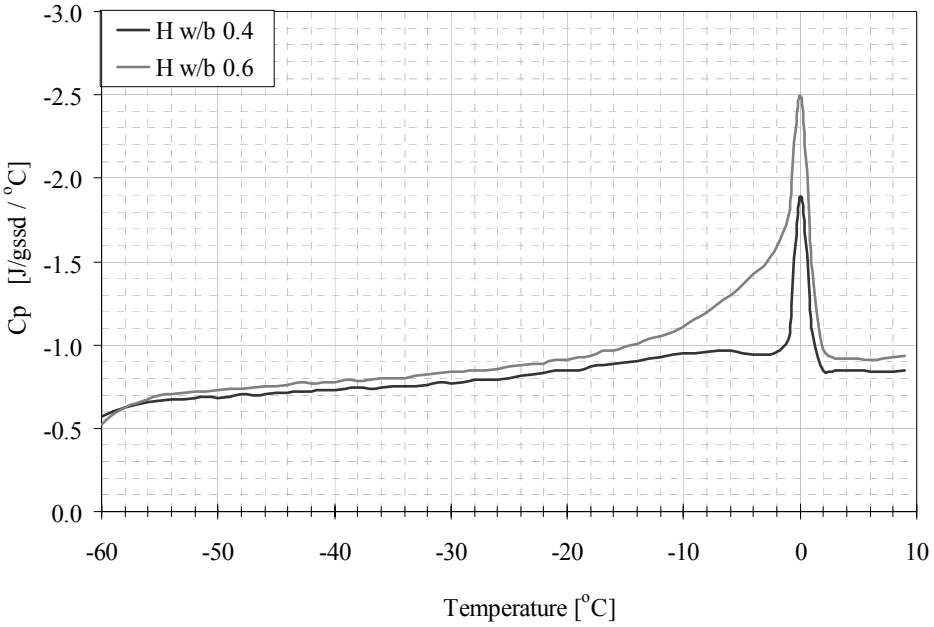


*Figure 4. 2 Heat flow during heating for mature water cured concrete specimens of the w/b 0.4 and w/b 0.6 concrete. Heat 4.1°C/h.*

*Table 4. 1 Relevant concrete properties for calculations of the amount of ice in the capillary pores*

| | w/b 0.4 | w/b 0.6 | |
|---|---|---|---|
| $Density_{ssd}$ | 2.394 | 2.313 | $[g_{ssd}/cm^3]$ |
| Evaporable water, $w_{es}$ | 0.056 | 0.080 | $[g/g_{dry}]$ |
| Porosity, ε | 12.7 | 17.2 | [(vol) %] |
| $Density_{dry}$ | 2.267 | 2.141 | $[g_{dry}/cm^3]$ |
| $Density_{solid}$ | 2.401 | 2.328 | $[g_{solid}/cm^3]$ |
| ssd = saturated surface dry | | | |

The calculated amounts of ice based on the heat flow data and the concrete properties, shown in Table 4. 1, are given in Table 4. 2 and Table 4. 3 for the w/b 0.4 and w/b 0.6 concrete, respectively.

*Table 4. 2 Amount of ice at specific temperatures during Cool and Heat for the w/b 0.4 concrete*

| COOL Increment | | | | |
|---|---|---|---|---|
| Temperature | Amount of ice | | $w_{nf}$ | $w_{nf}/w_{es}$ |
| [°C] | [mg/g$_{ssd}$] | [mg/g$_{dry}$] | [g/g$_{dry}$] | |
| -2 | 0.000 | 0.000 | 0.056 | 1.000 |
| -10 | 2.574 | 2.718 | 0.053 | 0.951 |
| -20 | 3.704 | 3.911 | 0.052 | 0.930 |
| -35 | 6.571 | 6.938 | 0.049 | 0.876 |
| -55 | 17.061 | 18.013 | 0.038 | 0.677 |
| HEAT Increment | | | | |
| Temperature | Amount of ice | | $w_{nf}$ | $w_{nf}/w_{es}$ |
| [°C] | [mg/g$_{ssd}$] | [mg/g$_{dry}$] | [g/g$_{dry}$] | |
| -55 | 17.071 | 18.025 | 0.038 | 0.677 |
| -35 | 15.911 | 16.800 | 0.039 | 0.699 |
| -20 | 12.538 | 13.238 | 0.043 | 0.763 |
| -10 | 8.099 | 8.551 | 0.047 | 0.847 |
| 4 | 0.000 | 0.000 | 0.056 | 1.000 |

$w_{nf}$ = *non frozen water*

*Table 4. 3 Amount of ice at specific temperatures during Cool and Heat for the w/b 0.6 concrete*

| COOL Increment | | | | |
|---|---|---|---|---|
| Temperature | Amount of ice | | $w_{nf}$ | $w_{nf}/w_{es}$ |
| [°C] | [mg/g$_{ssd}$] | [mg/g$_{dry}$] | [g/g$_{dry}$] | |
| -3 | 0.000 | 0.000 | 0.080 | 1.000 |
| -10 | 7.634 | 8.246 | 0.072 | 0.897 |
| -20 | 14.127 | 15.259 | 0.065 | 0.810 |
| -35 | 21.521 | 23.245 | 0.057 | 0.710 |
| -55 | 30.277 | 32.703 | 0.047 | 0.592 |
| HEAT Increment | | | | |
| Temperature | Amount of ice | | $w_{nf}$ | $w_{nf}/w_{es}$ |
| [°C] | [mg/g$_{ssd}$] | [mg/g$_{dry}$] | [g/g$_{dry}$] | |
| -55 | 35.080 | 37.891 | 0.042 | 0.527 |
| -35 | 34.156 | 36.893 | 0.043 | 0.540 |
| -20 | 29.287 | 31.634 | 0.048 | 0.605 |
| -10 | 22.492 | 24.295 | 0.056 | 0.697 |
| 4 | 0.000 | 0.000 | 0.080 | 1.000 |

The results given in Table 4. 2 and Table 4. 3 are shown graphically in Figure 4. 3.

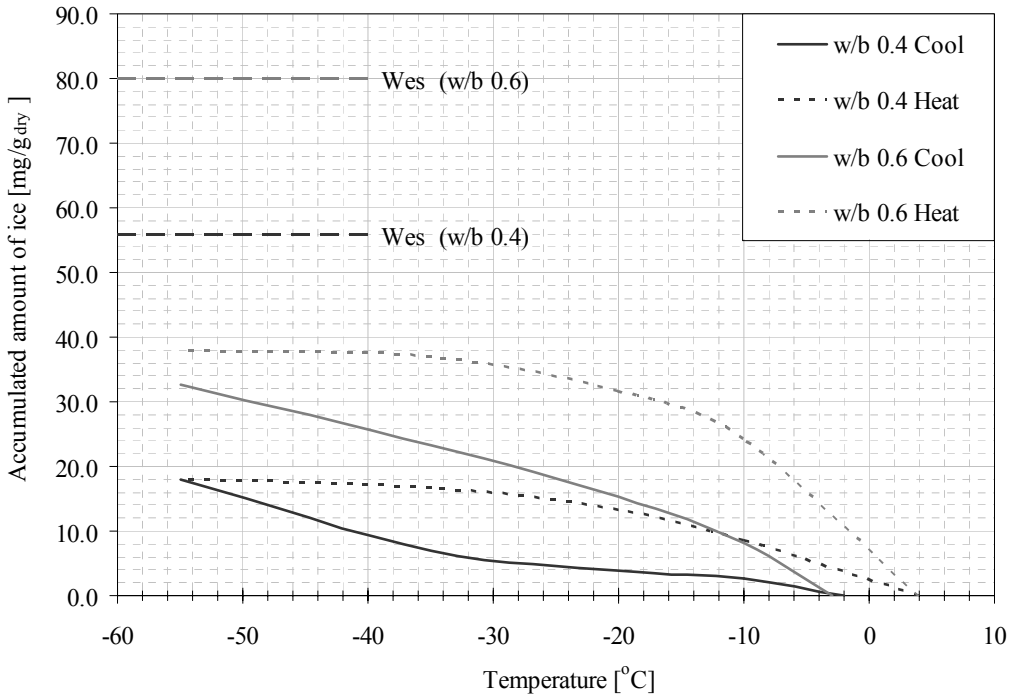


*Figure 4. 3 Accumulative ice formation ($w_f$) curves for the w/b 0.4 and w/b 0.6 concretes for cooling and heating increments. The horizontal long dashed lines indicate total evaporable water content ($w_{es}$) for the concretes.*

The results are discussed in the following sections.

## 4.3 Stability of measurements and choice of steady state

An effort was made in the planning of the CRR – experiments to ensure stability of the measurements. The stability of measurements was controlled by the time for stabilisation of the cell current (transient period) generated by temperature changes within an acceptable range.

### 4.3.1 Transients of the cathodic reaction rate due to temperature changes.

During Run 1 the transients for each temperature change was followed closely in order to define a level of satisfactory stability of measurements. It was expected a certain amount of drift in the measurements and particularly the first temperature changes was interesting with respect to time for stable conditions. The response of the cathodic reaction rate on the first temperature change is given in Figure 4. 4. All the temperatures are referred to operating temperatures in the chamber in the descriptions of the Figures.

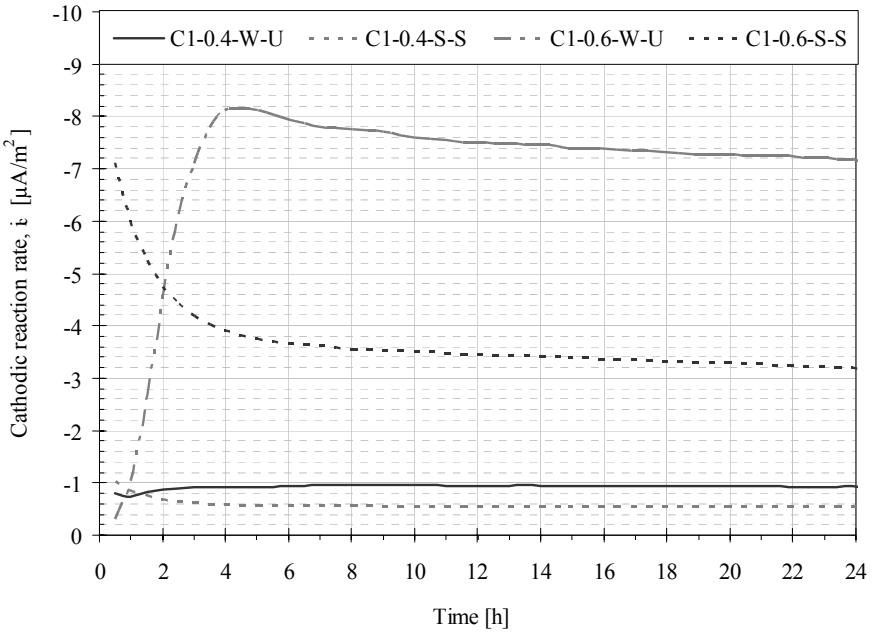


*Figure 4. 4 Response of the cathodic reaction rate on the first temperature change during the start-up of Run 1 at 0°C*

Figure 4. 4 shows the response of the cathodic reaction current on the temperature change for the tested specimens at constant polarisation (-0.6 V/MMO) for the first 24 hours of the experiments. The chamber had an initial temperature of 10°C (at start-up), and the programmed temperature was 0°C. The temperature in the chamber was decreased rapidly and generated a large temperature induced transient on the cell current. The temperature shift for this step was larger (10°C) compared to the later ones (5°C change). The corresponding temperature – time curve for the first temperature change is given in Figure 4. 5. The samples were polarised for about 5 – 10 minutes before the first measurements were taken. Some of the alteration in the thermal response on the cathodic

reaction rate may be connected to the lag between concrete temperature and the operating temperature in the chamber.

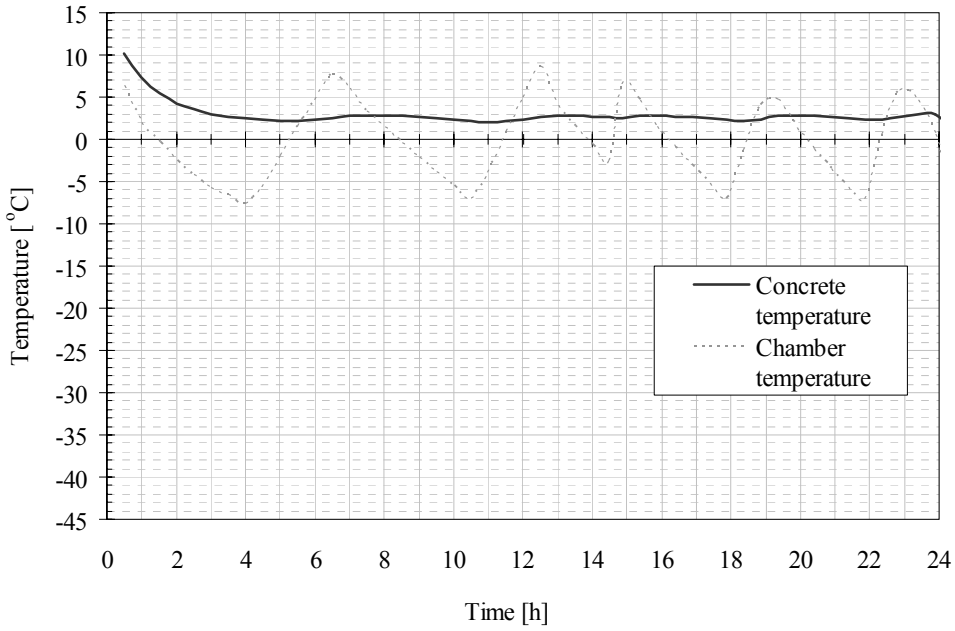


*Figure 4. 5 The temperature – time curve corresponding to the thermal response of the cathodic reaction rate (Figure 4. 4)*

The relative large thermal transients in the first temperature shifts were considerably reduced at decreasing temperatures. In the following Figures (Figure 4. 6 – Figure 4. 14) the transient for lower temperatures are shown, both for the freezing interval and for the thawing interval.

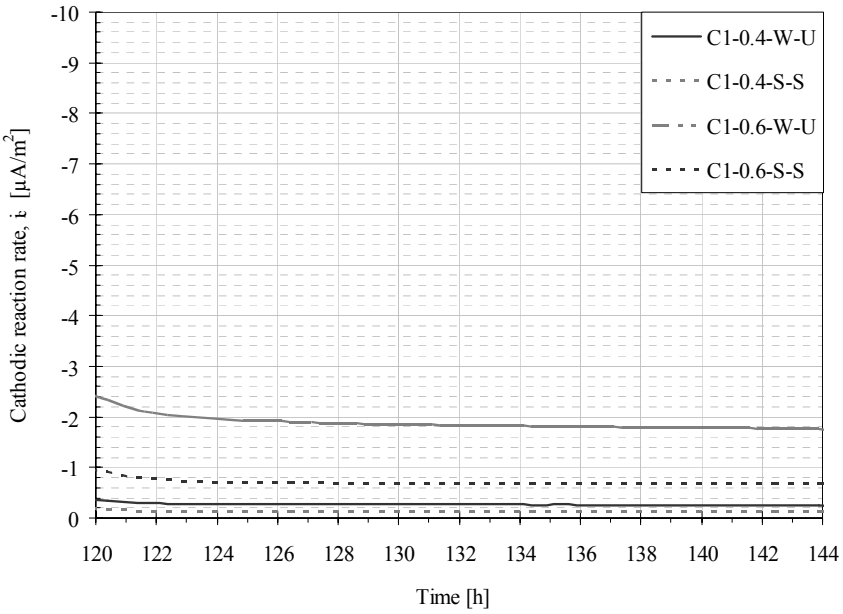


*Figure 4. 6 The thermal response on the cathodic reaction rate during Freezing at -20°C*

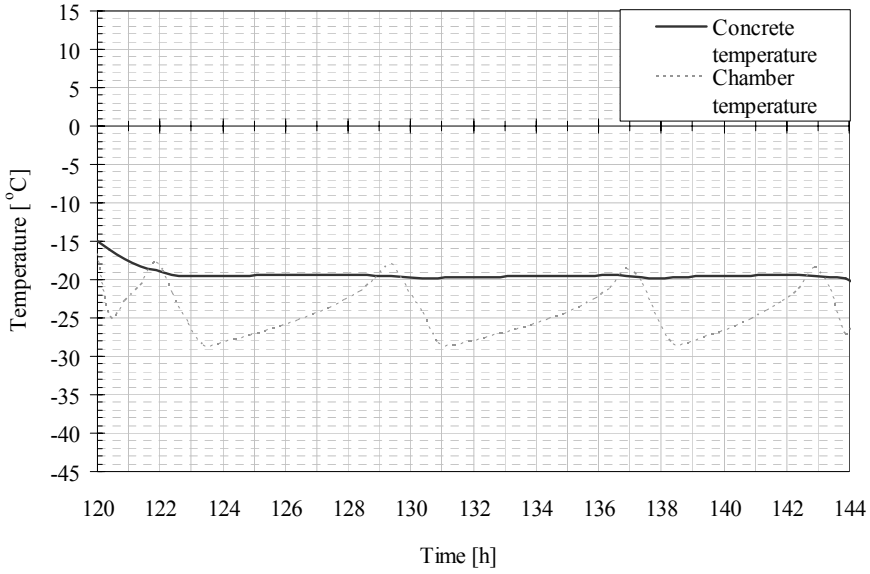


*Figure 4. 7 The temperature – time curve corresponding to Figure 4. 6*

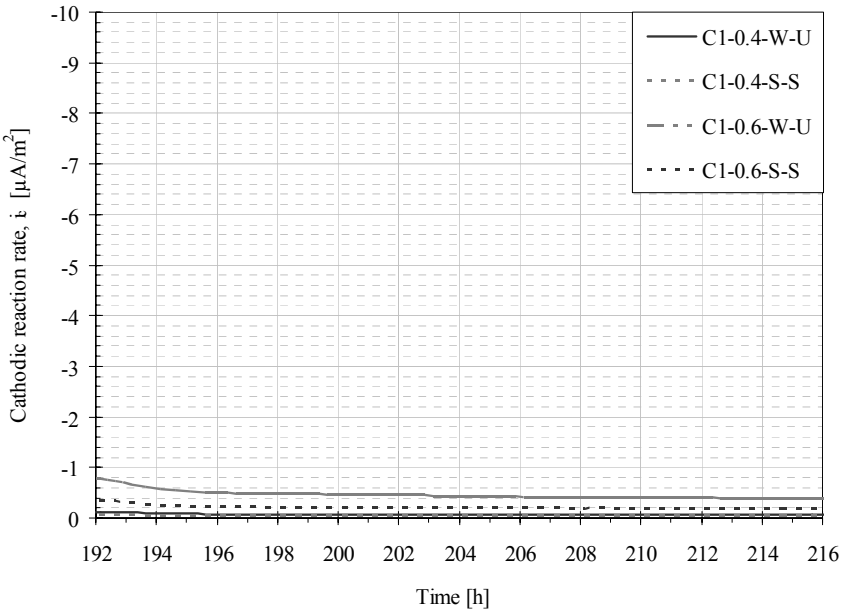


*Figure 4. 8 The thermal response on the cathodic reaction rate during Freezing at -40°C*

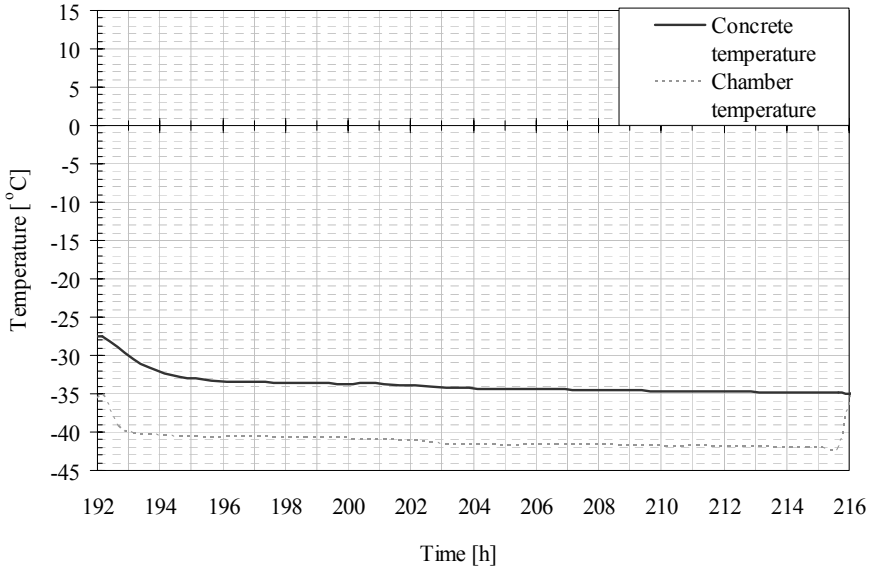


*Figure 4. 9 The temperature – time curve corresponding to Figure 4. 8*

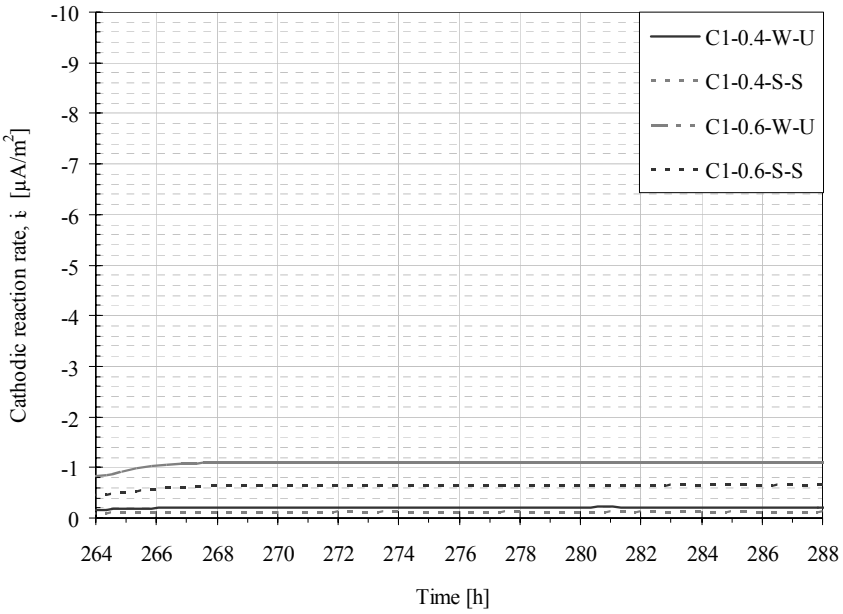


*Figure 4. 10 The thermal response on the cathodic reaction rate during Thawing at -20°C*

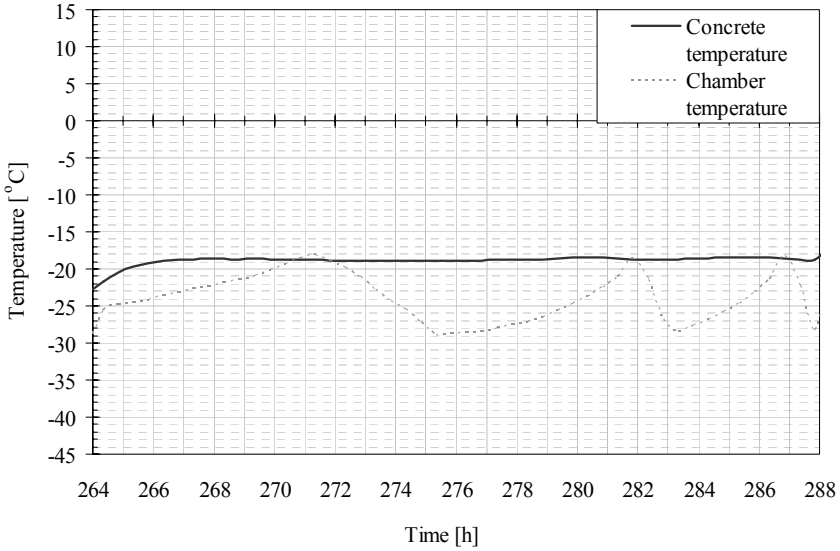


*Figure 4. 11 The temperature – time curve corresponding to Figure 4. 10*

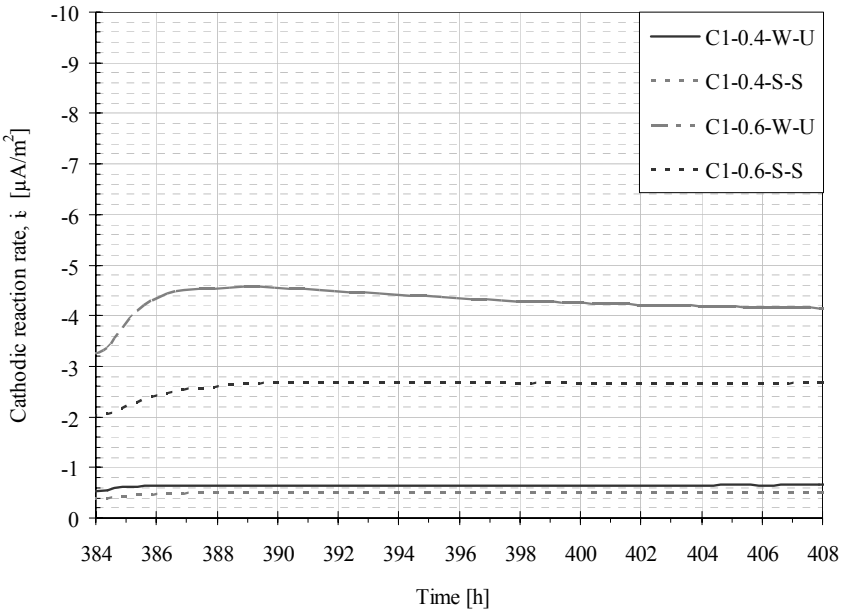


*Figure 4. 12 The thermal response on the cathodic reaction rate during Thawing at 0°C*

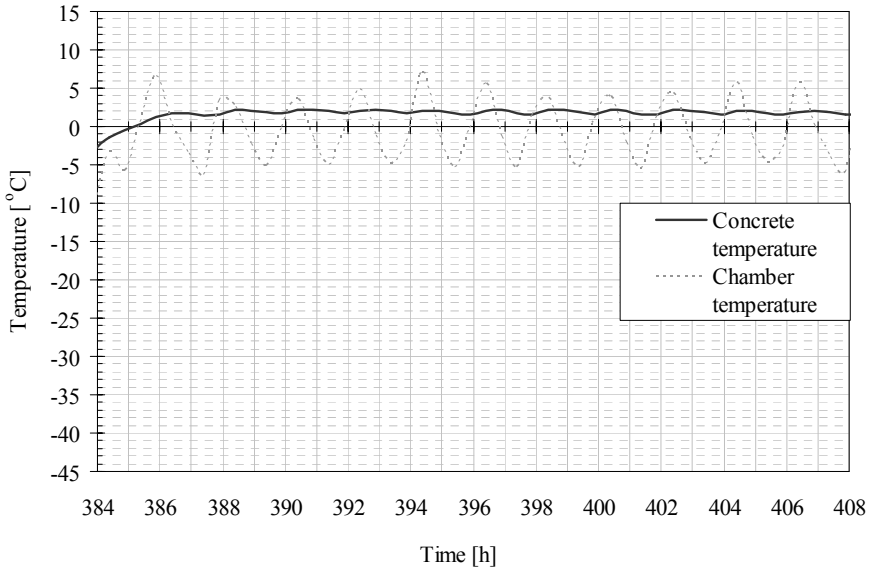


*Figure 4. 13 Temperature – time curve corresponding to Figure 4. 12*

After the completion of the temperature intervals: Freezing and Thawing, the samples were kept at 0°C for a period of more than 200 hours in order to observe long term changes in the system. The results are shown in Figure 4. 14.

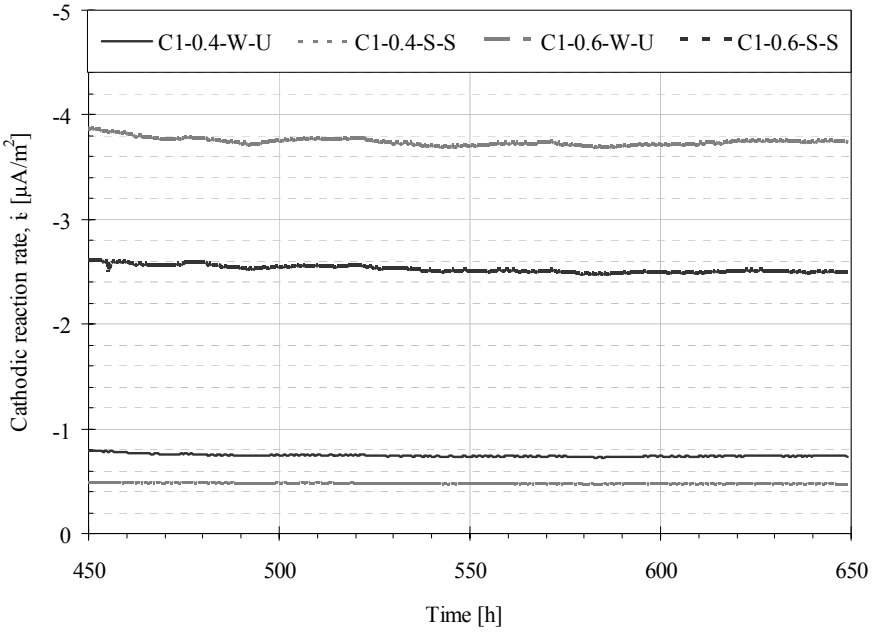


*Figure 4. 14 The long term effects of polarisation of -0.6 V/MMO during the Stable temperature interval (0°C) of Run 1*

### 4.3.2 Choice of steady state for the CRR – experiments

Based on the results given in section 4.3.1 it could be defined a range in which a "quasi steady state" could be defined after a temperature step. The "quasi steady state" was chosen to the average of the last 4 hours of measurements before the next temperature step and ignoring the first 20 hours of measurements. The logging interval was every 30 minutes. Hence, the averaged cell current of the last 8 measurements at each temperature step was defined as one "steady state" measurement.

The thorough control of the thermal response on the cathodic reaction rate were primarily performed during Freezing and Thawing of Run 1, and monitored in the later intervals of Run 1 and also in Run 2. The results show the same trend for both runs.

It was found that it was significantly harder to change the temperature in the samples at lower temperature. The effect can be found in Figure 4. 9 and Figure 4. 15.

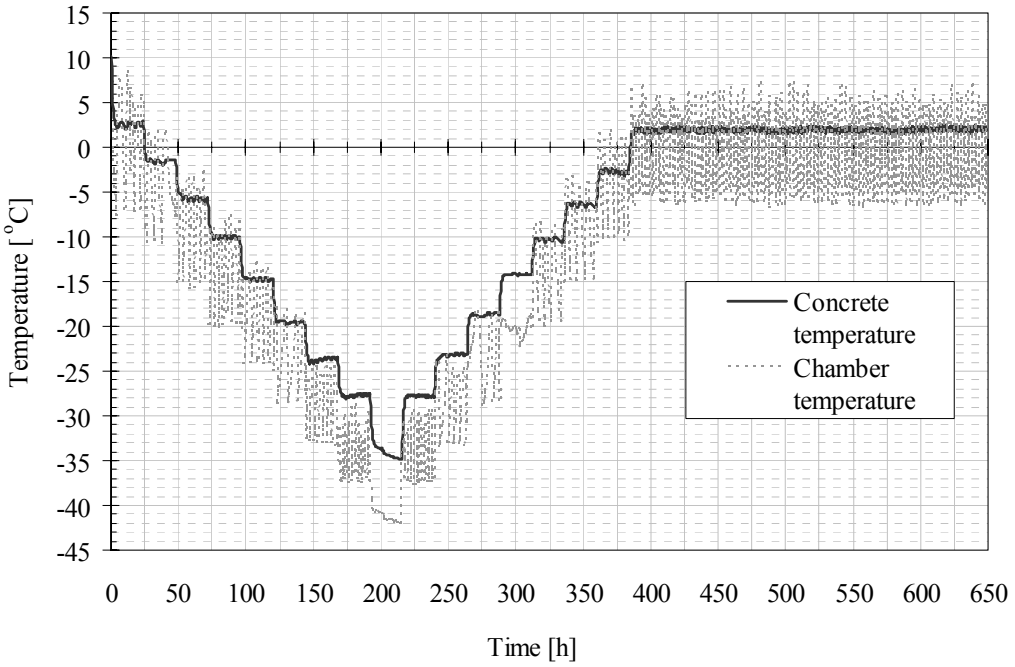


*Figure 4. 15 Comparison of the concrete temperature and the chamber temperature during freezing, thawing and stable temperature intervals of Run 1*

The minimum concrete temperature was measured to -34.9 °C, despite the minimum temperature in the chamber was measured to below -42 °C. This lack of temperature equilibrium (i.e. slow specimen cooling) may partly be due to ice formation in the capillaries. Ice nucleation generates heat.

From section 4.2 it can be found that a temperature of -35°C corresponds to amounts of frozen water, $w_f/w_{es}$ = 12.4% for the w/b 0.4 concrete and $w_f/w_{es}$ = 29.0% for the w/b 0.6 concrete. Both concretes (when saturated)

show a heat flow peak in the range from -35°C and lower during cooling (Figure 4. 1), which indicates that a considerable fraction of pores nucleate around this temperature.

The effect of water freezing in the pores may have induced the larger lag between concrete temperature and chamber temperature at the lowest temperatures.

During Run 1 an active temperature sensor was used to control the temperature inside the chamber. This high precision temperature sensor reacted too slowly, hence, the temperature fluctuations were unnecessary large. This was upgraded to a much faster reacting passive temperature sensor in Run 2. This run showed that the faster sensor reduced this problem.

The stability of the reference electrode was tested against a $MnO_2$ reference electrode at various temperatures in order to have an impression of the stability. These experiments were performed on mortar specimens that were well cured at 100% RH for 3 months before the test was initiated.

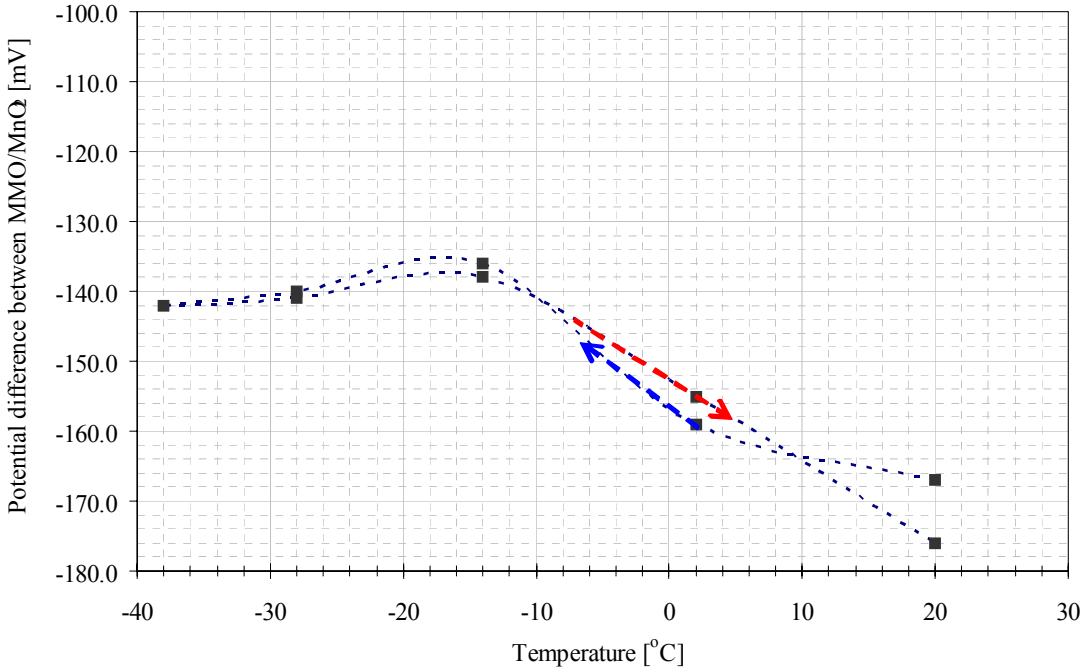


*Figure 4. 16 Stability of the potential difference between an ATM (MMO) reference electrode and a $MnO_2$ reference electrode at various temperatures. The data represents a single specimen.*

The results from the comparison of the reference electrodes indicate that either one or both electrodes show a thermal change. Since no parallel measurements were performed it is not possible to extract which electrode that is most temperature sensitive. The change of the potential difference between the reference electrodes was approximately 0.03 V in the temperature interval between 20°C and -20°C.

Based on the fact that the CRR – experiments showed relatively stable values and that a limited number of alternative reference electrode types will operate in actual temperature range, this type of reference electrode was found acceptable, having in mind that it potentially could introduce a small error.

## 4.4 Influence of temperature on cathodic polarisation curves

The potential level was chosen to -0.6 V against the ATM reference electrode. In order to verify that the selected potential level is within the range where oxygen reduction is the dominant cathodic reaction a series of polarisation experiments were performed.

These polarisation experiments were performed incrementally at different durations of the steps and at three different temperatures (20°C, 0°C and -20°C). It must be emphasised that all the polarisation experiments were performed without IR– compensation.

### 4.4.1 Cathodic polarisation curves at different incremental intervals

As stated in Chapter 3 one series was tested at different time intervals (duration of the steps) where the slow scanning (long interval) was 0.1V every 24 hours, and the fast scanning (short interval) was 0.1V every 15 minutes. The results from these tests are given in the Figure 4. 17 and Figure 4. 18. These test series were performed at a constant temperature of 20°C.

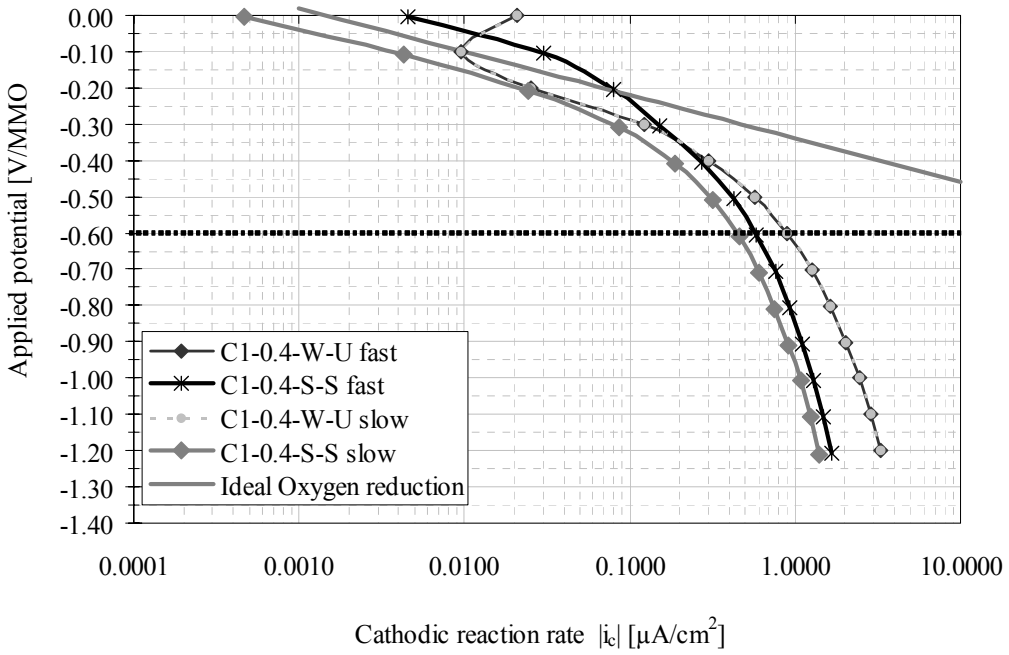


*Figure 4. 17 Evans-diagrams for the w/b ratio 0.4 specimens tested in Run 1 at slow and fast scanning at a constant temperature of 20°C. The ideal oxygen reduction slope indicates the theoretical curve for oxygen reduction without diffusion.*

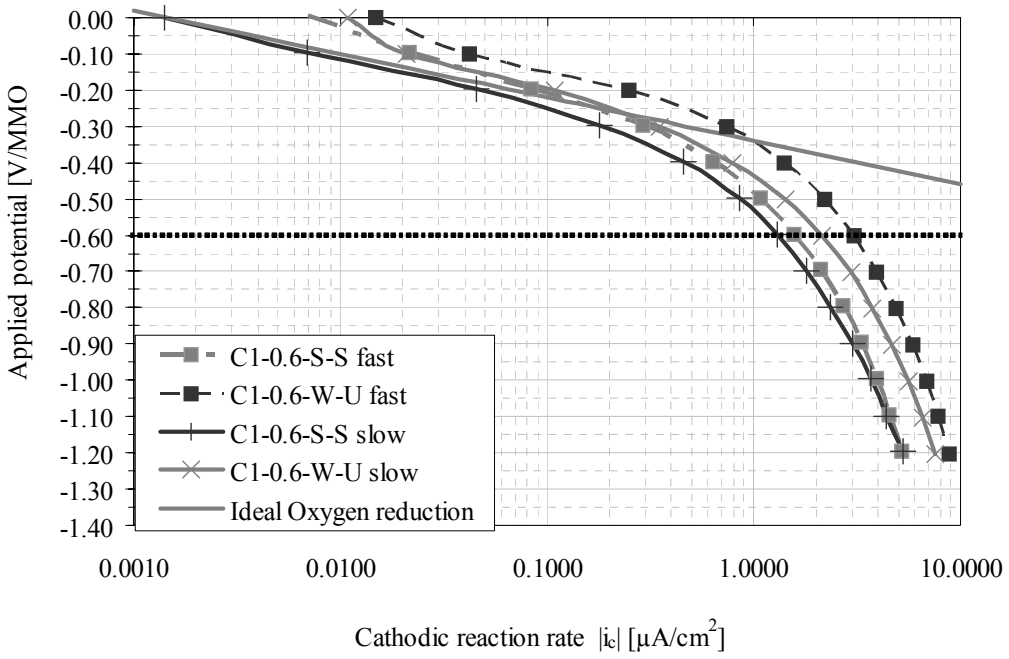


*Figure 4. 18 Evans-diagrams for the w/b ratio 0.6 specimens tested in Run 1 at slow and fast scanning at a constant temperature of 20°C.*

### 4.4.2 Influence of incremental intervals on cathodic polarisation curves

As can be seen from the polarisation curves given in Figure 4. 17 and Figure 4. 18 the effect of the intervals is notable. It is clear that the effect is largest on the samples with lowest moisture content and of poorest concrete quality. The C1-0.4-W-U samples show little change at different intervals between the incremental. The effect is largest on the C1-0.6-S-S samples. 0.1 V every 15 minutes corresponds to a scan rate of 6.7 mV/minute, which

is quite slow in comparison to normal practice (10 mV/minute). It was therefore decided to use the more practical fast scanning for later tests.

### 4.4.3 Cathodic polarisation curves for different temperatures

To obtain information on how the chosen potential level (-0.6V/MMO) agreed with the theoretical considerations, further cathodic polarisation experiments were carried out for specimens tested in Run 1. The polarisation experiments were made in the range from 0V to -1.2V.

The initial equilibrium potential of the electrodes was not taken into account. This can be seen as anodic currents (or current shifts) at given potentials for some of the samples. The experiments were performed at three different temperatures, 20°C, 0°C and -20°C.

In the following section the Evans diagrams for all specimens tested in Run 1 are shown for all three temperatures in one diagram. The diagrams are sorted by concrete composition, curing and sealing.

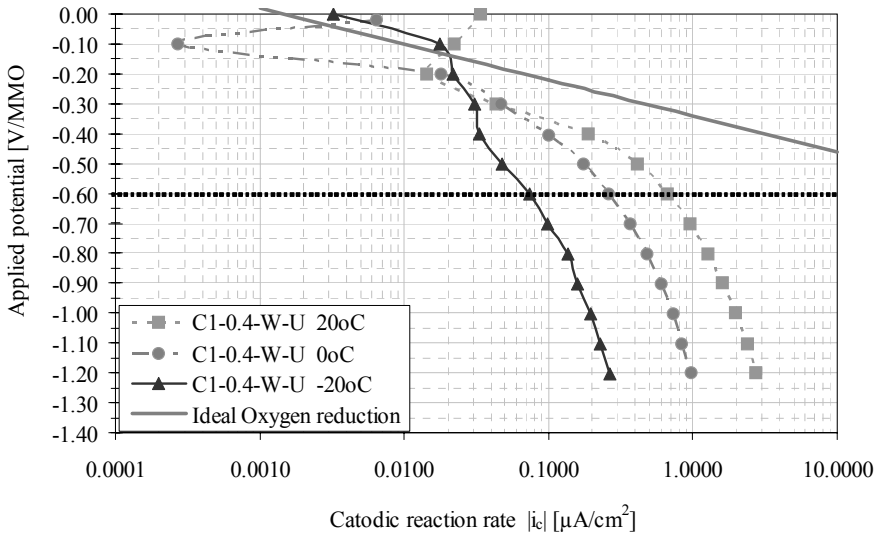


*Figure 4. 19 Comparison of the Evans diagram for the C1-0.4-W-U variant at three temperatures; 20°C, 0°C and -20°C*

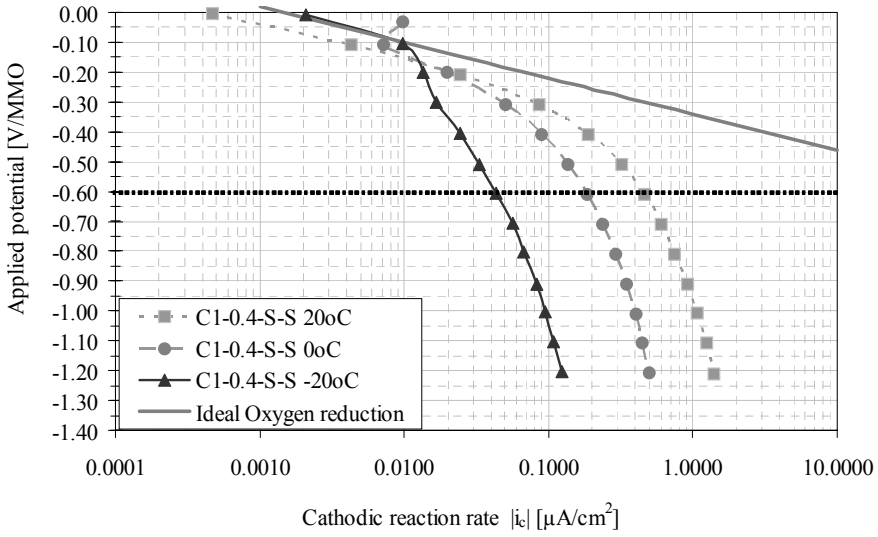


*Figure 4. 20 Comparison of the Evans diagram for the C1-0.4-S-S variant at three temperatures; 20°C, 0°C and -20°C*

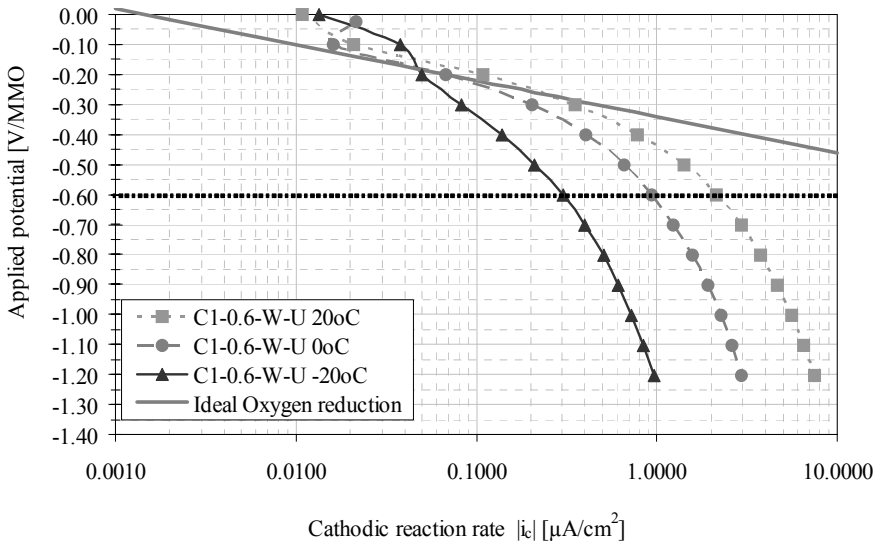


*Figure 4. 21 Comparison of the Evans diagram for the C1-0.6-W-U variant at three temperatures; 20°C, 0°C and -20°C*

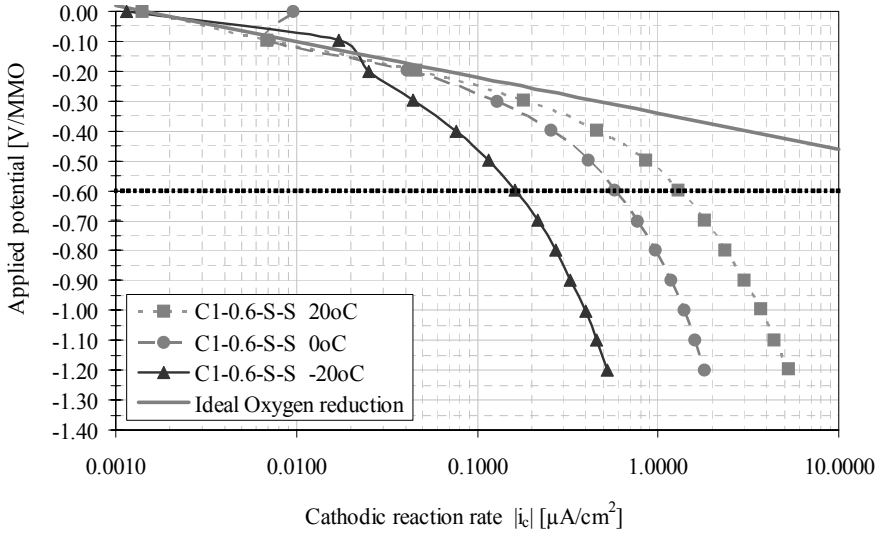


*Figure 4. 22 Comparison of the Evans diagram for the C1-0.6-S-S variant at three temperatures; 20°C, 0°C and -20°C*

### 4.4.4 Influence of temperature on cathodic polarisation curves

In the range between 0V and -0.3V the polarisation curves appears to be quite linear with calculated Tafel slopes (gradients) in the range from -0.1 to -0.2V/decade. These values of the Tafel slopes are quite comparable to the Tafel constant of oxygen reduction on pure platinum. However, deviations from linearity found in Figure 4. 19 – Figure 4. 22 indicate that the polarisation curves in some cases are influenced by other parameters. As emphasised initially the potential values are not IR – compensated. In the paragraph below a discussion is given on how the different parameters may affect the system.

The IR – loss was initially supposed to be a minimal problem due to the placing of the reference electrode. It is placed very close to the reinforcement steel electrode, still presumably shielded from the current field. By applying this design it was assumed that the IR – correction would be a moderate problem.

After some initial resistance measurements it was shown that the electrical resistance between the reference electrode and the working electrode was very much larger than expected.

It must also be taken into account that this electrical resistance between the reference electrode and the working electrode also increases with decreasing temperatures.

The resistance between the reference electrode (RE) and the working electrode (WE) was measured to 1.5 kΩ at 20°C for the concrete with w/b – ratio of 0.6 and 3.0 kΩ for the concrete with w/b – ratio of 0.4. It was estimated that the electrical resistance was doubled at 0°C and magnified ten times at -20°C. Thereby, the resistances were assumed to be:

| | w/b 0.4 | w/b 0.6 |
|---|---|---|
| • 20°C | 3.0 kΩ | 1.5 kΩ |
| • 0°C | 6.0 kΩ | 3.0 kΩ |
| • -20°C | 30 kΩ | 15 kΩ |

Based on the above resistance values a manual IR – correction of the potentials for most of the variants were performed. To illustrate the effect of the IR – correction, the corrected values are compared to the original data for the C1-0.6-S-S variant at all three temperatures as an example. The comparison is given in Figure 4. 23.

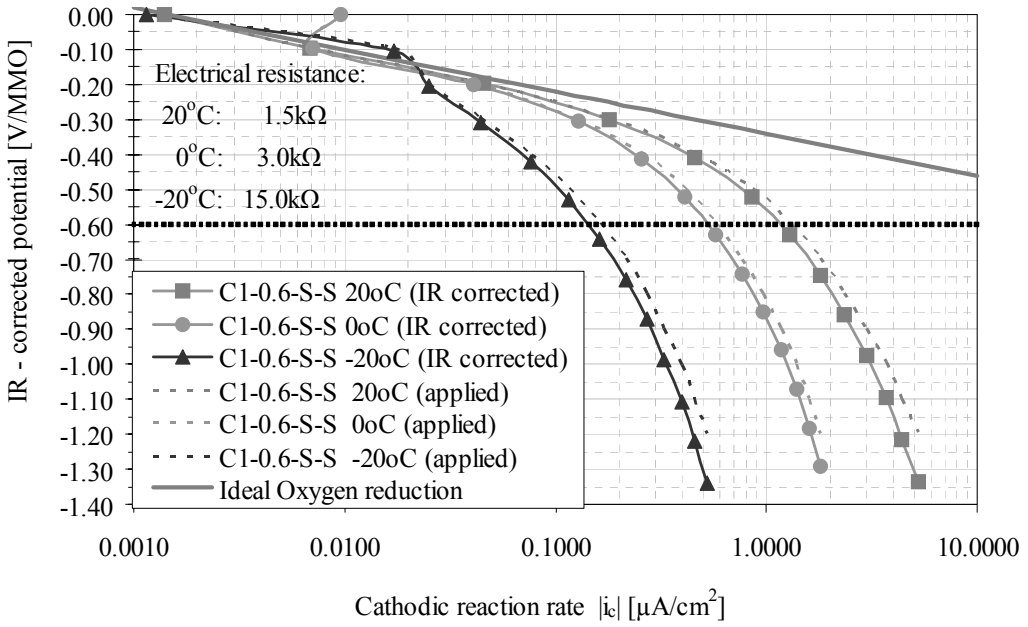


*Figure 4. 23 Illustration of the effect of IR – compensation for the cathodic polarisation curves. The values for the electrical resistance (between RE and WE) are estimated for 0°C and -20°C. The corrected curves are shown with continuous lines, while original data as dotted lines.*

As Figure 4. 23 indicates, the IR – drop correction would not affect the curve shape considerably. Even for very high resistance values (approximately 15kΩ at -20°C, estimated for the w/b 0.6 concrete) the correction would not be proportionally larger due to a very low current density.

The obtained values of the Tafel slopes compared to the Tafel slope of e.g. oxygen reduction (-0.12V/decade) may indicate that there are other charge-transfer reactions taking place on the electrodes that also influence the total gradient.

Most likely these reactions are reduction of oxides, mainly Ferrous oxides and Ferric oxides, on the electrode surface. As stated in Chapter 2 the oxidation of $Fe_3O_4$ to $\gamma$-$Fe_2O_3$ has been reported to be a reversible process by Stratmann et al. [15] and reduction of $\gamma$-$Fe_2O_3$ to $Fe_3O_4$ may interfere in the total reaction.

These aspects could be clarified by performing an investigation of the oxide layers on the electrode surfaces using Raman spectroscopy. Such an investigation was considered but was found to be outside the scope for this project. However, it would be very interesting from a scientific point of view. This may have provided important information about the changes in the oxide layers that may explain or partly explain the effect on the Tafel slopes.

According to Yeager [11] oxygen reduction may go directly (direct 4 – electron pathway) or by a secondary state producing an instable super oxide (peroxide pathway). Bocris et al. [3] supported this and stated that when dealing with passive steel the reduction of oxygen stops at peroxide ($H_2O_2$) formation, not going the step further to hydroxide ($OH^-$) formation. The peroxide formation reaction has a lower Tafel-gradient (~-0.04V/decade) than oxygen reduction; hence, this reaction should result in an overall

lower Tafel gradient. This reaction, however, is very unstable at lower temperatures and it is assumed that the overall effect is small.

When dealing with steel embedded in concrete one should be aware of the complexity of the electrolytic system. When an electrode-system (such as in the CRR – specimens) is polarised the whole electrode surfaces of the electrodes are not active. Only on the parts of the surface in contact with pore solution charge transfer reaction occurs. This leads to an uneven distribution of current, where some enclosed parts of the electrode surface remains inactive.

Furthermore, when a large potential is applied one may assume that a larger part of the pore system will be influenced by the current field. In smaller pores where the mobility of the molecules is limited due to physical barriers this may have an effect. These small pores will contribute only if the applied field exceeds a limit.

The most important aspect that affects the overall gradient of the Tafel constants are transport related phenomena like migration and especially diffusion.
The cell current may have diffusion control (concentration polarisation) in some potential ranges. This would yield a very much higher Tafel gradient. Limited transport would limit the amount of charge transfer reactions and ultimately result in a limiting reduction current density. Research by Raupach [24, 25] indicates that normally in atmospheric conditions diffusion limiting processes are doubtful under normally polarised conditions. Still the results from the polarisation experiments

substantiates that some degree of concentration polarisation occurs, especially at lower temperatures.

Based on the given results in Figure 4. 17 – Figure 4. 22 it appears as if diffusion starts to act as a barrier on the current already at -0.3V in most of the cases. The curves have departure points from linearity around this potential value. The alteration which presumably is related to diffusion increases at a lower potential. There is no decisive point where reduction of water takes over in the interval around -1.1V/MMO as expected. However, this will probably occur at even lower potentials.

From the results it can be deduced that in the interval from 0 V to -0.3 V an "impure" oxygen reduction, i.e. other charge transfer reactions influencing the dominant oxygen reduction, takes place and that in this potential region the dominant processes are related to charge-transfer. This interval is influenced less by the lack of IR-drop correction due to small current densities. The "impurities" may be other charge-transfer reactions, such as reduction of oxides, and/or effects induced by the initial equilibrium potential of the electrodes. Another uncertainty is the specific surface in contact with the electrolyte and inhomogeneities in the active surface.

The interval from -0.3V to -1.2V seem to be dominated by transport limiting processes. Presumably this is due to limited diffusion of dissolved oxygen from the bulk solution to the interface of the electrode, however, the current still increases by increasing overpotential and it is not observed a situation comparable to concentration polarisation. IR-drop correction may also influence here due to larger current densities.

The main deductions are illustrated in Figure 4. 24.

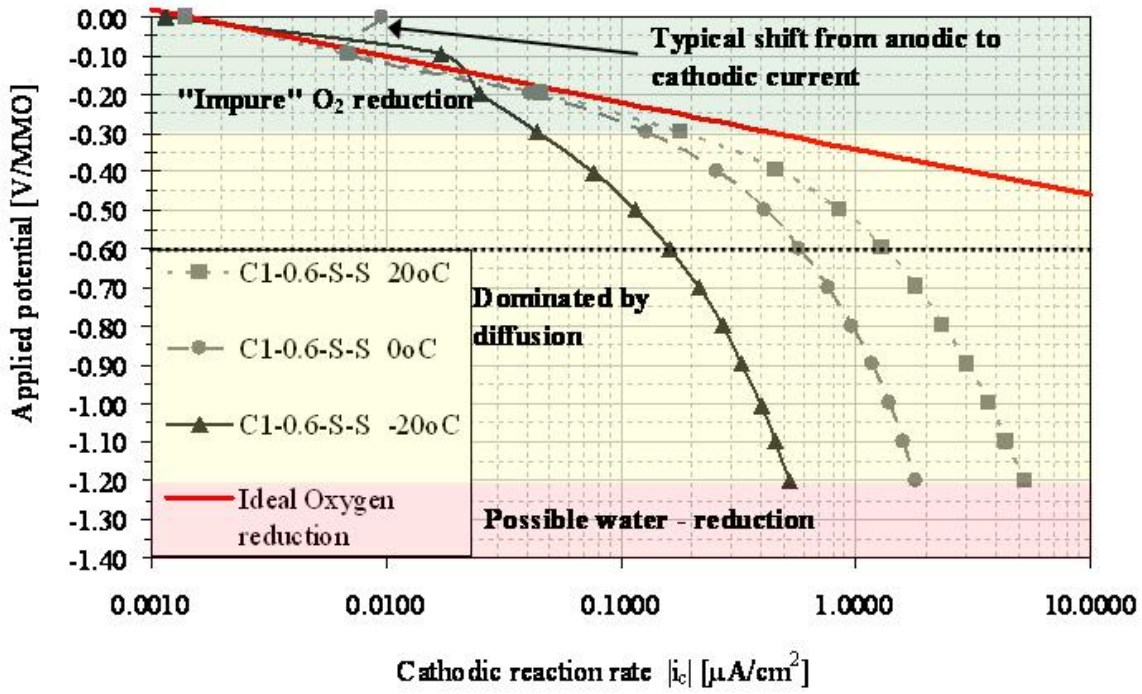


*Figure 4. 24 Typical Evans Diagram from the polarisation experiments*

From Figure 4. 19 – Figure 4. 24 it can be seen that temperature has a considerable influence on the cathodic polarisation response. The diffusion limiting processes occurs at lower overpotential and slow increase in current generates steeper gradients by decreasing temperatures, i.e. the current density increases less at given overpotentials.

In the interval from 0V to -0.15V it seems to be relatively unaffected by temperature, but at such low current densities the accuracy of the

measurements may interfere and conceal the real behaviour. As a general observation the current shifts to lower intensity at lower temperatures.

## 4.5 Influence of temperature on cathodic reaction rate

The experiments to detect the influence of temperature on the cathodic reaction rate were performed on concrete specimens containing a 3-electrode system as described in Chapter 3. The programme was divided in two runs where the second included more specimen variation and more thorough control.

### 4.5.1 Test programme and results

Run 1 was executed with temperatures ranging from +40°C to -40°C. The low temperature range was of most interest; however, the higher temperatures were interesting by means of being able to compare the results with other similar projects. In Run 1 this full temperature range were investigated. However, in Run 2 only temperatures from 0°C to -40°C were tested.

Run 1 included both concrete compositions and 2 curing regimes. This gives a total of four variants where two specimens for each variant were tested.

In the following the results from the various temperature intervals of Run 1 are given. The results from:

- Freezing (0°C to -40°C) presented in Figure 4. 25
- Thawing (-40°C to 0°C) presented in Figure 4. 26
- Heating (0°C to +40°C) presented in Figure 4. 27
- Cooling (+40°C to 0°C) presented in Figure 4. 28

The cell current development during the Stable temperature interval was displayed earlier (Figure 4. 14).

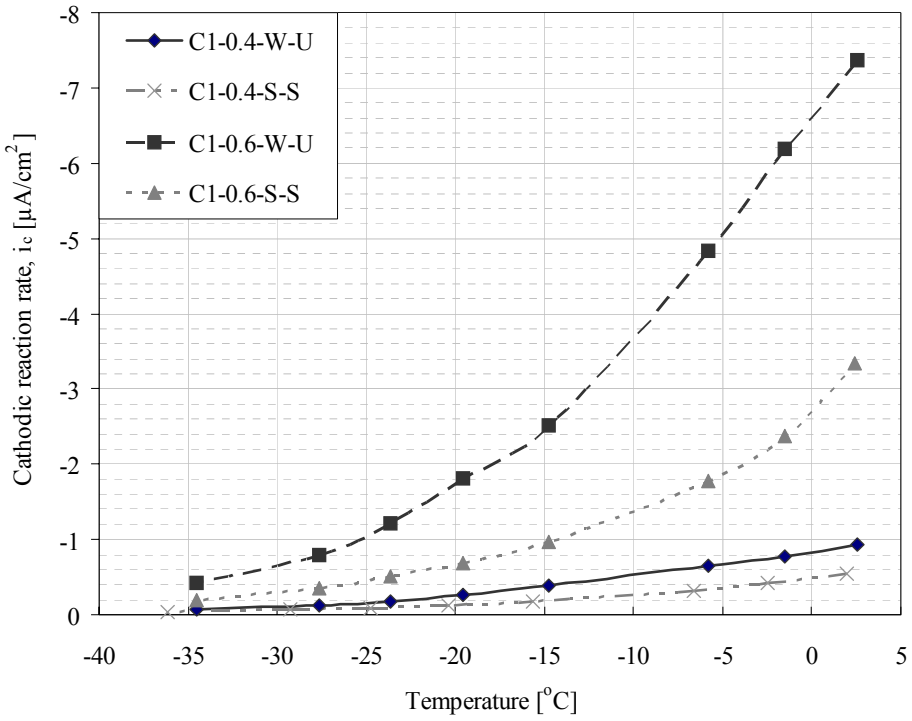


*Figure 4. 25 Temperature response on the cell current of the polarised specimens during the Freezing interval of Run 1*

In Figure 4. 13 it can be observed that the results at a temperature of -10°C are missing. Due to loss of logging data resulting from a power failure these results were regrettably not recovered.

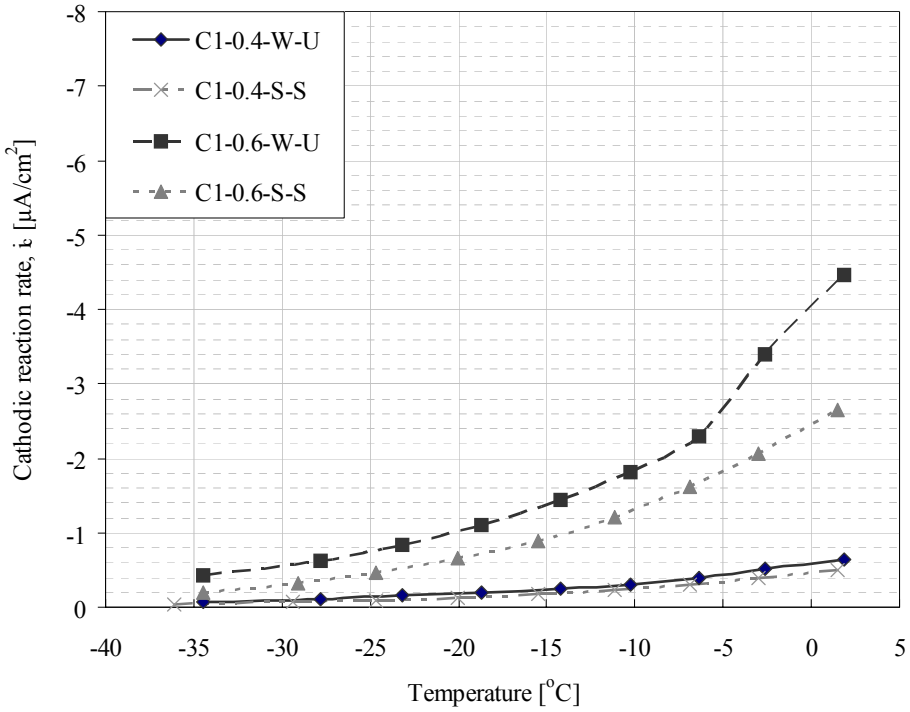


*Figure 4. 26 Temperature response on the cell current of the polarised specimens during the Thawing interval of Run 1.*

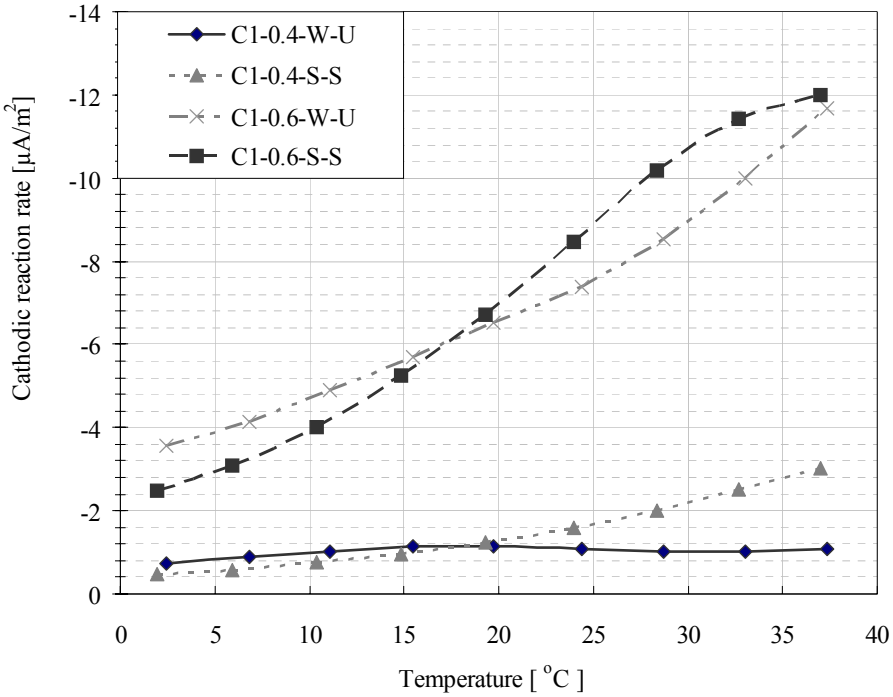


*Figure 4. 27 Temperature response on the cell current of the polarised specimens during the Heating interval of Run 1*

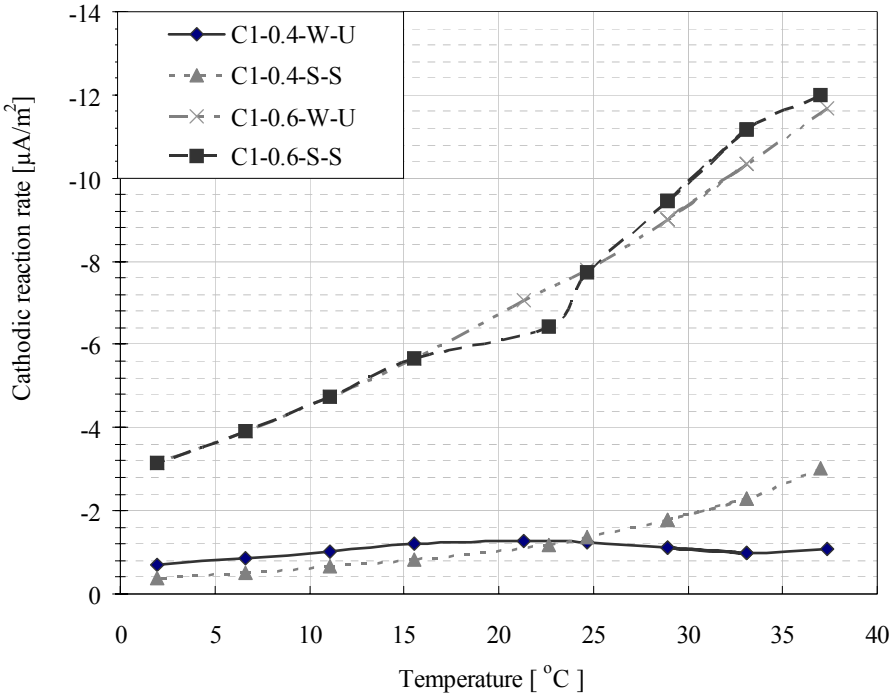


*Figure 4. 28 Temperature response on the cell current of the polarised specimens during the Cooling interval of Run 1*

Run 2 included a larger number of curing regimes. Here a total of eight variants were tested, four for each concrete composition. Three parallel samples for each variant were run through the temperature cycle. Due to extensive and repeated problems with the logging equipment it has only been possible to reconstruct the Freezing interval of Run 2 of the experiments in the temperature range from -5°C to -40°C.

The results from the Freezing interval of Run 2 are displayed in Figure 4. 29.

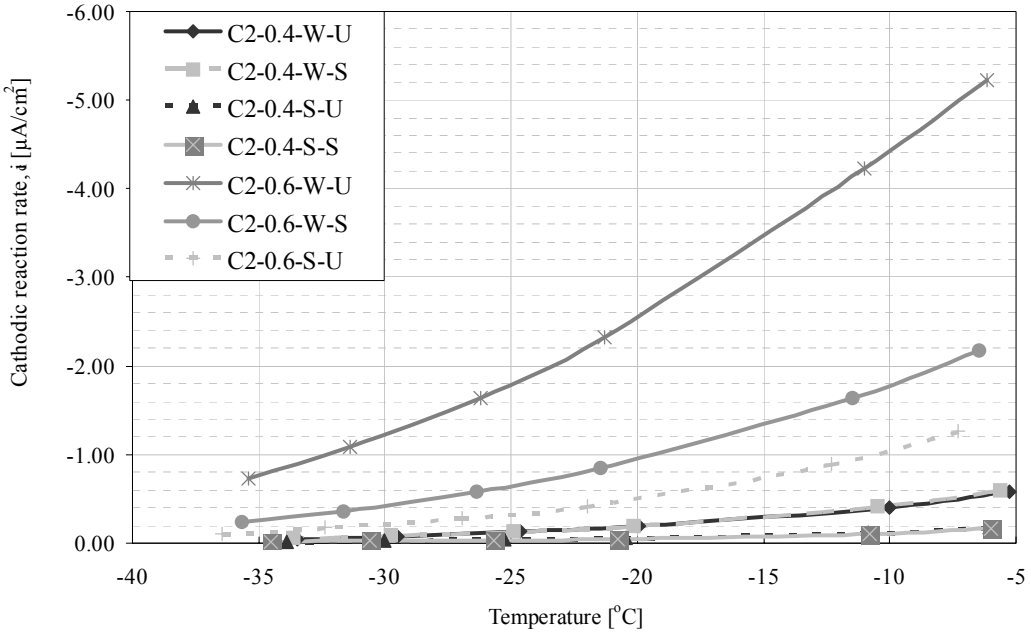


*Figure 4. 29 Temperature response on the cell current of the polarised specimens during the Freezing interval of Run 2*

### 4.5.2 Discussion of the influence of temperature on the cathodic reaction rate

Temperature influences nearly all chemical processes. From the results given in section 4.5.1 it can be clearly seen that temperature influence the system. The activation energy constant, a, according to Equation 2.16 characterises the temperature sensitivity of a particular chemical reaction.

Temperature sensitivity of the cathodic reaction rate

To obtain the activation energy constants for the variants, the results were plotted as reciprocal of temperature given in Kelvin vs. logarithm of the current intensities. The activation energy constant is then proportional to the absolute slope value. This presentation is abbreviated "Arrhenius plots" in the following. The Arrhenius plots corresponding to Figure 4. 25 to Figure 4. 29 are given in Figure 4. 30 to Figure 4. 34.

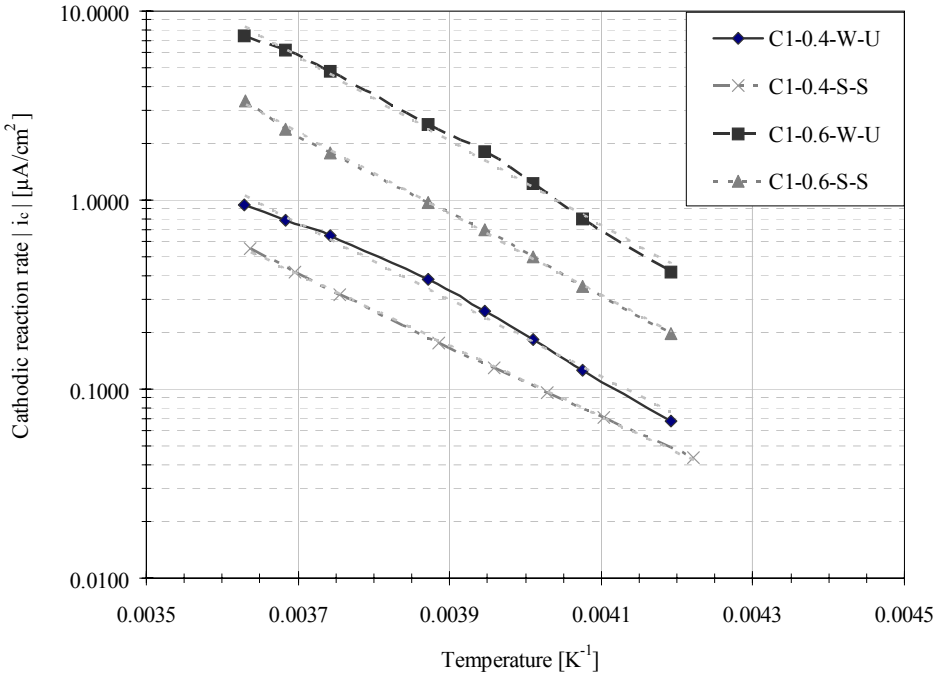


*Figure 4. 30 Arrhenius plots for Freezing of Run 1*

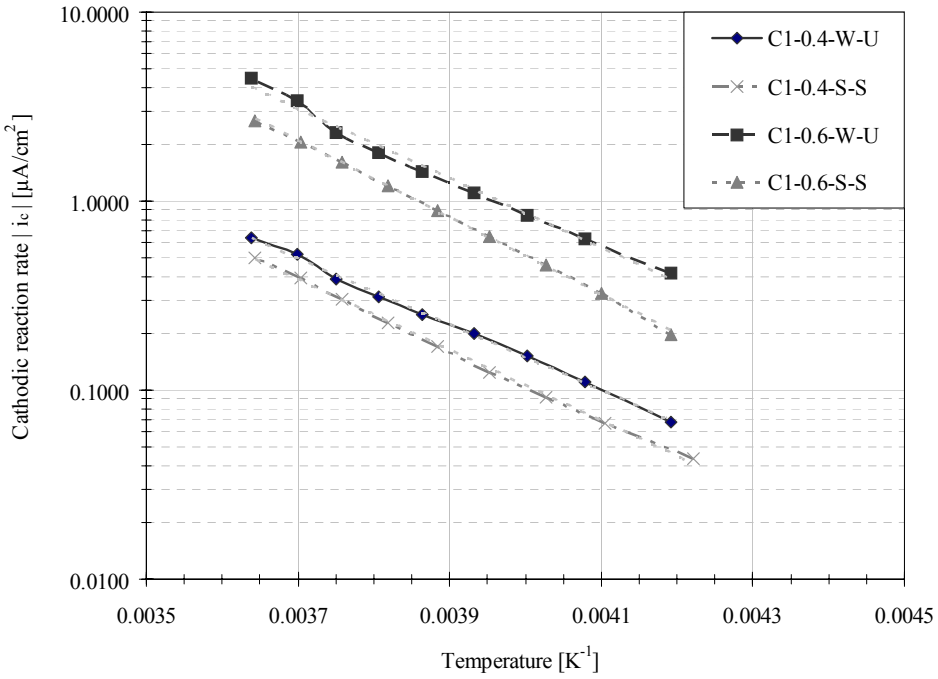


*Figure 4. 31 Arrhenius plot for Thawing of Run 1*

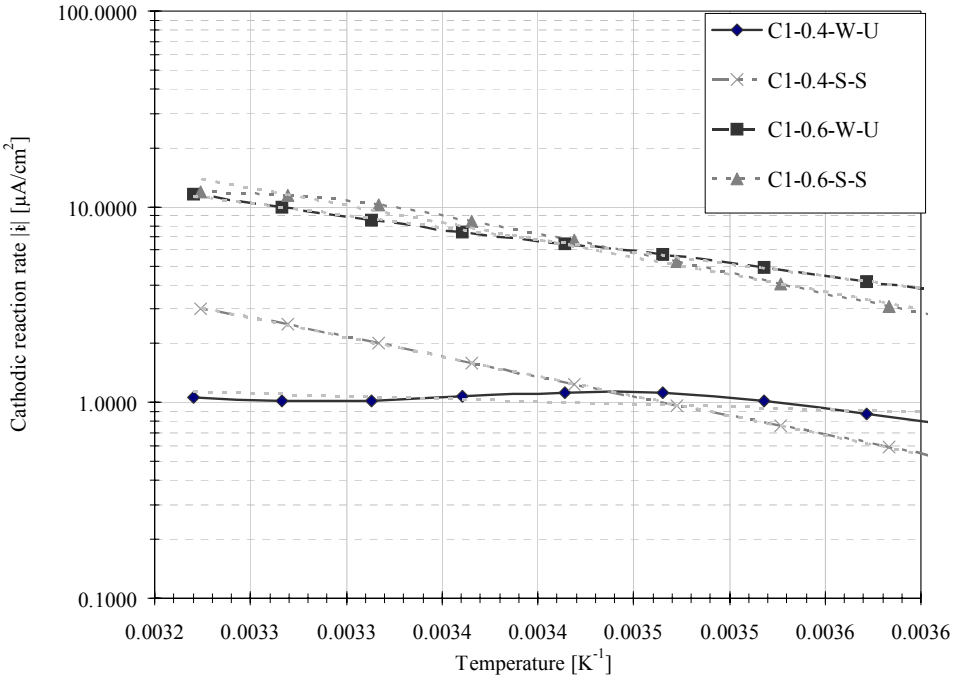


*Figure 4. 32 Arrhenius plot for Heating of Run 1*

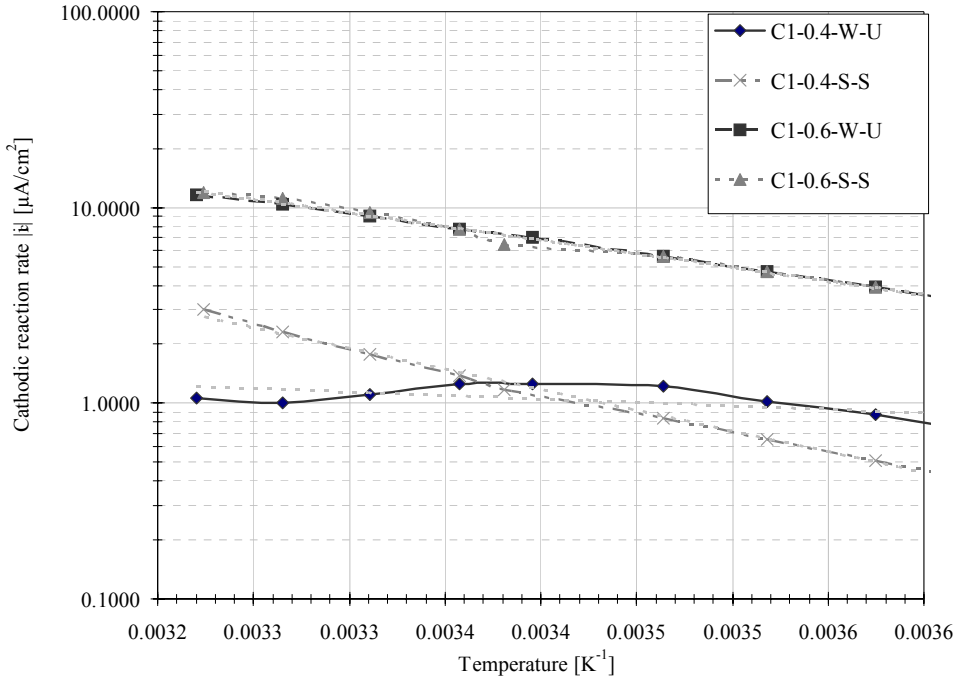


*Figure 4. 33 Arrhenius plot for Cooling of Run 1*

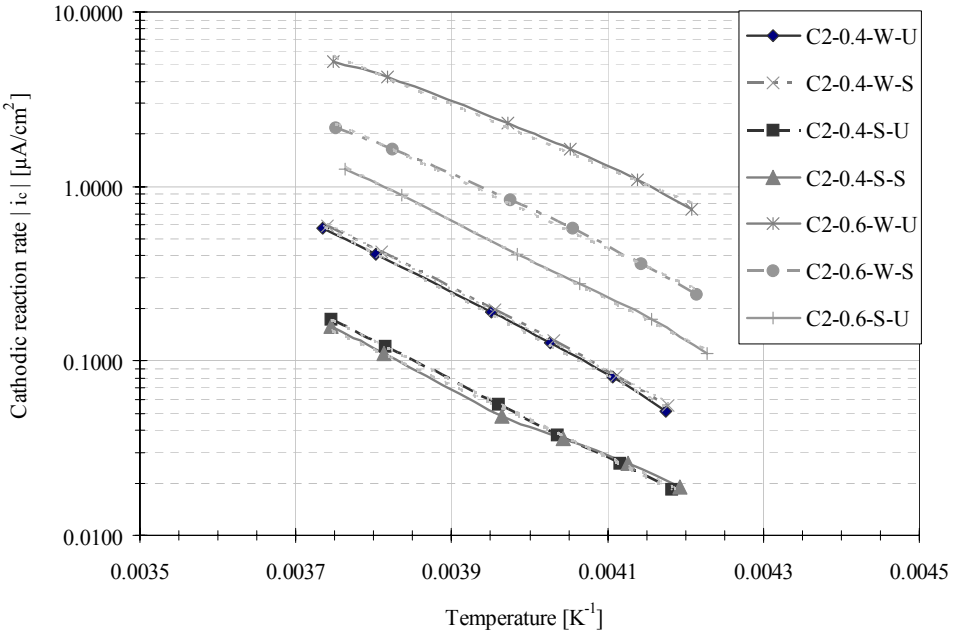


*Figure 4. 34 Arrhenius plots for Freezing of Run 2*

A summary of the activation energy constants for both runs in the CRR – experiments is given in Table 4.4.

*Table 4. 4 Activation energy constants for the CRR experiments. Calculated based on regression analysis of Figure 4. 30 – Figure 4. 34*

| **w/b -ratio** | | **Curing** | | **Sealing** | | **Activation energy constants** | | | | |
|---|---|---|---|---|---|---|---|---|---|---|
| | | | | | | Run 1 | | | | Run 2 |
| 0.4 | 0.6 | W | S | S | U | Freezing | Thawing | Heating | Cooling | Freezing |
| | | | | | | [K] | [K] | [K] | [K] | [K] |
| X | | X | | | X | 4660 | 4000 | 630 | 820 | 5410 |
| X | | X | | X | | | | | | 5400 |
| X | | | X | | X | | | | | 5150 |
| X | | | X | X | | 4340 | 4305 | 4600 | 4860 | 4730 |
| | X | X | | | X | 5130 | 4230 | 2850 | 3150 | 4220 |
| | X | X | | X | | | | | | 4740 |
| | X | | X | | X | | | | | 5200 |
| | X | | X | X | | 4960 | 4700 | 4060 | 3270 | |

Erroneous data (logging failure)

Not tested in Run 1

Higher activation energy constants indicate higher temperature sensitivities for the reactions.

The fact that the curves presented in Figure 4. 30 – Figure 4. 34 are quite linear in most cases demonstrates that the activation energy constant is a function of temperature within the investigated intervals. However, deviations from linearity indicate that the systems are also influenced by other parameters. When comparing the results between intervals there are differences which indicate quite considerable hysteresis. In the following each of the variants are discussed briefly.

C-0.4-W-U (Figure 4. 30 – Figure 4. 34)

This variant was tested in all temperature intervals of Run 1 and Run 2.

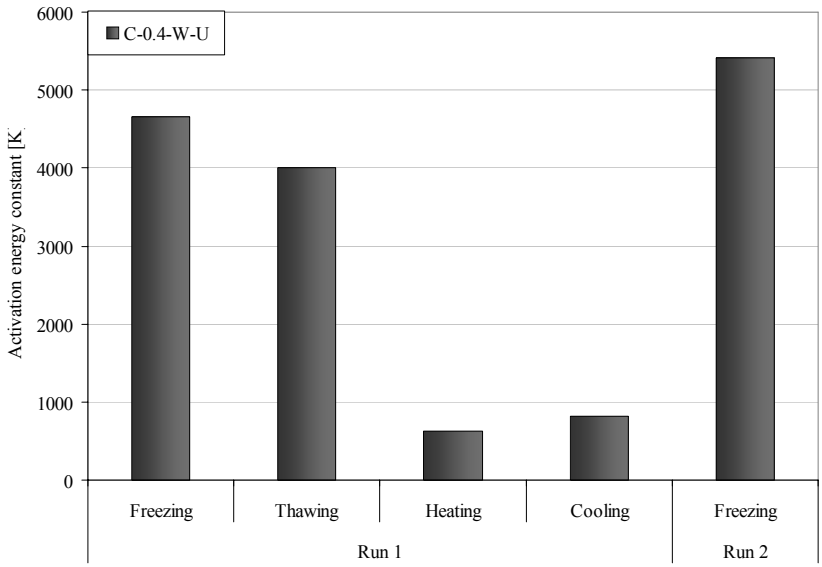


*Figure 4. 35 Development of the activation energy constant for the C-0.4-W-U variant between the temperature intervals in the CRR – experiments*

Between Freezing and Thawing of Run 1 the activation energy constant decreases by more than 10%, indicating less temperature sensitivity during thawing compared to freezing. This difference in temperature sensitivity is probably related to frozen capillary water. During freezing about 12% of the evaporable water is frozen.

The Arrhenius curves on Freezing and Thawing are fundamentally different for this variant. During Freezing the curve appears to decline towards the lowest temperatures, while on Thawing the reversed behaviour is found.

This observation is in accordance with accumulated ice amounts given in Figure 4.3 and the different amounts of ice on freezing and thawing.

When the pore water freezes it is assumed that the ice-front moves from the surface and inwards inhibited in its progress by “ink-bottles” in the pore system. These obstacles correspond to the amount of super-cooling needed for the ice front to progress beyond this obstacle. Thawing of water in small pores will occur at a specific temperature for a specific pore size unaffected by these “ink-bottles”. The systems on freezing and on thawing are therefore fundamentally different. When comparing the two cases, one would expect to observe a clear hysteresis, which in this case was found to be about 10% change in activation energy constant.

The activation energy constant is in the range of 4000K which is comparable to similar research found in the literature. However, during the Heating and Cooling intervals of Run 1 this variant stands out. The activation energy constants are very much lower compared to the other variants.

The curve shape for these two temperature intervals is very different compared to the other temperature intervals and far from linear. The lack of linearity indicates that this variant is affected by other processes to a large degree.

Since its behaviour stands clearly out compared to the other variants no conclusion can be made on which processes that are affecting it most

during heating and cooling. It is supposed that a large part of the effect is connected to moisture exchange with the surrounding environment.

In the Freezing interval of Run 2 the activation energy constant is higher compared to the corresponding interval of Run 1. The increase was about 20 %. The change in temperature sensitivity can be due to differences between the specimens since these were cast at different points in time.

C-0.4-W-S (Figure 4. 34)

This variant was only tested in Run 2. The activation energy constant and the curve are close to identical to that of the C-0.4.W-U variant in the same run.

This variant has no comparable values from previous testing and the discussion of its temperature sensitivity is only based on comparison to the other variants tested in Run 2. The similar behaviour of the water cured variants suggests that the sealing would not change the transport conditions of oxygen to the cathodic electrode; neither induces changes in the moisture condition to a notable degree.

C-0.4-S-U (Figure 4. 34)

Similarly to the C-0.4-W-S this type has only been tested in Run 2 and no comparable results from previous testing exist. The activation energy constant of this type is slightly (5%) lower than the water-cured variants of the 0.4 concrete. This variant behaves similarly as the C-0.4-S-S variant.

However, the variation between the sealed cured variants of the w/b 0.4 concrete is notably larger than that of the water-cured variants of the same concrete.

The difference in the calculated activation energy constants between the sealed variants is approximately 400K. The curves are more or less overlapping for temperatures higher than -20°C where the curve for the sealed variant deviates to lower values than the unsealed variant. The observation may indicate that either there is a change in the moisture conditions in the unsealed variant by water uptake from the surrounding air, or that the transport of oxygen to the cathodic electrode is slightly inhibited in the sealed variant.

C-0.4-S-S (Figure 4. 30 – Figure 4. 34)

This variant was tested in both runs.

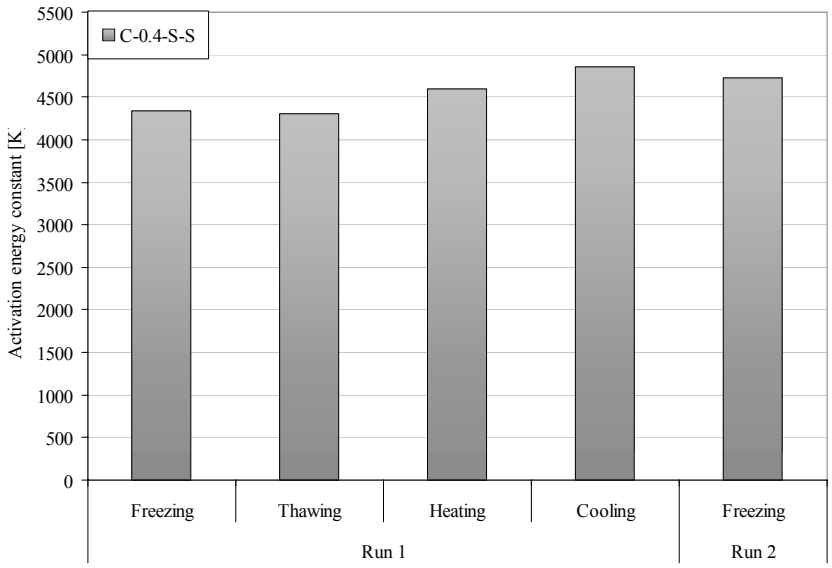


*Figure 4. 36 Development of the activation energy constant for the C-0.4-S-S variant between the temperature intervals in the CRR – experiments*

In contrast to the water-cured and unsealed variant the variation of the activation energy constants within the different temperature intervals was not too large. There is a slight decrease in temperature sensitivity from Freezing to Thawing in Run 1. The decrease was less than 1% and was therefore within the error range of the experiments. Between Heating and Cooling intervals the increase was about 5%. The activation energy constant for Run 2 Freezing interval are higher compared to the corresponding temperature interval in Run 1. The difference is approximately 10%. Generally, it appears as if the variation is smaller on the sealed-cured and sealed variant compared to the water-cured variant.

The sealed cured variant had lower moisture content (due to self-desiccation) and was therefore probably less affected by ice formation in the capillaries.

C-0.6-W-U (Figure 4. 30 – Figure 4. 34)

This variant was one of four variants tested both in Run 1 and Run 2.

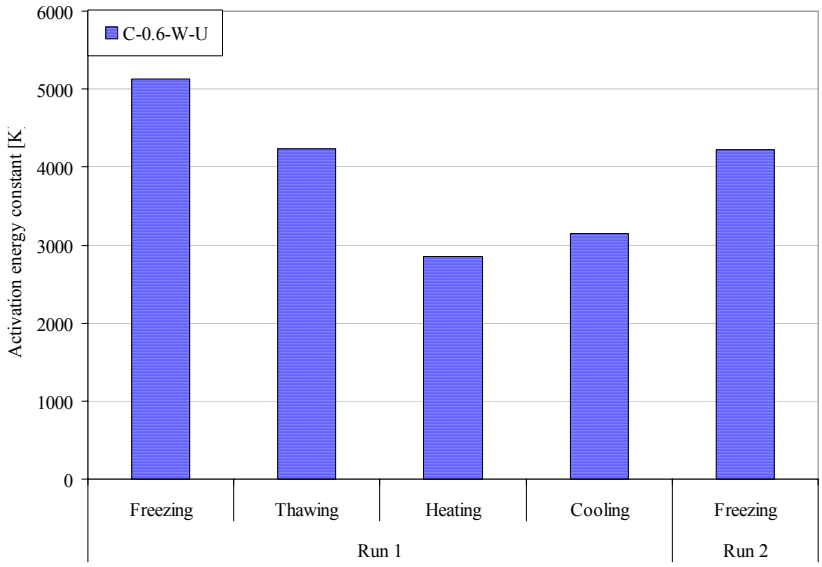


*Figure 4. 37 Development of the activation energy constant for the C-0.6-W-U variant between the temperature intervals in the CRR – experiments*

The activation energy constant is relatively high (5130K) during the Freezing interval of Run 1 and has a significant drop during the Thawing interval (4230K). This considerable drop is close to 20%. Variations in activation energy constants of such magnitude suggest big differences, i.e. ice formation, in the system on freezing and on thawing.

The large hysteresis between freezing and thawing is in all likelihood connected to freezing of capillary water. Similarly as the C-0.4-W-U variant the C-0.6-W-U variant has quite high moisture content and therefore has a quite high probability for ice formation in the largest capillary voids. From section 4.2 it can be found that approximately 29% of the evaporable water is frozen at -35°C given that the specimens are water saturated.

Due to the large fraction of frozen capillaries and the differences in how water freezes and ice melts in a porous system, one should expect a relatively large hysteresis. In this case the hysteresis can be expressed as 20% reduction in activation energy constant on thawing compared to freezing.

The difference in activation energy constant between C1-0.6-W-U and C1-0.4-W-U is 530K during the Freezing interval, but during the Thawing interval this difference is reduced to 230K.

This observation shows the difference between the concrete qualities. The concrete with w/b ratio of 0.6 has a larger fraction of capillary pores; in addition to a larger fraction, the capillaries in the w/b 0.6 concrete will presumably be larger and better connected. The amount of frozen capillaries illustrates these differences. The w/b 0.4 concrete has a fraction of 12% of the evaporable water frozen while the w/b 0.6 concrete has about 29% of the evaporable water frozen in the capillaries. The variation between the concretes on thawing is not so different, and this may be explained in that the amount of capillaries blocked due to ice in the w/b 0.6

concrete makes the transport behaviour similar to that of the w/b 0.4 concrete, which initially has a finer pore structure and fewer capillaries blocked of ice. Since a large fraction of ice melts around 0°C the systems will be comparable during better parts of this temperature interval.

On the higher temperatures, the Heating and Cooling intervals, there is a large change in the activation energy constant. This drop, however, is not as large as that of the concrete with w/b ratio of 0.4.

During Freezing of Run 2 the activation energy constant is lower compared to the corresponding temperature interval of Run 1, but similarly as for the C1-0.4-W-U this may be due to differences between the mixes.

C-0.6-W-S (Figure 4. 34)

This variant was only tested in Run 2. It has an activation energy constant of 4740K in the Freezing interval, which is right in between the W-U variant and the S-U variant.

This variant has no comparable values from previous testing and the discussion of its temperature sensitivity is only based on comparison to the other variants tested in Run 2. The notable difference to the water cured and unsealed suggests that the sealing has kept the moisture condition so high that diffusion of oxygen is inhibited, i.e. the conditions for transport of oxygen to the cathodic electrode are dominated by diffusion in water. Diffusion in water is very much slower than diffusion in air that might result in lower current densities and explain the results for this variant.

C-0.6-S-U (Figure 4. 34)

Similarly to the C-0.6-W-S this type has only been tested in Run 2. This variant has the highest activation energy constant of the variants of the concrete with w/b ratio of 0.6.

This variant has no comparable values from previous testing and the discussion of its temperature sensitivity is only based in comparison to the other variants tested in Run 2. Initially (at 0°C) this variant has the lowest current density of the w/b 0.6 concrete variants. At decreasing temperatures this variant catches up with the other w/b 0.6 concrete variants. This is observed by its large activation energy constant that is 1000K and 500K larger than the W-U and the W-S variants, respectively.

C-0.6-S-S (Figure 4. 30 – Figure 4. 33)

This type was initially planned to be tested in both Run 1 and Run 2. Due to malfunction of the logger during Run 2 the results for this variant was not recoverable.

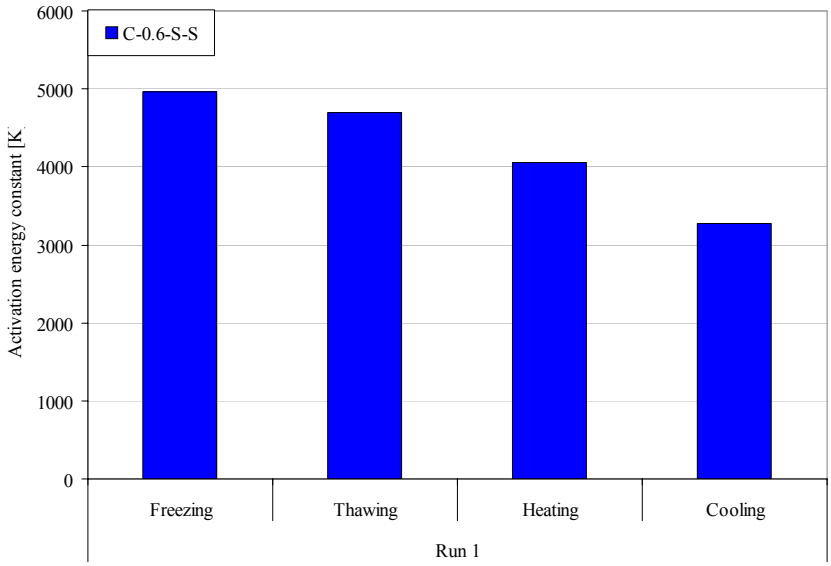


*Figure 4. 38 Development of the activation energy constant for the C-0.6-S-S variant between the temperature intervals in the CRR – experiments*

In Run 1 this variant shows the same trend as the other variants. It has a decrease in activation energy constant between Freezing and Thawing. The decrease is approximately 5%. The small hysteresis may be explained by that the S-S variants have less water content than the W-U variants due to self-desiccation.

It is highly probable that the C-0.6-S-S variant has less non-frozen water than the similarly cured and handled variant of the w/b 0.4 concrete and therefore has a larger hysteresis than the similar variant of the 0.4 variant.

On the high temperature intervals this variant stands out. On the contrary of the other variants this variant has a decreased activation energy constant between the Heating and Cooling intervals. The decrease is almost 20% compared to the other variants which have an increase in the range of 5-10% between the same intervals. The reason to this irregular behaviour has not been recognised.

### 4.5.3 Discussion of the influence of moisture condition on the cathodic reaction rate

The moisture condition of the concrete clearly influences the cathodic reaction rate. This can be seen by the different behaviour between the various curing regimes and sealing levels. Though, it seems as the temperature sensitivity of the reaction is not affected in the investigated range of moisture conditions as discussed in section 4.5.2. In the low temperature ranges there is a notable change in the progress of the cathodic reaction intensities (hysteresis) on Freezing and on Thawing for some of the variants. A discussion of these observations is given below.

By combining the results from Freezing and Thawing of Run 1, given in Figure 4. 39, a substantial hysteresis for some of the variants can be observed.

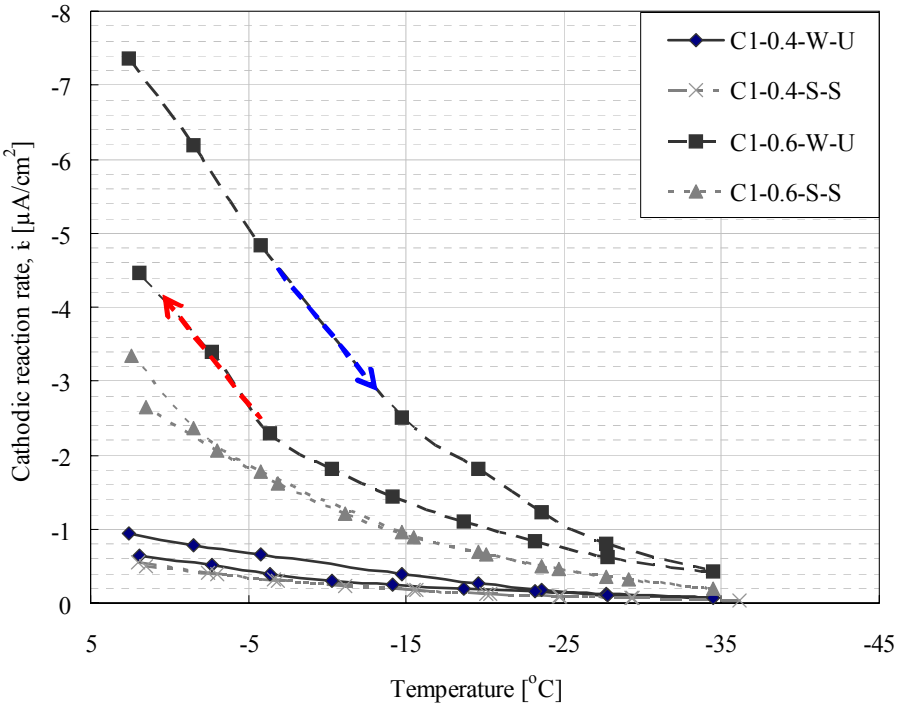


*Figure 4. 39 Combination of Freezing and Thawing of Run 1*

While the hysteresis is not so obvious for the same combination of Heating and Cooling, given in Figure 4. 40.

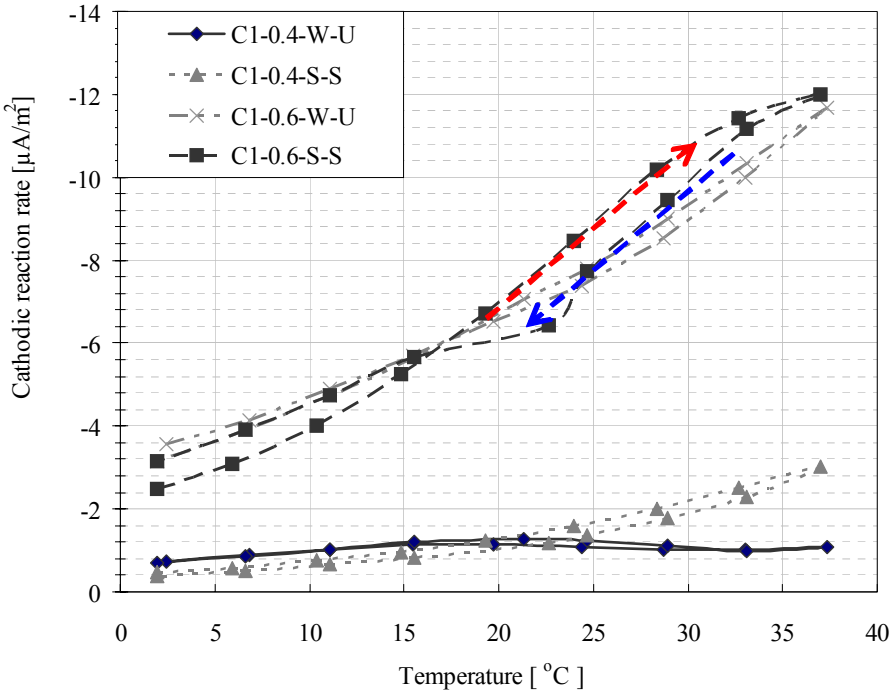


*Figure 4. 40 Combination of Heating and Cooling of Run 1*

The water-cured and unsealed variants of both concrete compositions show a clear change between Freezing and Thawing.

It is expected that some of these changes were generated by moist exchange with the surroundings in the chamber during testing. The sealed variants seem to be unaffected between the intervals and have a more or less identical curve both on Freezing and on Thawing. The sealed variants contained less moisture initially (DS = 75%), and presumably they were prevented from evaporation by the sealing, e.g. securing a stable moisture content.

It is assumed that the unsealed variants had a significant moist loss during the testing period. The drying effect is presumably generated by the continuously running fans on the heat exchanger inside the chamber. The fans that secured an even temperature distribution in the chamber, but did presumably dry out the unsealed specimens during the testing period.

A quantification of the drying effect requires reliable data on the moisture condition of the variants before, during and after testing, which were not performed in Run 1. The moisture data from Run 2 is shown in Table 4. 5, and based on these values an estimate of the consequence of the drying effect by means of change in degree of saturation is given.

*Table 4. 5 Data on moisture state of the CRR – variants tested in Run 2*

| Variant | DCS | Δ DCS | Porosity | Evaporable water | |
|---|---|---|---|---|---|
| | End test | During test | Total | | |
| | [%] | | [%] | [g] | [%] |
| C-0.4-W-U | 89 | 8 | 13.8 | 28.1 | 5.7 |
| C-0.4-W-S | 97 | | 13.1 | 27.3 | 5.3 |
| C-0.4-S-U | 58 | 17 | 15.7 | 35.0 | 6.4 |
| C-0.4-S-S | 75 | | 15.0 | 35.6 | 6.2 |
| C-0.6-W-U | 80 | 19 | 18.5 | 30.9 | 7.8 |
| C-0.6-W-S | 99 | | 19.0 | 35.8 | 8.0 |
| C-0.6-S-U | 62 | 14 | 18.3 | 42.4 | 7.7 |
| C-0.6-S-S | 77 | | 18.4 | 44.7 | 7.8 |

In the Δ DCS column in Table 4. 5 it is assumed that the variants sealed during testing represent the initial state of moisture condition. The drying is calculated as the difference in moisture condition between the unsealed and sealed variants of the same concretes with the same curing. This way of

calculating the drying is not accurate, however, it gives an estimate of how much water that is lost during the test cycle.

From the values in Table 4. 5 it can be found that a significant moist loss took place during testing. Close to 20% change in moisture condition in the worst case (C-0.6-W-U). The hysteresis may therefore partly represent a change in moisture condition.

Between Heating and Cooling (Figure 4. 40) (where one should expect a considerable drying) the effect of drying is not clear. This may indicate that although it is found a change in moisture condition during the whole run, it is plausible that the wettest variants were more affected by the ice formation in the capillaries during Freezing and Thawing than the effect drying introduces on the high temperature intervals.

The Kelvin Equation expresses a relation between pore size and the freezing point depression. In short: water in small capillaries will remain liquid, while water in larger capillaries will nucleate ice.

By low temperature calorimetry it has been found that approximately 12% and 29% of the evaporable water will freeze within the temperature interval during freezing for fully saturated specimens of the concrete with w/b ratio of 0.4 and w/b ratio of 0.6, respectively. Ice formation was anticipated to result in a significant and sudden drop in current density. However, no such observations were made, and the conclusion is that any possible ice formation is not significant for the current response and that transport of reactants finds alternate pathways.

### 4.5.4 Discussion of the combined influence of temperature and moisture condition on the cathodic reaction rate

The forgoing discussions lead to an assumption that there is a connection between temperature and the moisture content of the concrete and that the total effect is superimposed by both parameters.

The calculated activation energy constants found from on the Arrhenius plots in the CRR – experiments alone give little basis to conclude which parameters are controlling the temperature sensitivity of the reaction rate.

In Figure 4. 41 the activation energy constants are plotted vs. the concretes moisture condition, represented by their degrees of capillary saturation. It can be observed from Figure 4. 41 that an overweight of the activation energies are in the range 4000 – 5000K, and that the dispersion do not seem to have a direct correlation to moisture state.

The observation may indicate that the temperature sensitivity is not moisture dependent in the investigated range of moisture conditions. Furthermore, the activation energy constants seem to be independent on the w/b ratio. More research is clearly needed on this subject for verification.

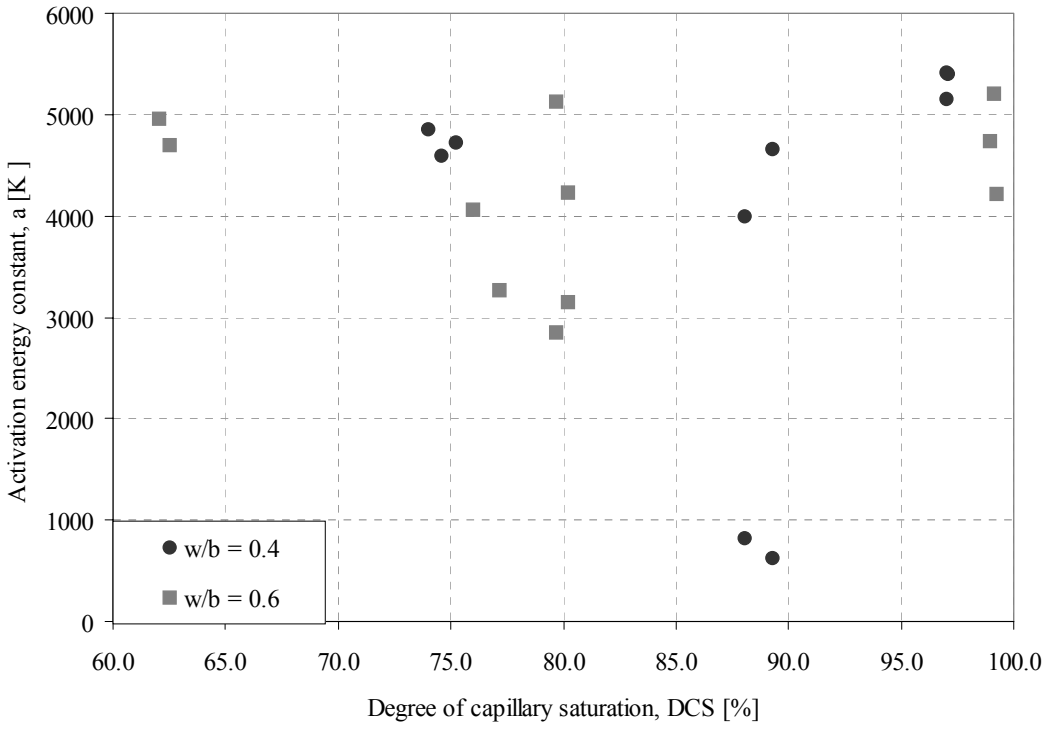


*Figure 4. 41 Activation energy constant as a function of degree of capillary saturation*

The reduction reaction itself is assumed not to be very dependent on the moisture content as long as it is sufficiently supported. However, this supply, i.e. diffusion of oxygen is dependent on the bulk phase concrete properties and its moisture condition. The transport of hydroxyl from the cathodic electrode has the same dependency on the concrete moisture condition and physical properties.

Figure 4. 39 shows considerable hysteresis for the water-cured and unsealed specimens of both concrete compositions between Freezing and Thawing of Run 1. Some of this effect is supposed to be related to moist

exchange with the surrounding atmosphere in the chamber. The hysteresis may also partly be generated by ice formation.

There is no obvious connection between temperature and moisture condition of the concrete for the cathodic reaction rate neither from the results or theoretical, as long as the reaction is not undergoing concentration polarisation.

## 4.6 Concluding discussion

Reduction of oxygen, which assumingly is the dominant reaction occurring in the CRR experiments, is a temperature dependent electrochemical reaction. This reaction is dependent on sufficient supply of water and oxygen at the electrode surface and the ability for hydroxyl ions to diffuse from the electrode surface.

It is known from the literature [5] that diffusion of oxygen is very fast in air compared to water. Saturated concrete will have slow diffusion of oxygen, but plenty supply of water. Clearly, there is a balance where there is plenty supply of oxygen and still plenty supply of water on the electrode. The solubility of oxygen in water is temperature dependent and increases by decreasing temperature.

As shown in section 4.3 the temperature responses are giving transient periods of approximately 4 hours in average when the temperature is changed 5°C. A "quasi steady-state" was found as the average of the last 4 hours of the 24 hours steps disregarding the first 20 hours of measurements. Some of the transient period is due to a lag between concrete temperature and the chamber temperature. The slow temperature change in the concrete is related to its large mass. The concrete temperature had a lag of approximately 2 hours compared to the chamber temperature. The difference between concrete temperature and chamber temperature is summarised in Figure 4. 15.

At the lowest temperature the specimen cooling was slow; hence, the lag was very much longer at this temperature step in comparison to all others.

The concrete seemed to be very energy consuming to freeze further from around -35°C. This may be due to a fraction of the capillaries having their ice nucleation point around this temperature. -35°C represents a Kelvin radius of about 2 nm presumed a solid liquid governing interfacial energy in the pore according to Sellevold and Bager [72].

This is a strong indicative that ice was present in the pores, at least for the wettest specimens of the w/b 0.6 concrete. The presence of ice did not result in any notable and sudden changes in the reaction rate as first suspected.

By investigating the systems at a fixed temperature of 0°C for more than 200 hours it was found a slight decrease in current intensity over this period. The decrease was less than 5% over this period for the most affected variant (C-0.6-S-S). This small reduction in reaction rate may be induced by a local change in pH in the environment adjacent to the cathodic electrode. A pH increase due to formation of hydroxyl would decrease the equilibrium potential of the electrode, and therefore decrease the cathodic overpotential needed to obtain the certain potential. The decrease in driving force would, evidently, result in a decreased reaction rate.

Still, the profound stability over a period of more than 200 hours is an indicative that the reaction is well supported by oxygen and that

concentration polarisation is not likely at least at this temperature. It is therefore assumed that the reaction is not impaired by diffusion of neither oxygen nor hydroxyl ions.

The cathodic polarisation experiments (reported in section 4.4) indicate in contrast to the steady polarisation that the reaction is impaired by diffusion phenomena at -0.6 V/MMO. These experiments are performed without IR-drop corrections, but it is indicated that the IR-drop corrections are negligible for the curve shape.

The Evans Diagrams plotted from the results show that the systems appear to have diffusion barriers on surprisingly low (cathodic) overpotentials.

Already at -0.3 V/MMO diffusion appeared to have dominant effect on the progress of reaction intensity by increased cathodic overpotentials. In the potential interval from 0 to -0.3 V/MMO the systems show a linear behaviour (Tafel region) in a linear logarithmic diagram. It is assumed that the results are representative for the polarisation behaviour of steel in concrete at various temperatures.

Compared to an idealised oxygen reduction curve (Tafel gradient of 0.12V/decade) the systems show quite good correlation to this in this potential interval.

In the actual potential range -0.6V/MMO the systems were affected by transport phenomena. Presumably the systems were limited by diffusion of oxygen from the bulk solution to the interface of the steel electrode.

The diffusion seemed to occur on decreased overpotentials when the temperature was decreased. This is coherent to limited mobility of species by decreasing temperature. On the other hand the solubility of dissolved oxygen in water is increasing with decreasing temperature. However, the solubility plays a secondary role as diffusion is clearly more dominant in the accessibility at the electrode surface than the reactants solubility.

# 5

# TEMPERATURE EFFECTS ON ELECTRICAL RESISTIVITY OF CONCRETE

*This chapter gives a detailed description of the experimental results. In the latter part a thorough discussion of the interpretation and conclusions are given.*

## 5.1 Introduction

It has been shown by others [32, 34] that temperature is a vital parameter for the electrical resistivity of concrete, and accordingly also important for the overall corrosion rate of embedded steels.

To identify the temperature effects on the concrete system, hence, how the electrolyte reacts on temperature, the ER – research was initiated. Other electrical properties than the electrical resistivity of the electrolytic system were evaluated since Electrochemical Impedance Spectroscopy was chosen as one of the measuring techniques.

The ER – experiments includes additional parameters in combination with temperature such as moisture state and concrete quality.

The investigations were made using three different measurement techniques:

- Electrochemical Impedance Spectroscopy (EIS)
- Positive feedback (PF)
- Potential square pulse (PSP)

Positive feedback were compared and validated against EIS.

## 5.2 Temperature influence on electrical resistivity of concrete

The electrical resistivity of concrete was measured at four specific temperatures (20°C, 2°C, -14°C and -28°C).

The experiments were executed in different Runs:

- Run 1 was primarily to test the validity of the measurement techniques and to record temperature changes in the concrete specimens.

- The aim of Run 2 was to identify moisture effects using parallel measurements with both EIS and the positive feedback circuit. Both Run 1 and Run 2 were performed at Instituto Eduardo Torroja (IETcc), Madrid.

- Run 3 was executed at NTNU with a different measurement technique, chronoamperometry, or as more commonly abbreviated, potential square pulse measurements. Run 3 was carried out in order to add more moisture states to extend the range of moisture conditionings.

- Run 4 was made with the same samples as in Run 3. The specimens were saturated for 8 weeks immersed in water before initiation of Run 4, through before they were Run through a temperature cycle.

- Run 5 was only a moisture state control test where the electrical resistivities of the samples were followed during changing moisture states (resaturation by immersion in water). These samples were not run through a temperature cycle.

### 5.2.1 Influence of temperature on electrical resistivity of concrete – results

The results for each temperature interval of each Run are presented in the following.

Run 1

The results for Freezing in Run 1 are shown in Figure 5. 1 and Figure 5. 2 for the concrete with w/b of 0.4 and with w/b 0.6, respectively. The measurements were performed by EIS.

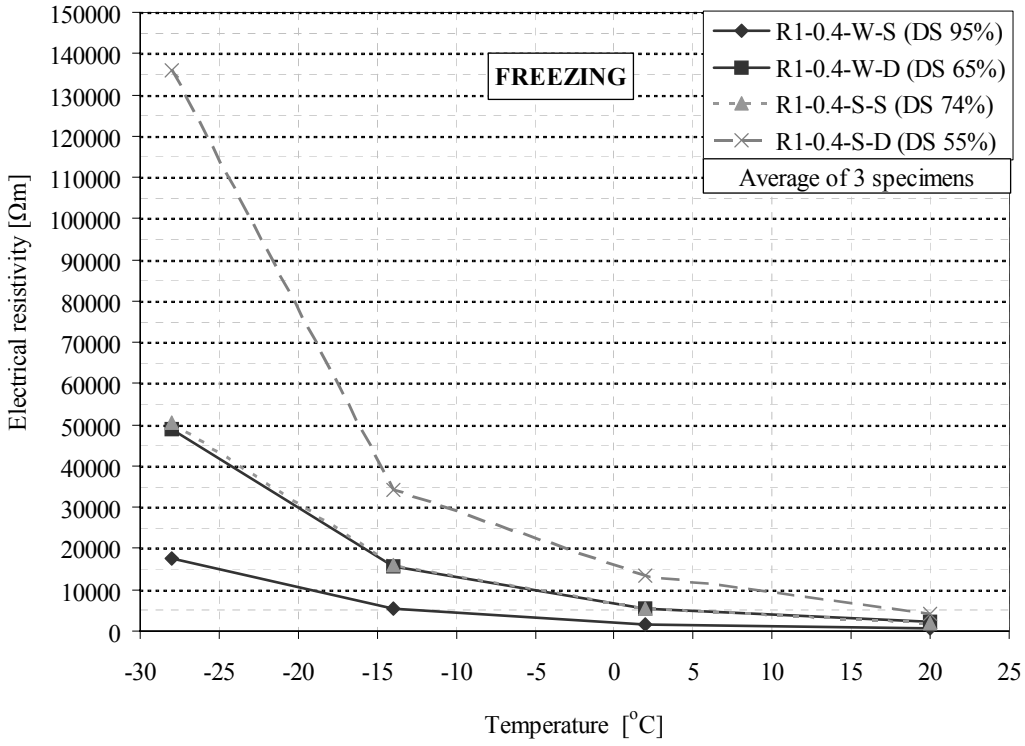


*Figure 5. 1 Effect of temperature on the electrical resistivity of the w/b 0.4 concrete during Freezing in Run 1. Measured by EIS.*

The results are the calculated average of the measurements for three parallel samples.

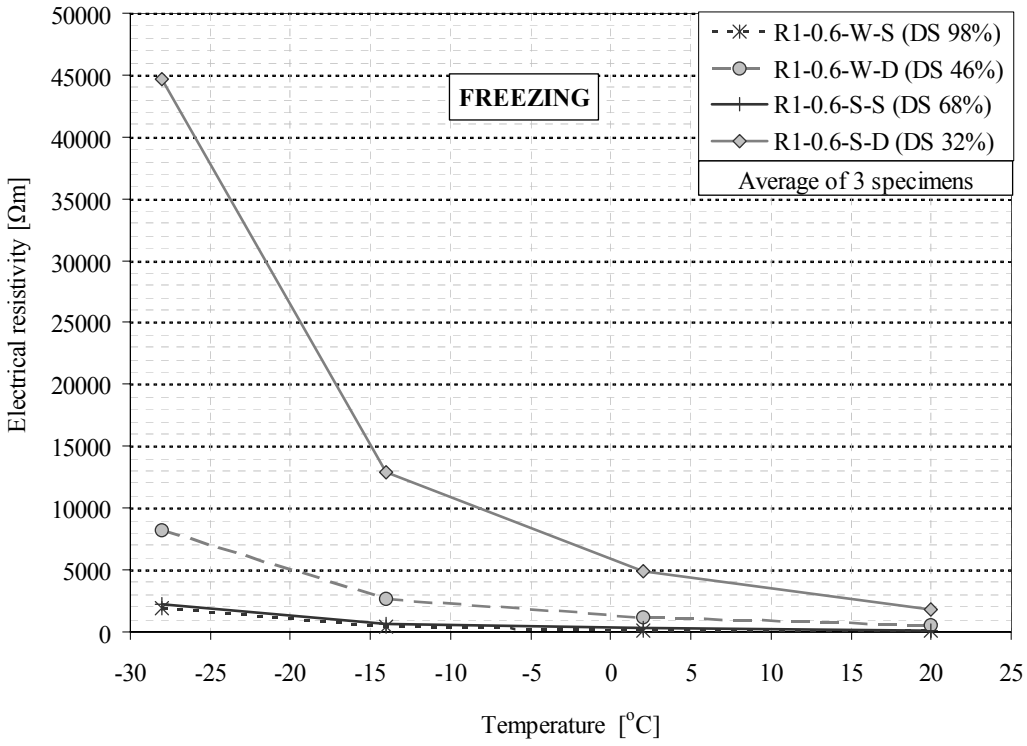


*Figure 5. 2 Effect of temperature on the electrical resistivity of the w/b 0.6 concrete during Freezing in Run 1. Measured by EIS.*

In Figure 5.3 the statistical variation between the parallel samples is illustrated. The results for variant R1-0.4-W-S are shown with the standard deviation added and withdrawn.

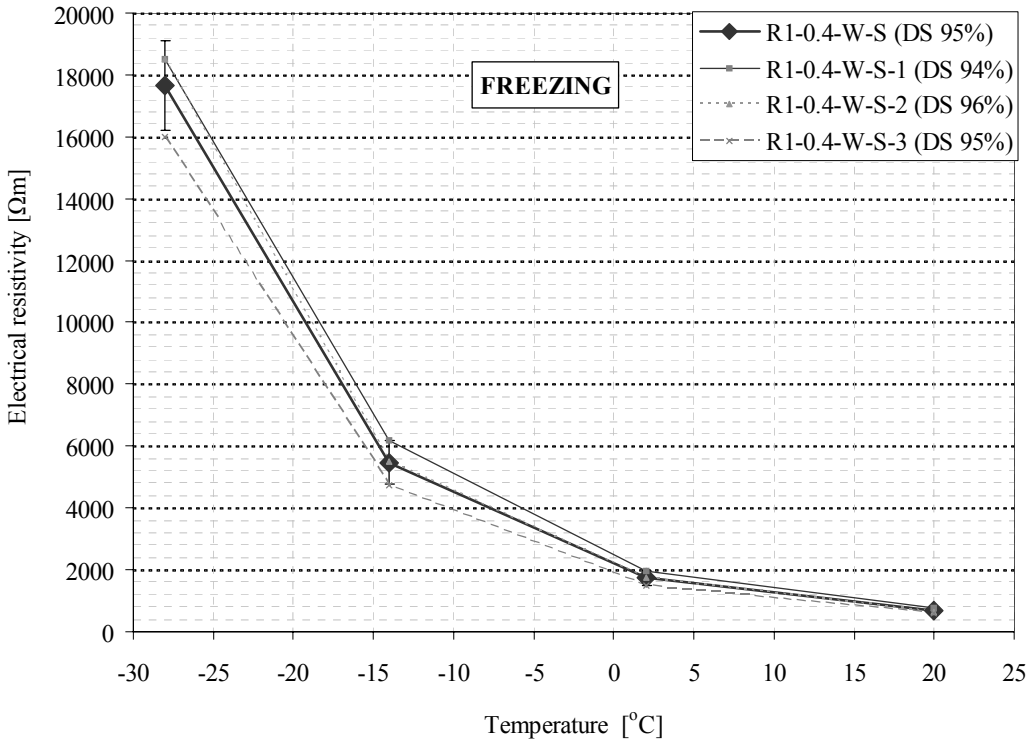


*Figure 5. 3 Statistical variation for variant R1-0.4-W-S during Freezing in Run 1. The standard deviation is marked by the error bars. Measured by EIS.*

During Thawing in Run 1 the measurements were performed with positive feedback. The results are shown in Figure 5. 4 and Figure 5. 5 for the concrete with w/b of 0.4 and w/b of 0.6, respectively.

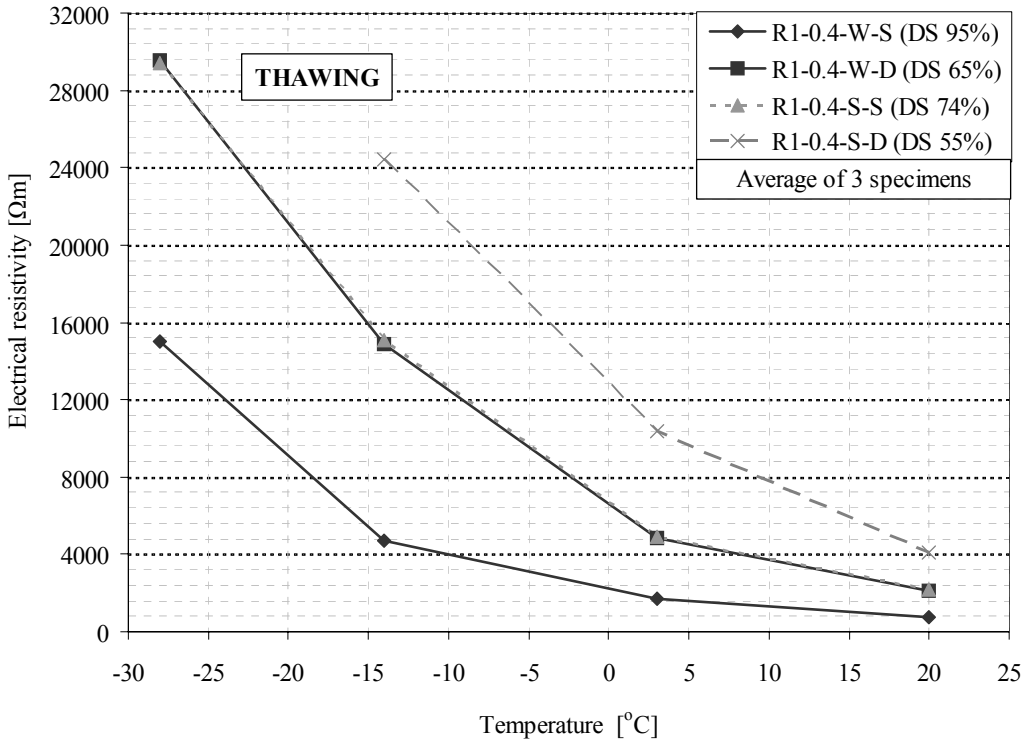


*Figure 5. 4 Effect of temperature on the electrical resistivity of the w/b 0.4 concrete during Thawing in Run 1. Measured by Positive Feedback.*

It was not possible to obtain any values for the R1-0.4-S-D variant at -28°C. The interpretation of the results is therefore based on the points obtained at the other temperatures.

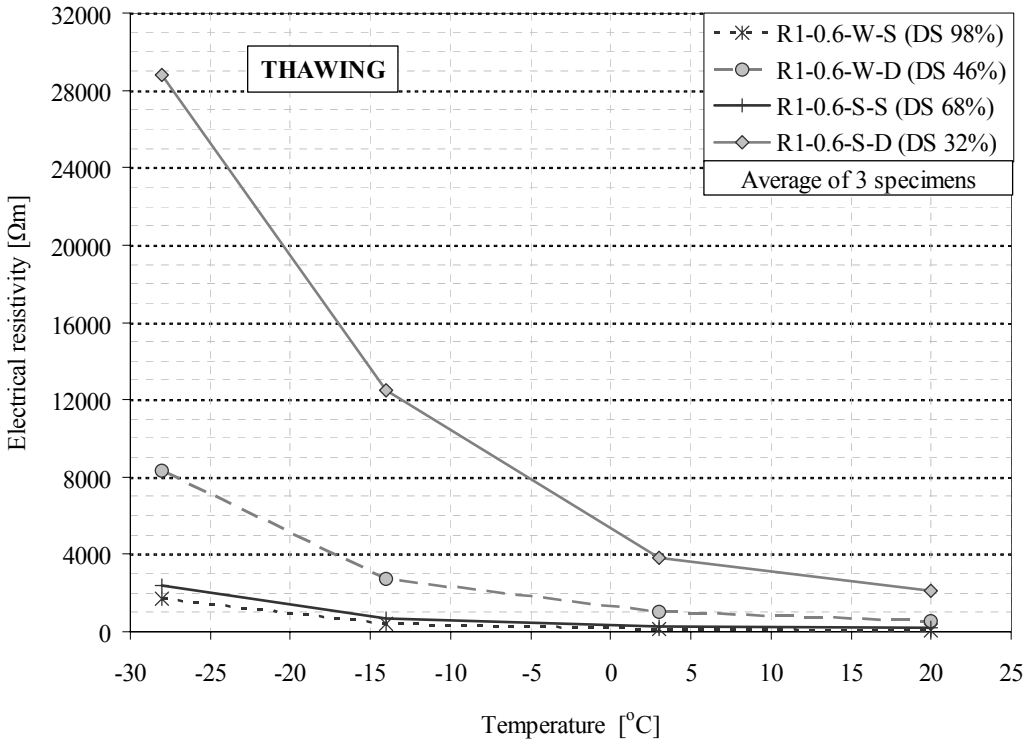


*Figure 5. 5 Effect of temperature on the electrical resistivity of the w/b 0.6 concrete during Thawing in Run . Measured by Positive Feedback.*

Run 2

This Run was performed using parallel measurements by electrochemical impedance spectroscopy and by the positive feedback circuit on a potentiostat. Each variant were represented by a single specimen only.

It is important to notice that in Run 2 only one specimen of each variant were tested An exception is that for the water-cured sealed variants of both concrete compositions an additional specimen were included. These

specimens were saturated by vacuum for 36 hours, and then tested (specimen R2-0.4-W-S-2 and R2-0.6-W-S-2). This treatment was performed in order to have higher moisture content and observe moisture related phenomena.

In Figure 5. 6 the EIS results from the Freezing are shown for all variants. The parallel results from positive feedback are displayed in Figure 5. 7.

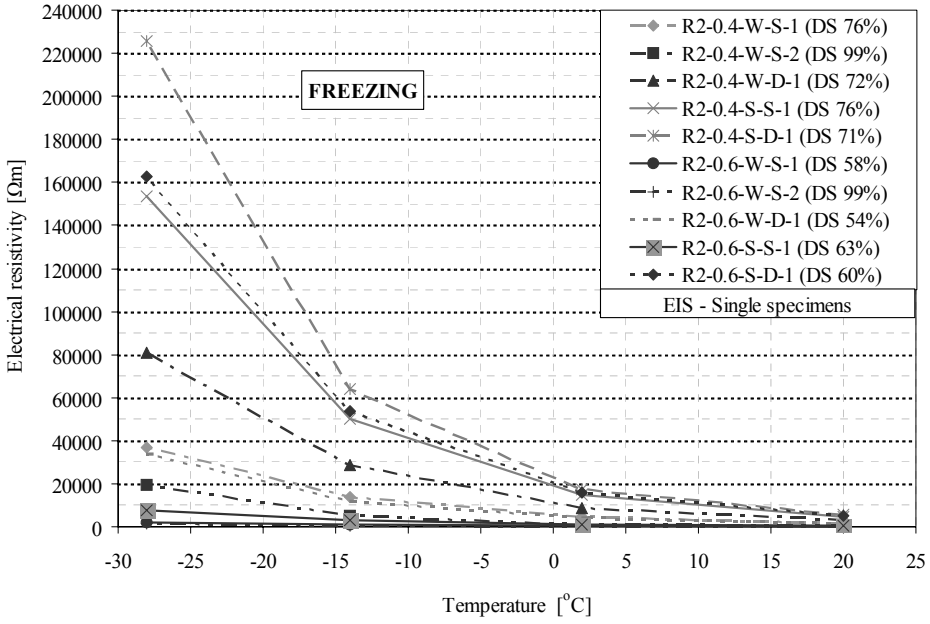


*Figure 5. 6 Effect of temperature on the electrical resistivity for all variants during Freezing in Run 2. Measured by EIS.*

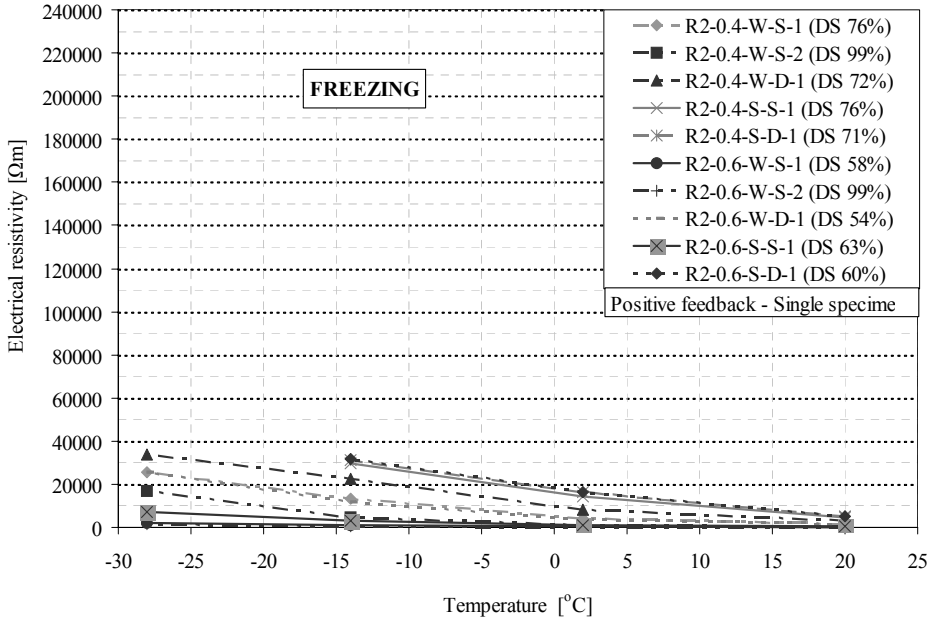


*Figure 5. 7 Effect of temperature on the electrical resistivity for all variants during Freezing in Run 2. Measured by positive feedback.*

The results for the R2-0.4-S-S, R2-0.4-S-D and R2-0.6-S-D at -28°C were not within the limits of the positive feedback circuit of the potentiostat. The interpretation of the results for these variants is based on the other temperatures.

The results from Thawing are shown in the same way in Figure 5. 8 and Figure 5. 9 for EIS and positive feedback, respectively.

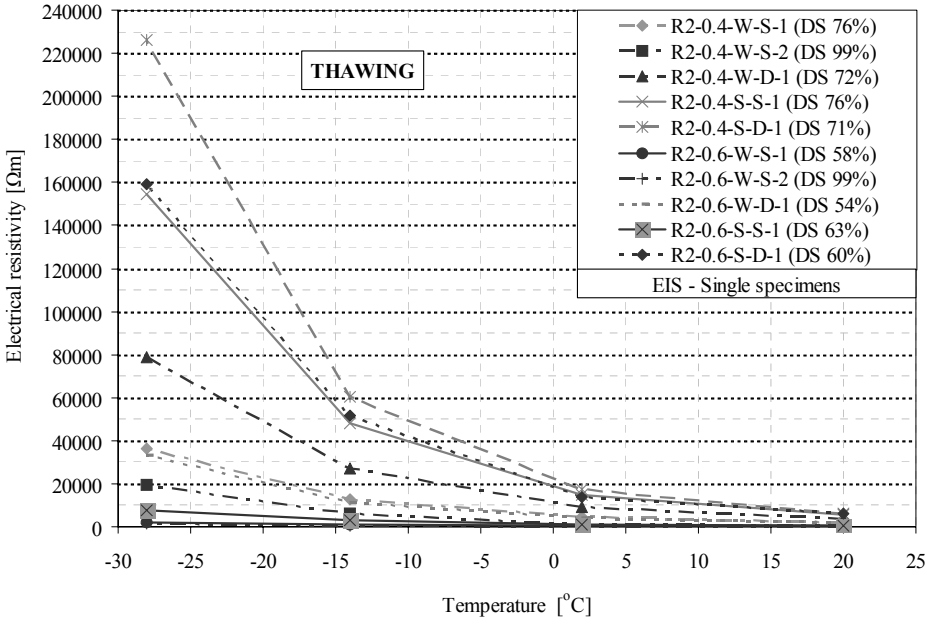


*Figure 5. 8 Effect of temperature on the electrical resistivity for all variants during Thawing in Run 2. Measured by EIS.*

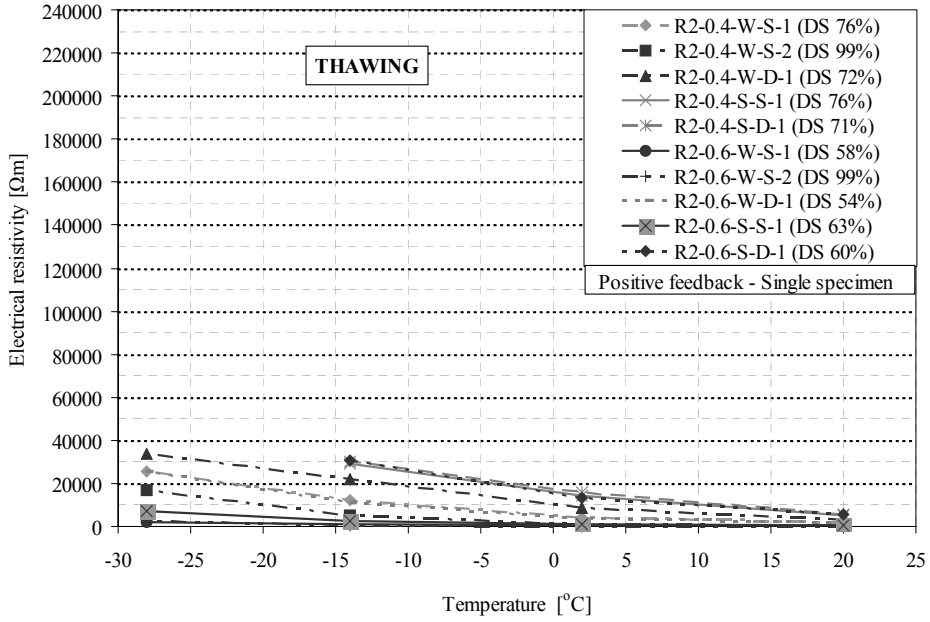


*Figure 5. 9 Effect of temperature on the electrical resistivity for all variants during Thawing in Run 2. Measured by positive feedback*

Run 3

In Run 3 the measurements were performed by a different method than in Run 1 and Run 2. These measurements were performed by a handheld potential square pulse meter (Escort LCR meter) at a fixed frequency of 1 kHz. The results from Run 3 are shown in Figure 5. 10 and Figure 5. 11 for Freezing and Thawing, respectively.

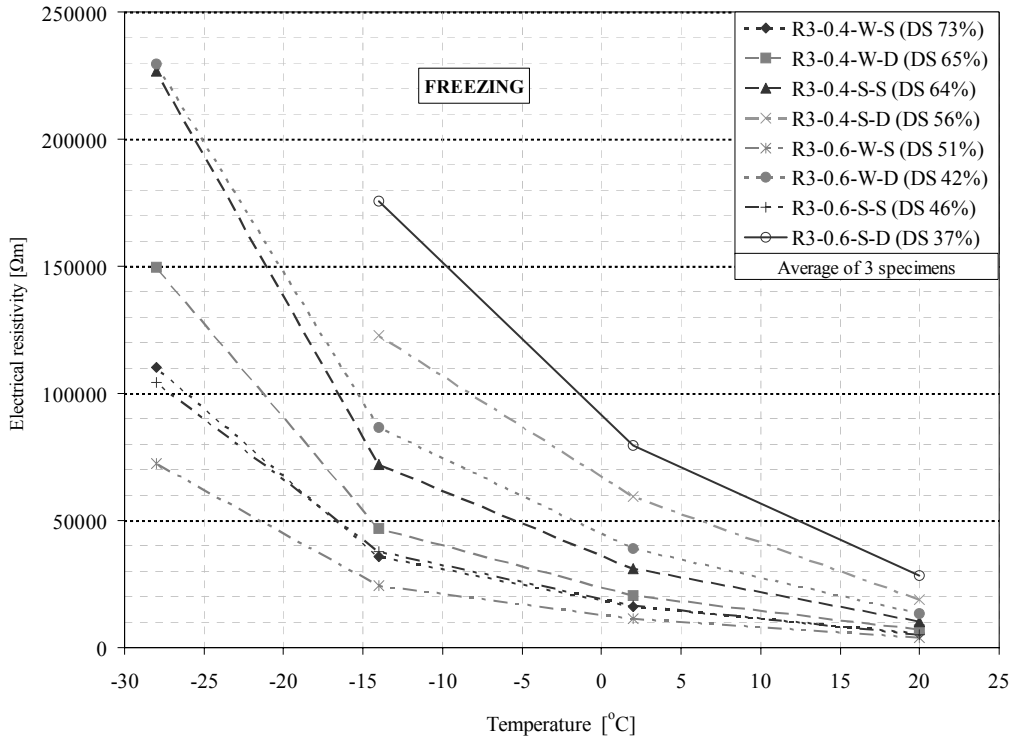


*Figure 5. 10 Effect of temperature on the electrical resistivity for all variants during Freezing in Run 3. Each point is the average of three parallel specimens. Measurements performed by Potential Square Pulse (PSP).*

The resistivities of the sealed-cured and dried (40°C for 1 week) samples for both concrete compositions were out of range for the equipment at -28°C.

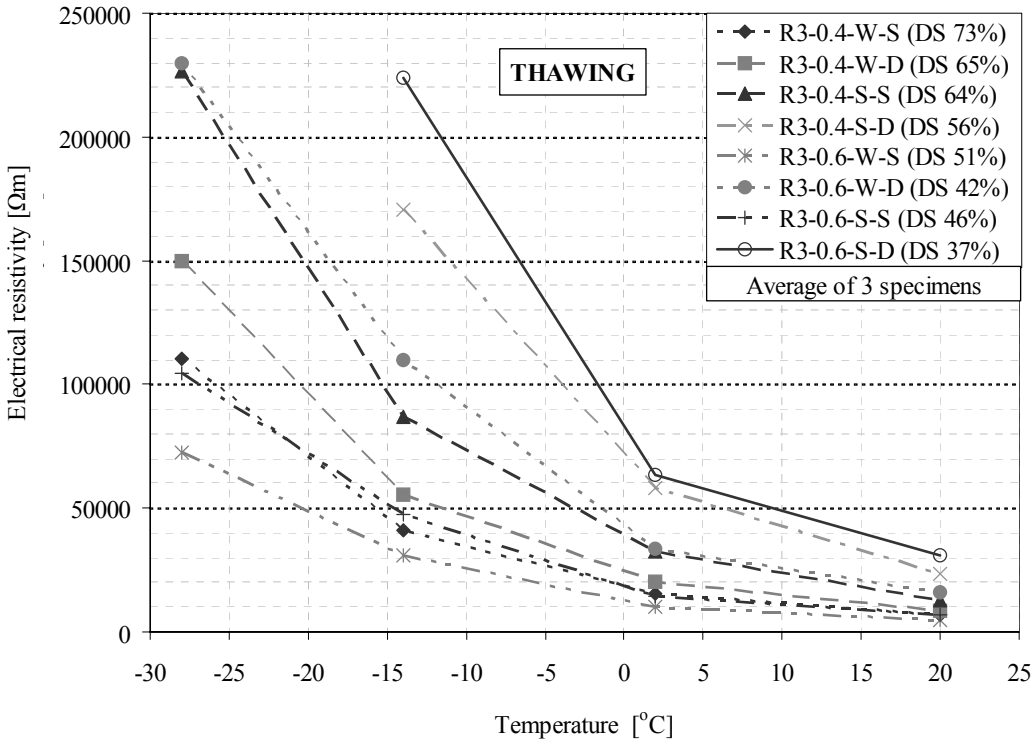


*Figure 5. 11 Effect of temperature on the electrical resistivity for all variants during Thawing in Run 3. Each point is the average of three parallel specimens. Measurements performed by PSP.*

Run 4

Run 4 was executed on the same samples as tested in Run 3. Before start of Run 4 the specimens were immersed in water for 8 weeks in order to saturate as much as possible. During the immersion period the specimens were controlled for changes in the electrical resistivity. When the decrease

between the weekly measurements was less than 5 %, the electrical resistivity was considered to have sufficient stability for initiation of Run 4.

The results are shown in Figure 5. 12 and Figure 5. 13 for Freezing and Thawing, respectively.

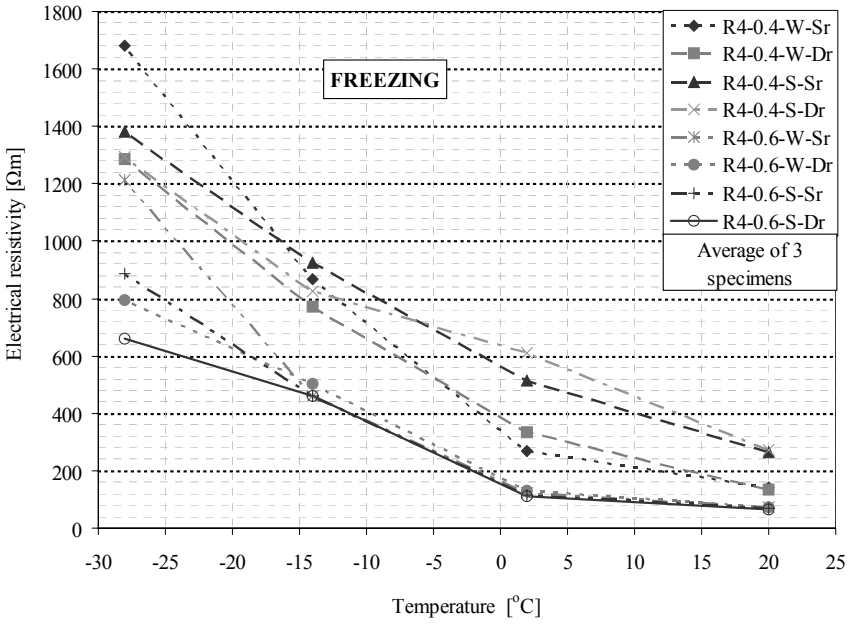


*Figure 5. 12 Effect of temperature on the electrical resistivity for all variants during Freezing in Run 4. Each point is the average of three parallel specimens. Measurements performed by PSP.*

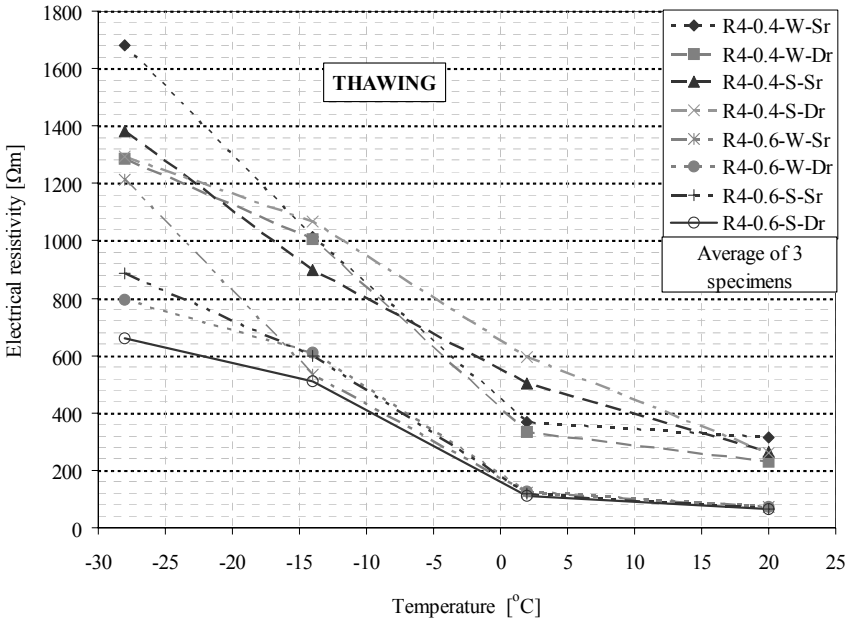


*Figure 5. 13 Effect of temperature on the electrical resistivity for all variants during Thawing in Run 4. Each point is the average of three parallel specimens. Measurements performed by PSP.*

### 5.2.2 Hysteresis between Freezing and Thawing

The results given in section 5.2.1 show a nearly consequent hysteresis between Freezing and Thawing.

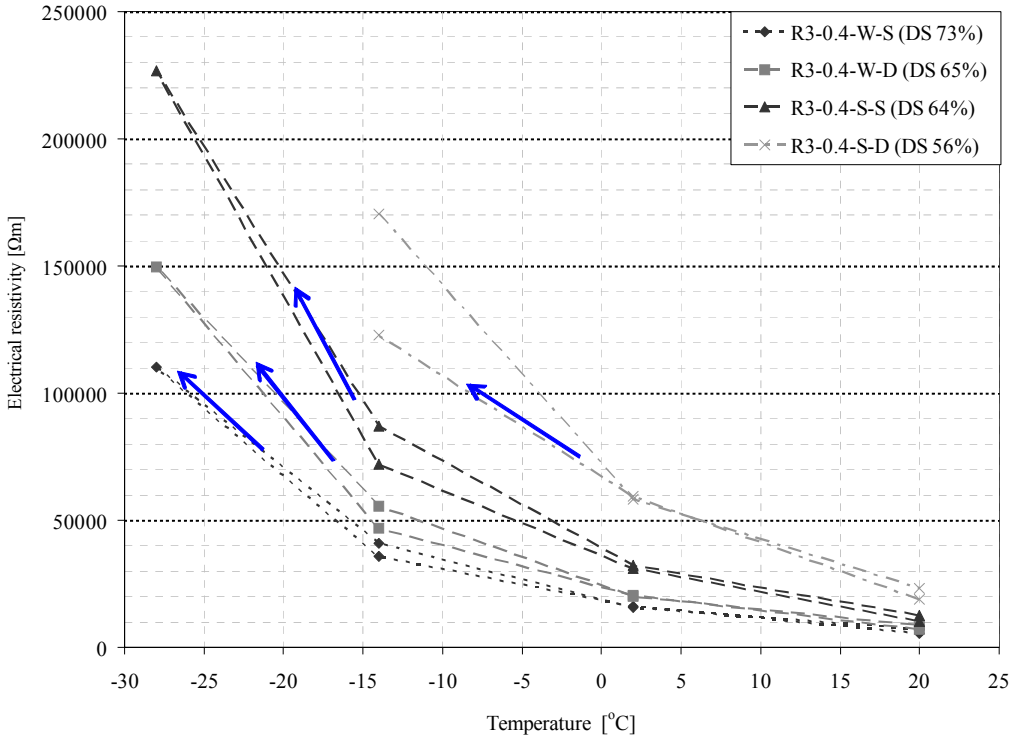


*Figure 5. 14 An example for the w/b 0.4 concrete of the hysteresis found between the temperature intervals; Freezing and Thawing. The Figure corresponds to a combination of Figures 5.10 and 5.11 (Run 3). The measurements were performed by PSP. Freezing is marked by arrows on the curves.*

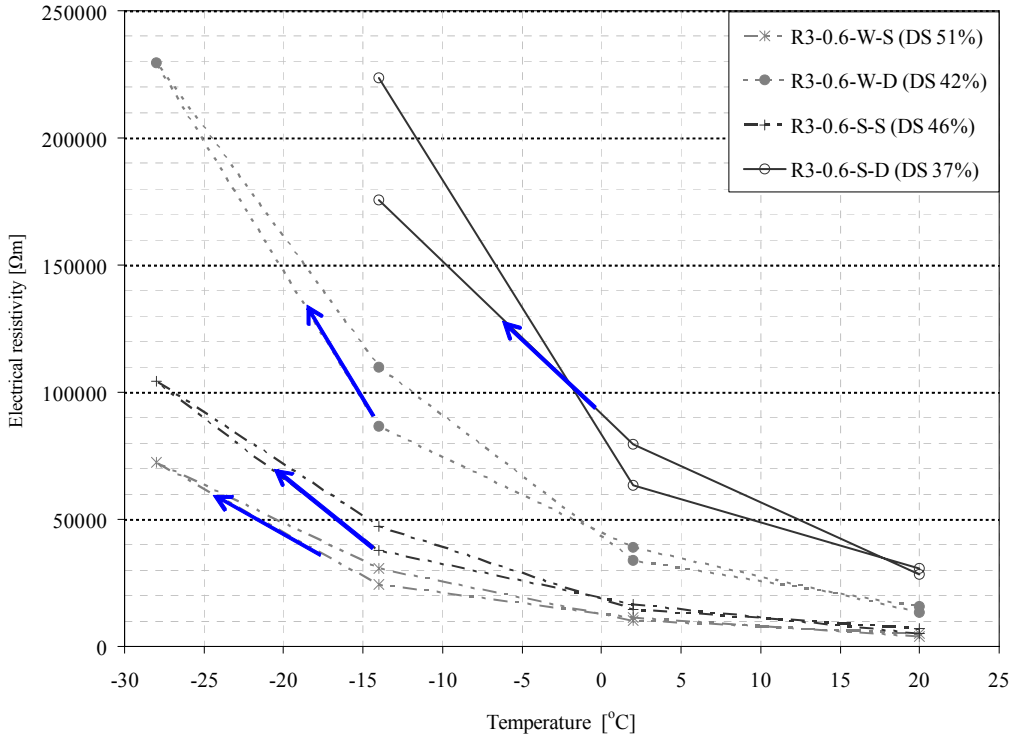


*Figure 5. 15 An example for the w/b 0.6 concrete of the hysteresis found between the temperature intervals; Freezing and Thawing. The Figure corresponds to a combination of Figures 5.10 and 5.11 (Run 3). The measurements were performed by PSP. Freezing is marked by arrows on the curves*

Figure 5. 14 and Figure 5. 15 show that the resistivity values on Thawing were generally higher or equal on 20°C and on -14°C than those of Freezing while they seem generally lower or equal for 2°C. The hysteresis is presumably generated by moisture phenomena and may also be connected to irreversible changes in the pore system due to ice formation in the pores. This will be discussed further in a later section.

### 5.2.3 Comparison of measurement techniques

Run 2 was partly performed to validate positive feedback as method for resistance measurements in concrete, therefore parallel measurements by electrochemical impedance spectroscopy and positive feedback were performed. This enabled comparison of the methods. EIS was regarded as the "true" method since the internal resistor is 10 MΩ while the capacity of the positive feedback equipment is 1MΩ.

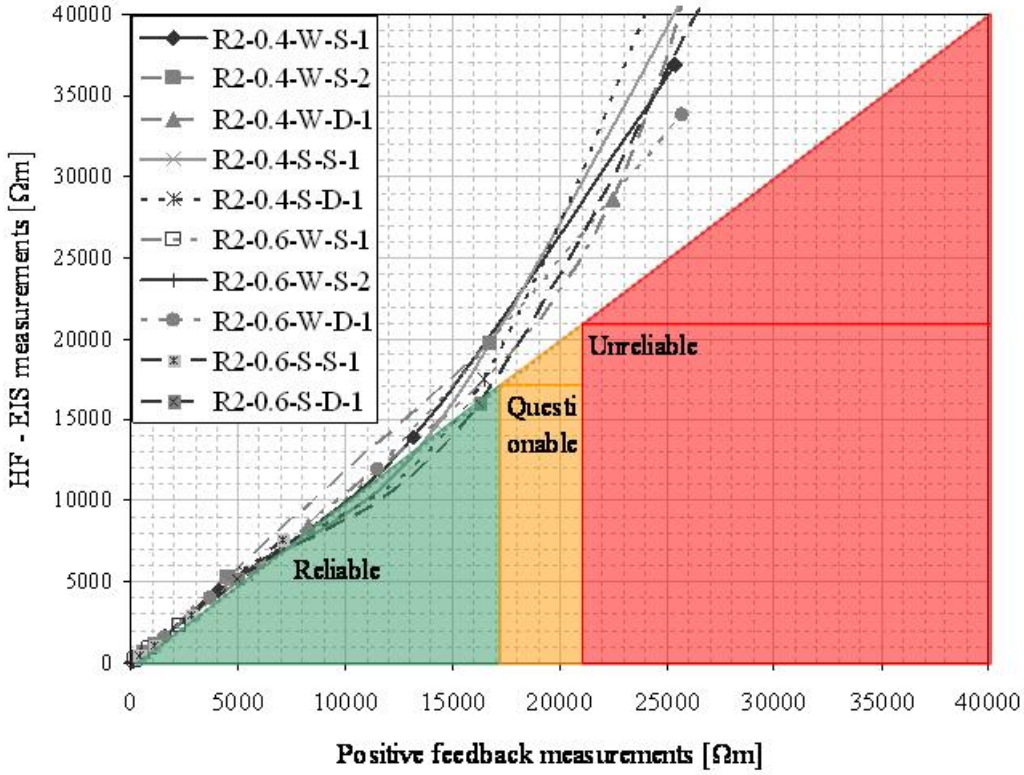


*Figure 5. 16 Comparison of EIS and positive feedback measuring techniques. The deviation of positive feedback started at 17 kΩm.*

Figure 5. 16 show electrical resistivity values recorded with EIS compared to corresponding simultaneously recorded values with positive feedback.

Apparently, positive feedback deviates at higher values of electrical resistivity than 17 kΩm, which correspond to an electric resistance of 485 kΩ.
The positive feedback circuit of the potentiostat sends out an AC current signal of variable frequency dependent upon the magnitude (amplitude) of the current signal.

At high resistances the current needs to be very small and thus the frequency is increased (above 100 kHz at 500 kΩ). Since the measurement at such high frequencies represents an impedance with a substantial capacitive contribution an error is introduced. The measurement will therefore not represent the circuit real impedance (resistance).

From Figure 5. 6 and Figure 5. 7 the big difference between the measurement techniques can be found during Freezing, and from Figure 5. 8 and Figure 5. 9 during Thawing. Generally, by comparing the results from Freezing and Thawing the results from the positive feedback (Thawing) generally give less steep slopes. Additionally the maximum values for some variants are more than a factor of two higher for the EIS results (Freezing).

The results from the positive feedback measurements show a critical point around 17 kΩm where the values deviate to lower values compared to the corresponding results from the EIS measurements.

The data during Freezing of Run 2 is given in Table 5. 1 and Table 5. 2 for the w/b 0.4 concrete and the w/b 0.6 concrete, respectively.

*Table 5. 1 Comparison of measured values of resistivity for the w/b 0.4 concrete with positive feedback and EIS. The ratios between the measured values are given in respect to EIS measurements.*

| Temp. | R2-0.4-W-S-1 | | R2-0.4-W-S-2 | | R2-0.4-W-D-1 | | R2-0.4-S-S-1 | | R2-0.4-S-D-1 | |
|---|---|---|---|---|---|---|---|---|---|---|
| [°C] | [Ωm] | | [Ωm] | | [Ωm] | | [Ωm] | | [Ωm] | |
| 20 | 1579 | **1.01** | 625 | **0.95** | 2926 | **1.06** | 4568 | **1.05** | 5320 | **1.04** |
| 20 | 1598 | | 595 | | 3108 | | 4808 | | 5525 | |
| 2 | 4095 | **1.09** | 1173 | **0.97** | 8278 | **1.03** | 14245 | **1.03** | 16503 | **1.06** |
| 2 | 4474 | | 1132 | | 8490 | | 14700 | | 17450 | |
| -14 | 13160 | **1.06** | 4550 | **1.16** | 22470 | **1.27** | 29505 | **1.70** | 31115 | **2.06** |
| -14 | 13913 | | 5280 | | 28613 | | 50100 | | 64050 | |
| -28 | 25410 | **1.45** | 16765 | **1.17** | 33600 | **2.40** | N/A | | N/A | |
| -28 | 36883 | | 19638 | | 80613 | | 153750 | | 225500 | |
| | Positive feedback | | | | EIS | | EIS/Positve feedback ratio | | | |

*Table 5. 2 Comparison of measured values of resistivity for the w/b 0.6 concrete with positive feedback and EIS. The ratios between the measured values are given in respect to EIS measurements*

| Temp. | R2-0.6-W-S-1 | | R2-0.6-W-S-2 | | R2-0.6-W-D-1 | | R2-0.6-S-S-1 | | R2-0.6-S-D-1 | |
|---|---|---|---|---|---|---|---|---|---|---|
| [°C] | [Ωm] | | [Ωm] | | [Ωm] | | [Ωm] | | [Ωm] | |
| 20 | 192 | **0.97** | 68 | **0.96** | 1575 | **0.98** | 434 | **1.06** | 4953 | **1.05** |
| 20 | 186 | | 65 | | 1548 | | 459 | | 5178 | |
| 2 | 396 | **0.99** | 104 | **0.94** | 3703 | **1.09** | 1134 | **0.99** | 16303 | **0.99** |
| 2 | 392 | | 98 | | 4053 | | 1121 | | 16075 | |
| -14 | 896 | **1.02** | 417 | **1.19** | 11533 | **1.04** | 2860 | **1.02** | 31745 | **1.69** |
| -14 | 917 | | 494 | | 11981 | | 2918 | | 53688 | |
| -28 | 2282 | **1.01** | 1575 | **1.06** | 25725 | **1.31** | 7123 | **1.06** | N/A | |
| -28 | 2296 | | 1664 | | 33800 | | 7544 | | 162625 | |
| | Positive feedback | | | | EIS | | EIS/Positve feedback ratio | | | |

The data given in Table 5. 1 and Table 5. 2 illustrates the difference between the measurement techniques. On lower resistivity values both techniques show similar results and the ratio between EIS and Positive feedback (in respect to EIS values) are close to 1, while on resistivities values larger than 17kΩm the values are very different. The difference was up to 2.4 times larger value obtained with EIS compared to corresponding measurement with positive feedback. This measurement of 33.8 kΩm corresponds to an electrical resistance of 966 kΩ which is very close to the limitations of the equipment (1MΩ).

Generally, it can be concluded that the positive feedback measurements contains an error on resistivity values larger than 17 kΩm which apparently increases on increasing resistivities. Caution has therefore been made when interpreting the positive feedback results higher than this critical value.

The potential square pulse equipment was not available for comparison, and therefore no verification against EIS was performed for this device.

### 5.2.4 Activation energy constants for the electrical resistivity

The results given in section 5.2.1 demonstrate a clear relation between temperature and the electrical resistivity of concrete. In general, the electrical resistivity increases exponentially with decreasing temperature, but the moisture content has a strong influence on the magnitude of the temperature effect.

This observation agrees with results found in the literature [32, 40]. In order to control if the results agree with the Hinrichson-Rasch Law [59] (Equation 2.34) the results are plotted as Arrhenius plots, i.e. log (resistivity) vs. reciprocal of temperature (1/T).

In the following section the Arrhenius plots for the various Runs and temperature intervals are given. Succeeding activation energy constants according to Hinrichson-Rasch Law are calculated and listed in Tables for all variants. In the end a general discussion is given.

If the results show a linear behaviour in the Arrhenius presentations then the temperature dependency of the progress of the electrical resistivity can be described by a single constant according to Hinrichson-Rasch law. However, if a deviation from linearity is observed this indicates that other processes influence the temperature sensitivity, and that the activation energy constant is a function of temperature, rather than a constant.

A nonlinear behaviour may indicate occurrence of irreversible changes in water distribution, irreversible changes in the pore system, and changes in the chemical composition of the pore water. Further it may also indicate freezing of pore water or a change in the conduction phase.

This will be discussed further after the presentation of Arrhenius plots.

Run 1

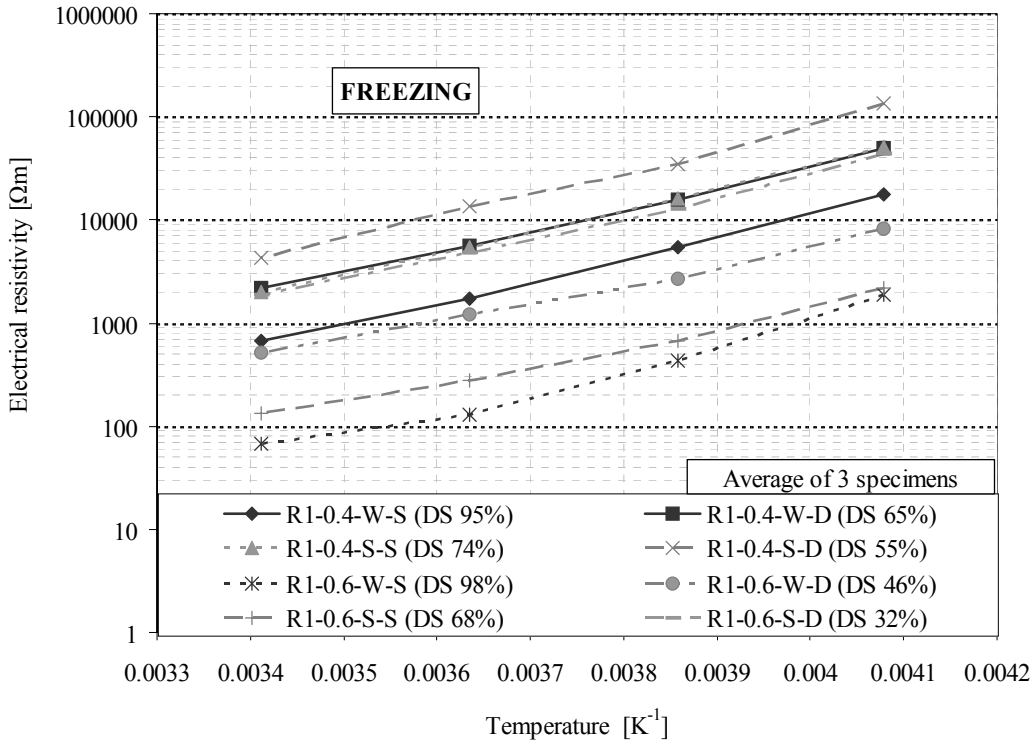


*Figure 5. 17 Arrhenius plot for all variants during the Freezing of Run 1. The results are averaged from 3 specimens of each variant. Corresponds to results presented in Figure 5.1 and Figure 5.2*

From Figure 5. 17 it may seem as if all the variants could be expressed by individual activation energy constants. Due to the linearity in the Arrhenius-plot it may be deduced that during Freezing all variants follow the Hinrichson-Rasch law. The calculated activation energy constants are given in Table 5. 3.

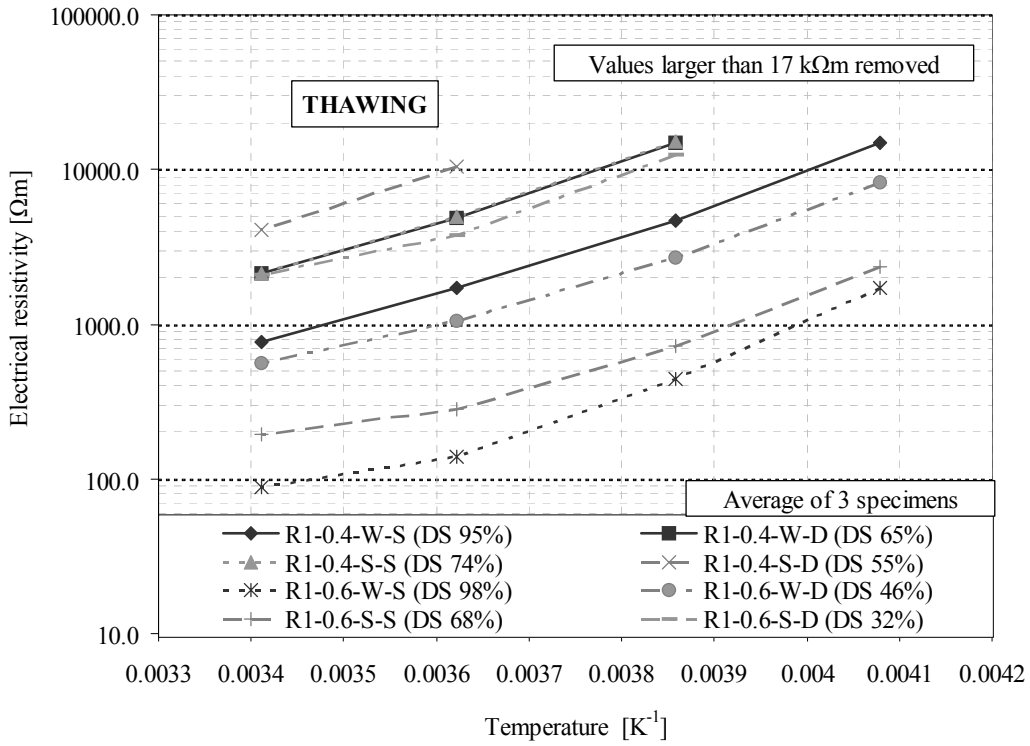


*Figure 5. 18 Arrhenius plot for all variants during Thawing in Run 1. The results are averaged from 3 specimens of each variant. Corresponds to results presented in Figure 5.4 and Figure 5.5 with values larger than 17 kΩm removed.*

On Thawing, given in Figure 5. 18, more deviation from linearity can be observed compared to that found for Freezing. The deviation from

linearity indicates that other processes influence the temperature sensitivity. The measurements were performed by positive feedback and some of the deviations from linearity on resistivity values greater than 17 kΩm are probably influenced by uncertainties in the measurements.

The calculated activation energy constants (according to Hinrichson-Rasch law) are presented in Table 5. 3. The correlation coefficients ($R^2$) are shown in a separate column to illustrate the deviation from linearity of each variant.

*Table 5. 3 Calculated activation energy constants with corresponding correlation coefficients for all variants tested in Run 1*

| Variant | Freezing | | Thawing | |
|---|---|---|---|---|
| | EIS | | Positive Feedback | |
| | Activation energy constant [K] | $R^2$ | Activation energy constant [K] | $R^2$ |
| R1-0.4-W-S (DS 95%) | 4925 | 0.998 | 4441 | 0.995 |
| R1-0.4-W-D (DS 65%) | 4652 | 0.998 | 4015 | 0.995 |
| R1-0.4-S-S (DS 74%) | 4820 | 0.999 | 4002 | 0.993 |
| R1-0.4-S-D (DS 55%) | 5063 | 0.994 | 3976 | 0.997 |
| R1-0.6-W-S (DS 98%) | 5047 | 0.973 | 4512 | 0.965 |
| R1-0.6-W-D (DS 46%) | 4068 | 0.994 | 4050 | 0.987 |
| R1-0.6-S-S (DS 68%) | 4160 | 0.988 | 3778 | 0.959 |
| R1-0.6-S-D (DS 32%) | 4713 | 0.995 | 4047 | 0.990 |

The hysteresis between Freezing and Thawing observed in Figure 5. 17 – Figure 5. 18 and in the values of the activation energy constants are

probably related to water transport mechanisms and or phase transformations. This will be further discussed in the general discussion.

Run 2

It must be emphasised that in Run 2 there were no parallel specimens and false measurements on one specimen will play a large role.

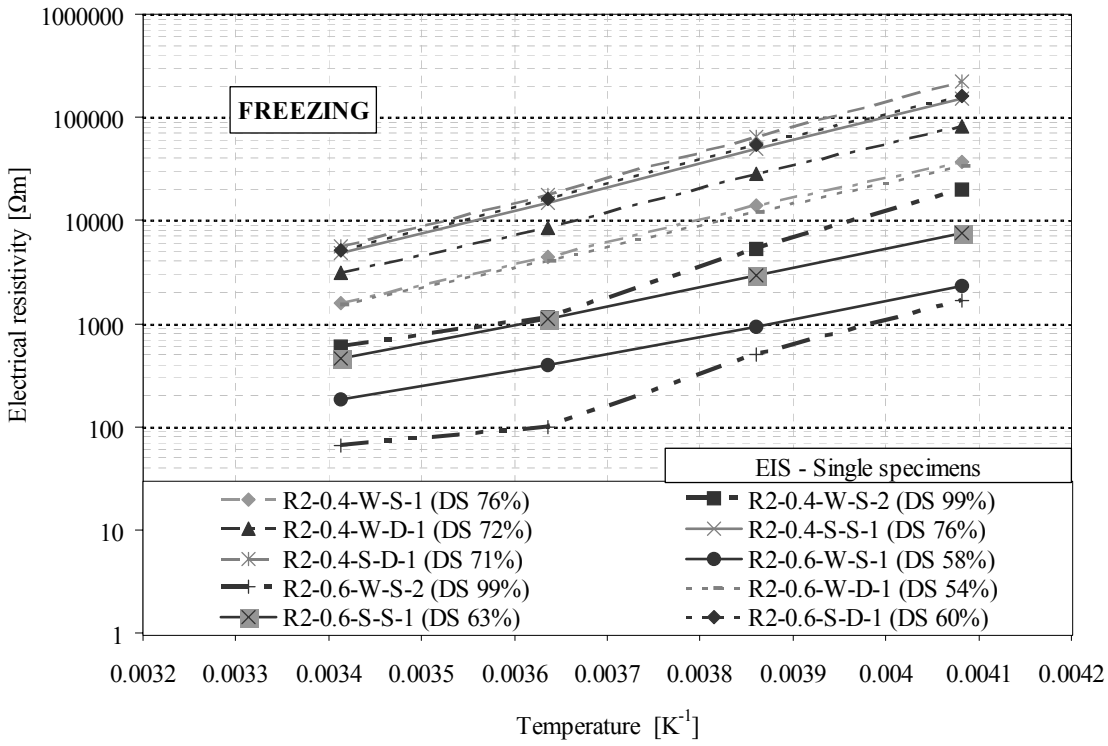


*Figure 5. 19 Arrhenius plot for all variants during the Freezing of Run 2. Each variant is represented by a single specimen. The measurements are performed by EIS. The Figure corresponds to results presented in Figure 5.6*

The deviation from linearity in the Arrhenius-plots, given in Figure 5. 19, are very small, except for the specimens that were saturated by vacuum

suction (R2-0.4-W-S-2 and R2-0.6-W-S-2). These specimens have higher moisture content than the other tested specimens in Run 2. Therefore, it is reasonable to anticipate that the moisture condition generates the deviation from linearity. It may seem as the activation energy constants for the anomalies have a departure value somewhere between 2°C and -14°C. No data is obtained in the range between these temperatures. Ice may have formed during Freezing in the largest pores between 2°C and -14°C and therefore a change in the conduction phases due to ice formation may explain the behaviour of the anomalies.

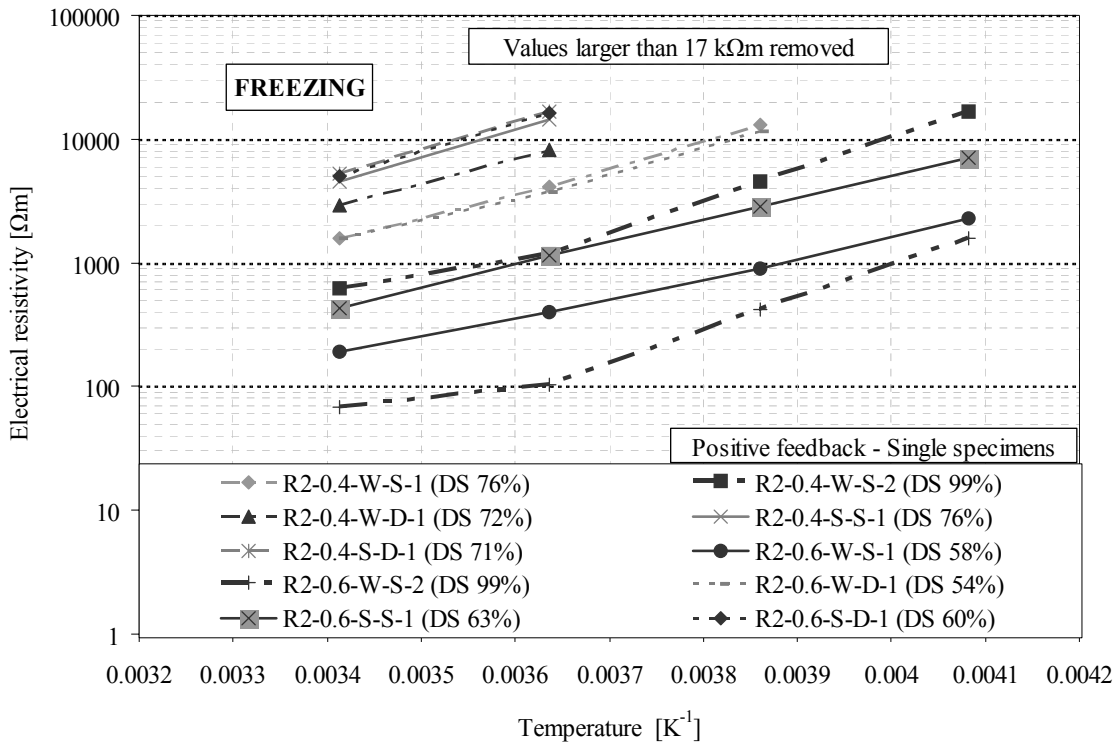


*Figure 5. 20 Arrhenius plot for all variants during Freezing in Run 2. Each variant is represented by a single specimen. The measurements are performed by positive feedback. The Figure corresponds to results presented in Figure 5.7*

The parallel measurements by positive feedback compared to those performed by EIS show more deviation from linearity in the Arrhenius presentation. Also in these results the R2-0.4-W-S-2 and R2-0.6-W-S-2 specimens stands out with large deviation from linearity compared to the other variants. As for Run 1 the measurements performed with positive feedback were influenced by errors in the measurements introduced by the equipment.

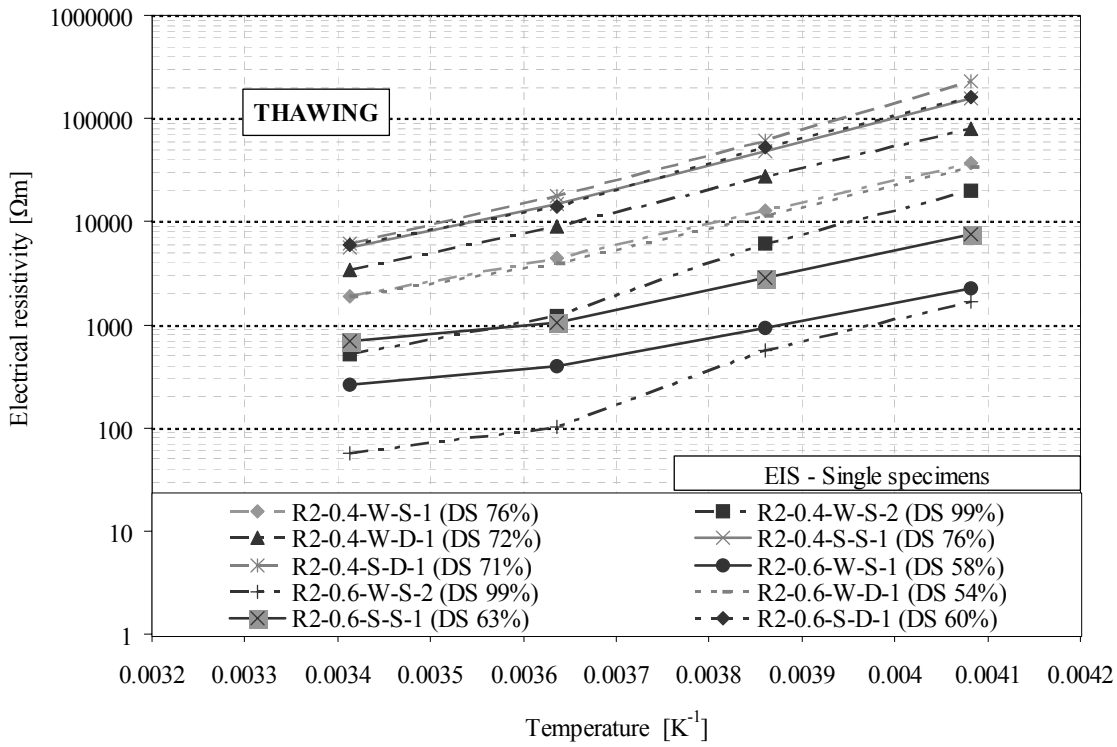


*Figure 5. 21 Arrhenius plot for all variants during Thawing in Run 2. Each variant is represented by a single specimen. The measurements are performed by EIS. The Figure corresponds to results presented in Figure 5.8*

The specimens that behaved differently on Freezing continue their anomalous behaviour also on Thawing. Furthermore, some of the specimens of the concrete with w/b ratio of 0.6 seem to have similar deviation from linearity as the two specimens treated by vacuum. This is a further statement that moisture is affecting the temperature sensitivity of the concrete, but it also introduces the possibility that the layout of the concrete physical interior is an influencing parameter. Since the w/b 0.6 concrete have a coarser pore structure than the w/b 0.4 concrete it is

expected that more ice formation should have take place on the higher w/b – ratio. The observation of anomalous behaviour on several of the w/b 0.6 variants sustains the possibility of ice formation influencing the progress of the electrical resistivity.

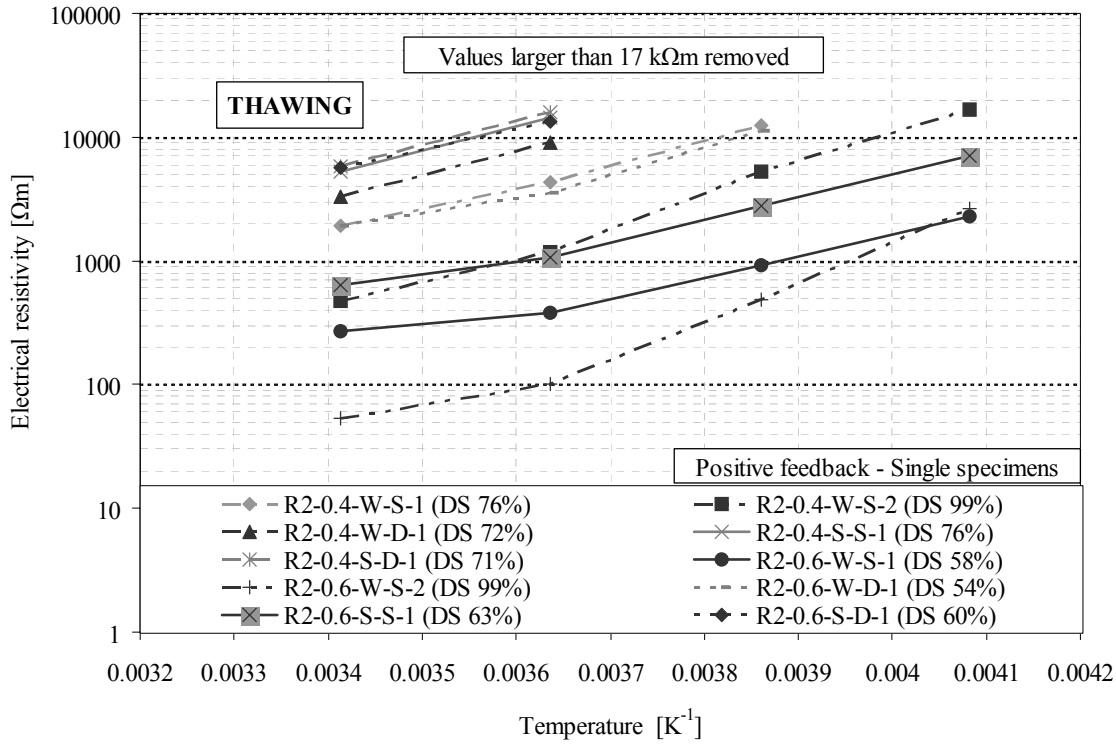


*Figure 5. 22 Arrhenius plot for all variants during Thawing in Run 2. Each variant is represented by a single specimen. The measurements are performed by positive feedback. The Figure corresponds to results presented in Figure 5.9*

Similarly as for Freezing the measurements performed by positive feedback show a larger anomaly than those performed by EIS.

In Figure 5. 22 it can be observed the same tendencies indicated in Figure 5. 21 with more specimens deviating from linearity in the Arrhenius presentation.

The calculated activation energy constants for all results in Run 2 are presented in Table 5. 4 in the same manner as it was presented for Run 1.

*Table 5. 4 Calculated activation energy constants with corresponding correlation coefficients for all variants tested in Run 2*

| Variant | Freezing | | Thawing | |
|---|---|---|---|---|
| | Activation energy constant [K] | $R^2$ | Activation energy constant [K] | $R^2$ |
| **Electrochemical Impedance Spectroscopy** | | | | |
| R2-0.4-W-S-1 (DS 76%) | 4378 | 0.996 | 4102 | 0.988 |
| R2-0.4-W-S-2 (DS 99%) | 4943 | 0.956 | 5160 | 0.972 |
| R2-0.4-W-D-1 (DS 72%) | 4547 | 0.993 | 4354 | 0.993 |
| R2-0.4-S-S-1 (DS 76%) | 4823 | 0.995 | 4583 | 0.989 |
| R2-0.4-S-D-1 (DS 71%) | 5148 | 0.993 | 4980 | 0.988 |
| R2-0.6-W-S-1 (DS 58%) | 3464 | 0.989 | 2995 | 0.955 |
| R2-0.6-W-S-2 (DS 99%) | 4643 | 0.931 | 4871 | 0.950 |
| R2-0.6-W-D-1 (DS 54%) | 4282 | 0.993 | 3993 | 0.979 |
| R2-0.6-S-S-1 (DS 63%) | 3873 | 0.994 | 3368 | 0.948 |
| R2-0.6-S-D-1 (DS 60%) | 4787 | 0.996 | 4619 | 0.981 |
| **Positive feedback** | | | | |
| R2-0.4-W-S-1 (DS 76%) | 3945 | 0.990 | 3644 | 0.991 |
| R2-0.4-W-S-2 (DS 99%) | 4619 | 0.957 | 5040 | 0.981 |
| R2-0.4-W-D-1 (DS 72%) | 3476 | 0.980 | 3308 | 0.984 |
| R2-0.4-S-S-1 (DS 76%) | 3705 | 0.996 | 3416 | 0.999 |
| R2-0.4-S-D-1 (DS 71%) | 3512 | 0.991 | 3284 | 0.996 |
| R2-0.6-W-S-1 (DS 58%) | 3404 | 0.987 | 2995 | 0.939 |
| R2-0.6-W-S-2 (DS 99%) | 4426 | 0.931 | 5437 | 0.942 |
| R2-0.6-W-D-1 (DS 54%) | 3945 | 0.991 | 3681 | 0.976 |
| R2-0.6-S-S-1 (DS 63%) | 3873 | 0.998 | 3368 | 0.962 |
| R2-0.6-S-D-1 (DS 60%) | 3705 | 0.991 | 3356 | 0.998 |

Table 5. 4 indicate the same trends as found in Figure 5. 19 – Figure 5. 22. There is a general hysteresis between freezing and thawing. However,

there are exceptions. For the wettest specimens and specimens of the concrete with w/b of 0.6 the hysteresis is less clear. For the vacuum treated variants an increase in the calculated activation energy constants appears. Table 5.4 sustains the theory of water transport mechanisms influencing the temperature sensitivity of the wettest specimens. This is indicated by lower $R^2$ values. However, the observation undermines the theory of ice formation in the pores. Ice formation is expected to result in irreversible changes in the pores. This should have resulted in a larger hysteresis.

Run 3

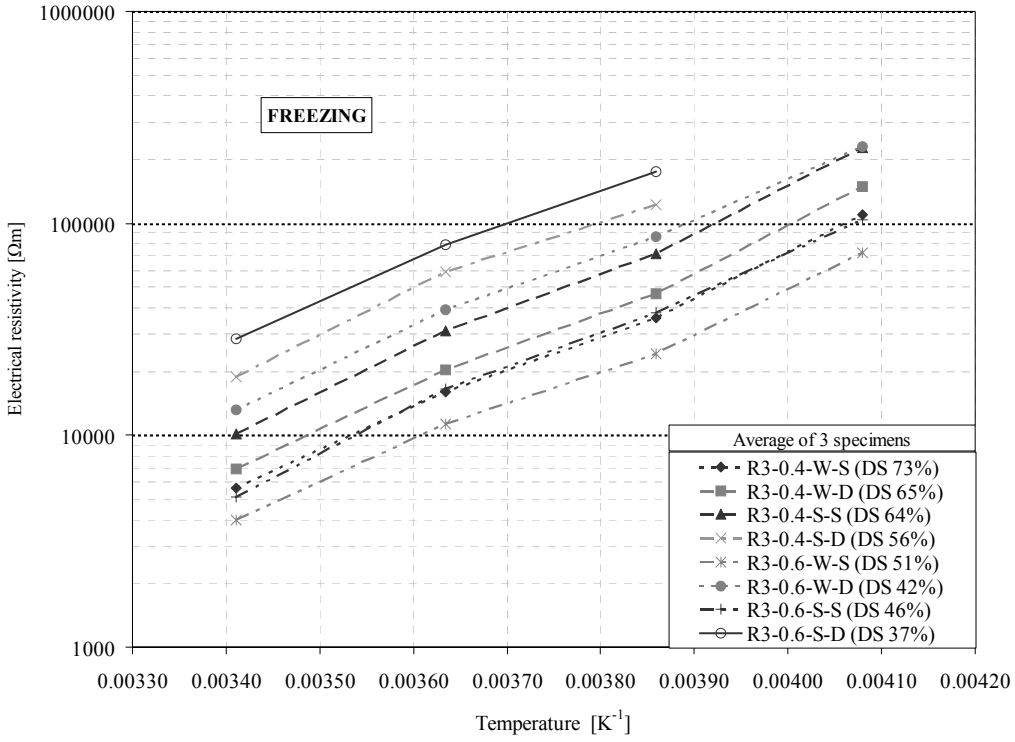


*Figure 5. 23 Arrhenius plot for all variants during Freezing in Run 3. The results are averaged from 3 specimens of each variant. Measurements are performed by PSP. The Figure corresponds to results presented in Figure 5.10*

The Arrhenius plot presented in Figure 5. 23 show similar tendencies to deviation from linearity as the presentations for Run 1 and Run 2. However, for the temperature interval in Run 3 the deviations from linearity seem more general. In Run 3 the measurements were performed by a different method that may behave differently than the previously described methods.

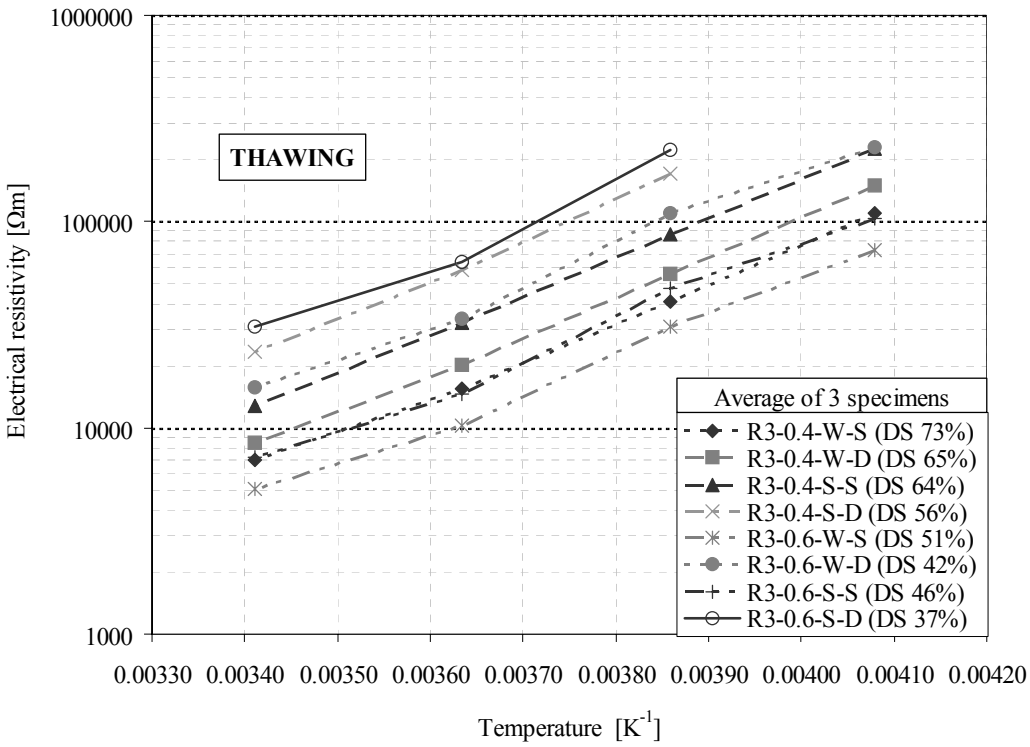


*Figure 5. 24 Arrhenius plot for all variants during Thawing in Run 3. The results are averaged from 3 specimens of each variant. Measurements are performed by PSP. The Figure corresponds to results presented in Figure 5.11*

The general deviation from linearity found on Freezing is less evident during Thawing shown in Figure 5. 24. However, there are changes for several of the variants in Run 3. The calculated activation energy constants for the variants tested in Run 3 are listed in Table 5.5.

*Table 5. 5 Calculated activation energy constants with corresponding correlation coefficients for all variants tested in Run 3*

| Variant | Freezing | | Thawing | |
|---|---|---|---|---|
| | Activation energy constant [K] | $R^2$ | Activation energy constant [K] | $R^2$ |
| R3-0.4-W-S (DS 73%) | 4354 | 0.996 | 4150 | 0.998 |
| R3-0.4-W-D (DS 65%) | 4510 | 0.996 | 4318 | 0.999 |
| R3-0.4-S-S (DS 64%) | 4559 | 0.996 | 4318 | 1.000 |
| R3-0.4-S-D (DS 56%) | 4198 | 0.983 | 4450 | 0.998 |
| R3-0.6-W-S (DS 51%) | 4246 | 0.995 | 4077 | 0.994 |
| R3-0.6-W-D (DS 42%) | 4210 | 0.997 | 4138 | 0.992 |
| R3-0.6-S-S (DS 46%) | 4438 | 0.996 | 4138 | 0.991 |
| R3-0.6-S-D (DS 37%) | 4077 | 0.994 | 4438 | 0.977 |

In Table 5.5 a hysteresis can be observed as a decrease in activation energy constants between Freezing and Thawing. The sealed-cured and dried (S-D) variant for both concrete compositions, however, stands out. This is observed as an increase in activation energy constant for both variants. These variants had a lower moisture condition than the other variants resulting in larger electrical resistivities. Apparently from Figure 5.23 and Figure 5.24 these dry variants had more profound hysteresis effects, which are also indicated by the correlation coefficients.

Run 4

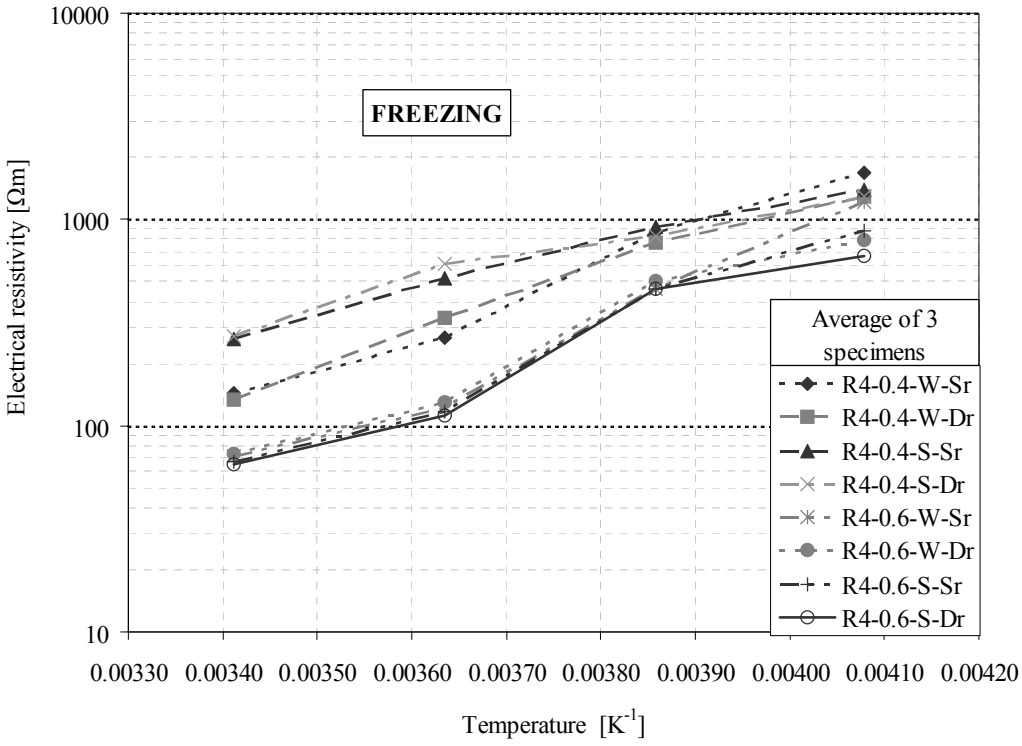


*Figure 5. 25 Arrhenius plot for all variants during the Freezing of Run 4. The results are averaged from 3 specimens of each variant. Measurements are performed by PSP. The Figure corresponds to results presented in Figure 5.12. All specimens had DS = 1.0.*

The specimens tested in Run 4 were saturated by immersion in water for 8 weeks before the run was initiated. The various specimens, therefore, had quite high moisture content. The deviations from linearity for the variants appears larger for all variants in comparison to the results from Run 1, Run

2 and Run 3. Similarly as observed by the results from the vacuum treated specimens in Run 2 the curves have a break point between 2°C and -14°C.

In Figure 5. 25 the concrete compositions are clearly separated at higher temperatures. For the concrete with w/b of 0.4 it is further possible to separate the various curing conditions. However, the variants which were oven dried at 40°C for one week do not stand out in comparison to the variants which were sealed directly after curing.

The divergence between the variants of the concrete with w/b 0.6 seems less dependent on curing and handling, i.e. the scatter between the w/b of 0.6 variants is significantly smaller compared to the w/b of 0.4 variants.

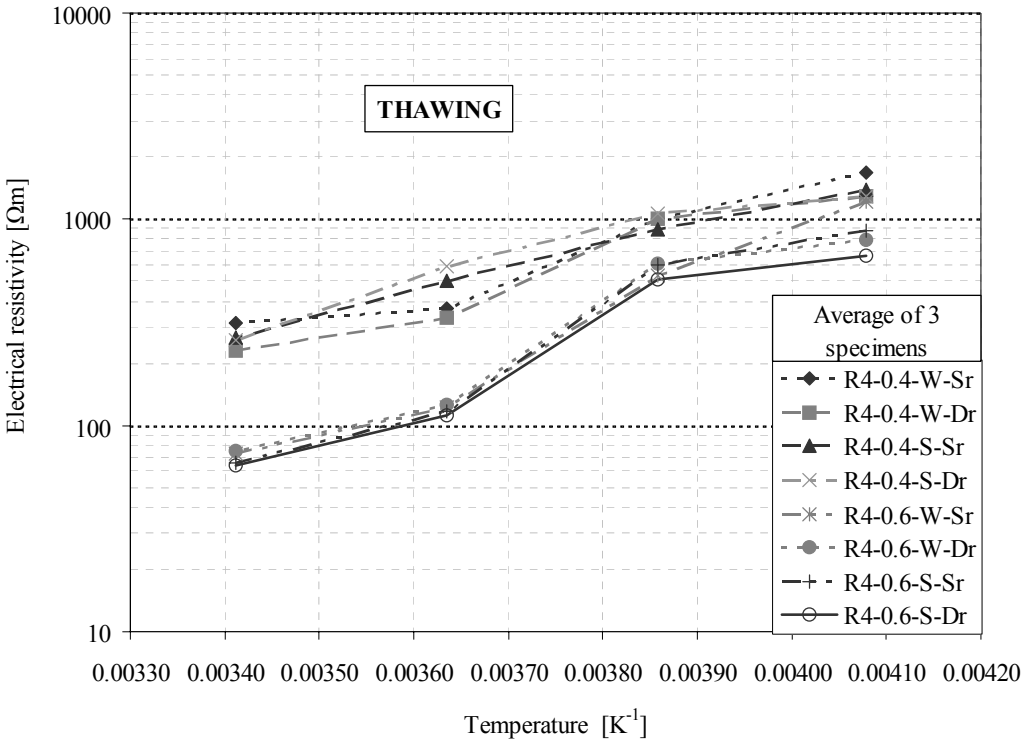


*Figure 5. 26 Arrhenius plot for all variants during the Thawing of Run 4. The results are averaged from 3 specimens of each variant. Measurements are performed by PSP. The Figure corresponds to results presented in Figure 5.13. All specimens had DS = 1.0.*

Figure 5. 26 illustrated the same effects as Figure 5. 25. However, the scatter for the w/b 0.4 variants appears smaller. There is hardly any change in the behaviour of the w/b 0.6 variants.

The activation energy constants are given in Table 5. 6 with corresponding correlation coefficients.

*Table 5. 6 Calculated activation energy constants with corresponding correlation coefficients for all variants tested in Run 4*

| Variant | Freezing | | Thawing | |
|---|---|---|---|---|
| | Activation energy constant [K] | $R^2$ | Activation energy constant [K] | $R^2$ |
| R4-0.4-W-Sr | 3849 | 0.985 | 2718 | 0.938 |
| R4-0.4-W-Dr | 3416 | 0.986 | 2815 | 0.940 |
| R4-0.4-S-Sr | 2502 | 0.989 | 2478 | 0.994 |
| R4-0.4-S-Dr | 2237 | 0.959 | 2418 | 0.937 |
| R4-0.6-W-Sr | 4414 | 0.977 | 4450 | 0.970 |
| R4-0.6-W-Dr | 3825 | 0.963 | 3897 | 0.928 |
| R4-0.6-S-Sr | 4089 | 0.972 | 4234 | 0.944 |
| R4-0.6-S-Dr | 3765 | 0.950 | 3825 | 0.933 |

The calculated activation energy constants, given in Table 5. 6, support the statement that the w/b 0.6 variants differ only marginally between Freezing and Thawing. However, between Freezing and Thawing there is a hysteresis for the water cured w/b 0.4 variants.

Since the specimens tested in Run 4 have high moisture contents it is probable that some of the water is able to freeze in the pores. This will be further elaborated in the following general discussion.

### 5.2.5 General discussion of the temperature effect on the electrical resistivity of concrete

The results given in section 5.2.1 show that the relationship between temperature and the electrical resistivity of concrete can be described by an activation energy constant following the Hinrichson-Rasch law.

*Table 5. 7 Summary of the apparent activation energy constants calculated from the results found in the ER – experiments.*

| w/b-ratio | | Curing | | Handling | | | | | Apparent activation energy constants | | | | | | | | | |
|---|---|---|---|---|---|---|---|---|---|---|---|---|---|---|---|---|---|---|
| | | | | | | | | | Run 1 | | Run 2 | | | | Run 3 | | Run 4 | |
| | | | | | | | | | EIS* | P.F.** | EIS* | | P.F.** | | PSP*** | PSP*** | PSP*** | PSP*** |
| 0.4 | 0.6 | W | S | S | D | V | Sr | Dr | Freeze | Thaw | Freeze | Thaw | Freeze | Thaw | Freeze | Thaw | Freeze | Thaw |
| | | | | | | | | | [K] | [K] | [K] | [K] | [K] | [K] | [K] | [K] | [K] | [K] |
| X | | X | | X | | | | | 4925 | 4441 | 4378 | 4102 | 3945 | 3644 | 4354 | 4150 | | |
| X | | X | | | X | | | | 4652 | 4015 | 4547 | 4354 | 3476 | 3308 | 4510 | 4318 | | |
| X | | X | | X | | X | | | | | 4943 | 5160 | 4619 | 5040 | | | | |
| X | | X | | | | | X | | | | | | | | | | 3849 | 2718 |
| X | | X | | | | | | X | | | | | | | | | 3416 | 2815 |
| X | | | X | X | | | | | 4820 | 4002 | 4823 | 4583 | 3705 | 3416 | 4559 | 4318 | | |
| X | | | X | | X | | | | 5063 | 3976 | 5148 | 4980 | 3512 | 3284 | 4198 | 4450 | | |
| X | | | X | | | | X | | | | | | | | | | 2502 | 2478 |
| X | | | X | | | | | X | | | | | | | | | 2237 | 2418 |
| | X | X | | X | | | | | 5047 | 4512 | 3464 | 2995 | 3404 | 2995 | 4246 | 4077 | | |
| | X | X | | | X | | | | 4068 | 4050 | 4282 | 3993 | 3945 | 3681 | 4210 | 4138 | | |
| | X | X | | X | | X | | | | | 4643 | 4871 | 4426 | 5437 | | | | |
| | X | X | | | | | X | | | | | | | | | | 4414 | 4450 |
| | X | X | | | | | | X | | | | | | | | | 3825 | 3897 |
| | X | | X | X | | | | | 4160 | 3778 | 3873 | 3368 | 3873 | 3368 | 4438 | 4138 | | |
| | X | | X | | X | | | | 4713 | 4047 | 4787 | 4619 | 3705 | 3356 | 4077 | 4438 | | |
| | X | | X | | | | X | | | | | | | | | | 4089 | 4234 |
| | X | | X | | | | | X | | | | | | | | | 3765 | 3825 |

***) EIS = Electrochemical Impedance Spectroscopy **) P.F. = Positive Feedback ***) PSP = Potential Square Pulse**

**Not tested** **V in handling refers to specimens treated by vacuum**

In Table 5. 7 it can be observed that the activation energy constants are in the range 2000 K – 5000 K. These activation energy constants give the

temperature sensitivity of the electrical resistivity of the variants tested in the ER – experiments. In general the correlation coefficients suggest that the temperature sensitivity can be described by a constant. However, there are exceptions.

In several cases deviation from linearity in the Arrhenius presentation were found. In these cases the temperature sensitivity of the electrical resistivity varies with temperature. The calculated activation energy constants are therefore termed "Apparent activation energy constants".

Deviation from linearity in the Arrhenius presentations occurred in nearly all four Runs. This deviation is presumably generated by several interacting mechanisms, but the dominant appears to be related to moisture. Higher moisture contents results in larger deviations, but lower activation energies. This substantiates a clear connection between temperature, moisture content and the electrical resistivity.

Concrete is a complex electrolytic system. Conduction in concrete will occur in different parallel pathways. The main contributor to conduction in concrete is pore water solution which is highly conductive due to the presence of ions, mostly $K^+$, $Na^+$ and $OH^-$, with small amounts of $Ca^{2+}$, $SO_4^{2-}$. Additional ions (such as chlorides) can also be present due to infiltration from other sources (such as seawater and de-icing salt solutions), increasing the concentration of ions in the pore water and, presumably, reducing the electrolytic resistance. The electrical resistivity of pore water is in the range of 0.1 – 0.3 Ωm dependent on the ionic strength; thereby, primarily controlled by the pH. It is also supposed that

much of the conduction is done along the adsorbed layers of the pore walls (adsorbate phase). This ionised layer contains high concentrations of conductive ions in a very porous structure that may lead to locally very low electrical resistivity.

The cement paste is in itself conductive. Even in oven dried state it acts as a semiconductor according to Whiting and Nagi [27]. This is assumed to be due to the presence of non-evaporable water.

*"Any temperature change imposed on wet concrete leads to different chemical potential changes in the various water phases (adsorbed, vapour, capillary, gel and interlayer), and therefore to internal redistribution which is time dependent"* according to Radjy, Sellevold and Hansen [73].

To repeat; temperature has an effect on the moisture distribution between the different water states in concrete. Time is a parameter for the redistribution of water.

Such large temperature changes on the exposed concrete as in the ER – experiments, lead to a redistribution of the water phases which presumably are not stabilised between the measurements. This time-dependency generates a possible drift in the measurements. However, total redistribution before measurement takes impractically long time until stable values are obtained; if at all a total stabilisation is feasible.
To perform measurements of effects of temperature on either property of concrete will suffer by such redistribution effects.

At higher moisture contents more of the capillaries are water-filled. With more water present in larger pores more water is able to freeze. Ice formation in the largest capillaries is likely. As stated in the start of this section a hysteresis was found nearly always between Freezing and Thawing (Figure 5. 14). The values of the resistivity at 20°C was generally lower or equal on Freezing compared to Thawing, and more or less equal at the other temperatures.

The observation of hysteresis indicates either that some of the moisture evaporates and is exchanged with the atmosphere in the fridge between 2°C and 20°C during Thawing or that during Freezing ice formation has caused irreversible changes in the pore system that shows when all the ice is melted. These observations substantiates that any temperature change generates redistribution effect in the various water phases, and may also be an indication on that ice formation have occurred in the pores. The hysteresis was largest for the variants of the concrete with w/b – ratio of 0.6.

Obviously, the moisture condition of the concrete and the concrete temperature are very closely connected. Before a further discussion is performed it is necessary to process the effect of moisture condition on the electrical resistivity of the specimens tested in the various Runs.

## 5.3 Influence of moisture state on electrical resistivity in concrete

After some initial test of the electrical resistivity of concrete below 0°C temperatures it was deemed necessary to simultaneously keep control of the moisture condition of the specimens. Moisture control was performed by weighing the samples before and after the run for Run 1 and Run 2, while for Run 3 and Run 4 the weighing was performed also during the runs.

The moisture content in concrete is here related to degree of saturation, calculated by:

$$DS = \frac{Weight(in\ situ) - Weight\ after\ drying\ at\ 105°C}{Weight\ after\ pressuration - Weight\ after\ drying\ at\ 105°C} \quad (Equation\ 5.1)$$

The dry weights were not measured in Run 2, therefore the data from this run has not been taken into consideration in the present section.

No measurements of the relative humidity inside the pores were performed. A decrease in temperature results in immediate change in the relative humidity inside the pores. This parameter was therefore not considered as reliable to measure.

### 5.3.1 Influence of moisture state on the electrical resistivity

By combining all the results from Run 1, Run 3 and Run 4 sorted by moisture state and temperature a correlation between moisture state and the electrical resistivity was found. A presentation of the results for both concrete qualities is given in Figure 5. 27 for a temperature of 20°C.

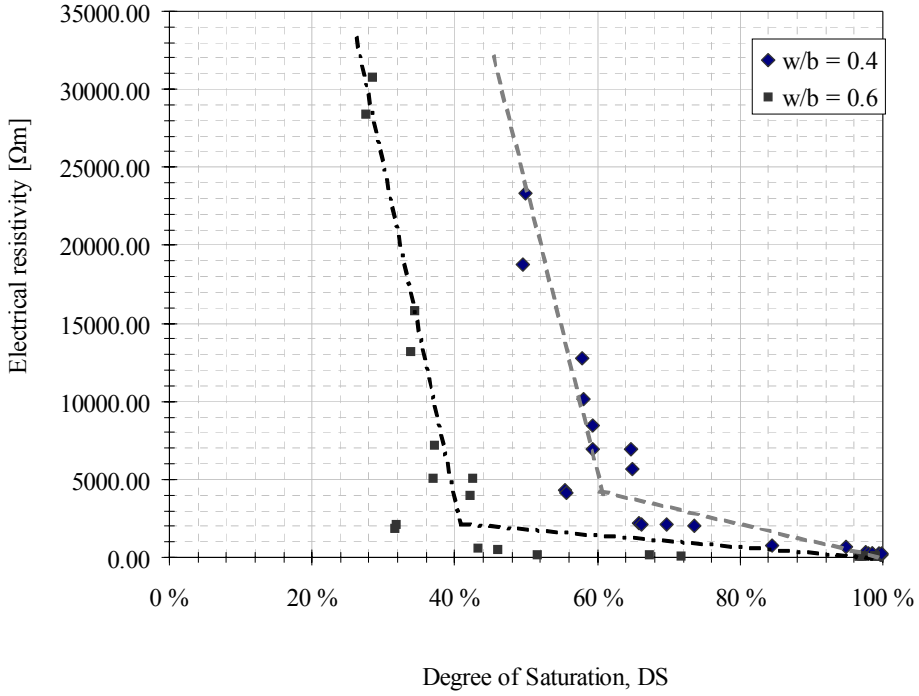


*Figure 5. 27 Comparison of the effect of moisture state (displayed as degree of saturation, DS) on the electrical resistivity for w/b 0.4 and w/b 0.6 concrete mixes at 20°C. The dotted lines indicate the breaking point in electrical resistivity at the respective degrees of saturations for the w/b 0.4 concrete and the w/b 0.6 concrete, respectively.*

By Figure 5. 27 an effect of water – binder ratio can be observed. All four variants for the respective w/b – ratios are included in the plot.

In Figure 5. 28 the differences introduced by the curing and handling are illustrated.

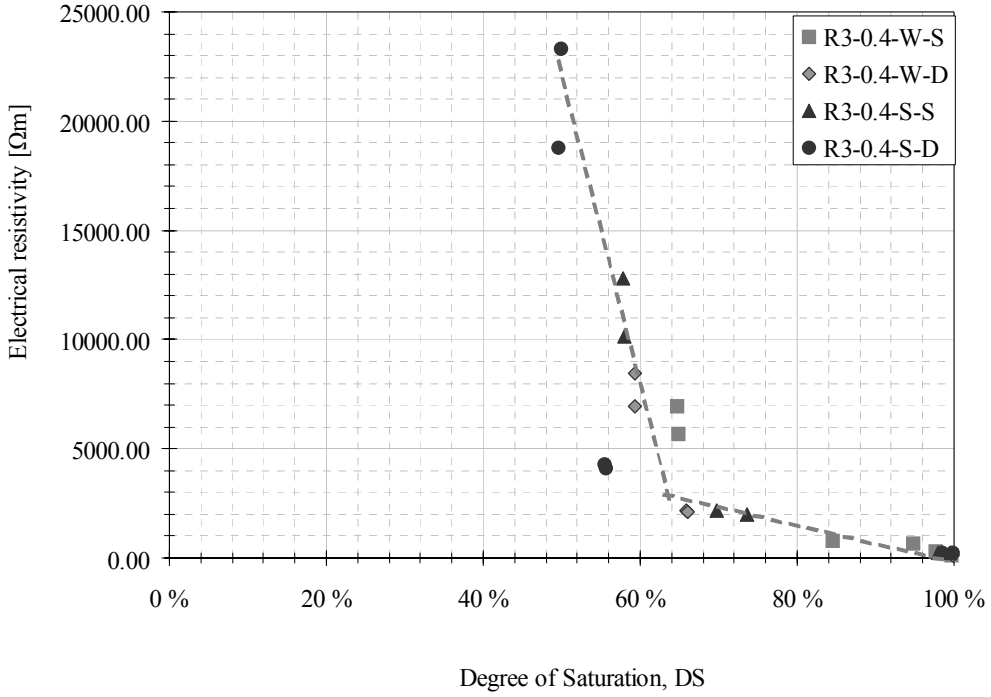


*Figure 5. 28 Comparison of the variants for the w/b 0.4 concrete. The Figure illustrates the effect of curing and handling on the relationship between electrical resistivity at 20°C and moisture condition (displayed as degree of saturation, DS).*

From Figure 5. 28 it can clearly be seen that curing and handling affects the results. Generally the water cured and sealed variant appear to be most moisture sensitive of the variants. The sealed cured and dried variant

seems less moisture sensitive of the variants. The sealed cured variants seem less moisture sensitive than the water cured which is in agreement with observations of a coarser structure caused by internal forces from drying effects during early curing on self-desiccated concrete compared with water-cured concrete. By drying the concrete pores are inflicted by large forces which may have lead to profound and irreversible changes in the layout of the pores even at such gentle drying as 40°C for 1 week.

However, the effect of curing and handling appears to be quite marginal and acceptably small in order to illustrate the overall effect of moisture state on the electrical resistivity between the different w/b – ratios. A similar effect was found for the w/b 0.6 concrete.

### 5.3.2 Discussion of the influence of moisture state on the electrical resistivity of concrete

Figure 5. 27 clearly confirm previous observations [32-35, 41-49] that the moisture state is the main contributor to the electrical resistivity. The moisture state decides the degree of pore filling; hence, it decides the amount of available current-pathways.

Conduction in concrete has to go in the water phases. All theories found in the literature states that the capillary conduction is the dominant. However, the results are discussed based on two main assumptions.

1. Conduction in concrete takes place in the continuous capillary water phase where ever these are available and
2. when and where continuous capillary water is not present the conduction in concrete goes in the adsorbed water phase on the pore walls and through the gel/interlayer spaces which are water filled at quite low degrees of saturation.

The above implies: At higher moisture contents the capillary water dominates the total conduction and is nearly only a function of the ionic strength of the pore water and the porosity of the concrete. At lower moisture contents the adsorbed layer play a larger role, and when the moisture content reach the critical value the conduction is dominated by conduction in the adsorbed water phase. When the adsorbed layer is dominant the thickness of the adsorbed layer is the critical parameter. It is assumed that the tortuous path the current has to pass reach a limiting value at this critical value of moisture content.

The resistivity for both concrete qualities increases very strongly below a critical value of the moisture content. These critical values are, presumably, related to loss of continuity and that the current paths change from capillary water to the other water phases. The critical points occur at degrees of saturations of 60% and 40% for the concretes with w/b ratios 0.4 and 0.6, respectively.

This different moisture sensitivity may be explained by the differences in porosity. The w/b 0.6 concrete has a higher measured total porosity, 18% compared to 15% for the w/b 0.4 concrete (averaged values). The w/b 0.6

concrete has a relative larger fraction of capillary pores. This concrete will have more available pathways for the current to flow than the w/b 0.4 concrete and therefore be less moisture sensitive at higher moisture contents. Additionally the w/b 0.6 concrete will allow the current to flow more or less linear in the high moisture range, while the w/b 0.4 concrete will form more tortuous current paths. An illustration of this effect is displayed in Figure 5. 29.

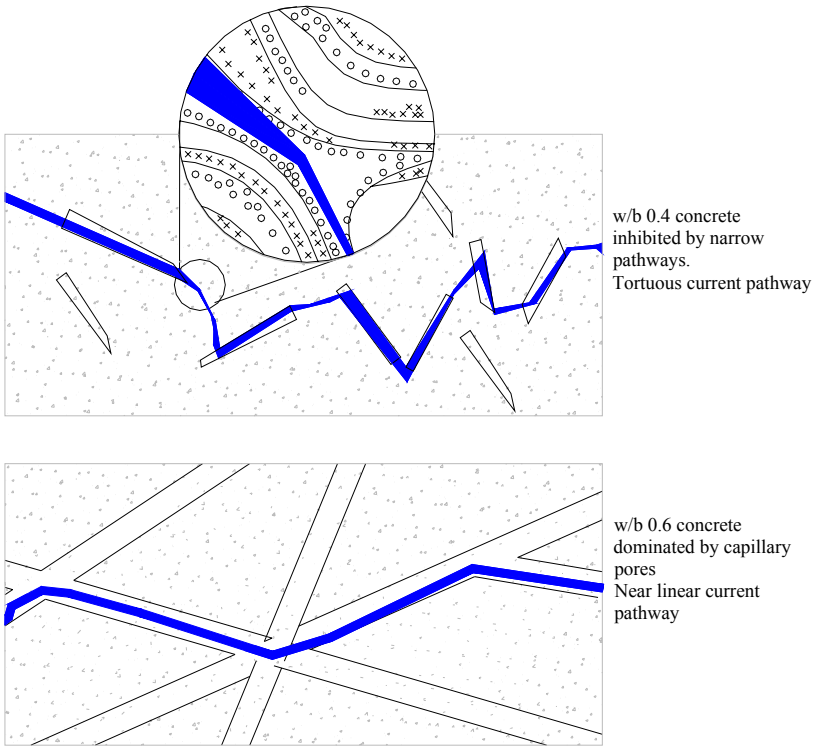


*Figure 5. 29 Illustration of the differences in conduction between the concretes. The capillaries are displayed as tubes. In the magnified section the adsorbed water is displayed as circles in and the interlayer water as crosses. The silicate model (in the magnified section) is based on the Feldman and Sereda model according to Soroka [74].*

Figure 5.29 illustrates the differences on how the conduction occurs in the two concrete qualities. For the w/b 0.6 concrete the current pathways are continuously following the capillary (water filled) spaces, with little constriction. The w/b 0.4 concrete, however, narrow sections where the current follows the adsorbed water phase dominates, and thereby increases the effective length of the pathway.

The w/b 0.6 concrete tend to be very moisture sensitive at lower moisture contents, with very rapid increase in electrical resistivity when the moisture content drops below this point. The w/b 0.4 concrete appears to be quite moisture sensitive already from about 70% saturation degree.

Powers [75] developed a model for volumetric determinations in cement paste and concrete based on the BET – theory by Brunauer, Emmett and Teller [76] The BET - theory is based on 6 main assumptions which can be found elsewhere [77].

Powers model states that the total porosity is given by:

$$\varepsilon_T = \frac{\frac{w}{c} - 0.17 \cdot \alpha}{0.32 + \frac{w}{c}} \qquad \textit{(Equation 5.2)}$$

where:

$\varepsilon_T$ is the total porosity in %

$w/c$ is the water-cement ratio

$\alpha$ is the degree of hydration

and that the gel porosity is given by:

$$\varepsilon_{GEL} = \frac{0.185 \cdot \alpha}{0.32 + \frac{w}{c}} \qquad \textit{(Equation 5.3)}$$

where:

$\varepsilon_{GEL}$ is the gel porosity in %.

The capillary porosity is then given by the difference between the total porosity and the gel porosity:

$$\varepsilon_{C} = \frac{\frac{w}{c} - 0.357 \cdot \alpha}{0.32 + \frac{w}{c}} \qquad \textit{(Equation 5.4)}$$

By using Equations 5.2 – 5.4 it is possible to estimate the respective porosities of concretes. By assuming that the w/b 0.6 concrete had a degree of hydration, $\alpha$=0.8 and that the w/b 0.4 concrete had a degree of hydration, $\alpha_c$=0.6 for the cement and that the 8% silica fume is fully reacted, $\alpha_s$=1.0, and generates 3 times the amount of gel generated by an equivalent amount of cement the porosities of the binder phases in the respective concretes were calculated.

The results from these calculations are given in Table 5. 8.

*Table 5. 8 Calculated porosity distribution by the BET – theory.*

| w/b ratio | w/c | Silica fume s/c | α | Total porosity | Gel porosity | Capillary porosity |
|---|---|---|---|---|---|---|
| | | [%] | | [%] | [%] | [%] |
| 0.4 | 0.44 | 0.08 | 0.6 | 43 % | 20 % | 23 % |
| 0.6 | 0.6 | 0 | 0.8 | 50 % | 16 % | 34 % |

The Powers model illustrates the differences between the concretes quite well. The w/b 0.4 concrete has lower total porosity, higher gel porosity and very much lower capillary porosity compared to the w/b 0.6 concrete.

The Powers model estimations above illustrate the differences between the concretes and allow visualisation of the physical distinctions in the respective pore systems.

Intuitively, the highly porous (w/b 0.6) concrete should be less moisture sensitive with respect to electrical resistivity than the concrete dominated by interlayer spaces (w/b 0.4 concrete). The estimations substantiate the illustration given in Figure 5.29.

By using the values in Table 5.8 it is possible to express the relation between moisture content and the electrical resistivity based on a simple assumption:

- At higher degrees of saturation the water loss comes only from the capillaries, and that the gel/interlayer pores are remained water filled until practically all capillary water is lost.

At the degrees of saturations where the resistivity increases more strongly the volume of the evaporated water corresponds to the volume of the capillary porosity for both concretes.

This may be illustrated by examples:

> The w/b 0.4 concrete has a total porosity of 43%, and at 60% saturation the remaining water corresponds to 26% of the total volume. If it is assumed that no gel/interlayer is evaporated the remaining capillary water is only 6%.
>
> The w/b 0.6 concrete has a total porosity of 50%, and at 40% saturation the remaining water corresponds to 20% of the total volume. Making the same assumption that the gel-water is remained, the remaining capillary water is 4%.

Another approach to illustrate differences between the concretes and to illustrate the effect of moisture on the electrical resistivity is by analysing sorption isotherms.

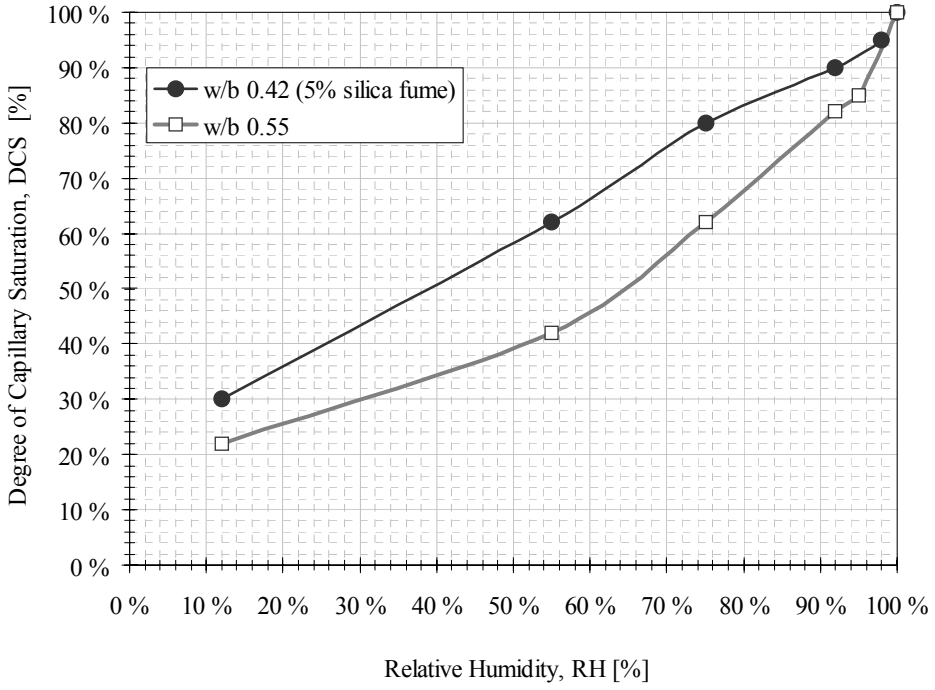


*Figure 5. 30 Desorption isotherms for concrete discs by degree of capillary saturation, DCS as a function of the relative humidity, RH for laboratory concrete with w/b=0.42 (5% silica fume) and w/b=0.55. Based on Relling [78].*

Figure 5. 30 shows desorption isotherms for w/b 0.55 and w/b 0.42 (5% silica fume) concretes performed by Relling [78]. By analysing Figure 5.27 and assuming that the w/b 0.4 concrete resembles the w/b 0.42 concrete and the 0.6 resembles the 0.55 concrete it can be deduced that the concretes tested in the ER - experiments have approximately the same RH at their respective departure points.

The departure points are at DCS of 60% and 40% for the w/b 0.4 and the w/b 0.6 concretes, respectively. This corresponds to an RH of approximately 55% taken from Figure 5.30. If it is assumed that the conduction in concrete is concentrated on the adsorbed solution layer on the pore wall below a certain moisture content, i.e. that the adsorbed water layers on the pore wall surface is the main contributor to conduction, then a RH of 55% should represent a critical thickness of this adsorbed layer. A RH of 55% means about 2 monolayers of water adsorbed on a free surface. Surely, it is not appropriate to assume what amounts of monolayers of water which are available in the pores at the corresponding RH during adsorption while the real process is desorption. Still, while some of the pores will be more or less water filled during the desorption stage the general adsorbed amount of water represents 2 monolayers.

In order to estimate the amount of water present during both adsorption and desorption an example based on sorption isotherms for thin discs of bridge concrete performed by Sellevold [79] is given:

For the found RH of 55% the available water in percent of dry mass is 3.5% and 2% for desorption and adsorption, respectively. Assuming there is 400 kg/m$^3$ of hydrated cement and a dry mass of 2200 kg/m$^3$, then the available water percentage in cement paste would be approximately: (400/2200)•3.5 = 19% and (400/2200)•2 = 11%. Both values are representing about 2 monolayers of water.

Evidently, the estimations above are based on very rough assumptions and represent only a slight indication of the effect of adsorbed water in the pores. However, this may give a hint that a thickness of the adsorbed layer of approximately 6 Å (equivalent to 2 monolayers of water) is a critical value for conduction in water. Since no experiments are performed on this, a further discussion of the implications of this theory would not be appropriate.

The two approaches are conflictive in that the represent different critical thicknesses. The volumetric considerations based on the Powers model gives that the breaking points represent the moisture condition when the gel-water is starting to loose water. Gel/interlayer spaces are defined by Powers as spaces smaller than 3 monolayers of water.

The approach through sorption isotherms gave a thickness of the adsorbed layers of 2 monolayers, and therefore conflicts with the assumptions behind Powers model.

Since both attempts are based on underlying assumptions and limited data neither of the methods can be conclusive in their current presentation, however, they may give a foundation for further elaborations based on specific research.

## 5.4 Combined effect of temperature and moisture condition on the electrical resistivity of concrete

Stated in the previous sections the effects of temperature and moisture are closely connected, and simultaneously affecting the electrical resistivity.

### 5.4.1 Combined effects of temperature and moisture condition on the electrical resistivity of concrete – results

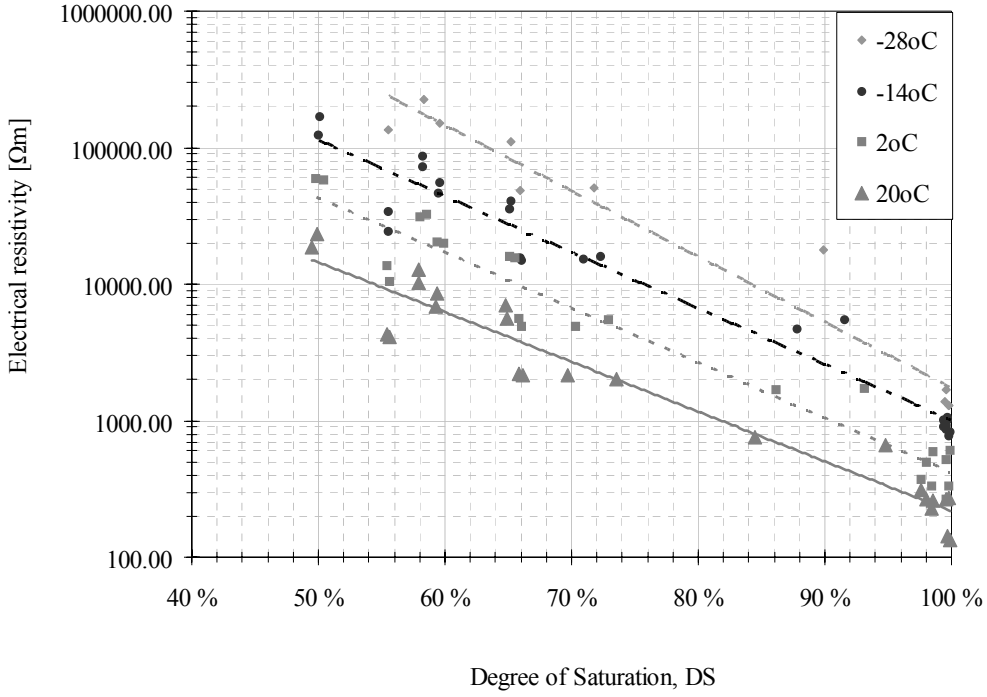


*Figure 5. 31 Combined effect of temperature and moisture condition displayed as Degree of Saturation, DS on the electrical resistivity of concrete for the concrete with w/b of 0.4. The ordinate is in log scale. The curves represent all results from Run 1, Run 3 and Run 4. Regression performed by exponential functions.*

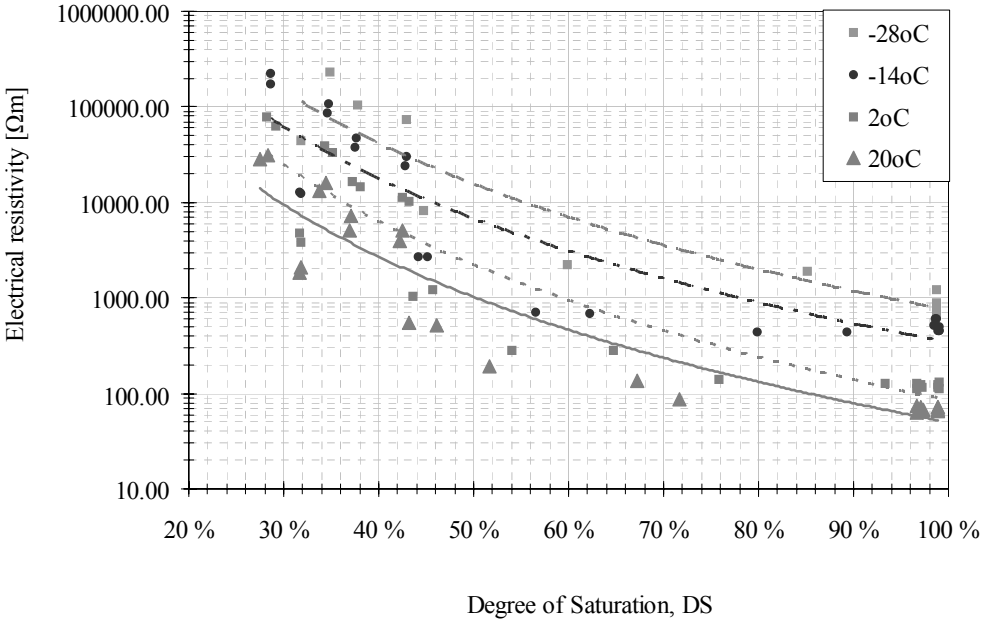


*Figure 5. 32 Combined effect of temperature and moisture condition displayed as Degree of Saturation, DS on the electrical resistivity of concrete for the concrete with w/b of 0.6. The ordinate is in log scale. The curves represent all results from Run 1, Run 3 and Run 4. Regression performed by geometrical functions.*

Figure 5. 31 and Figure 5. 32 show the combined effect of temperature and moisture condition for the w/b 0.4 and w/b 0.6 concretes, respectively. The results are based on Run 1, Run 3 and Run 4. Of practical reasons the ordinate was shown in logarithmic scale in order for the lower values at the higher temperatures to be separable.

### 5.4.2 Discussion of the combined effects of temperature and moisture condition on the electrical resistivity of concrete

Figure 5. 31 and Figure 5. 32 indicate that the temperature introduces a shift in level on the electrical resistivity of concrete. By decreasing temperatures the electrical resistivity increases quite remarkably as previously discussed. However, the different moisture conditions of the concretes appear to have similar effect at all temperatures.

The relationship between the activation energy constants and the moisture contents give a large scatter as shown in Figure 5.33, but there seem to be no systematic trend.

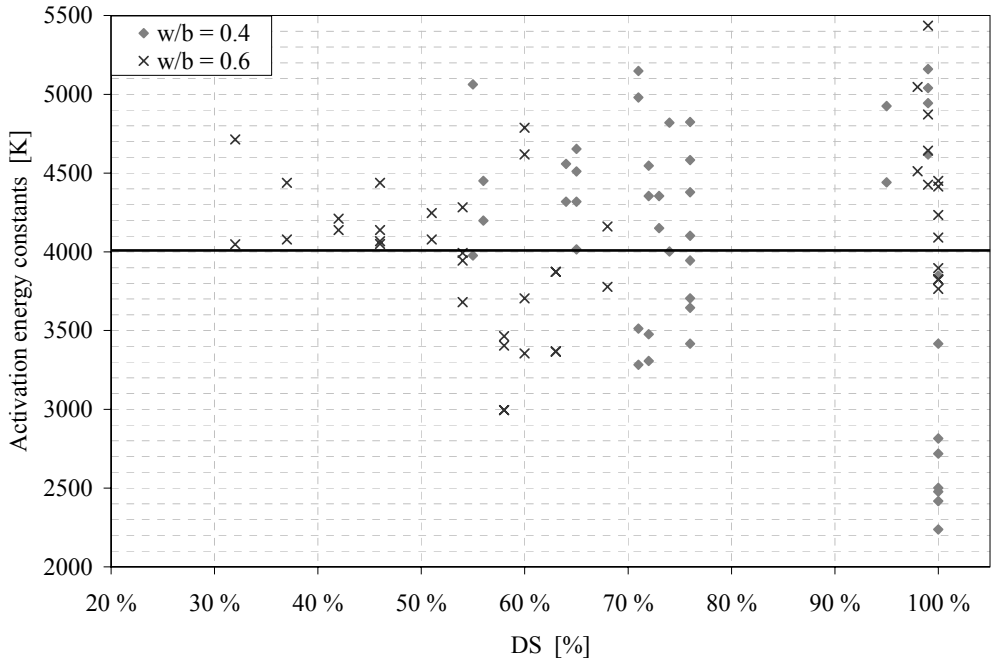


*Figure 5. 33 Relationship between the activation energy constants and the moisture contents of the specimens tested in the ER – experiments.*

This temperature induced shift in level is most profound on the concrete with w/b ratio of 0.4. It is indicated that the effect of temperature is relatively unaffected by moisture for the w/b 0.4 concrete by the conformity of the curves in Figure 5. 31. As discussed in section 5.3.2 the w/b 0.4 concrete have a finer pore size distribution and it is assumed that ice formation will not obstruct the current pathways in a large scale. However, for the w/b 0.6 concrete the shift in level is not as clear as for the w/b 0.4 concrete. The curves appear to be more similar to the 0.4 concrete on the low moisture contents (lower than 50%). This may be an indication that there are interfering processes occurring in the pore system which assumingly could be related to ice in the capillaries blocking the current pathways.

From the low temperature calorimetry results given in section 4.2 it can be deduced that approximately 10% of the evaporable water content will be frozen at a temperature of -28°C for the w/b 0.4 concrete, while for the w/b 0.6 concrete this amount is about 22%.

The corresponding amount of the porosity that contains frozen water at -28°C can be calculated from porosity data given in Table 4.1:
For the w/b 0.4 concrete the porosity is found to be 12.7% and if it is assumed that the sample is water saturated then the ice volume in the pores for this concrete at -28°C would be 1.3% of the total concrete volume.

Correspondingly, for the w/b 0.6 concrete the porosity is 17.2 % that results in an ice volume of 3.8% with respect to the total concrete volume.

Clearly, the w/b 0.6 concrete will have more ice present in the pores in the low temperatures, especially on thawing. The ice will presumably block the largest capillaries which result in more tortuous current pathways. This may explain the fundamentally different behaviour of the electrical resistivity between the w/b 0.4 concrete and the w/b 0.6 concrete.

At lower degrees of saturation the amount of frozen water will decrease. Below a certain degree of saturation no ice formation will occur due to no water present in the pores where the thermodynamic conditions for ice nucleation are present. Therefore frozen capillary water will only affect the systems profoundly in the high range of moisture contents.

Ice formation has a similar effect to the systems as drying. The pores blocked by ice will redirect the current pathways to smaller pores where liquid water is present. This increases the effective length of the current pathway resulting in an increased electrical resistivity. However, ice nucleation results in considerable forces inside the pores which in turn results in a change in the appearance of the pores. The volume increase due to the phase shift will result in damages on the pores resulting in a collapse of pores and thereby irreversible changes in the pore system.

## 5.5 Effect of temperature on other electrical properties in concrete

In Run 1 and Run 2 measurements were performed using Electrochemical Impedance Spectroscopy, EIS. EIS measurements on a concrete sample give information on several other interesting electrical properties besides the electrical resistivity, e.g. the impedance of the system (which is more descriptive than resistivity), the capacitance of the system (ability to hold a charge of electrons) and the depression angle (indicating whether or not there are parallel processes (phases) present in the system).

### 5.5.1 Interpreting EIS data – Equivalent circuit

EIS data can be visualised and interpreted by several equivalent circuits or Randles circuits, RC. Often data from EIS measurements are hardly interpretable, and it is very challenging to identify a representative RC for the measured system. Concrete introduces interpretation difficulties since it is a complex composite material and its various components have different electrical behaviour.

Initial measurements on concrete specimens were attempted to be interpreted using several equivalent circuits. Due to depression of the semicircles (flattening of the arc) it was supposed that the concrete was best represented by a combination of 2 RC in combination:

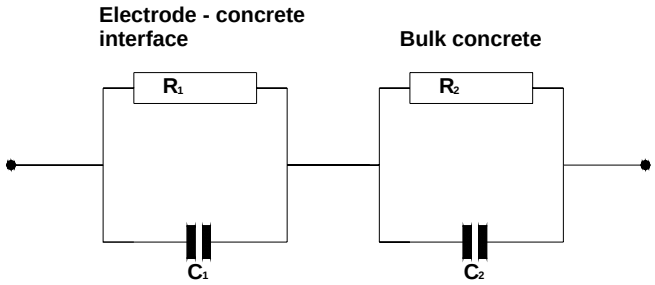


*Figure 5. 34 Equivalent circuit with 2 serial RC*

The equivalent circuit is presented in Figure 5.34, and the resulting semicircles generated by this equivalent circuit is illustrated along with results from Run 1 in Figure 5. 35.

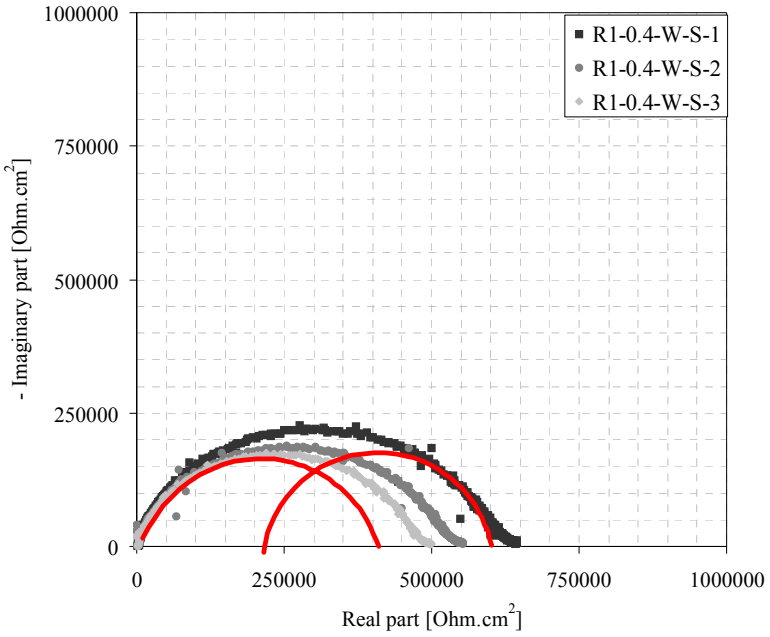


*Figure 5. 35 Nyquist diagram for the R1-0.4-W-S variant. The scatter shows the internal variation between the parallel specimens. Semicircles generated by the 2 serial RC are shown by red arcs. The results relates to an electrode area of 28 cm$^2$.*

By this interpretation the concrete resistivity could be calculated from the sum of the resistances of semicircle 1 and 2. This would make disproportionately much work.

It was chosen to use a single RC to describe the concrete. Depression of the semicircle would still be detected by the depression angle, $\alpha$.

The chosen equivalent circuit is shown in Figure 5.36 and the corresponding interpretation in Figure 5.37.

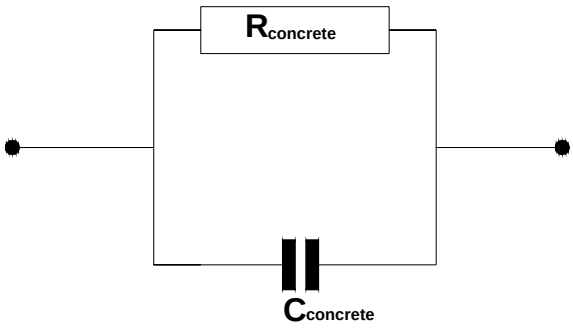


*Figure 5. 36 The chosen equivalent circuit. A single RC.*

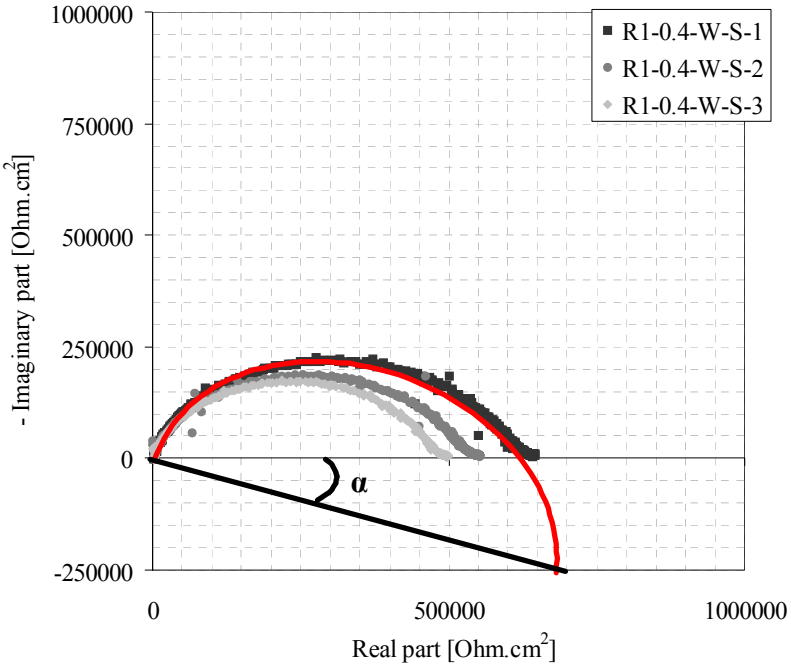


*Figure 5. 37 Nyquist diagram for the R1-0.4-W-S variant. The scatter shows the internal variation between the parallel specimens. The semicircle generated single RC is shown by a red arc. The suppression angle, α, is marked below the abscissa. The results relates to an electrode area of 28 cm$^2$.*

### 5.5.2 EIS results from Run 1 and Run 2

Measurements with Electrochemical Impedance spectroscopy were performed during Freezing of Run 1 and during Freezing and Thawing of Run 2. The results are given in Table 5. 9 – Table 5. 14.

*Table 5. 9 Calculated values of the electrical properties for the w/b 0.4 concrete during Freezing of Run 1. The EIS results were interpret using a single RC. The results are averaged from three parallel samples.*

| Variant | Temperature | | Electrical properties | | | | | |
|---|---|---|---|---|---|---|---|---|
| | | | ρ | α | $F_m$ | C | C | ε |
| | [°C] | [°K] | [Ωm] | | [Hz] | [F/cm$^2$] | [pF/m$^2$] | |
| R1-0.4-W-S | 20 | 293 | 678 | 0.823 | 5.5E+05 | 5.44E-13 | 5440 | 18 |
| | 2 | 275 | 1748 | 0.816 | 2.2E+05 | 5.18E-13 | 5179 | 17 |
| | -14 | 259 | 5464 | 0.814 | 8.0E+04 | 4.61E-13 | 4609 | 15 |
| | -28 | 245 | 17929 | 0.810 | 2.4E+04 | 4.73E-13 | 4727 | 15 |
| R1-0.4-W-D | 20 | 293 | 2203 | 0.792 | 1.1E+05 | 5.31E-13 | 5308 | 17 |
| | 2 | 275 | 5685 | 0.829 | 8.4E+04 | 2.84E-13 | 2838 | 9 |
| | -14 | 259 | 15571 | 0.811 | 2.0E+04 | 7.55E-13 | 7547 | 24 |
| | -28 | 245 | 49675 | 0.806 | 1.0E+04 | 4.06E-13 | 4058 | 13 |
| R1-0.4-S-S | 20 | 293 | 2053 | 0.829 | 2.0E+05 | 4.96E-13 | 4956 | 16 |
| | 2 | 275 | 5538 | 0.814 | 8.0E+04 | 3.49E-13 | 3489 | 11 |
| | -14 | 259 | 15971 | 0.791 | 2.7E+04 | 4.74E-13 | 4743 | 15 |
| | -28 | 245 | 51346 | 0.788 | 9.6E+03 | 4.06E-13 | 4065 | 13 |
| R1-0.4-S-D | 20 | 293 | 4414 | 0.826 | 9.3E+04 | 5.02E-13 | 5021 | 16 |
| | 2 | 275 | 13723 | 0.803 | 3.7E+04 | 3.08E-13 | 3080 | 10 |
| | -14 | 259 | 34238 | 0.786 | 1.2E+04 | 4.83E-13 | 4826 | 16 |
| | -28 | 245 | 141758 | 0.828 | 4.2E+03 | 3.36E-13 | 3361 | 11 |

*Table 5. 10 Calculated values of the electrical properties for the w/b 0.6 concrete during Freezing of Run 1. The EIS results were interpret using a single RC. The results are averaged from three parallel samples.*

| Variant | Temperature | | Electrical properties | | | | | |
|---|---|---|---|---|---|---|---|---|
| | | | ρ | α | $F_m$ | C | C | ε |
| | [°C] | [°K] | [Ωm] | | [Hz] | [F/cm$^2$] | [pF/m$^2$] | |
| R1-0.6-W-S | 20 | 293 | 66.95 | 0.818 | 8.0E+06 | 3.73E-13 | 3728 | 12 |
| | 2 | 275 | 131.43 | 0.836 | 4.8E+06 | 3.17E-13 | 3169 | 10 |
| | -14 | 259 | 441.05 | 0.843 | 1.7E+06 | 2.73E-13 | 2731 | 9 |
| | -28 | 245 | 1894.2 | 0.842 | 4.0E+05 | 2.63E-13 | 2628 | 8 |
| R1-0.6-W-D | 20 | 293 | 534.68 | 0.847 | 1.1E+06 | 3.31E-13 | 3314 | 11 |
| | 2 | 275 | 1232.9 | 0.841 | 5.9E+05 | 2.93E-13 | 2925 | 9 |
| | -14 | 259 | 2748.3 | 0.826 | 2.8E+05 | 2.74E-13 | 2736 | 9 |
| | -28 | 245 | 8248.8 | 0.832 | 8.3E+04 | 3.05E-13 | 3053 | 10 |
| R1-0.6-S-S | 20 | 293 | 135.56 | 0.862 | 4.7E+06 | 3.34E-13 | 3335 | 11 |
| | 2 | 275 | 286.21 | 0.847 | 2.6E+06 | 2.87E-13 | 2871 | 9 |
| | -14 | 259 | 690.75 | 0.841 | 1.2E+06 | 2.58E-13 | 2583 | 8 |
| | -28 | 245 | 2192.1 | 0.843 | 4.0E+05 | 2.59E-13 | 2591 | 8 |
| R1-0.6-S-D | 20 | 293 | 1889.9 | 0.831 | 3.4E+05 | 3.17E-13 | 3165 | 10 |
| | 2 | 275 | 4865.8 | 0.820 | 1.4E+05 | 3.02E-13 | 3023 | 10 |
| | -14 | 259 | 12900 | 0.805 | 4.3E+04 | 3.6E-13 | 3603 | 12 |
| | -28 | 245 | 43925 | 0.802 | 1.1E+04 | 4.03E-13 | 4033 | 13 |

The variation between the three parallel specimens was generally satisfactory on all calculated values, with standard deviations within 10% of the values.

*Table 5. 11 Calculated values of the electrical properties for the w/b 0.4 concrete during Freezing of Run 2. The EIS results were interpret using a single RC. The measurements represent a single specimen of each variant.*

| **Specimen Id** | | **Temperature** | | **Electrical properties** | | | | | |
|---|---|---|---|---|---|---|---|---|---|
| Variant | No | | | ρ | α | $F_m$ | C | C | ε |
| | | [°C] | [°K] | [Ωm] | | [Hz] | [F/cm$^2$] | [pF/m$^2$] | |
| R2-0.4-W-S | 1 | 20 | 293 | 1598 | 0.815 | 3.60E+05 | 3.45E-13 | 3454 | 11 |
| | 1 | 2 | 275 | 4474 | 0.799 | 1.20E+05 | 3.70E-13 | 3701 | 12 |
| | 1 | -14 | 259 | 13913 | 0.817 | 3.73E+04 | 3.83E-13 | 3834 | 12 |
| | 1 | -28 | 245 | 36883 | 0.813 | 1.19E+04 | 4.55E-13 | 4545 | 15 |
| R2-0.4-W-S | 2 | 20 | 293 | 595 | 0.786 | 7.30E+05 | 4.58E-13 | 4581 | 15 |
| | 2 | 2 | 275 | 1132 | 0.800 | 3.55E+05 | 4.95E-13 | 4954 | 16 |
| | 2 | -14 | 259 | 5280 | 0.819 | 8.84E+04 | 4.26E-13 | 4263 | 14 |
| | 2 | -28 | 245 | 19638 | 0.826 | 1.86E+04 | 5.44E-13 | 5443 | 18 |
| R2-0.4-W-D | 1 | 20 | 293 | 3108 | 0.815 | 1.87E+05 | 3.52E-13 | 3520 | 11 |
| | 1 | 2 | 275 | 8490 | 0.829 | 5.52E+04 | 4.24E-13 | 4242 | 14 |
| | 1 | -14 | 259 | 28613 | 0.812 | 1.69E+04 | 4.11E-13 | 4108 | 13 |
| | 1 | -28 | 245 | 80613 | 0.807 | 6.86E+03 | 3.60E-13 | 3596 | 12 |
| R2-0.4-S-S | 1 | 20 | 293 | 4808 | 0.830 | 1.34E+05 | 3.09E-13 | 3089 | 10 |
| | 1 | 2 | 275 | 14700 | 0.820 | 3.65E+04 | 3.70E-13 | 3703 | 12 |
| | 1 | -14 | 259 | 50100 | 0.799 | 1.25E+04 | 3.18E-13 | 3176 | 10 |
| | 1 | -28 | 245 | 153750 | 0.828 | 4.29E+03 | 3.02E-13 | 3021 | 10 |
| R2-0.4-S-D | 1 | 20 | 293 | 5525 | 0.808 | 9.46E+04 | 3.81E-13 | 3805 | 12 |
| | 1 | 2 | 275 | 17450 | 0.858 | 2.95E+04 | 3.86E-13 | 3858 | 12 |
| | 1 | -14 | 259 | 64050 | 0.817 | 8.21E+03 | 3.79E-13 | 3792 | 12 |
| | 1 | -28 | 245 | 225500 | 0.814 | 2.26E+03 | 3.91E-13 | 3909 | 13 |

*Table 5. 12 Calculated values of the electrical properties for the w/b 0.6 concrete during Freezing of Run 2. The EIS results were interpret using a single RC. The measurements represent a single specimen of each variant.*

| Specimen Id | | Temperature | | Electrical properties | | | | | |
|---|---|---|---|---|---|---|---|---|---|
| Variant | No | | | ρ | α | $F_m$ | C | C | ε |
| | | [°C] | [°K] | [Ωm] | | [Hz] | [F/cm$^2$] | [pF/m$^2$] | |
| R2-0.6-W-S | 1 | 20 | 293 | 186 | 0.847 | 4.22E+06 | 2.53E-13 | 2526 | 8 |
| | 1 | 2 | 275 | 392 | 0.838 | 1.94E+06 | 2.62E-13 | 2622 | 8 |
| | 1 | -14 | 259 | 917 | 0.848 | 8.19E+05 | 2.65E-13 | 2648 | 9 |
| | 1 | -28 | 245 | 2296 | 0.856 | 3.11E+05 | 2.78E-13 | 2784 | 9 |
| R2-0.6-W-S | 2 | 20 | 293 | 65 | 0.798 | 1.00E+07 | 3.05E-13 | 3051 | 10 |
| | 2 | 2 | 275 | 98 | 0.818 | 6.45E+06 | 3.13E-13 | 3133 | 10 |
| | 2 | -14 | 259 | 494 | 0.853 | 1.47E+06 | 2.75E-13 | 2745 | 9 |
| | 2 | -28 | 245 | 1664 | 0.864 | 4.51E+05 | 2.65E-13 | 2651 | 9 |
| R2-0.6-W-D | 1 | 20 | 293 | 1548 | 0.828 | 4.86E+05 | 2.65E-13 | 2645 | 9 |
| | 1 | 2 | 275 | 4053 | 0.830 | 1.71E+05 | 2.87E-13 | 2869 | 9 |
| | 1 | -14 | 259 | 11981 | 0.815 | 5.40E+04 | 3.08E-13 | 3076 | 10 |
| | 1 | -28 | 245 | 33800 | 0.817 | 1.63E+04 | 3.61E-13 | 3608 | 12 |
| R2-0.6-S-S | 1 | 20 | 293 | 459 | 0.854 | 1.80E+06 | 2.41E-13 | 2407 | 8 |
| | 1 | 2 | 275 | 1121 | 0.859 | 7.23E+05 | 2.45E-13 | 2454 | 8 |
| | 1 | -14 | 259 | 2918 | 0.841 | 2.71E+05 | 2.52E-13 | 2520 | 8 |
| | 1 | -28 | 245 | 7544 | 0.850 | 1.06E+05 | 2.50E-13 | 2496 | 8 |
| R2-0.6-S-D | 1 | 20 | 293 | 5178 | 0.827 | 1.48E+05 | 2.59E-13 | 2590 | 8 |
| | 1 | 2 | 275 | 16075 | 0.853 | 5.00E+04 | 2.48E-13 | 2479 | 8 |
| | 1 | -14 | 259 | 53688 | 0.807 | 1.47E+04 | 2.52E-13 | 2522 | 8 |
| | 1 | -28 | 245 | 162625 | 0.841 | 5.09E+03 | 2.40E-13 | 2399 | 8 |

*Table 5. 13 Calculated values of the electrical properties for the w/b 0.4 concrete during Thawing of Run 2. The EIS results were interpret using a single RC. The measurements represent a single specimen of each variant.*

| **Specimen Id** | | **Temperature** | | **Electrical properties** | | | | | |
|---|---|---|---|---|---|---|---|---|---|
| Variant | No | | | ρ | α | $F_m$ | C | C | ε |
| | | [°C] | [°K] | [Ωm] | | [Hz] | [F/cm$^2$] | [pF/m$^2$] | |
| R2-0.4-W-S | 1 | 20 | 293 | 1900 | 0.833 | 2.92E+05 | 3.58E-13 | 3584 | 12 |
| | 1 | 2 | 275 | 4438 | 0.844 | 1.21E+05 | 3.72E-13 | 3723 | 12 |
| | 1 | -14 | 259 | 12700 | 0.844 | 4.00E+04 | 3.93E-13 | 3931 | 13 |
| | 1 | -28 | 245 | 36425 | 0.858 | 1.19E+04 | 4.59E-13 | 4592 | 15 |
| R2-0.4-W-S | 2 | 20 | 293 | 521 | 0.807 | 8.66E+05 | 4.40E-13 | 4403 | 14 |
| | 2 | 2 | 275 | 1198 | 0.786 | 3.40E+05 | 4.88E-13 | 4882 | 16 |
| | 2 | -14 | 259 | 6079 | 0.830 | 7.94E+04 | 4.12E-13 | 4120 | 13 |
| | 2 | -28 | 245 | 19638 | 0.851 | 1.86E+04 | 5.48E-13 | 5481 | 18 |
| R2-0.4-W-D | 1 | 20 | 293 | 3431 | 0.831 | 1.43E+05 | 4.07E-13 | 4072 | 13 |
| | 1 | 2 | 275 | 8986 | 0.859 | 5.75E+04 | 3.87E-13 | 3869 | 12 |
| | 1 | -14 | 259 | 27175 | 0.840 | 2.18E+04 | 3.36E-13 | 3363 | 11 |
| | 1 | -28 | 245 | 78762 | 0.824 | 7.22E+03 | 3.50E-13 | 3499 | 11 |
| R2-0.4-S-S | 1 | 20 | 293 | 5680 | 0.860 | 9.16E+04 | 3.82E-13 | 3824 | 12 |
| | 1 | 2 | 275 | 14750 | 0.830 | 3.52E+04 | 3.83E-13 | 3830 | 12 |
| | 1 | -14 | 259 | 48250 | 0.860 | 1.31E+04 | 3.14E-13 | 3140 | 10 |
| | 1 | -28 | 245 | 154375 | 0.825 | 4.27E+03 | 3.02E-13 | 3018 | 10 |
| R2-0.4-S-D | 1 | 20 | 293 | 6168 | 0.853 | 8.04E+04 | 4.01E-13 | 4011 | 13 |
| | 1 | 2 | 275 | 17600 | 0.832 | 2.75E+04 | 4.11E-13 | 4106 | 13 |
| | 1 | -14 | 259 | 60425 | 0.811 | 8.53E+03 | 3.89E-13 | 3891 | 13 |
| | 1 | -28 | 245 | 226250 | 0.804 | 2.24E+03 | 3.97E-13 | 3965 | 13 |

*Table 5. 14 Calculated values of the electrical properties for the w/b 0.6 concrete during Thawing of Run 2. The EIS results were interpret using a single RC. The measurements represent a single specimen of each variant.*

| Specimen Id | | Temperature | | Electrical properties | | | | | |
|---|---|---|---|---|---|---|---|---|---|
| Variant | No | | | ρ | α | $F_m$ | C | C | ε |
| | | [°C] | [°K] | [Ωm] | | [Hz] | [F/cm$^2$] | [pF/m$^2$] | |
| R2-0.6-W-S | 1 | 20 | 293 | 264 | 0.860 | 2.97E+06 | 2.54E-13 | 2535 | 8 |
| | 1 | 2 | 275 | 399 | 0.860 | 1.89E+06 | 2.63E-13 | 2629 | 8 |
| | 1 | -14 | 259 | 936 | 0.865 | 7.92E+05 | 2.68E-13 | 2684 | 9 |
| | 1 | -28 | 245 | 2263 | 0.879 | 3.15E+05 | 2.79E-13 | 2791 | 9 |
| R2-0.6-W-S | 2 | 20 | 293 | 57 | 0.817 | 9.28E+06 | 4.33E-13 | 4333 | 14 |
| | 2 | 2 | 275 | 102 | 0.798 | 6.26E+06 | 3.11E-13 | 3113 | 10 |
| | 2 | -14 | 259 | 568 | 0.860 | 1.33E+06 | 2.64E-13 | 2642 | 9 |
| | 2 | -28 | 245 | 1671 | 0.869 | 4.48E+05 | 2.66E-13 | 2657 | 9 |
| R2-0.6-W-D | 1 | 20 | 293 | 1900 | 0.847 | 3.90E+05 | 2.68E-13 | 2682 | 9 |
| | 1 | 2 | 275 | 3920 | 0.814 | 1.78E+05 | 2.85E-13 | 2850 | 9 |
| | 1 | -14 | 259 | 11501 | 0.856 | 5.34E+04 | 3.25E-13 | 3246 | 10 |
| | 1 | -28 | 245 | 33350 | 0.823 | 1.65E+04 | 3.62E-13 | 3615 | 12 |
| R2-0.6-S-S | 1 | 20 | 293 | 686 | 0.864 | 1.17E+06 | 2.49E-13 | 2487 | 8 |
| | 1 | 2 | 275 | 1043 | 0.864 | 8.35E+05 | 2.28E-13 | 2284 | 7 |
| | 1 | -14 | 259 | 2818 | 0.854 | 2.68E+05 | 2.64E-13 | 2639 | 9 |
| | 1 | -28 | 245 | 7574 | 0.868 | 1.05E+05 | 2.50E-13 | 2498 | 8 |
| R2-0.6-S-D | 1 | 20 | 293 | 5969 | 0.874 | 1.38E+05 | 2.41E-13 | 2411 | 8 |
| | 1 | 2 | 275 | 13788 | 0.820 | 3.92E+04 | 3.69E-13 | 3685 | 12 |
| | 1 | -14 | 259 | 51913 | 0.866 | 1.10E+04 | 3.48E-13 | 3482 | 11 |
| | 1 | -28 | 245 | 159000 | 0.853 | 5.14E+03 | 2.44E-13 | 2444 | 8 |

### 5.5.3 Effect of temperature on other electrical properties of concrete

The values of the electrical resistivity are discussed in previous sections and will not be discussed further here. These values represent the impedance of the system where the imaginary component is cero.

The suppression angle, α, when lower than one, demonstrates that the relaxation time is not single valued but distributed. The values of α, is connected to the variation of the relaxation times in the system. This variation indicates that the system has different phases with different electrical properties between the phases. However, the differences in relaxation times were so small that the results described a single semicircle in the complex plane plot.

In concrete these phases may represent a paste rich phase including the calcium hydroxide rich transition layer surrounding the electrodes as one phase and the bulk concrete as another phase.

The values of the suppression angle appear very little temperature sensitive and no clear variations induced by temperature were observed from the results.

It was expected that the suppression angle could change if ice nucleated and introduced another phase in the system. However, since no clear change was found in the values of α, it is supposed that ice, when present, will not change the ratio between the phases. Stated in section 5.5.1 it was

chosen to regard the system as a single phase accepting the small misinterpretation this introduces by viewing the system as a combined phase of the two mentioned phases.

The frequency of maximum capacitance, $F_m$, appears to decrease by decreasing temperature. This is observed for all of the variants in both Run 1 and Run 2.

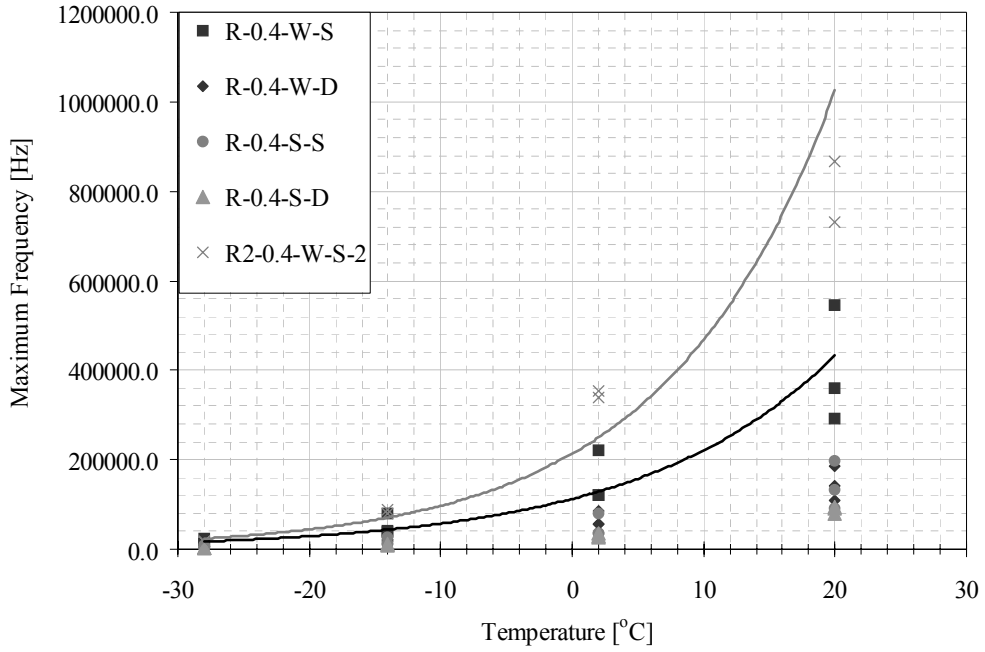


*Figure 5. 38 Relationship between temperature and frequency of maximum capacitance for the w/b 0. 4 concrete at different moisture conditions. The results are combined for Run 1 and Run 2. The R2-0.4-W-S-2 represents the wettest variant (single specimen) and is only tested in Run 2. Regression performed by exponential functions.*

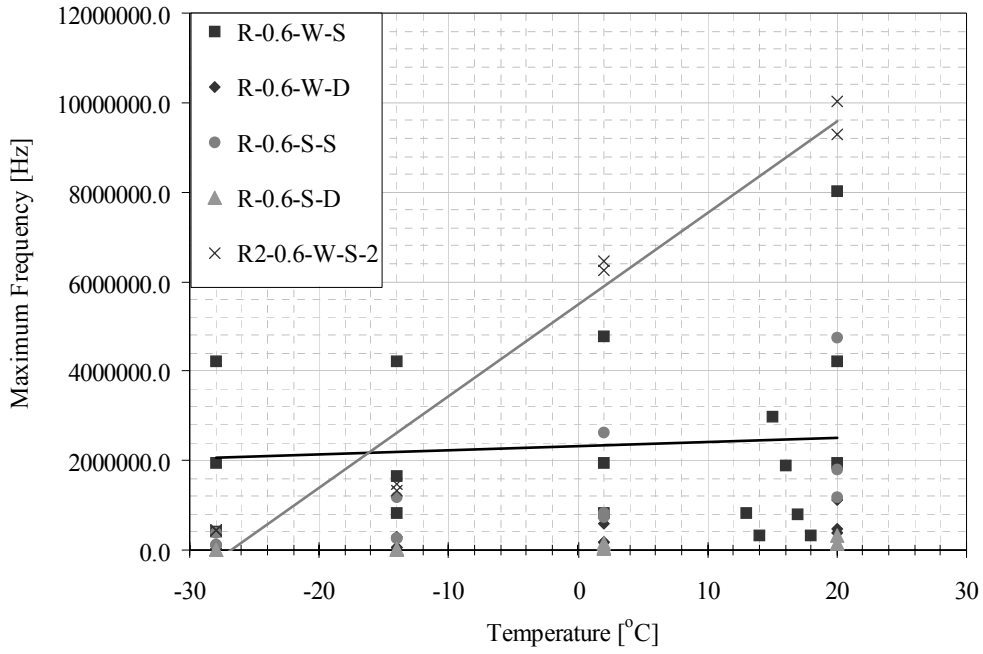


*Figure 5. 39 Relationship between temperature and frequency of maximum capacitance for the w/b 0. 6 concrete at different moisture conditions. The results are combined for Run 1 and Run 2. The R2-0.6-W-S-2 represents the wettest variant (single specimen) and is only tested in Run 2. Regression performed by linear functions.*

The capacitance is a function of frequency and the total resistance described by the semicircular arc by the function [71]:

$$C = \frac{1}{F_m \cdot R_{concrete}} \qquad \text{(Equation 5.5)}$$

Where:

| | | |
|---|---|---|
| $C$ | Capacitance of the concrete system | [F/cm$^2$] |
| $R_{concrete}$ | Electrical resistance of the concrete | [Ωcm$^2$] |
| $F_m$ | Maximum frequency (top of arc) | [Hz] |

For the w/b 0.4 concrete $F_m$ decreased significantly with temperature. Its relationship with temperature could be well described by an exponential function. We found earlier in this chapter that the electrical resistivity (and therefore also the area related electrical resistance of the circuit) increases exponentially by decreasing temperature. As a result the values for the capacitance for the w/b 0.4 concrete should vary only slightly with temperature which agrees well with the recorded values. However, for the w/b 0.6 concrete the relationship between temperature and the $F_m$ is more scattered and is only poorly described by a linear function. This agrees well with the recorded values of the capacitance which show an unclear scatter.

Overall, the recorded values for the capacitance are in the expected range for concrete.

The dielectric constant, ε, is the relative permittivity of a dielectric material. It is an important parameter in characterising capacitors. From the results the dielectric constants were found to be nearly constant and appeared relatively independent of the temperature. The obtained values of the dielectric constant were in the range 8 – 15 in most cases. This is in the expected range for concrete.

However, the dielectric constant should be related to the moisture content.

The calculated dielectric constants are plotted against the moisture contents of the concrete specimens during testing in Figure 5.40.

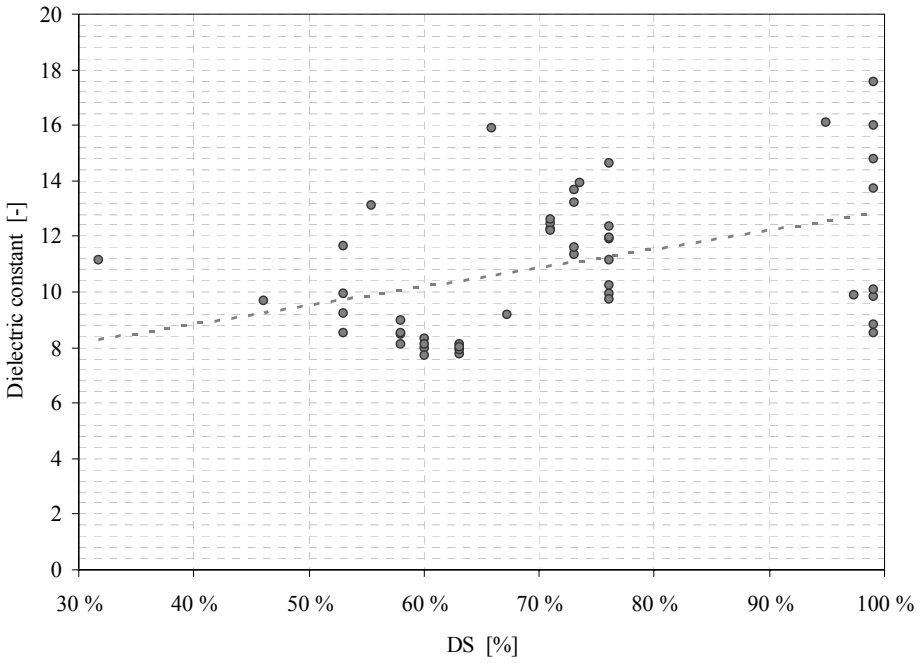


*Figure 5. 40 The relationship between dielectric constant and the moisture content of both concrete qualities. Regression performed by a linear function.*

The data indicates a weak relationship between the dielectric constant and the moisture content. It appears that the dielectric constant increases by increasing moisture contents; however, since the results are showing a large scatter, it is not possible to quantify the relationship.

### 5.5.4 Effect of temperature on the frequency sensitivity

The observation of the temperature dependency of the maximum frequency indicates that the appropriate measuring frequency may change with temperature. By combining the Bode plots for the variants it is possible to illustrate these changes.

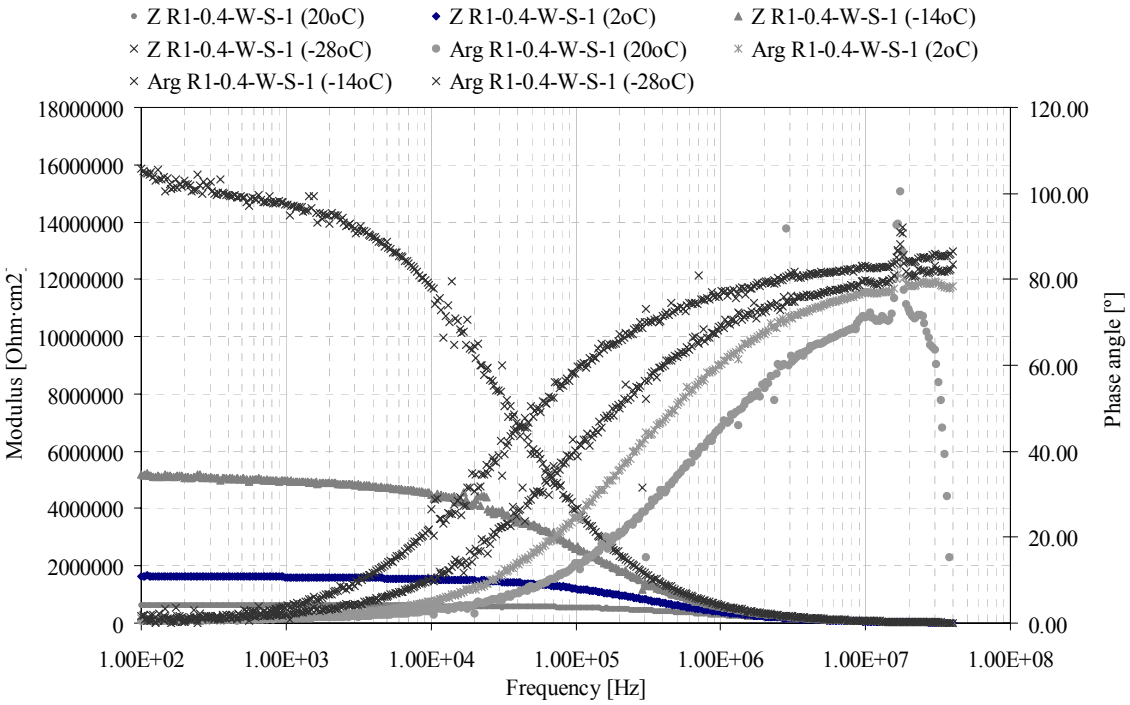


*Figure 5. 41 Combined Bode plots illustrating the effect of temperature on the frequency dependency in the low frequency range for the R1-0.4-W-S-1 specimen (DS = 95%).*

From Figure 5.41 it can be found that the measurement frequency results in only slight changes in the measured impedance (modulus) within a frequency range from 100 Hz – 10 kHz for temperatures higher than 0°C.

On temperatures lower than 0°C; however, there is an increased change in the modulus by decreasing temperature. This indicates that the measurement frequency (especially when dealing with stationary frequencies) is significant for the values of the electrical resistance of concrete even on wet concrete.

The effect showed also moisture dependency and the effect is increased by decreasing moisture contents.

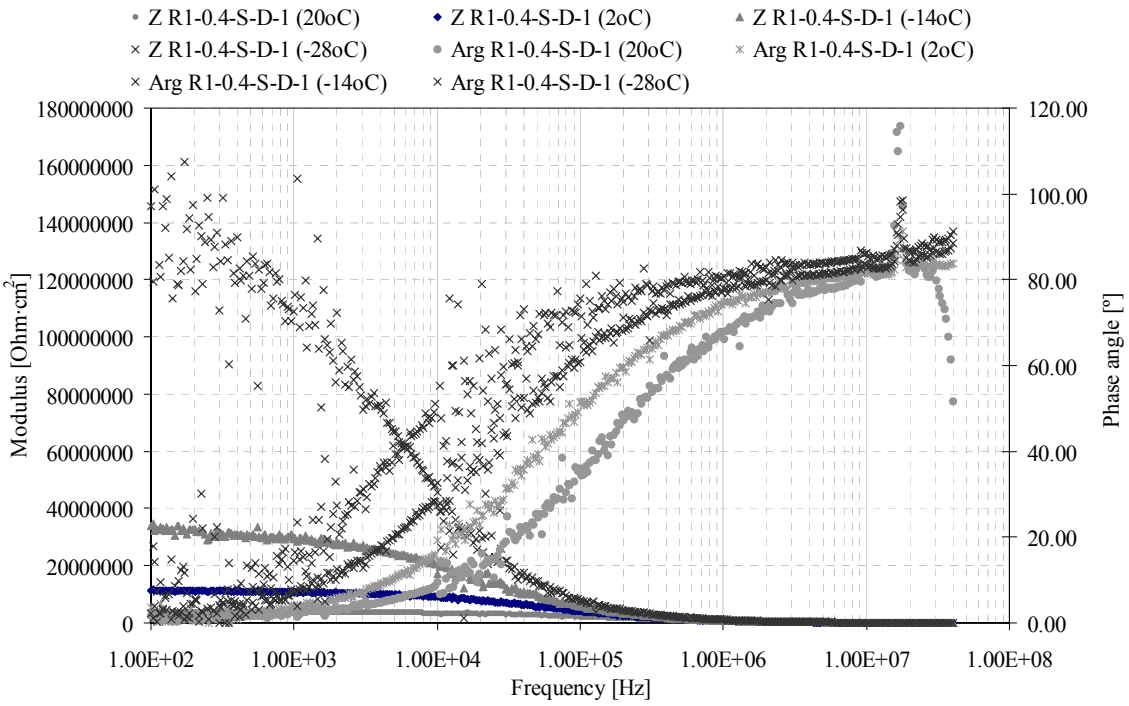


*Figure 5. 42 Combined Bode plots illustrating the effect of temperature on the frequency dependency in the low frequency range for the R1-0.4-S-D-1 specimen (DS = 55%).*

Figure 5.42 illustrates the same effects as found in Figure 5. 41. The effect appears more profound on the lowest temperature for this drier variant.

For both the water-cured – sealed variant and the sealed-cured – dried variant the effect seem largest at -28°C. At a temperature of -14°C the modulus decreases by increasing frequencies, however very much less than at -28°C. The departure point for the phase angle indicates that the frequency where the capacitive contribution to the impedance increases, i.e. where the imaginary component of the impedance vector start to influence. These departure points appear to trend to decreasing frequencies at decreasing temperatures. An attempt to visualise this trend by an impedance plot (Nyquist Diagram) is given in Figure 5.43.

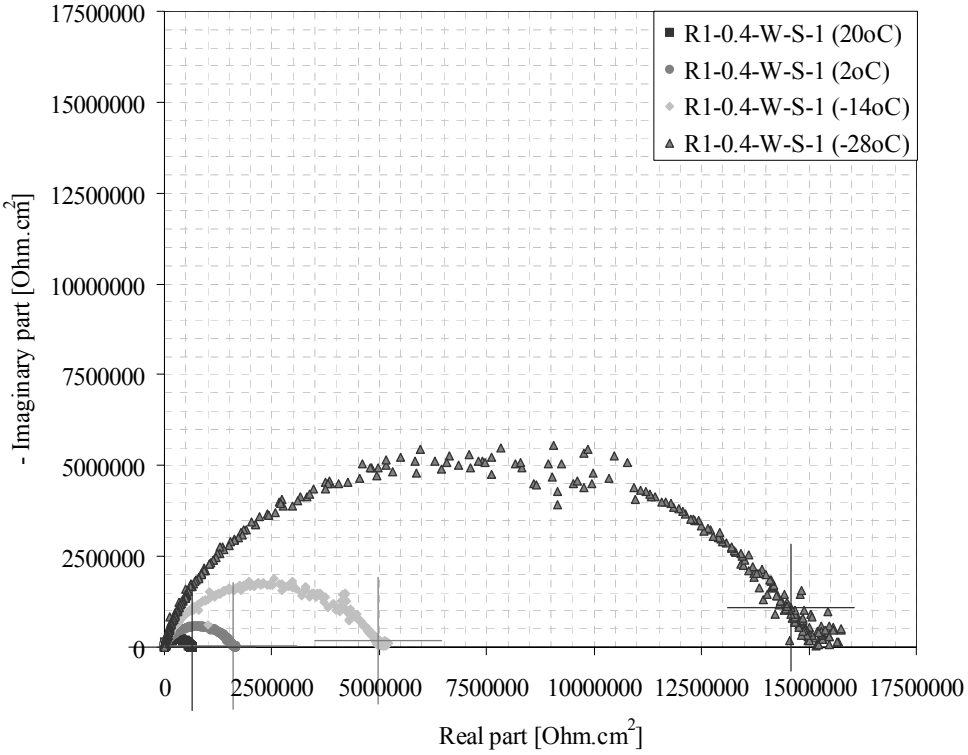


*Figure 5. 43 Nyquist diagram for the R1-0.4-W-S-1 specimen at the four tested temperatures. The large crosses show the impedance at 1 kHz.*

As Figure 5.43 shows a constant frequency of 1 kHz describes the impedance with an increasing imaginary component on decreasing temperature. This observation indicates that a lower measurement frequency would be more appropriate at lower temperatures for this particular specimen than a stationary frequency of 1 kHz as commonly used. Similar effects were found for the w/b 0.6 concrete, which substantiate the observations.

# 6

# THE EFFECT OF TEMPERATURE ON CORROSION OF STEEL IN CONCRETE

*This chapter is the overall concluding discussion of this thesis. Here the two parameters investigated are connected to visualise the effect of temperature on corrosion of steels embedded in concrete.*

## 6.1 Introduction and connection between the experiments and corrosion of steel in concrete.

It has in the forgoing discussions been established that corrosion of steel in concrete is dependent on four main elements as illustrated in Figure 6.1.

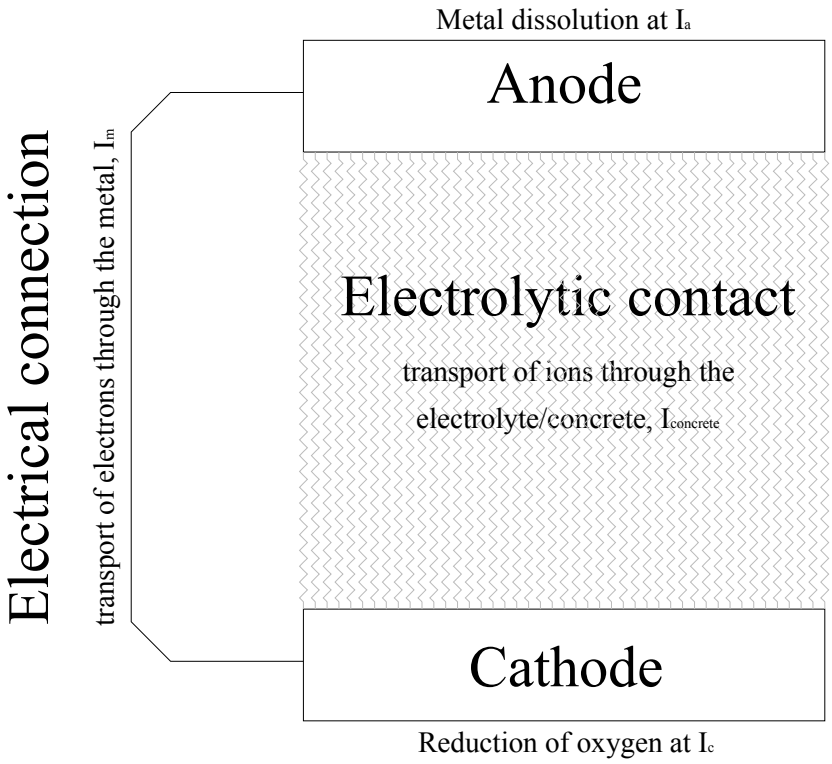


*Figure 6. 1 Illustration of the corrosion cell and the interconnected elements*

These four elements, or processes, are complementary, i.e. they occur at the same rate; Anodic dissolution rate, $I_a$ = cathodic reduction rate, $|I_c|$ = electrons transported by the electrical connection (metallic), $I_{metal}$ = ion charge transported through the electrolyte (concrete), $I_{concrete}$.

The current generated in the corrosion cell is mutually connected and equal to all these partial currents, i.e. all partial currents are equal to the corrosion rate, and all partial processes may be rate determining.

By the CRR and the ER experiments, it is (for these particular systems) given an effect on the current bearing capacity of the cathode and the electrolyte by changes in temperature and moisture contents.

## 6.2 Main observations from the experiments

### 6.2.1 Main observations from the CRR – experiments

- The lag between concrete temperature and the temperature in the chamber was approximately two hours. The total transient time was about four hours until a more or less "quasi steady state" was achieved.

- By stationary polarisation (-0.6V/MMO) at a stable temperature (0°C) it was observed a small decrease in cathodic reaction rate. The decrease was about 5% over a period of 200 hours. This may indicate increased pH in the adjacent areas of the electrode due to insufficient diffusion of hydroxide ions from the cathodic electrode surface. Increased pH makes the electrode nobler and thereby less energy consuming to polarise. The decrease may possibly also owe to changes in the reference electrode and eventual polarisation of these electrodes. The MMO – reference electrodes has been reported by Castro, Sagüés, Maldonado and Genescá [80] to have slight polarisation over longer periods.

- Polarisation of the cathodic reaction resulted in steeper Tafel gradients in the low-overpotential range (less than -0.3V/MMO) than the reported for oxygen reduction on platinum, however, the results are quite in range of what is normally observed for cathodic polarisation curves in the literature [17 – 19]. The observation of higher slopes may indicate that other charge-transfer reactions are taking part in the overall reaction and that oxygen reduction occurs by first peroxide or superoxide formation before completing the reactions. Even though the experiments were performed without any compensation for the ohmic drop (IR corrections) they provide relevant information.

- At higher cathodic overpotentials the reaction appears to be restricted by the availability of the cathodic reactant (oxygen). Already at a potential of approximately -0.3V/MMO the reaction appears to be restricted by mass transport of reactants by diffusion to the electrode surface. The reaction may additionally be restricted by diffusion/migration of resultants of the reaction from the electrode surface. Funahishi and Young [17] indicates without being able to conclude that diffusion of hydroxide from the electrode may be rate determining if the water film surrounding the electrode is particularly thin (i.e. the moisture content is low). It is assumed due to relatively moderate moisture contents in the CRR – experiments that the availability of oxygen will dominate the rate of the reaction in this research.

- Cathodic polarisation of steel in concrete is clearly temperature dependent. By decreasing the temperature the restriction of the reaction due to lack of reactants appears at lower overpotentials (as low as -0.15 V/MMO at -20°C) and the total current increases clearly slower by increased overpotentials at lower temperatures. However, at low overpotentials (linear Tafel region) the reaction appears to have nearly the same development by overpotential as for higher temperatures.

- It was not observed cases comparable to concentration polarisation in the cathodic polarisation curve experiments. Even though the reaction was clearly restricted, no limited state could be found within the potential interval investigated ($0 > \eta > -1.0$ [V]). It is therefore assumed that the reaction is decelerated by the supply of reactants without reaching a state of concentration polarisation.

- The polarisation rate was tested by two rates at 15 minutes and 24 hours at each potential step. The polarisation curves were corresponding for both steps; however, there were a lag between the different stabilisation times which appeared to be more or less consistent through the testing interval. Of practical reasons the shorter rate was chosen. The difference between the polarisation rates are illustrated in Figure 6.2 by a potentiostatic transient.

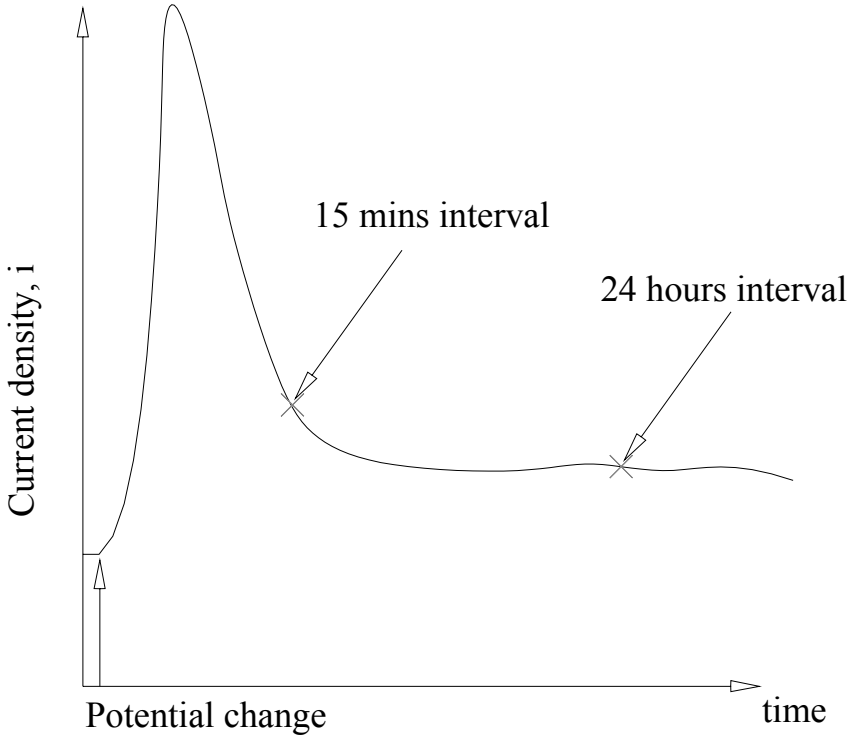


*Figure 6. 2 Potentiostatic transient for the CRR visualising the two polarisation rates. Based on Bockris et al. [3].*

- The variation of the polarisation curves by temperature indicates that the increased solubility of oxygen in the pore water by decreasing temperature play a secondary role for the overall reaction rate.

- It was observed that the cathodic reaction rate decreased by decreasing temperature, giving activation energy constants in the range of 3000 – 5000 K. The calculated activation energies were within the expected range compared to information found in the literature. A list of activation energy constants found by several authors is given in Table 6.1:

*Table 6. 1 Comparison of activation energy constants found in the literature compared to obtained values*

| Project | Polarisation type | Temperature range | Activation energy constant | | |
|---|---|---|---|---|---|
| | | | SPS* | Mortar | Concrete |
| Jäggi, Böhni and Elsener [19] | Macrocell of depassivated steel/ Constant | 0°C to 50°C | 4310K | 4250K | |
| Vennesland [20] | Constant (-0.8V/SCE) | 1°C to 30°C | | | 2500K |
| Elsener, Flükiger, Woytas and Böhni [21] | Macrocell measurements | -10°C to 18°C | | | 3789K |
| This project | Constant (-0.6V/MMO) | -40°C to 40°C | | | 3000K – 5500K |

*) SPS = Simulated Pore Solution (KOH and $Ca(OH)_2$)

The very extensive range of activation energy constants may owe to that the cathodic reaction rate is influenced by transport mechanisms simultaneously with the temperature effect. The effect of temperature on the cathodic reaction rate is given in Figure 6.3 as a temperature scaling factor given an estimated upper and a lower range.

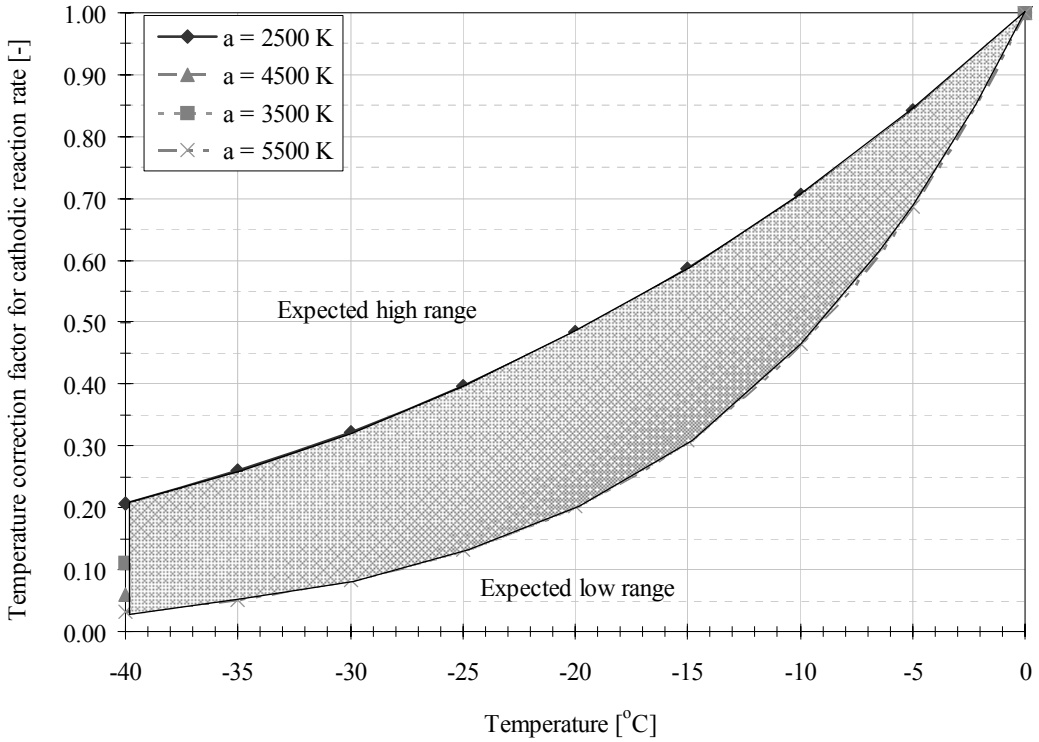


*Figure 6. 3 Temperature reduction curve for the cathodic reaction rate in respect to a measured reaction rate at 0°C. Low temperature range (-40°C ≤ T ≤ 0°C).*

- The cathodic reaction rate appears to be connected to the permeability of the concrete. Generally, the concrete with w/b-ratio 0.6 generated far higher currents than the concrete with w/b-ratio 0.4, which can be attributed to the permeability of the concretes.

- Between freezing and thawing there were found considerable hysteresis effects for the water-cured variants. These hysteresis effects were assumed to be induced by frozen capillary water. From calorimetric testing it was found that approximately 29% (w/b 0.6) and 12% (w/b 0.4) of the evaporable water were able to freeze within the temperature range (down to -35°C concrete temperature) given a fully saturated concrete. With such considerable amounts of frozen capillaries the hysteresis effects were well expected. The theory of ice in the pores was substantiated in that no clear hysteresis effects were found between heating and cooling and that nearly no hysteresis effects were found for the variants with lower moisture contents.

- The moisture content of concrete seems to play a secondary role for the cathodic reaction rate. At higher moisture contents however, the diffusion of oxygen mainly takes place in the aqueous phase, which is very much slower than in air. Reduction of oxygen is on the other side dependent upon a water film present in the adjacent areas to the electrode, and also to be interconnected by an ionic conductive pathway to the anode for the reaction to occur.

### 6.2.2 Main observations from the ER – experiments

- The experiments verify in general the numerous observations that the electrical resistivity increases by decreasing w/b-ratios. Monfore [32] reported observations of that the electrical resistivity of a cement paste with a w/b-ratio of 0.4 was about the double of that of a cement paste with w/b-ratio of 0.6. Generally for the investigated concretes the electrical resistivity of the concretes with w/b-ratio of 0.4 were relatively larger than that of the concretes with w/b-ratio 0.6 at comparable curing regimes and moisture contents. However, a clear ratio between the two w/b-ratios is not found. The ratios between the concretes ($\rho_{0.4}/\rho_{0.6}$) were observed to be in the range 1.5 – 3.5 dependent upon the curing and handling. It is important to note that the concretes were fundamentally different with a view to cement content, silica fume additive and amounts and gradation of the aggregates. Therefore a clear indication of the impact of the various parameters regarding the concrete mix on the electrical resistivity is not conclusive. However, the observations show the same trend as indicated in the literature.

- The electrical resistivity of concrete is clearly and decisively dependent upon the moisture condition of the concrete. The observations in this project correspond to that found in the literature. Gjørv et al. [49] and Woelfl and Lauer [59] reported dramatic increasing electrical resistivity (Woelfl and Lauer investigated electrical resistance of concretes) at decreasing moisture contents. This has in general later been verified by several authors and is

verified by the present experimental results. However, the results do not agree in detail. The electrical resistivity in the present results for both concretes increases more strongly at certain moisture contents. Based on quite rough assumptions it appears as these critical moisture contents coincide with the capillary cores being empty and/or a thickness of the adsorbed water layers of approximately 2 to 3 monolayers. The slope of the increase in the electrical resistivity by decreasing moisture contents may be a valuable tool to describe the pore structure, i.e. a division into gel and capillary pores, thereby describing the various concrete qualities by means of durability of concrete. If properly investigated and verified this may give an important tool to characterise the concretes. Supporting literature for these observations was not found.

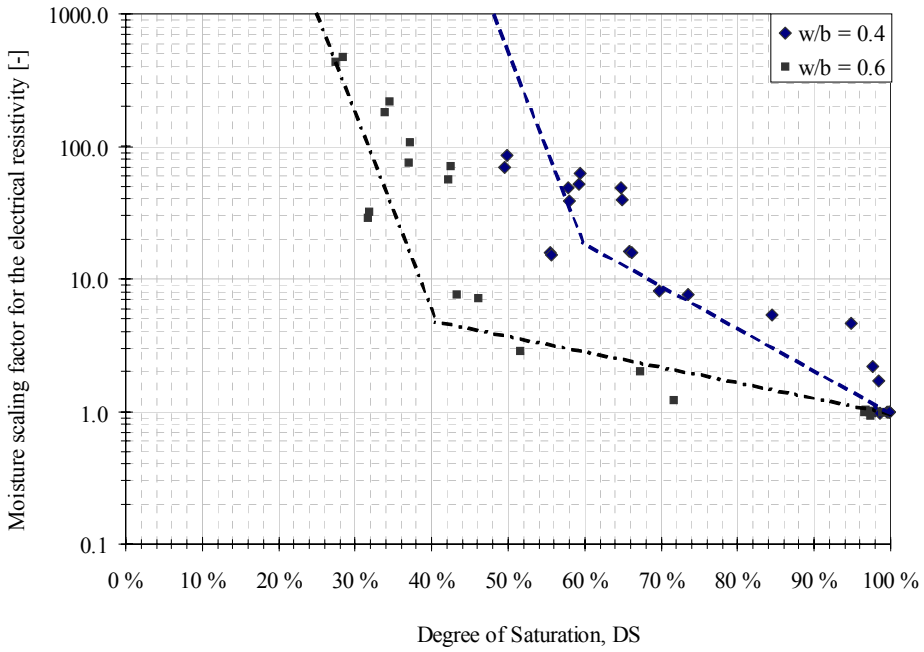


*Figure 6. 4 Moisture scaling factor for electrical resistivity. The reference (1.0) is the electrical resistivity of fully saturated concrete (DS =100%).*

- The electrical resistivity of concrete increases with decreasing temperatures yielding activation energy constants (according to Hinrichson – Rasch law) in the range 2200 K – 5500 K. This range of temperature sensitivity is in agreement with the statement of Elkey and Sellevold [40] that the activation energy constants may vary between 2000 K and 5000 K in some cases.

*Table 6. 2 Comparison of activation energy constants found in the literature compared to obtained values*

| Project | Measurement type (frequency) | Temperature range | Activation energy constant | | |
|---|---|---|---|---|---|
| | | | Cement paste | Mortar | Concrete |
| Monfore [32] | DC and AC (0.1 – 10 kHz) | | 2200 K | | |
| Hope et al. [61] | AC (1 kHz) | 5°C to 25°C | | | 2900 K |
| This project | AC (0.1 – 40 MHz) (0.1 – 10 kHz) (1 kHz) | -28°C to 20°C | | | 2200 K – 5500 K |

- When temperature and the moisture contents of concrete are viewed in combination, the effect on the electrical resistivity can be summarised as follows: The effect of moisture contents appears to follow the same trend at all temperatures, however, the temperature introduces a level shift (increased to a higher level at decreased temperature).

- The measurements appear to be frequency dependent at lower temperatures and lower moisture contents. It seems as if a constant measurement frequency will describe impedances with increasing imaginary components at lower temperatures and lower moisture contents. No conclusion is possible to make due to the low amounts

of data, however, the indication is clear. It is recommended that more research is performed to map out the frequencies proper for measurements at lower temperatures and lower moisture contents. However, for practical purposes constant measurements frequencies between 100 and 5000 Hz appears to be appropriate at normal moisture contents ( >70 %) and at temperatures above 0°C.

- The presentation of the EIS data by impedance plot (Nyquist diagrams) confirm the observations made by Bürcheler, Elsener and Böhni [44] that the semicircles describing the impedance in concrete are suppressed which indicates dispersed relaxation times, i.e. the impedance describes the different phases of conduction in concrete (e.g. cement particles, liquids, adsorbate). The impedance will therefore describe a semicircle that is suppressed below the real axis.

## 6.3 Effect of temperature on corrosion of steel in concrete

### 6.3.1 Effect of temperature on corrosion of steel in concrete highlighted by an example

Based on the observations summarised in section 6.2 it is now possible to estimate the effect of temperature on the corrosion rate of steel embedded in concrete based on certain assumptions. The assumptions and observations are:

- The electrodes are identically sized on both the anode and the cathode.

- The cathodic reaction is impeded by the supply of reactants at lower overpotentials by decreasing temperatures as observed in the CRR experiments.

- The anodic electrode is assumed to be easier polarised tending towards a transpassive state for decreasing temperatures, i.e. the slope of the anodic polarisation curve will increase for decreasing temperatures.

- The electrical resistivity of concrete increases quite intensively with decreasing temperatures, and even though the current density is assumed to decrease in the corrosion circuit, one may predict that the

ohmic drop induced (by the concrete resistance) in the corrosion circuit remains more or less stable.

- The respective anodic and cathodic corrosion potentials will attend approximately the same values at various temperatures. Slight changes will occur, but in eyes of the effect of the temperature on the other processes this will only play a second order role.

Based on the above assumptions and observations Evans diagrams for four temperatures are given in Figure 6.5.

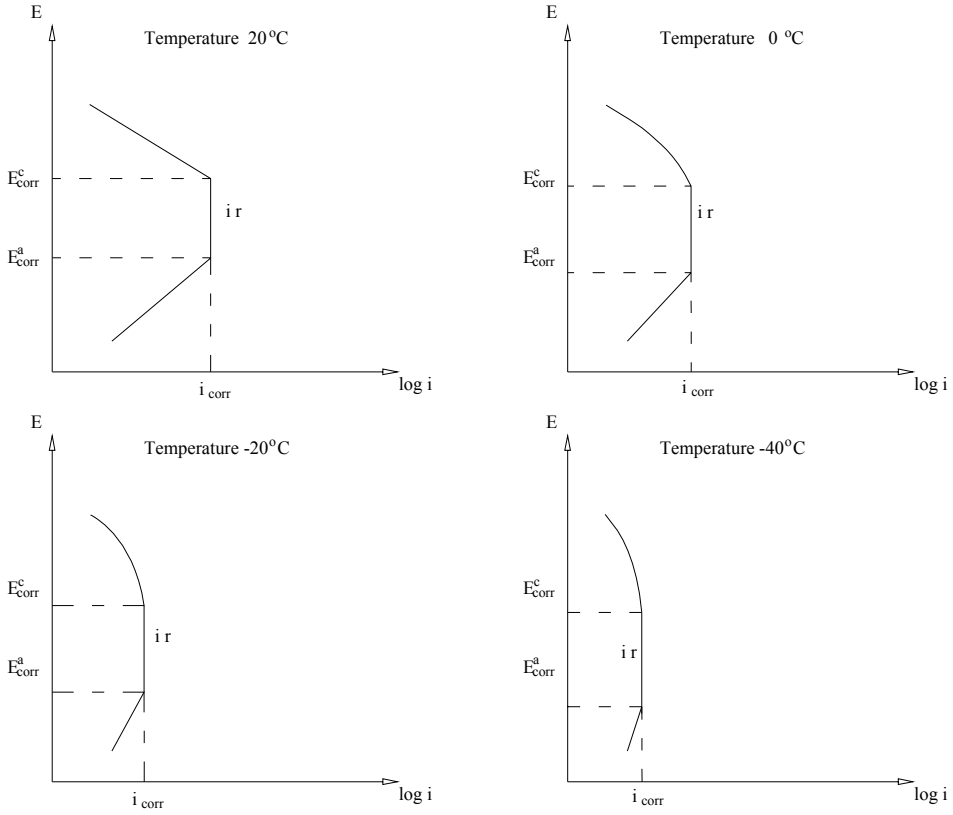


*Figure 6. 5 Plausible effect of temperature on the corrosion couple illustrated by Evans diagrams for temperatures of 20°C, 0°C, -20°C and -40°C.*

Certainly , the illustrated effect on the corrosion rate (Figure 6.5) represents only a qualified guess based on my best knowledge; however, it is plausible that it illustrates the effect of temperature on a corrosion couple in concrete given the assumed conditions.

At 20°C the cathodic electrode is assumed to be in the linear region of the polarisation curve at its corrosion potential, the anodic electrode is in the active part and the ohmic drop (ir) is quite substantial due to the high activity, though the electrolytic resistance is low.

At 0°C the cathodic process starts to be restricted by the supply of oxygen and the slope of the anodic curve is increased due to higher activation energy. The ohmic drop is the same although the activity is decreased since the electrolytic resistance is increased in the circuit.
At the temperatures of -20°C and -40°C the situation from 0°C is amplified. The cathodic electrode is reaching a situation similar to concentration polarisation and the anodic electrode is more and more steeply polarised.

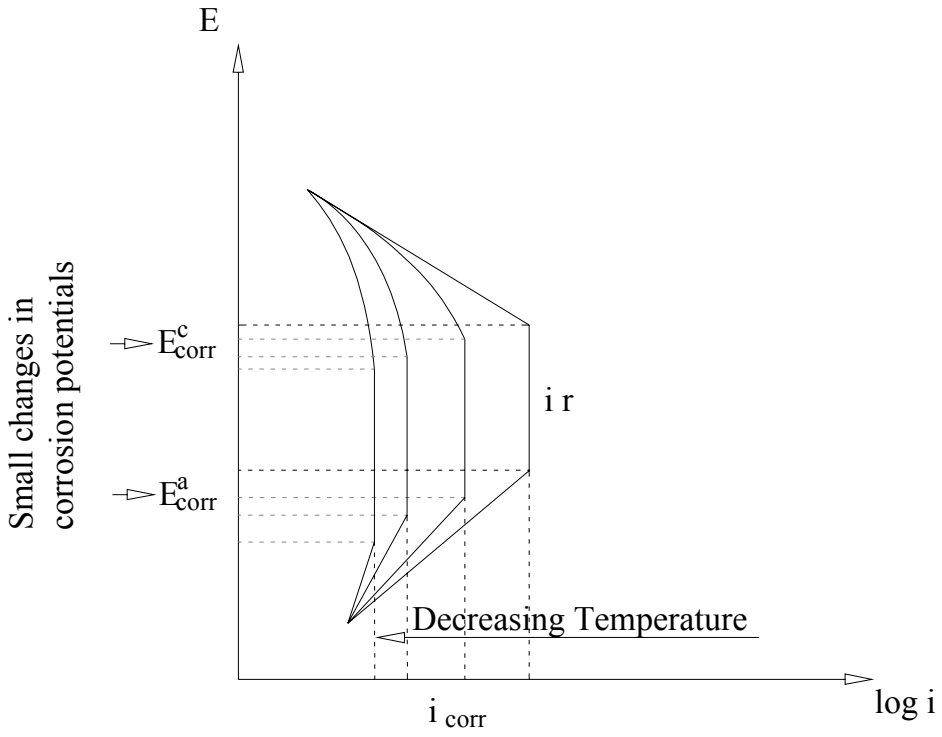


*Figure 6. 6 Summary of the assumed effect of temperature on corrosion rate of steel in concrete.*

Clearly, a quantification of the direct temperature effect on the corrosion rate is not possible by the observations in this project. However, it is strongly indicated that the corrosion rate decreases with decreasing temperature, and that it is inhibited by both the investigated corrosion parameters. The cathodic reaction current density was shown to decrease strongly by temperature with activation energy constants from 2500 K to 5000 K. Likewise, the electrical resistivity increased equally much with decreasing temperatures.

If the temperature effect of the cathodic reaction rate and the temperature effect of the electrical resistivity of concrete are superimposed, the effects should result in a decrease of the corrosion rate according an activation energy constant of approximately 25000 K. This implies that the corrosion rate should decrease by nearly 15% per °C. Clearly, the effect of temperature on the corrosion rate can not be estimated by superimposing the effects.

Due to the complexity of the corrosion processes in concrete, e.g. geometrical considerations, reaction kinetics, available current pathways etc, to go beyond the elaborations just made is too uncertain to justify the attempt.

In order to clarify the direct effect of temperature on the corrosion rate in the low temperature range a large and accurate laboratory study seen in conjunction with field measurements is needed.

# 7

# CONCLUSIONS

*This chapter summarises the main conclusions based on the experimental work, reported in Chapters 4 through 6, and their most important consequences. At the end some recommendations on further work is outlined.*

## 7.1 Main conclusions and their implications

The results in this study demonstrate that:

1) The cathodic reaction rate of passive steel embedded in concrete decreases for decreasing temperature.

2) Ice formation in the capillary pore structure generates considerable hysteresis effect on the cathodic reaction rate of steel in concrete.

3) The cathodic polarisation behaviour of passive steel is temperature dependent.

4) The electrical resistivity of concrete is increasing by decreasing temperature

5) The electrical resistivity of concrete is governed by the moisture condition of concrete, increasing for decreasing moisture contents.

### 7.1.1 Thermal effects on the cathodic reaction rate of passive state embedded steels in the low temperature range

The conclusion that the cathodic reaction rate of passive embedded steels in concrete decreases for decreasing temperatures is based on the results from the CRR – experiments (Chapter 4) where all tested specimens showed a decrease in reaction rate for decreasing temperatures. The decrease did in most cases follow the Arrhenius law. The calculated activation energy constants formed a scatter in the range 2000 – 5000 K (activation energies according to Arrhenius law -17 – -45 kJ/mole). The variation of the activation energy constants could not be related to either the concrete porosity characteristics or the moisture content of the concrete.

The observation of decreasing reaction rate for decreasing temperature confirms the reported findings for similar processes found in the literature and the range of the observed activation energy constants fits the reported range.

The practical implication of these observations is that one should expect a change in cathodic reaction rate of steel in concrete of approximately 3 % to 5 % per °C at 20°C.

Furthermore, this implies that cathodic protection systems that are controlled after a fixed current (density) principle may generate extreme potentials on both the anodic electrode and the cathodic electrode (reinforcements) with the consequences that such potentials may have.

### 7.1.2 Hysteresis effects due to ice formation in the capillary pores

The conclusion that ice formation in the capillary pores causes the hysteresis effects is based on the results from the CRR – experiments seen in conjunction with low-temperature calorimetric data.

The specimens having the highest moisture contents, i.e. thereby the largest potential for ice in the capillaries, behaved differently during thawing compared to during freezing. On freezing these specimens acted differently than the specimens containing less moisture, while on thawing the results were corresponding to those containing less moisture. The specimens that contained less moisture did not show hysteresis effects. This was a strong indicative that some of the capillaries were demobilised and did not contribute to the reaction rate. The fact that the data from the low-temperature calorimetry substantiated the hysteresis effects due to the difference in how water freezes and thaws in concrete gave this conclusion.

The practical consequences of these observations is that while working at low temperatures with wet or saturated concrete one has to bare in mind that ice may interfere measurements of all kind in concrete.

### 7.1.3 Temperature dependency of the cathodic polarisation curves for passive state steel in concrete.

The conclusion that the cathodic polarisation curves for passive steel in concrete have a temperature dependency is based on the polarisation experiments in the CRR – section of the experimental programme. During polarisation in the range, 0 to -1.2 V/MMO, at three specific temperatures, 20°C, 0°C and -20°C, the shapes of the polarisation curves changed by changes in temperature. It was found that the slope of the steepest parts of the polarisation curves increased by decreasing temperatures. For some of the variants the situation at -20°C approached a situation of concentration polarisation.

### 7.1.4 Thermal aspects of the electrical resistivity of concrete in the low temperature range.

The conclusion that the electrical resistivity increases by decreasing temperatures is based on the ER – experiments where the electrical resistivity of all specimens were found to increase by decreasing temperatures. The change in electrical resistivity was found to follow Hinrichson – Rasch law in many cases giving activation energy constants in the range 2000 – 5500 K. The wetter the concrete the less it could be described by a single activation energy constant according to Hinrichson – Rasch law, indicating presence of changes in the electrolyte that is not activation governed. It is assumed that some of these effects could be attributed to ice formation in the capillaries.

### 7.1.5 The moisture condition governs the electrical resistivity of concrete also in the low temperature range.

The conclusion that the moisture content of concrete governs the electrical resistivity was found previously by several authors. However, this study extends the conclusion to the electrical resistivity at low temperatures. This conclusion is based on the observations in the ER – experiments (chapter 5).

Temperature introduces a level shift to the relation between moisture content and the electrical resistivity. The curves for the four specific temperatures investigated in this project were nearly following the same course for all temperatures, however, with a temperature induced level change.

## 7.2 Recommendations for further work

More work should be made in order to clarify the effect ice has on the electrolytic behaviour of concrete. This could include a variety of experiments, but it is indeed recommended that finer resolutions on the temperature intervals are used, and that the range is widened compared to the experimental programme in this project.

More work on the relation between moisture content and electrical resistivity should be made in order to verify the indications found in this

project that a critical resistivity is reached at specific moisture contents given by the concrete porosity characteristics. Such an investigation is recommended to include a wider range of materials (e.g. cement types, additives) and concentrate on only one temperature. A thorough investigation could result in a method to characterise in-situ concrete in terms of durability by its moisture-resistivity relation.

It would be of great value to perform a statistical study of several structures suffering of reinforcement corrosion where in-situ measurements were correlated with the experimental data found in this project and similar projects in order to verify if the observations could be translated into existing structures.

# 8

# REFERENCES

[1] Andrade, C, Alonso, C, "Corrosion rate monitoring in the laboratory and on-site". *Construction and Building Materials*. Elsevier Science Ltd., London, pp 315-328, 1995

[2] Schiessl, P., Raupach, M., "Influence of Temperature on the Corrosion Rate of Steel in Concrete Containing Chlorides" in *First International Conference of Reinforced Concrete Materials in Hot Climates*, Alain, 1994.

[3] Bockris, O´M., Reddy, A., Gamboa-Aldeco, M. , *Modern Electrochemistry 2a, Fundamentals on Electrodics*, Kluwer Academics/Plenum Publishers, New York, 2000.

[4] Page, C. "Corrosion of steel in concrete", In, Sciessl, P (Ed.) *Project report TC-60-CSC Corrosion of Steel in Concrete*, Chapman and Hall, pp. 3-22, New York, 1988

[5] Tuutti, K., *Corrosion of steel in concrete,* Swedish Cement and Concrete Research (CBI) no 4-82, Stockholm, 1982

[6] Bockris, O´M., Reddy, A., Modern Electrochemistry 1, *Ionics*, Kluwer Academics/Plenum Publishers, New York, 2000.

[7] Neville, A.M., *Properties of concrete*, Prentice Hall, London, 2000.

[8] Cost 509 Workshop (1997) Part 2: Monitoring. In: Cox RN, Cigna R, Vennesland Ø, Valente T (Eds) *Corrosion and protection of metals in contact with concrete*. COST, Brussels, pp 39-103

[9] Bertolini, L., Elsener, B., Pedeferri, P., Polder, R., *Corrosion of Steel in Concrete – Prevention, Diagnosis and Repair*, Wieley – VCH, Weinheim, 2004.

[10] Bard, A.J., Faulkner, L.R, "Electrochemical Methods. Fundamentals and Applications, John Wiley & Sons, 1980.

[11] Yeager, E, "Electrocatalysts for $O_2$ Reduction", *Electrochemical Acta*, Vol. 29, No. 11, pp 1527-1537, London, 1984

[12] Sato, N., "Toward a more Fundamental Understanding of Corrosion Processes, *CORROSION, The journal of Science and Engineering*, Vol. 5, No. 9, pp. 969-985, 1983.

[13] Pruckner, F., *"Corrosion and Protection of Reinforcement in Concrete Measurement and Interpretation"* Dr. rer.nat. Thesis, University of Vienna, Vienna, Austria, pp. 4-106,2001

[14] Andrade, C., Merino, P., Nóvoa, X.R, Pérez, M.C, Soler, L., ”Passivation of Reinforcing Steel in Concrete, *Material Science Forum*, Trans Tech Publications, Switzerland, Vols. 192-194, pp. 891-898, 1995

[15] Stratmann, M., Bohnenkamp, K., Engell, H.J., “An Electrochemical Study of Phase-Transitions in Rust Layers”, *Corrosion Science*, Vol. 23, pp. 969-985,Pergamon Press, London, 1983

[16] Vennesland, Ø. Unpublished data from experiments on chloride extraction of steel in chloride contaminated concrete, (Personal communication), 2002.

[17] Funahishi, M., Young, W.T, “Investigation of E-Log I Tests and Cathodically Polarized Steel in Concrete”, *Corrosion 94*, Paper 301. NACE, Houston, pp 1-38, 1994.

[18] Jäggi, S., Elsener, B., Böhni, H. ”Oxygen Reduction on Mild Steel and Stainless Steel in Alkaline Solutions” In Mietz, J. Polder R., Elsener, B. (Eds.) *EFC 31 (Papers from EUROCORR `99)*, IOM Communications, London, 2000.

[19] Jäggi, S., Elsener, B., Böhni, H. ”Macrocell Corrosion of Steel in Concrete – Experiments and Numerical Modelling” (Presented at *EUROCORR 2001*), AIM, Milan, 2001.

[20] Vennesland, Ø. "Effect of Temperature on Oxygen Transport Through Submerged Concrete". In *Nordic Concrete Research*, publication no. 10, pp. 139-145, 1991

[21] Elsener, B., Flükiger, D., Woytas, H., Böhni, H., *"Methoden zur Erfassung der Korrosion von Stahl in Beton"* Eidgenössisches Verkers- und Energiewirtschaftsdepartement, Bundesamt für Strassenbau, Zürich, (In German), 1996.

[22] Raupach, M., *"Effect of Temperature on Chloride Induced Corrosion in Concrete"*, 2001

[23] Andrade, C., Alonso, C., Garcia, A.M., "Oxygen Availability in the Corrosion of Reinforcements", *Advances in Cement Research*, vol. 3 no. 11, pp.127-132, 1990

[24] Raupach, M., "Investigations on the Influence of Oxygen on Corrosion of Steel in Concrete – Part 1", *Materials and Structures*, V. 29, pp. 174-184, April 1996.

[25] Raupach, M., "Investigations on the Influence of Oxygen on Corrosion of Steel in Concrete – Part 2", *Materials and Structures*, V. 29, pp. 226-232, May 1996.

[26] RILEM. *Performance Criteria for Concrete Durability*. Proceedings. State of the Art Report prepared by RILEM Technical Committee TC 116-PCD, Performance of Concrete as a Criterion of Its Durability. RILEM Report 12. 1995, E & FN SPON, London,England, Kropp, J.; Hilsdorf, H. K., Editor(s), , 1995

[27] Esbach, O.E. and Souders, M., *Handbook of Engineering Fundamentals*, John Wiley & Sons, New York, 1975.

[28] Harper, C.A., "Fundamentals of Electrical Insulating Materials," *Industrial Research/Development*, Vol. 20, No. 12, pages 81 to 84, December 1978.

[29] Whiting, D.A, Nagi, M.A., *"Electrical Resistivity of Concrete – A Literature Review"*, R&D Serial No.2457, Portland Cement Association, Skokie, Illonois, USA, 57 pages, 2003.

[30] Maxwell, C., *Treatise on Elasticity and Magnetism*, Vol.1, Clarendon Press, Oxford, 1873.

[31] Keller, G.V., *"Electrical Properties of Rocks and Minerals,"* Chapter 2 in Handbook of Physical Properties of Rocks, Vol. I, Carmichael, R.S., ed. pages 217 to 293, CRC Press, Boca Raton, Florida, 1982.

[32] Monfore, G.E. “The Electrical Resistivity of Concrete,” *Journal of the PCA Research and Development Laboratories*, Vol. 10, No. 2, pages 35 to 48, May 1968.

[33] Fricke, H., "A Mathematical Treatment of the Electrical Conductivity and Capacity of Disperse Systems. The Electrical Conductivity of a Suspension of Homogeneous Spheroids," *Physics Review* – Vol. 24, 1924, pages 678 to 681.

[34] Whittington, H.W., McCarter, J., and Forde, M.C., “The Conduction of Electricity Through Concrete,” *Magazine of Concrete Research*, Vol. 33, No. 114, pages 48 to 60, 1981.

[35] Xie, P. P., Gu, Y.F., and Beaudoin, J.S., “Determination of Blast-Furnace Slag Content in Hardened Concrete by Electrical Conductivity Methods,” *Cement, Concrete, and Aggregates, CCAGDP*, Vol. 17, No. 1, June 1995, pages 79 to 83.

[36] Archie, G.E., "The Electrical Resistivity Log as an Aid in Determining Some Reservoir Characteristics," *Transactions of the American Institute of Mining and Metallurgical Engineers*, Vol. 146, pages 54 to 62, 1942.

[37] Atkins, E.R. and Smith, G.H., “The Significance of Particle Shape in Formation Resistivity Factor-Porosity Relationships,” *Transactions of the American Institute of Mining and Metallurgical Engineers*, Vol. 222, pages 285 to 291, 1961.

[38] Jackson, P.D., Taylor-Smith, D., and Stanford, P.N., "Resistivity–Porosity–Particle Shape Relationships for Marine Sands," *Geophysics,* Vol. 43, pages 1250 to 1268, 1978.

[39] Morelli, R. and Ford, M.C., "Electrical Conduction Through Concrete Using Formation Factor Theories," *Proceedings, International Conference on Structural Faults and Repair*, University of London, July 7-9, 1987, Engineering Technics Press, Edinburgh, 1987, pages 411 to 422.

[40] Elkey, W. and Sellevold, E.J., *Electrical Resistivity of Concrete*, Norwegian Road Research Laboratory, Publication No. 80, Oslo, July 1995.

[41] Berke, N.S., Scali, M.J., Regan, J.C., and Shen, D.F., "Long-Term Corrosion Resistance of Steel in Silica Fume and/or Fly Ash Containing Concretes," Proceedings, *Second CANMET/ACI International Conference on Durability of Concrete, SP-126*, pages 393 to 415, American Concrete Institute, Farmington Hills, MI, 1991.

[42] Berke, N.S., Dallaire, M.P., and Hicks, M.C., "Plastic Mechanical, Corrosion, and Chemical Resistance Properties of Silica Fume (Microsilica) Concretes," Proceedings, *Fourth CANMET/ACI International Conference on Fly Ash, Silica Fume, Slag, and Natural Pozzolans in Concrete, SP-132*, pages 1125 to 1149, American Concrete Institute, Farmington Hills, MI, 1992.

[43] Cabrera, J.G. and Ghoddoussi, P., "The Influence of Fly Ash on the Resistivity and Rate of Corrosion of Reinforced Concrete," Proceedings, *Fourth CANMET/ACI International Conference on Concrete Durability*, SP-145, pages 229 to 244, American Concrete Institute, Farmington Hills, MI, 1994.

[44] Bürchler, D., Elsener, B., and Böhni, H., *Electrical Resistivity and Dielectric Properties of Hardened Cement and Mortar*, Institute of Materials Chemistry and Corrosion, Swiss Federal Institute of Technology, ETH Hönggerber, CH-8093 Zurich, Switzerland, 1996.

[45] Hunkeler, F., "The Resistivity of Pore Water Solution - A Decisive Parameter of Rebar Corrosion and Repair Methods," *Construction and Building Materials*, Vol. 10, No. 5, pages 381 to 389, 1996.

[46] Baweja, D., Roper, H., and Sirivivatnanon, V., "Corrosion of Steel in Marine Concrete: Long-Term Half-Cell Potential and Resistivity Data," Proceedings, *Third CANMET/ACI International Conference on Concrete in Marine Environment, SP-163*, pages 89 to 110, American Concrete Institute, Farmington Hills, MI, 1996.

[47] Hammond, E. and Robson, T.D., "Comparison of Electrical Properties of Various Cements and Concretes," *The Engineer*, Vol. 199, No. 5156, pages. 78 to 80, January 21, 1955, and No. 5166, pages 114 to 115, January 28, 1955.

[48] Hughes, B.P., Soleit, A.K.O., and Brierly, R.W., "New Technique for Determining the Electrical Resistivity of Concrete," *Magazine of Concrete Research,* Vol. 37, No. 133, pages 243 to 248, 1985.

[49] Gjørv, O.E., Vennesland, Ø , and El-Busiady, A.H.S., "Electrical Resistivity of Concrete in the Oceans," *Proceedings – 9th Annual Offshore Technology Conference, Houston*, Texas, pages 581 to 588, May 2-5, 1977.

[50] Whiting, D., Todres, A., and Nagi, M., Synthesis of Current and Projected Concrete Highway Technology, *SHRP-C-345, Strategic Highway Research Program*, National Research Council, Washington, D.C., 1993, 286 pages.

[51] Ehtesham, S. and Rasheeduzzafar, H., "Corrosion Resistance Performance of Fly Ash Blended Cement Concrete," *ACI Materials Journal*, Vol. 91, No. 3, pages 264 to 271, May-June 1994.

[52] Lewis, D.W., "History of Slag Cements," *Paper Presented at University of Alabama Slag Cement Seminar*, American Slag Association, MF 186-6, April 1981.

[53] Malhotra, V.M., "Properties of Fresh and Hardened Concrete Incorporating Ground Granulated Blast Furnace Slag," *Supplementary Cementing Materials for Concrete*, ed. V.M. Malhotra, 291-331, Ottawa: Canadian Government Publishing Centre, 1987.

[54] Mobasher, B. and Mitchell, T.M., "Laboratory Experience with the Rapid Chloride Permeability Test," Permeability of Concrete, *ACI SP-108*, pages 117 to 140, American Concrete Institute, Farmington Hills, MI, 1988.

[55] ASTM C 1202-97, "Standard Test Method for Electrical Indication of Concrete's Ability to Resist Chloride Ion Penetration," *American Society for Testing and Materials*, West Conshohocken, PA.

[56] Rosenberg, A., Hansson, C. M., and Andrade, C., "Mechanisms of Corrosion of Steel in Concrete," *Materials Science of Concrete I*, Edited by J. P. Skalny, The American Ceramic Society, pages 285 to 315, 1989.

[57] Dhir, R.K., Ei-Mohr, M.A.K., and Dyer, T.D., "Chloride Binding in GGBS Concrete," *Cement and Concrete Research*, Vol. 26, No. 12, pages 1767 to 1773, 1996.

[58] Sellevold, E.J., Larsen, C.K., and Blankvoll, A.A., "Moisture State of Concrete in a Coastal Bridge," *Proceedings, Fourth CANMET/ACI International Conference on Concrete Durability, SP-170*, pages 825 to 833, American Concrete Institute, Farmington Hills, MI, 1997.

[59] Woelfl, G.A. and Lauer, K., "The Electrical Resistivity of Concrete with Emphasis on the Use of Electrical Resistance for Measuring Moisture Content," *Cement, Concrete, and Aggregates, CCAGDP*, Vol. 1, No. 2, pages 64 to 67, 1979.

[60] McNeill, J.D., Electrical Conductivity of Soils and Rocks, Technical Note TN-5, Geonics Ltd., Mississauga, Ontario, Canada, 1980.

[61] Rasch, E. and Hinrichsen, F.W., "Uber eine Beziehung zwischen Elektrischer Leitfahigkeit und Temperatur," *Zeitschrift fur Electrochemie*, (In German), Vol. 14, No. 41, pages 41 to 48, 1908.

[62] Spencer, R.W., "Measurement of the Moisture Content of Concrete," *Journal of the American Concrete Institute*, Vol. 9, No. 1, pages 45 to 61, Sept.-Oct. 1937.

[63] Hope, B.B., Ip, A.K., and Manning, D.G., "Corrosion and Electrical Impedance in Concrete," *Cement and Concrete Research*, Vol. 15, No. 3, pages 525 to 534, 1985.

[64] Castellote, M., Andrade, C., Alonso, M.C., "Standardisation, to a Reference of 25°C, of Electrical Resistivity for Mortars and Concretes in Saturated or Isolated Conditions", *ACI Materials Journal*, Vol 99, No 2, pp.119-128, 2002

[65] Hauck, C.J., The Effect of Curing Temperature and Silica Fume on Chloride Migration and Pore Structure of High Strength Concrete, Doctoral Dissertation, Norges Tekniske Høgskole (NTH), University of Trondheim, Norway, 1993.

[66] Bracs, G., Balint, E., and Orchard, D.F., "Use of Electrical Resistance Probes in Tracing Moisture Permeation Through Concrete," Journal of the American Concrete Institute, Vol. 67, No. 8, pages 642 to 646, August 1970.

[67] Schissl, P., Breit, W., Raupach, M., "Investigation into the Effect of Coatings on Water Distribution in Concrete using Multi-Ring Electrodes", Proceedings, ACI, Convention, Minneapolis, MN, Nov. 1993.

[68] Hansson, I.L.H. and Hansson, C.M., "Electrical Resistivity Measurements of Portland Cement Based Materials," Cement and Concrete Research, Vol. 13, No. 5, pages 675 to 683, 1983.

[69] Bhargava, J. and Rhenstrom, A., Electrochemical Aspects of Electrical Resistance Gauges for Concrete, Swedish Council for Building Research, Doc. D11:1978, 1978.

[70] Feliu, S., Feliu, V. *"Modelling and identification of corrosion processes to electrical signals"* Monografy n.380 (In Spanish/English summary), IETcc, CSIC, Madrid, 1985, 100 pages

[71] Macdonald, R., *"Impedance Spectroscopy, Emphasizing solid materials and systems"*, John Wiley and Sons, New York, 1987 396 pages.

[72] Sellevold, E.J., Bager, D., "Low Temperature Calorimetry as a Pore Structure Probe" In Proceedings Vol.IV from *The 7th International Congress on the Chemistry of Cement*, Paris, 1980

[73] Radjy, F., Sellevold, E. J., Hansen, K. K., *"Isothermic Vapor Pressure – Temperature Data for Water Sorption in Hardened Cement Paste: Enthalpy, Entropy and Sorption Isotherms at Different Temperatures."* Report BYG-DTU R-057 Technical University of Denmark (DTU), Lyngby, 2003.

[74] Soroka, I., *"Portland Cement Paste and Concrete"* The Macmillan Press, London, 1979, pp. 46-72.

[75] Powers, T. C., "Physical Properties of Cement Paste", in the proceedings of the *Fourth International Symposium in the Chemistry of Cement*, Washington, 1960, pp.577-613.

[76] Brunauer S., Emmett P. H., Teller E., Adsorption of gases in multimolecular layers. *Journal of the American Chemical Society* 60:309-19, 1938

[77] Sellevold, E. J., *"Lecture notes in Structure of Cement Paste and Concrete"*, PhD lecture, NTNU, Trondheim, 2001.

[78] Relling, R., *"Coastal Concrete Bridges: Moisture State, Chloride Permeability and Aging Effects"*, Dr. Ing. Thesis, NTNU, Trondheim, 1999.

[79] Sellevold, E. J., "Resistivity and Humidity Measurements on Repaired and Non-repaired Areas in Gimsøystraumen Bridge", In Proceedings *International Conference Repair of Concrete Structures – From Theory to Practice in a Marine Environment*, Svolvær, 1997, pp. 283-295.

[80] Castro, P., Sagüés, A. A., Maldonado, L., Genescá, J., "Charachterization of Activated Titanium Solid Reference Electrodes for Corrosion Testing of Steel in Concrete", Corrosion, Vol.52, No.8, 1996, pp.609-617.